

**TRANSPORT AND RETENTION OF COLLOIDS IN SATURATED
AND UNSATURATED POROUS MEDIA**

A Dissertation
Presented to
The Academic Faculty

by

Christopher Scott Gray

In Partial Fulfillment
of the Requirements for the Degree
Doctor of Philosophy in the
School of Civil and Environmental Engineering

Georgia Institute of Technology
May 2016

Copyright © 2016 by Christopher Scott Gray

TRANSPORT AND RETENTION OF COLLOIDS IN SATURATED AND UNSATURATED POROUS MEDIA

Approved by:

Dr. Susan E. Burns, Advisor
School of Civil and Environmental
Engineering
Georgia Institute of Technology

Dr. Chloè Arson
School of Civil and Environmental
Engineering
Georgia Institute of Technology

Dr. J. David Frost
School of Civil and Environmental
Engineering
Georgia Institute of Technology

Dr. Christian Huber
School of Earth and Atmospheric Sciences
Georgia Institute of Technology

Dr. Paul W. Mayne,
School of Civil and Environmental
Engineering
Georgia Institute of Technology

Date Approved: January 8, 2016

To Laura, Charles, and Terry-Ann Gray

ACKNOWLEDGEMENTS

I would like to express the deepest gratitude to my advisor Dr. Susan Burns, who has shown me so much kindness, support, and generosity throughout my time at Georgia Tech. She continues to encourage me to push myself further personally as well as professionally. I would like to acknowledge and thank my thesis committee for all of their contributions to this body of work: Dr. Chloé Arson, Dr. David Frost, Dr. Christian Huber, and Dr. Paul Mayne. I would also like to thank all of the Geosystems faculty for their contributions in the classroom, where they have influenced my approach to problem solving and research.

I would like to thank all of the members of the Geoenvironmental research group: Akin Akinsola, Bate B., Additya Bhatt, Hyunwook Choo, Nicole Caruso, Joan Larrahondo, Junghwoon Lee, Randy Pettyjohn, Cameron Troxel, Xenia Wirth, Jong Muk Won, Nortey Yeboah, and Qian Zhao. Thank you to each and every one of you for your friendship and for all that you have taught me inside and outside of the lab. I would like to acknowledge Jenny Eaton, Carol Maddox, Billy Plum, and Andrew Udell for all of their help over the years.

I would like to thank my family. I would not be where I am today without the love and support of my mother, father, two brothers, and grandparents. Last but not least I would like to thank my wife, Laura. Thank you for all of your love and the unwavering support that you've shown over the years. You inspire me!

TABLE OF CONTENTS

ACKNOWLEDGEMENTS	IV
LIST OF TABLES	IX
LIST OF FIGURES.....	X
SUMMARY	XVII
CHAPTER 1: INTRODUCTION	1
1.1 Research Motivation	1
1.2 Thesis Organization	7
CHAPTER 2: LITERATURE REVIEW.....	9
2.1 Colloidal Processes in Saturated Porous Media	9
2.1.1 Favorable Conditions: Physicochemical Attachment + DLVO Theory.	9
2.1.2 Unfavorable Attachment Conditions	11
2.2 Colloidal Processes in Unsaturated Porous Media	13
2.2.1 Transient Flow in Unsaturated Porous Media.....	15
2.3 Factors Influencing Colloid Retention and Transport	17
2.3.1 Colloidal Factors	17
2.3.2 Soil Roughness and Angularity.....	19
2.3.3 Soil Physical Heterogeneity	20
2.4 Colloid Transport in Permeable Reactive Media	21
2.5 The Role of Colloid Shape in Transport and Retention.....	25
CHAPTER 3: PHYSICAL AND HYDRAULIC CHARACTERIZATION OF PERMEABLE REACTIVE MEDIA	31
3.1 Introduction	31
3.2.1 Porous Media Preparation and Index Properties	31
3.2.2 Media Surface Characterization.....	33
3.3 Saturated and Unsaturated Hydraulic Characterization	36
3.3.1 Experimental Setup	39
3.3.2 Numerical Simulations	41

3.3.3 Results and Discussion	44
3.4 Conclusions	56
CHAPTER 4: THE TRANSPORT AND RETENTION OF COLLOIDS IN SATURATED PERMEABLE REACTIVE MEDIA: THE ROLE OF PH AND IONIC STRENGTH.....	58
4.1 Introduction	58
4.2 Materials and Methods.....	60
4.2.1 Theoretical Considerations	60
4.2.2 Experimental.....	63
4.3 Results and Discussion.....	67
4.3.1 Effect of pH.....	69
4.3.2 Effect of Ionic Strength	77
4.3.3 Modeling Results	88
4.4 Conclusions	93
CHAPTER 5: THE TRANSPORT AND RETENTION OF COLLOIDS IN UNSATURATED PERMEABLE REACTIVE MEDIA.....	95
5.1 introduction	95
5.2 Materials and Method	96
5.2.1 Colloid and Porous Media Preparation	96
5.2.2 Column Transport Experiments	98
5.2.3 Transport Modeling.....	100
5.3 Results and Discussion.....	102
5.4 Conclusions	116
CHAPTER 6: THE MOBILIZATION OF COLLOIDS FROM PERMEABLE REACTIVE MEDIA DURING DRAINAGE	118
6.1 Introduction	118
6.2 Materials and Method	119
6.2.1 Theoretical Considerations	119
6.2.2 Colloid and Porous Media Preparation	121

6.2.3 Column Mobilization Experiments.....	121
6.3 Results and Discussion.....	123
6.4 Conclusions	137

CHAPTER 7: THE EFFECT OF IONIC STRENGTH ON THE TRANSPORT AND RETENTION OF SPHERICAL AND ELLIPSOIDAL COLLOIDS IN SATURATED POROUS MEDIA 139

7.1 Introduction	139
7.2 Materials and Method	140
7.2.1 Colloid and Porous Media Preparation	140
7.2.2 Column Transport Experiments	142
7.2.3 Theoretical Considerations	144
7.3 Results and Discussion.....	148
7.3.1 Characterization of Colloids and DLVO Interaction Energies	148
7.3.2 Column Transport Experiments	154
7.4 Conclusions	160

CHAPTER 8: THE TRANSPORT AND RETENTION OF COLLOIDS IN UNSATURATED SAND: THE ROLE OF COLLOID SHAPE AND MOISTURE CONTENT 161

8.1 Introduction	161
8.2 Materials and Method	162
8.2.1 Colloid and Porous Media Preparation	162
8.2.2 Column Transport Experiments	164
8.2.3 Transport Modeling.....	166
8.3 Results and Discussion.....	168
8.4 Conclusions	182

CHAPTER 9: THE EFFECT OF IONIC STRENGTH AND HYDRAULIC FLUX ON THE MOBILIZATION OF SPHERICAL AND ELLIPSOIDAL COLLOIDS FROM SAND DURING DRAINAGE 183

9.1 Introduction	183
------------------------	-----

9.2 Materials and Method	184
9.2.1 Colloid and Porous Media Preparation	184
9.2.2 Column Mobilization Experiments.....	184
9.3 Results and Discussion.....	186
9.4 Conclusions	193
CHAPTER 10: CONCLUSIONS AND FUTURE WORK.....	194
REFERENCES	205

LIST OF TABLES

Table 3.1: Index Properties.....	32
Table 3.2: SWCC and HCF Parameter Prior Distribution	44
Table 3.3: Directly estimated soil properties	45
Table 3.4: SWCC and HCF Measured and Estimated Parameters	48
Table 3.5: Coefficient of Variation (COV) of Estimated Parameters	48
Table 3.6: Calculated RMSE and AIC.....	49
Table 4.1: Experimental conditions and mass balance information.....	68
Table 4.2: DLVO Calculation Results	74
Table 4.3: ADE Model Results.....	89
Table 5.1: Soil water characteristic curve and hydraulic conductivity parameters	97
Table 5.2: Experimental conditions and mass balance information.....	104
Table 5.3: Fitted model parameters and calculated standard errors.	115
Table 6.1: DLVO Interaction Energies and Attachment Force Calculations	120
Table 6.2: Experimental Conditions	123
Table 7.1: Geometric dimensions of spherical and ellipsoidal particles.....	149
Table 7.2: DLVO Interaction Potential Energy Results.....	153
Table 7.3: Experimental conditions and mass balance information.....	157
Table 8.1: Experimental conditions and mass balance	170
Table 8.2: Fitted model parameters and calculated standard errors.	181
Table 9.1: Experimental conditions and mass balance information.....	186

LIST OF FIGURES

Figure 1.1: Size ranges of organic and inorganic materials in the colloidal size range. Particles in the highlighted area are subject to electrostatic forces and considered to be in the colloidal size range.	2
Figure 2.1: DLVO interaction potential energies between colloid and soil surface under conditions favorable and unfavorable to attachment.	11
Figure 3.1: SEM micrograph of silica sand surface	33
Figure 3.2: SEM micrograph of iron oxide coated sand surface. The hematite coating was discrete in nature and nanoparticles were typically grouped together in patches of varying size.	34
Figure 3.3: SEM micrograph of zeolite. Cuboid crystals occurred in patches of varying size and covered the majority zeolite surface.	34
Figure 3.4: Zeta potential measurements at varying pH for milled sand and zeolite, and hematite nanoparticles used to prepare iron oxide coated sand. All measurements were made at a fixed ionic strength of 1 mM. Dashed line demarks positive and negative zeta potentials.	36
Figure 3.5: Suction measurements from top ($z = 7.5$ cm), middle ($z = 5$ cm), and bottom ($z = 2.5$ cm) tensiometers for clean sand MSO experiment (left axis). Cumulative flux (outflow) measurements (right axis). Simulated data was calculated in Hydrus using the average parameter values estimated from including β in the optimization.	46
Figure 3.6: Suction measurements from top ($z = 7.5$ cm), middle ($z = 5$ cm), and bottom ($z = 2.5$ cm) tensiometers for iron oxide coated sand MSO experiment (left axis). Cumulative flux (outflow) measurements from scale (right axis).	46
Figure 3.7: Suction measurements from top ($z = 7.5$ cm), middle ($z = 5$ cm), and bottom ($z = 2.5$ cm) tensiometers for zeolite MSO experiment (left axis). Cumulative flux (outflow) measurements from scale (right axis).	47
Figure 3.8: The effect of including β or K_{sat} as fitted parameters on the SWCC (top) and HCF (bottom) for clean sand.	51
Figure 3.9: SWCC for sand, iron oxide coated sand, and zeolite expressed in terms of volumetric moisture content (top) and effective saturation (bottom). Note SWCC is calculated from the average estimated parameters from the optimization that included β	52

Figure 3.10: HCF for sand, iron oxide coated sand, and zeolite expressed in terms of volumetric moisture content (top) and effective saturation (bottom). Note HCF is calculated from the average estimated parameters from the optimization that included β55

Figure 4.1: Colloid transport results for clean sand at various pHs and constant ionic strength of 1 mM. Top: measured and simulated normalized effluent concentration breakthrough curves for colloids. Effluent concentration is normalized by influent concentration C_o . Bottom: measured and simulated normalized soil surface concentrations as a function of depth (distance from outlet). Surface concentration, S , refers to the mass of colloids retained per mass of soil. Simulated curves are shown as solid lines.70

Figure 4.2: Colloid transport results for iron oxide coated sand at various pHs and constant ionic strength of 1 mM. Top: measured and simulated normalized effluent concentration breakthrough curves for colloids. Bottom: measured and simulated normalized soil surface concentrations as a function of depth.71

Figure 4.3: Colloid transport results for zeolite at various pHs and constant ionic strength of 1 mM. Top: measured and simulated normalized effluent concentration breakthrough curves for colloids. Bottom: measured and simulated normalized soil surface concentrations as a function of depth.73

Figure 4.4: Mass of retained colloids as measured by integration of the breakthrough curve for all permeable reactive materials at varying pH.....76

Figure 4.5: Colloid transport results for clean sand at various ionic strengths and a constant pH of 5.5. Top: measured and simulated normalized effluent concentration breakthrough curves for colloids. Bottom: measured and simulated normalized soil surface concentrations as a function of depth.....79

Figure 4.6: Colloid transport results for iron oxide coated sand at various ionic strengths and a constant pH of 5.5. Top: measured and simulated normalized effluent concentration breakthrough curves for colloids. Bottom: measured and simulated normalized soil surface concentrations as a function of depth.80

Figure 4.7: Colloid transport results for zeolite at various ionic strengths and a constant pH of 5.5. Top: measured and simulated normalized effluent concentration breakthrough curves for colloids. Bottom: measured and simulated normalized soil surface concentrations as a function of depth.....81

Figure 4.8: Colloid transport results for clean sand at various ionic strengths and a constant pH of 10. Top: measured and simulated normalized effluent concentration breakthrough curves for colloids. Bottom: measured and simulated normalized soil surface concentrations as a function of depth.....82

Figure 4.9: Colloid transport results for iron oxide coated sand at various ionic strengths and a constant pH of 10. Top: measured and simulated normalized effluent concentration breakthrough curves for colloids. Bottom: measured and simulated normalized soil surface concentrations as a function of depth.83

Figure 4.10: Colloid transport results zeolite at various ionic strengths and a constant pH of 10. Top: measured and simulated normalized effluent concentration breakthrough curves for colloids. Bottom: measured and simulated normalized soil surface concentrations as a function of depth.84

Figure 4.11: Mass of retained colloids as measured by integration of the breakthrough curve for all permeable reactive materials at varying ionic strength at pH 5.5 and 10. ...87

Figure 4.12: Estimated kinetic attachment coefficients for permeable reactive materials at varying pH.90

Figure 4.13: Estimated kinetic attachment coefficients for permeable reactive materials at varying ionic strength at pH 5.5 and 10.....91

Figure 4.14: Estimated S_{max} coefficients for iron oxide coated sand and zeolite at varying ionic strength at pH 5.5 and 10. N_T refers to recovered colloids in the sand, N_i refers to number of colloids in a unit volume of injected colloid suspension.....92

Figure 5.1: Effective saturation profiles for unsaturated experiments measured at termination of experiments. Dashed lines show the general trend of decreasing saturation with depth.103

Figure 5.2: Colloid transport results for sand under varying degrees of saturation. Top: measured and simulated normalized effluent concentration breakthrough curves for colloids. C_0 is the concentration of the injected colloids. Bottom: measured and simulated normalized soil surface concentrations as a function of depth (distance from outlet). Surface concentration, S , refers to the mass of colloids retained per mass of soil. Simulated curves are shown as solid lines.106

Figure 5.3: Colloid transport results for iron oxide coated sand under varying degrees of saturation. Top: measured and simulated normalized effluent concentration breakthrough curves for colloids. Bottom: measured and simulated normalized soil surface concentrations as a function of depth.....107

Figure 5.4: Colloid transport results for zeolite under varying degrees of saturation. Top: measured and simulated normalized effluent concentration breakthrough curves for colloids. Bottom: measured and simulated normalized soil surface concentrations as a function of depth.	109
Figure 5.5: Mass of eluted colloids as measured by integration of the breakthrough curve at varying degrees of saturation.....	111
Figure 6.1: Measured effluent colloid concentration breakthrough curves in saturated clean sand under varying ionic strength and pH during first stage of experiment. Error bars are the standard deviations from three replicates. C_0 is the concentration of the injected colloids.	124
Figure 6.2: Measured effluent colloid concentration breakthrough curves in saturated iron oxide coated sand under varying ionic strength and pH during first stage of experiment. Error bars are the standard deviations from three replicates.	126
Figure 6.3: Measured effluent colloid concentration breakthrough curves in zeolite under varying ionic strength and pH during first stage of experiment. Error bars are the standard deviations from three replicates.	127
Figure 6.4: Percent mass of retained colloids (mass of retained colloids as measured by integration of the breakthrough curve divided by the injected mass of colloids) for all soil types under varying ionic strength and pH. Retained mass calculated from integration of the breakthrough curve.....	128
Figure 6.5: Measured drainage effluent colloid concentrations in clean sand under varying ionic strength and pH during second stage of experiment.	129
Figure 6.6: Measured drainage effluent colloid concentrations in iron oxide coated sand under varying ionic strength and pH during second stage of experiment.	130
Figure 6.7: Measured drainage effluent colloid concentrations in zeolite under varying ionic strength and pH during second stage of experiment.....	130
Figure 6.8: Top and Bottom: Percent mass of mobilized colloids (bars, left axis) compared with actual mass of mobilized colloids (lines, right axis) for all soil types under varying pH and ionic strength. Bottom portion of figure has cropped percent mobilized (left) axis to allow for easier comparison in low mobilization experiments.	132
Figure 6.9: Effluent colloid concentrations measured during drainage at varying hydraulic flux. Q is normalized flux, $Q = q_{\text{experiment}}/q$, where q is the hydraulic flux (0.24 cm/min) during the saturated portion of the experiment. All experiments were carried out at IS = 10 mM and pH = 10.	135

Figure 6.10: Percent mass of mobilized colloids (bars, left axis) compared with actual mass of mobilized colloids (lines, right axis) for all soil types under varying hydraulic flux. Q is normalized hydraulic flux, $Q = q_{\text{experiment}}/q$, where q is the hydraulic flux (0.24 cm/min) during the saturated portion of the experiment. All experiments carried out at IS = 10 mM, pH = 10. 136

Figure 7.1: Illustrated representation of the geometrical considerations when modeling an ellipsoidal particle and an infinite flat plate using surface element integration. In the case of a prolate ellipsoid, a and c are the semi-minor and semi-major axis respectively. \mathbf{n} is the unit vector normal to the surface element. \mathbf{k} is the unit vector normal to the plate. h is the distance between a surface element and the infinite flat plate. r , θ , and ϕ are the radial and angular coordinates in a spherical coordinate system. ϕ is the orientation of the ellipsoid relative to the surface. Only the two limiting cases for particle orientation were considered, that is $\phi = 0$ for an end-on configuration and $\phi = 90^\circ$ for a side-on configuration. 146

Figure 7.2: SEM micrograph of spherical (top) and ellipsoidal (bottom) colloids. 150

Figure 7.3: DLVO Interaction energy as a function of separation distance for spheres and ellipsoids at an ionic strength of 10 mM. For the ellipsoidal particles, only the limiting configurations were considered. That is, side-on, with the major semi-axis parallel to the soil surface, and end-on, with the major semi-axis perpendicular to the soil surface. 151

Figure 7.4: Expanded view of DLVO Interaction energies for spheres and ellipsoids at an ionic strength of 10 mM. The secondary minimum for ellipsoids in the side-on orientation is both deeper and broader than that of spherical colloids. 153

Figure 7.5: Measured and simulated normalized effluent concentration breakthrough curves for spherical and ellipsoidal colloids. Effluent concentration is normalized by influent concentration C_0 . Simulated breakthrough curves for each experiment are shown as solid lines. 155

Figure 7.6: First order attachment coefficients from estimated from simulated breakthrough curves. Error bars denote the standard deviation of the estimated parameters. 158

Figure 7.7: Measured normalized surface concentrations for spherical colloids as a function depth (distance from inlet). Surface concentration, S , has been normalized by influent concentration, C_0 . Solid lines are simulated retention profiles. 159

Figure 7.8: Measured and modeled normalized surface concentrations for ellipsoidal colloids as a function depth (distance from inlet).	159
Figure 8.1: Moisture content profiles for unsaturated experiments measured during dissection. Dashed lines show the general trend of decreasing moisture content with depth.	168
Figure 8.2: Matric suction measurements for untreated spherical colloids for both unsaturated flow cell tests. Upper data set is from the $\theta = 0.292$ experiment, lower data set is from the $\theta = 0.169$ experiment.....	169
Figure 8.3: Measured and simulated conservative NaNO_3 tracer breakthrough curves for untreated spherical colloid transport experiments for saturated and unsaturated flow cells. C_o is the concentration of the injected tracer.....	171
Figure 8.4: Measured and simulated normalized colloid breakthrough curves for untreated spherical colloids under varying degrees of saturation. C_o is the concentration of the injected colloids.	173
Figure 8.5: Measured and simulated normalized colloid breakthrough curves for treated spherical colloids under varying degrees of saturation.....	173
Figure 8.6: Measured and simulated breakthrough curves for ellipsoidal colloids under varying degrees of saturation.	174
Figure 8.7: Mass of eluted colloids as measured by integration of the breakthrough curve.	175
Figure 8.8: Measured and simulated normalized soil surface concentrations as a function of depth (distance from outlet) for untreated spherical colloids. Surface concentration, S , refers to the mass of colloids retained per mass of soil. Simulated curves are shown as solid lines.	177
Figure 8.9: Measured and simulated normalized soil surface concentrations as a function of depth for treated spherical colloids.	178
Figure 8.10: Measured and simulated normalized soil surface concentrations as a function of depth for ellipsoidal colloids.....	178
Figure 9.1: Measured effluent colloid concentration breakthrough curves for spherical and ellipsoidal colloids under varying ionic strength during first stage of experiment. Error bars are the standard deviations from three replicates. C_o is the concentration of the injected colloids.	187
Figure 9.2: Measured drainage effluent colloid concentrations under varying ionic strength for spherical and ellipsoidal colloids during second stage of experiment.....	188

Figure 9.3: Percent mass of mobilized colloids (bars, left axis) compared with actual mass of mobilized colloids (lines, right axis) at high and low ionic strength..... 189

Figure 9.4: Spherical and ellipsoidal colloid effluent concentrations measured during drainage at varying hydraulic flux. Q is normalized flux, $Q = q_{\text{experiment}}/q$, where q is the hydraulic flux (0.24 cm/min) during the saturated portion of the experiment. All experiments carried out at IS = 10 mM. 190

Figure 9.5: Percent mass of mobilized spheres and ellipsoids (bars, left axis) compared with actual mass of mobilized colloids (lines, right axis) under varying hydraulic flux. Q is normalized hydraulic flux, $Q = q_{\text{experiment}}/q$, where q is the hydraulic flux (0.24 cm/min) during the saturated portion of the experiment. All experiments were carried out at IS = 10 mM. 191

SUMMARY

The transport of colloidal particles in subsurface geological deposits plays an important role in many natural processes, from geochemical cycling of elements in aquifers to the transport of highly mobile bacteria and viruses. Colloids are of importance in geotechnical systems, where engineers are typically concerned with controlling the hydraulic conductivity of filters, such as in dam cores or landfill liners, or improving soil stiffness by utilizing microbial induced precipitation. Colloids are of particular importance to geoenvironmental engineers, as these highly mobile particles can act as vectors for immobile contaminants, effectively bypassing groundwater treatment systems. The transport of colloids themselves may be of concern such as in the case of pathogenic biocolloids and toxic nanoparticles.

This study explored the transport and retention of colloids in saturated and unsaturated silica sand, iron oxide coated sand, and natural zeolite, all of which are common components in permeable reactive barriers. Column flow cell studies demonstrate that colloid mobility is significantly affected by porewater chemistry and theoretical DLVO calculations elucidate differing colloid retention mechanisms in the three geomaterials. Results reveal that colloid transport in geomaterials is reduced in steady-state unsaturated flow, with zeolite significantly enhancing colloid retention. Studies exploring the mobilization of colloids from reactive geomaterials by a downward propagating drying front indicate that reactive geomaterials can enhance colloid retention.

This work also investigated the role of colloid shape on transport and retention in saturated and unsaturated silica sand using spherical and ellipsoidal colloids. Theoretical DLVO interaction potential energies calculated using surface element integration reveal that colloid shape affects interaction with the soil surface, while column studies

demonstrate colloid shape affects transport, retention, and mobilization in saturated and unsaturated sand.

CHAPTER 1:

INTRODUCTION

1.1 RESEARCH MOTIVATION

The transport of fine particles in subsurface geological deposits plays an important role in many natural processes, from geochemical cycling of elements in aquifers to engineered systems like dam cores and landfill liners (Reddi 1997; Ryan and Gschwend 1992). Colloidal particles, which are commonly defined as particles with a characteristic size in the 0.1-1 μm range, are of particular interest in transport phenomena. The range of sizes for particles considered colloidal is not set, and many definitions extend this range from as low as 10 nm (just above the size of larger dissolved macromolecules) up to 10 μm as shown in Figure 1.1 (Bradford and Torkzaban 2008; McGechan and Lewis 2002). Natural colloids are common in the environment, and can form due to a variety of mechanisms. Clay minerals such as kaolinite, montmorillonite, and illite, are colloids that are readily carried in suspension (Mitchell and Soga 2005; Shein and Devin 2007). Under certain geochemical conditions, soil minerals may dissolve, resulting in a pore fluid that is super saturated locally. Supersaturation can lead to precipitation of additional mineral phases, and the formation of mineral colloids. Additionally, mineral rock fragments may form from fracture of larger porous media particles and become mobile in the groundwater (McCarthy and McKay 2004; Sen and Khilar 2006). Other types of colloids include natural organic matter which can aggregate and form colloidal size particles, as well as other hydrophobic compounds that may form colloidal micelles in the presence of surfactants (McDowell-Boyer et al. 1986). Biocolloids such as bacteria, protozoa, and viruses are also present in the subsurface (Bradford, Morales, et al. 2013; Engström et al. 2014; Rockhold et al. 2004; Sen 2011; Yates et al. 1985). Reported concentrations of natural colloids

have varied widely, in the range of 10^8 to 10^{17} particles/L (Kim 1991), and in some cases have been found to be in excess of 1000 mg/L (Cheng and Saiers 2009, 2010; DeNovio et al. 2004; Rousseau et al. 2004; Sharma, Abdou, et al. 2008).

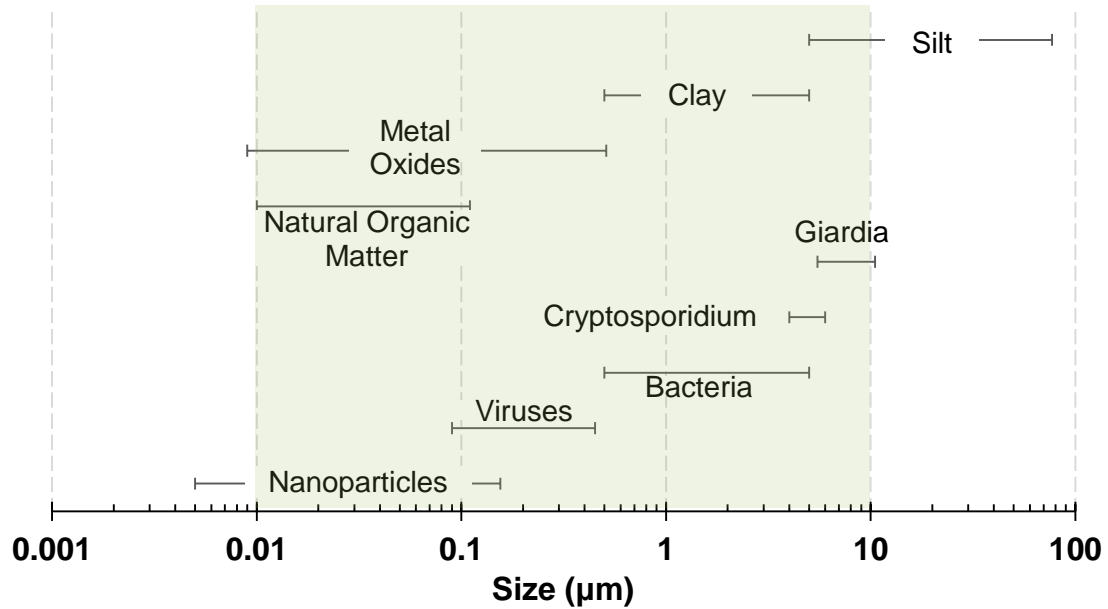


Figure 1.1: Size ranges of organic and inorganic materials in the colloidal size range. Particles in the highlighted area are subject to electrostatic forces and considered to be in the colloidal size range.

The implications for transport in the subsurface are significant because these particles are highly mobile and readily and reversibly transfer between the mobile aqueous phase and immobile porous media (DeNovio et al. 2004; Flury and Qiu 2008; Frimmel et al. 2007; Köhne et al. 2009; Shein and Devin 2007). Colloids have been shown to act as a vector for non-colloidal contaminants that would otherwise have a lower mobility in the dissolved phase. Many dissolved contaminants readily associate with the high surface area of colloidal particles through the mechanisms of ion exchange, surface complexation, or hydrophobic interactions (Sen and Khilar 2006). Colloid facilitated transport has been cited in the enhanced transport of radionuclides (Bates et al. 1992; Novikov et al. 2006;

Utsunomiya et al. 2009) and heavy metals (Bin et al. 2011; Shaoping et al. 2008), as well as organic contaminants such as polycyclic aromatic hydrocarbons (Laegdsmand et al. 2004; Roy and Dzombak 1998; Villholth 1999). Colloids enhance the transport of many contaminants associated with agriculture, such as hormones (Steiner et al. 2010), antibiotics (Zou and Zheng 2013), and pesticides (de Jonge et al. 1998; Kjær et al. 2011; Sprague et al. 2000; Villholth et al. 2000). Colloids have been found to enhance the transport of nutrients such as nitrogen and phosphorus, as well (Jarvie et al. 2012; de Jonge, Moldrup, et al. 2004; Rostad et al. 1998; Schelde et al. 2006). Finally, colloids have been implicated in the transport of contaminants through engineered systems that are designed to limit pollution of the environment, such as stormwater best management practices and landfill liners (Baumann et al. 2006; Béchet et al. 2006; Massoudieh and Ginn 2008).

In several instances, the colloidal particles themselves may be the contaminant of interest. Many bacteria and protozoans, such as *Escherichia coli*, *Listeria monocytogenes*, and *Cryptosporidium parvum* are pathogenic and are prevalent in groundwater due to wide spread contamination through agriculture, stormwater runoff, and waste treatment (Bradford, Morales, et al. 2013; Mohanty et al. 2013; Stevik et al. 2004; Tufenkji et al. 2006). Viruses, while smaller than bacteria, are a significant colloidal contaminant commonly encountered in the environment and can be highly mobile in both the saturated and unsaturated zone (Melnick and Gerba 1980; Schijven and Hassanizadeh 2000; Shein and Devin 2007; Yates et al. 1985). Biocolloids are subject to many of the same phenomena as non-biological colloids, as well as additional phenomena such as inactivation or the formation of biofilms (Ginn et al. 2002; Rockhold et al. 2004; Sen 2011; Tufenkji 2007). Increasingly, biocolloids are being considered as more than contaminants in the subsurface, but are instead being engineered as a mechanism to enhance soil properties. Engineers have injected bacteria, which may have to be

transported long distances, for bioremediation of contaminated soil, for the creation of biobarrriers, and to stiffen liquefaction susceptible soil (Bossolan et al. 2005; Díaz et al. 2010).

Another class of colloidal contaminants are engineered nanoparticles. While nanoparticles have at least one dimension in the 1 to 100 nm range, their overall size is often larger than the nanoscale, and they are subject to the same colloidal phenomena as micron sized particles (Baalousha et al. 2011; Hotze et al. 2010; Petosa et al. 2010). In other cases, nanoparticles may form aggregates that are in the colloidal size range (Fang et al. 2013). Manufactured nanoparticles include fullerenes, carbon nanotubes, metal oxides such as zinc and titanium nanoparticles, and quantum dots (Ju-Nam and Lead 2008). The small size and unique shapes of nanoparticles can result in high toxicity to bacteria and animal cells (Shi et al. 2008; Simon-Deckers et al. 2009). While many laboratory scale studies have demonstrated the high mobility of nanoparticles in saturated and unsaturated porous media (Chen et al. 2008; Jaisi et al. 2008; Lecoanet et al. 2004; Tian et al. 2012; Uyusur et al. 2010), there remain many unanswered questions as to their impact on and fate in the natural environment (Baalousha et al. 2011; Ju-Nam and Lead 2008; Lin et al. 2010).

From a geotechnical engineering standpoint, the retention and transport of colloids is important in the prediction or control of the hydraulic conductivity of engineered systems. Geotechnical engineers are often tasked with the design of filters, such as those found adjacent to dam cores. These filters must maintain high hydraulic conductivity, prevent the buildup of pore pressure, and limit the infiltration of fine grained soils into the coarse grained drainage filter (Mays 2010; McDowell-Boyer et al. 1986; Reddi et al. 2000, 2005; Sherard and Dunnigan 1989; Sherard et al. 1984a; b). Filter clogging by colloids is of interest in landfill design, where transport of bacteria through the leachate collection system can lead to biofouling and a subsequent drop in performance of the engineered

system (Hoffman et al. 1985; Koerner and Koerner 1992; Martin et al. 2006; McIsaac and Rowe 2006; Palmeira et al. 2008). In other cases, geotechnical engineers may seek to reduce hydraulic conductivity by inducing clogging with colloidal particles during the formation of filter cakes adjacent to boreholes or within a slurry cutoff wall (Evans and Ryan 2005; Hansmire et al. 1989; McDowell-Boyer et al. 1986; Weggel and Dortch 2012).

Geotechnical engineers are often interested in improving the stiffness of soils using a relatively new process known as microbial induced calcite precipitation (MICP). This technique relies on optimizing bacterial mediated precipitation to form calcite cementation between soil grains, which in turn improves soil stiffness (Burbank et al. 2013). Understanding the transport and retention of the colloidal sized bacteria is extremely important in this process, as engineers need to be able to control the delivery of both bacteria and nutrients to the zone of interest (Inagaki et al. 2011; Tobler et al. 2012). Abiotic mineral colloids can influence soil stiffness as well. Fine particles are transported to granular contacts during drying, where they can subsequently increase the dynamic resistance of the soil (Alramahi et al. 2010).

Colloids are important in energy related issues such as hydrocarbons extraction and the disposal of energy related waste. Geologic disposal sites have been considered as a potential option for long term storage of nuclear waste products (Bird and Fyfe 1982; Birkholzer et al. 2012); however, concerns have been expressed about the potential for colloid facilitated transport of radionuclides out of these disposal sites (Dai et al. 2002; Stockdale and Bryan 2013; Utsunomiya et al. 2009). Clay particles have a relatively high affinity for dissolved radionuclides and can serve as a vector for facilitated transport (Buddemeier and Hunt 1988; Kersting et al. 1999; Penrose et al. 1990). Radionuclide concentrations in groundwater at these site have been found in concentrations that are high enough to form metal precipitates that are subject to enhanced transport (Bates et al. 1992). Additionally, colloidal transport plays an extremely important role in energy

extraction. Engineers have long recognized how colloids can be mobilized, resulting in formation damage and a subsequent decrease in hydraulic conductivity (Gray 1966; Wilson et al. 2014), and practitioners are acutely aware of the impact of ionic strength and pH on the extent of formation damage by mobilized colloids (Khilar and Fogler 1984; McDowell-Boyer et al. 1986; Potter and W.E. 1985). Additionally, the transport and retention of biocolloids is extremely important in the microbial enhanced recovery of oil (Bossolan et al. 2005; Sen 2008). The recent boom in hydraulic fracking in the United States has resulted in a large supply of previously inaccessible natural gas becoming available. It has also resulted in a renewed focus on the potential environmental hazards associated hydraulic fracking, in part due to mobilization of colloidal particles (Haluszczak et al. 2013; Warner et al. 2013). The Marcellus Shale deposit is one of the largest shale gas deposits in the US and is rich in colloid sized clay particles that may become mobilized during fracking (Kargbo et al. 2010). Sang et al., (2014) recently demonstrated the potential effect of hydrofracking fluids on promoting colloid transport in the vadose zone.

It is clear that colloids will continue to play an important role in both the natural environment as well as in engineered systems for the foreseeable future. While the body of knowledge on this subject has continued to grow over the past three decades, there is still a need for better understanding of the mechanisms and processes involved in the transport and retention of colloids through porous media. To date, significant focus has been placed on the idealized systems made from model porous media such as glass spheres, and model colloidal polystyrene latex spheres. Additional research is needed to understand important processes and phenomena taking place in more complex systems.

1.2 THESIS ORGANIZATION

The thrust of this study was to examine the transport and retention of colloids in complex, non-idealized systems. The first half of this dissertation investigated the transport and mobilization of colloids in saturated and unsaturated engineered geomaterials that are commonly used in permeable reactive barriers. The geomaterials investigated include clean graded silica sand, hematite coated sand, and clinoptilolite zeolite. In the second half of the dissertation the role of colloid shape in transport and mobilization from saturated and unsaturated silica sand was investigated using spherical and ellipsoidal colloids.

Chapter 2 reviews the relevant processes associated with the transport and retention of colloids in saturated and unsaturated porous media. In Chapter 3, the porous media used throughout the study is characterized, including the measurement of geotechnical index properties and electrokinetic mobilities, and scanning electron microscopy. The saturated and unsaturated hydraulic characteristic of these geomaterials was assessed using the multistep outflow method, and unsaturated soil water characteristic curves and hydraulic conductivity functions were estimated. Chapter 4 explored the coupled effects of pH and ionic strength on the transport and retention of colloids through permeable reactive geomaterials under saturated conditions. Retention mechanisms were elucidated using Derjaguin, Landau, Verwey, and Overbeek (DLVO) theory and emphasis was placed on modeling effluent breakthrough curves and depth dependent retention profiles. In Chapter 5 the role of moisture content on the transport of colloids through unsaturated permeable reactive media under steady-state flow conditions was examined. Chapter 6 explored the role of drying fronts in mobilizing retained colloids from the surface of reactive media and investigated the role of pH, ionic strength, and drainage rate on colloid mobilization.

The role colloid shape plays in the transport and retention of colloids in porous media was investigated by modifying the shape of carboxylated polystyrene microspheres into ellipsoidal rod-like colloids. In Chapter 7 the ellipsoidal colloids were characterized using scanning electron microscopy and electrokinetic measurements. Saturated steady-state experiments examined the impact of ionic strength on the transport and retention of spherical and ellipsoidal colloids in saturated clean silica sand, while surface element integration was used to explore the effect of colloid shape on DLVO interaction potential energies. Chapter 8 investigated the unsaturated steady-state transport and retention of spherical and ellipsoidal colloids in clean sand. In Chapter 9 the mobilization of spherical and ellipsoidal colloids by a drying front was quantified, and the effect of ionic strength and drainage rate was assessed.

CHAPTER 2: LITERATURE REVIEW

2.1 COLLOIDAL PROCESSES IN SATURATED POROUS MEDIA

Retention of colloids in porous media is controlled by three primary processes: physical filtration, physicochemical attachment, and straining. Physical filtration is a constriction-based mechanism of particle removal and occurs when a particle larger than the pore throat becomes entrapped. This constriction-based method of particle immobilization can subsequently lead to the formation of a filter cake as retained particles accumulate at the surface boundary of the porous media (McDowell-Boyer et al. 1986). Physicochemical attachment refers to the process whereby particles become immobilized by electrostatic forces on the media surface through two sequential steps: transport to the surface and attachment to the surface; in some cases, detachment from the surface may also occur (McGechan and Lewis 2002). Finally, particles can become immobilized within the porous media in the smallest portion of the pore space within the soil matrix and at granular contacts in a general process termed straining (Bradford et al. 2002, 2006; Bradford, Torkzaban, et al. 2013).

2.1.1 Favorable Conditions: Physicochemical Attachment + DLVO Theory

Particles that are small enough to pass into the porous media are subject to physicochemical attachment at the soil water interface (SWI). When submersed in water, most surfaces or interfaces are charged due to a variety of mechanisms, including ionization of surface functional groups, isomorphic substitution, and adsorption of specific ions from solution (Benjamin 2002). As a direct consequence of electrostatics, dissolved, free ions of opposite charge are attracted to the charged surface. This redistribution of counterions leads to the formation of a diffuse electric double layer. Electric double layer interactions are a direct function of the surface potential (typically taken to be the zeta

potential), as well as the Debye Huckel parameter, which is a function of the solution ionic strength (Benjamin 2002). When two charged surfaces approach each other, their double layers begin to overlap, with similarly charged surfaces repelling each other and oppositely charged surfaces attracting each other. Surfaces experience additional interaction energy as they approach each other due to the spontaneous polarization of neighboring molecules in the space between the two surfaces. These dispersion forces, known London-van der Waals forces, lead to a net attraction between surfaces (Gregory 1981). Interaction energies between two surfaces are typically calculated using Derjaguin, Landau, Verwey, Overbeek (DLVO) theory, which simply states that the total interaction energy between two surfaces is the sum of the electric double layer interaction energy and the London-van der Waals interaction energy (Adamczyk and Weroński 1999; Elimelech et al. 1995).

DLVO theory has proven to be a very useful means of understanding and predicting phenomena associated with colloid transport and is a central feature of classical clean bed filtration theory. The Happel sphere-in-cell model simplifies the porous media as a representative single spherical collector surrounded by the pore fluid (Elimelech et al. 1995; Happel 1958; Nelson and Ginn 2005). Under favorable conditions (e.g. oppositely charged surfaces, and/or high ionic strength), no energy barrier between the two surfaces is present (Figure 2.1) and particles are readily attached and immobilized on the surface of the idealized collector in the primary energy well (Elimelech et al. 1995). For similarly charged surfaces, competition between electric double layer repulsion and London-van der Waals attraction leads to interaction profiles similar to the unfavorable profile (Figure 2.1). The salient features of the unfavorable interaction profile are a primary energy well at small separation distances, an energy barrier which prevents colloid attachment to the soil surface in the primary well, and a secondary energy well at larger distances. Colloids can become reversibly attach to the soil surface in the secondary

minimum. While classic filtration theory adequately describes the deposition of particles with a surface charge opposite to the soil media (i.e. favorable conditions), it is well recognized that it fails to adequately predict both the tendency for colloids to become immobilized when they share the same charge as the porous media, as well as the spatial distribution of immobilized colloids within the soil matrix (Bradford et al. 2002; Elimelech et al. 1995; Johnson et al. 2011; Loveland et al. 2003; Tufenkji and Elimelech 2005; Xu et al. 2006).

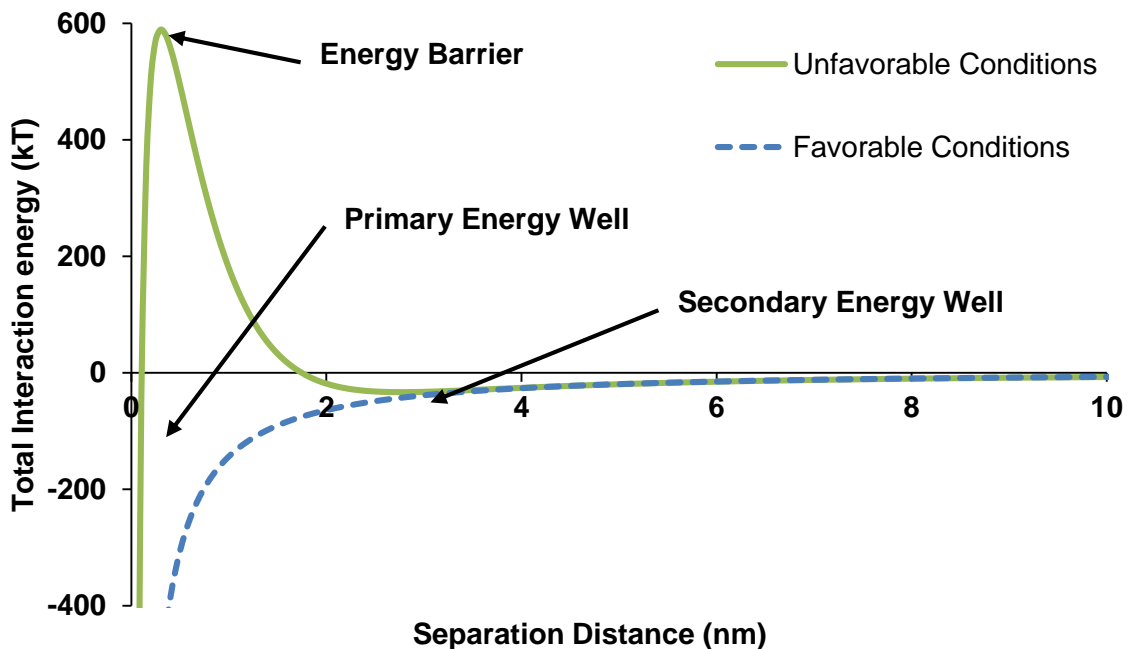


Figure 2.1: DLVO interaction potential energies between colloid and soil surface under conditions favorable and unfavorable to attachment.

2.1.2 Unfavorable Attachment Conditions

One of the earliest identified mechanisms of colloid immobilization under unfavorable conditions was the recognition that the presence of macro and micro scale chemical heterogeneities in porous media have a significant impact on retention (Johnson et al. 1996; Ryan and Gschwend 1992; Walz 1998). While the zeta potential is often used

to characterize surface charge for the purposes of DLVO and colloid filtration theory, it is effectively a coarse measurement that represents the average potential of the surface. Elimelech et al., (2000) demonstrated the disproportionate role chemical heterogeneities can play in colloid retention by introducing a relatively small fraction of media containing favorable attachment sites. Despite the net unfavorable conditions at the macroscale, the experiment demonstrated favorable media controlled retention behavior. At the microscale, small patchy chemical heterogeneity introduced to sand surfaces has been shown to be capable of immobilizing colloids that would otherwise be prevented from attachment due to the energy barrier (Bolster et al. 2001; Santore and Kozlova 2007; Walz 1998).

Straining within the soil matrix has received considerable attention in the past decade. In the context of this review, straining refers to retention of colloids within the smallest portion of the pore space near granular contacts (Bradford, Torkzaban, et al. 2013). This stands in contrast to physical filtration, which refers to particle retention in pore throats that can lead to the formation of filter cakes and result in a drop in hydraulic conductivity of the porous media (McDowell-Boyer et al. 1986). Straining is typically considered to become important as the empirical size ratio between the colloid and mean grain size ($d_{\text{colloid}}/d_{50}$) increases above 0.005-0.008 for monodisperse particles in saturated media (Bradford et al. 2002, 2006; Sang et al. 2013; Xu and Saiers 2009; Xu et al. 2006), while physical filtration is predominate at size ratios above 0.03-0.05 (McDowell-Boyer et al. 1986; Pazmino et al. 2011). However, the use of the median grain size, d_{50} , is not representative of the smallest grain sizes. Researchers have suggested that the particle number averaged grain size should be used instead, as it better captures the important role that finer sand grains play in straining by occupying the void space between larger grains (Pazmino et al. 2011; Porubcan and Xu 2011).

Just as DLVO theory plays a role in classical filtration theory, similar mechanisms are important in straining. Straining increases when ionic strength is increased, and the energy barrier to deposition is decreased (Bradford et al. 2007, 2009; Shen et al. 2008; Torkzaban et al. 2010). Straining is differentiated from physicochemical attachment in the secondary minimum at the soil surface because particles immobilized by straining are not remobilized by ionic strength transients, and colloids are typically located at grain contacts (Bradford et al. 2002; Bradford, Torkzaban, et al. 2013). Several mechanisms directly related to straining have been suggested to explain behavior observed under unfavorable conditions including wedging of colloids in low velocity stagnation points such as at the grain-to-grain contact of porous media (Johnson et al. 2010). In this case, particles can become loosely attached to the soil surface in the secondary minimum, then either roll or slide into flow stagnation points where they become immobilized (Johnson et al. 2007). At these locations, the low fluid velocities are ideal for immobilization of colloids in the secondary minimum (Bradford et al. 2006; Li et al. 2006). Additionally, once located in granular contacts, colloid-colloid interactions can become important as colloids begin to aggregate and form larger particles which contribute to filter ripening (Tong et al. 2008). Regardless of the mechanisms behind straining, its inclusion in models has led to accurate predictions of depth dependent profiles of immobilized colloid concentrations that classical models have failed to produce (Bradford et al. 2003, 2006; Johnson et al. 2011).

2.2 COLLOIDAL PROCESSES IN UNSATURATED POROUS MEDIA

The presence of a gas phase in steady unsaturated flow in porous media adds additional complexity to colloid transport and retention. A simple approach involves treating the air-water interface (AWI), which is typically negatively charged, as an additional collector, similar to classical filtration theory's treatment of the soil water interface (Karraker and Radke 2002; Wan and Wilson 1994b). Colloids that approach the

AWI experience electrostatic forces, thus retention at the AWI is affected by pH and typically increases as ionic strength increases (Saiers and Lenhart 2003a; Wan and Tokunaga 2002). Unlike the soil water interface in many natural minerals (e.g., silica), hydrophobic interactions at the AWI are considered extremely important. As such, retention at the AWI increases with colloid hydrophobicity and the process of attachment to the AWI by capillary forces is usually considered to be irreversible (Chen and Flury 2005; Crist et al. 2005; Gargiulo et al. 2008; Lazouskaya and Jin 2008; Wan and Tokunaga 2002; Wan and Wilson 1994a; b; Zevi et al. 2005; Zhuang et al. 2005). This is due largely to the fact that capillary forces which retain particles at the AWI are greater than DLVO forces, and this relative disparity in magnitude of forces increases as colloid size decreases (Chatterjee et al. 2012a; Shang et al. 2009). Media hydrophobicity can play an important role either by diverting preferential flow paths of water or by serving as a stronger collector for hydrophobic colloids (Chen et al. 2012; Goebel et al. 2013; Han et al. 2006).

In soils with low moisture contents, it has been suggested that colloids can become entrapped in the thin films, or pendular water, surrounding soil grains in a process known as film straining (Lenhart and Saiers 2002; Wan and Tokunaga 1997). Film straining becomes significantly more important as moisture content decreases, causing flow paths to become increasingly constrained to smaller pores (Lenhart and Saiers, 2002; Saiers and Lenhart, 2003a). Similar observations have been made when examining the role of ionic strength and moisture content. While increases in ionic strength increase colloid retention, as the moisture content decreases, thin film straining becomes more important than simple SWI physicochemical attachment (Gamerding and Kaplan 2001a; Torkzaban et al. 2008). Pore scale and visualization experiments have further elucidated processes taking place in the air-water meniscus solid (AWS) region, encompassing pendular water and the thin films that surround soil grains (Crist et al. 2004; Steenhuis et al. 2005; Wan and Tokunaga 2005; Zevi et al. 2005). Researchers have observed that

colloids can become trapped in hydrodynamic vortices in pendular water where they can undergo aggregation, suggesting that further transport would be retarded due to these larger aggregates settling out of suspension or being otherwise strained in pore throats (Zevi et al. 2012; W. Zhang et al. 2010).

2.2.1 Transient Flow in Unsaturated Porous Media

A phenomena unique to unsaturated porous media is the potential for different fluids to displace one another. Water displacing air in dry soil is referred to as imbibing, or infiltration, while air displacing water is referred to as drainage, though saturation levels can also change as a result of water table or surface water fluctuations and evapotranspiration. Numerous studies have demonstrated that the transient passage of a phase-phase interface has been shown to have the potential to mobilize in-situ colloids and highlight the complex coupled interplay between preferential flow in natural structured soils and soil water hysteresis (Kjaergaard, Moldrup, et al. 2004; Kjaergaard, Poulsen, et al. 2004). Hysteresis in unsaturated soils refers to the fact that the water content of a soil during drainage will always be greater than for a soil during wetting for the same given matric head or suction (Dane and Topp 2002). In natural systems, the amount of in-situ colloids mobilized during a storm event has been found to be dependent on the level of rainfall intensity (Rousseau et al. 2004; Shang et al. 2008), as well as on the antecedent dry period (Levin et al. 2006; Majdalani et al. 2008). Additionally, the mobilization of in-situ colloids is dependent on both water hysteresis and ionic strength, with higher ionic strength suppressing mobilization by wetting and drying fronts (Cheng and Saiers 2009, 2010; Zhuang et al. 2007).

Colloids can be transported by a wetting front, such as when water is imbibed into dry soil (Kenst et al. 2008). The work of Zhuang et al. (2010) investigated the role of surface tension in colloid transport during imbibition of a dry soil by varying the surface

tension of the imbibing water with 2-propanol and found that decreased surface tension led to a slower traveling wetting front allowing for increased physicochemical attachment to the SWI. Retained colloids can also be mobilized by a wetting front when colloids attached to soil grains are detached by capillary forces, or when colloids constrained by thin film straining are released by expanding films around soil grains. Saiers and Lenhart, (2003b) investigated colloid mobilization by step increases in soil moisture content and found a close relationship between the magnitude of the moisture change and the fraction of mobilized colloids. Their work demonstrated that the kinetic release of colloids was sensitive to the pore water velocity, highlighting the importance of fluid shear forces, but that overall the mobilization by the wetting front was rapid. Similar observations have been made in the imbibition based mobilization of in-situ colloids from disturbed natural sediments (Shang et al. 2008).

Drying fronts have been found to mobilize physicochemically immobilized colloids, and as with imbibition, behavior is coupled to chemical conditions. Measurements of the mobilization of in-situ colloids made by Cheng and Saiers (2009) suggest that drainage may be more effective than wetting in mobilizing colloids, though it is likely that this observation is related to soil water hysteresis. Saiers et al. (2003) found that the amount of colloids scoured by drying increased with the decreasing ionic strength of the pore water. It was found that as the discharge rate was increased, the probability of remobilization increased, an observation also made by others (Chen et al. 2008; Zhuang et al. 2009). Bridge et al. (2009) used a flat 2D flow cell to observe the transport of colloids during drainage and found that at low ionic strengths or drainage rate, particles tended to accumulate at the drying front, while at higher ionic strengths or drainage rate, mobilized particles were deposited over increasingly shorter distances. Aramrak et al. (2014) used confocal microscopy to observe colloid transport in response to a wetting and drying front

and observed similar behavior, with colloids retained in the secondary minimum being transported along the SWI.

Most work has focused on the role of flow transients on either mobilization of in-situ colloids from undisturbed or remolded soil cores, or on mobilization of colloids from model porous media such as clean silica sand or glass beads. Numerous studies have focused on the transport of colloids through chemically heterogeneous saturated porous media (Johnson et al. 1996; Ryan and Gschwend 1992). The presence of even extremely small chemical heterogeneities can cause colloids to become immobilized in either primary or secondary minimum, and this process can dominate transport and retention behavior from the nanoscale to the field scale (Bradford and Torkzaban 2012; Elimelech et al. 2000; Loveland et al. 2003; Santore and Kozlova 2007). The presence of air in the porous medium will not change interactions taking place at the SWI, thus it is unlikely that the presence of geochemical heterogeneities present in unsaturated media will significantly affect transport under steady-state flow conditions. It is less clear what the impact of geochemically heterogeneous media will be on mobilization of colloids by flow transients. Mohanty et al. (2013) measured the mobilization of bacteria in clean sands and hematite coated sands subjected to drainage by gravity, followed by imbibition and found that including 50% of hematite coated sand reduced the amount of mobilized bacteria by 97.9% while pure hematite coated sand reduced mobilized bacteria by 99.6%. This suggests that even a small amount of media favorable to colloid attachment may largely mask the mobilization of colloids by fluid transients.

2.3 FACTORS INFLUENCING COLLOID RETENTION AND TRANSPORT

2.3.1 Colloidal Factors

Colloid size and concentration play an important role in transport and retention in porous media. Colloids travel faster than solutes in porous media due to their tendency to

follow the fastest stream line in pore throats, which is even more pronounced as colloid size decreases (Sirivithayapakorn and Keller 2003b). In terms of retention, classical filtration theory has been successfully used to describe the impact of size under conditions favorable to attachment. Under these conditions, collector efficiency typically reaches a maximum in the 1-2 micron size range (Elimelech et al. 1995; Tong and Johnson 2006).

Under unfavorable attachment conditions, experimental observations deviate from filtration theory and are typically best described based on the ratio of the colloid diameter to the mean grain size of the porous media. Retention by straining becomes important as this empirical size ratio ($d_{\text{colloid}}/d_{50}$) increases above 0.005-0.008 for monodisperse particles in saturated media (Bradford et al. 2002, 2006; Xu et al. 2006). Xu and Saiers (2009) examined the transport of a polydisperse colloid suspension consisting of colloids of two different sizes and demonstrated the difficulty in predicting deposition kinetics in porous media. Although higher colloid concentration can increase retention through mechanisms such as pore throat bridging (Ramachandran and Fogler 1999), colloid concentrations typically have lower mass fractions retained due to the blocking of straining sites under unfavorable conditions (Bradford and Bettahar 2006; Bradford et al. 2009; Kasel et al. 2013; C. Wang et al. 2012). However, Zhang et al. (2010) observed that colloid retention increased with input concentration in unsaturated porous media, though this was attributed to possible aggregation of colloids at low velocity vortices near the air-water-soil interface.

Colloid hydrophobicity can be extremely important in determining the fate of colloids in unsaturated porous media. Hydrophobic colloids will readily become immobilized at the air-water-interface, and are less mobile as the moisture content decreases and the total surface area of the air-water-interface increases (Gargiulo et al. 2008; Zhuang et al. 2005). Hydrophobic bacteria can also experience increased retention in saturated media if the soil surface is hydrophobic as well (Jacobs et al. 2007). While

most mineral colloids are relatively hydrophilic, in some cases the positively charged edges of clays may be attracted to the negatively charged air-water-interface (Chatterjee et al. 2012a; Wan and Tokunaga 2002).

2.3.2 Soil Roughness and Angularity

Numerous studies have cited the role of roughness at varying scales in the retention of colloids under unfavorable conditions to explain the difference in observed results between smooth glass beads and sands or other natural media (Barton and Buchberger 2007; Bradford and Kim 2012; Brown et al. 2002; Tong and Johnson 2006; Torkzaban et al. 2010; Yoon et al. 2006). Roughness at the macroscale, or more generally, grain angularity, results in an increased number of media contacts which in turn increases retention at granular contacts through straining (Basha and Culligan 2010; Tong et al. 2008). In the context of classical filtration theory, Saiers and Ryan (2005) demonstrated that media roughness and shape does not impact collector efficiency, while experimental work by Tong and Johnson (2006) showed that increased angularity instead enhanced the colloid collision/sticking efficiency. Shellenberger and Logan (2002) showed that nanoscale surface asperities can impact retention of colloids, observing a 30-50% increase in colloid retention in media with roughened surfaces over smooth media.

Several attempts have been made to use extended forms of DLVO theory to explain increased retention in rough media. Huang et al. (2010) used DLVO theory to highlight the importance of the relative size of asperities, their spatial distribution, and colloid size in enhanced retention by rough surfaces. Specifically, as the ratio between asperity size and colloid size is increased, the energy barrier to deposition is decreased as long range van der Waals forces are increased. Krishna Darbha et al. (2012) observed that rough asperities can also frustrate colloid rolling or translation along mineral surfaces to flow stagnation points, and can thus cause colloids to be retained at locations other

than granular contacts. Shen et al. (2011) highlighted importance of the locations between asperities, termed “valleys,” on rough surfaces. While asperities can serve as attachment sites in the primary and secondary minimum (Shen, Lazouskaya, et al. 2012; Shen, L.-P. Wang, Li, et al. 2012), colloids are largely sheltered from hydrodynamic drag between asperities (Bradford, Torkzaban, et al. 2013; Shen et al. 2011) and the secondary minimum is deeper in this location due to the sides of the valley, which aids colloid retention in unfavorable conditions (Shen, F. Wang, Li, et al. 2012). Media roughness and angularity can become even more important in unsaturated media because restrictive flow paths bring colloids closer to the grain surface where they can become immobilized by friction forces (Gamerding and Kaplan 2001a; b; Morales et al. 2009; Zevi et al. 2005; W. Zhang et al. 2012).

2.3.3 Soil Physical Heterogeneity

Physical heterogeneity can impact colloid transport and retention in different ways depending on the type and scales. As one might expect, many of the trends observed by geotechnical engineers regarding heterogeneity of porous media and hydraulic conductivity are similar to observations of colloid transport and retention by environmental engineers. While classical filtration theory originally focused on uniform spheres, it has since been extended to differing grain sizes and distributions. In general, as the grain size distribution becomes less uniform, the reduction in pore space leads to a greater retention of colloids (Bradford et al. 2002; Pazmino et al. 2011; Porubcan and Xu 2011). Similarly, studies have observed the importance of D_{10} in predicting retention of colloids (Martin et al. 1996; Pazmino et al. 2011). Physical heterogeneity can occur in the form of the interface between two differing geomaterials and has been found to influence the retention of colloids. Multiple studies have observed increased retention when colloids pass from a coarser sand to a finer sand or to a geotextile due to the sudden and increased likelihood

of flow entering smaller or dead-end regions of the pore space (Bradford 2005; Lamy et al. 2013; Silliman 1995).

Larger scale physical heterogeneity includes preferential flow paths that can be caused by natural striation of different geomaterials or by biological processes such as root growth and worm tunneling. Preferential flow paths have long been recognized to have the potential to govern the transport of colloids as well as dissolved contaminants in the field (Cey et al. 2009; Wang et al. 2014). In the lab, preferential flow paths are typically modeled as coarse lenses or tubes parallel to the direction of flow in a fine grained matrix. The coarse grained preferential flow paths leads to distorted breakthrough curves and typically result in increased transport due to the increased void space in the coarse material (Bradford et al. 2004; Fontes et al. 1991; Saiers et al. 1994; Y. Wang et al. 2013). Interestingly this can be reversed in the vadose zone, where water flow is driven by capillary forces. Mishurov et al. (2008) investigated the role of physical heterogeneity by conducting colloid transport experiments with fine grained tubes in a coarser matrix. These finer grained pipes had a higher moisture content and acted as preferential pathways, decreasing retention and increasing the arrival time of the breakthrough curve over the homogenous coarse sand case.

2.4 COLLOID TRANSPORT IN PERMEABLE REACTIVE MEDIA

The use of reactive porous media for treating a wide variety of contaminants found in stormwater runoff, acid mine drainage, landfill leachate, and wastewater has received much attention (Chang et al. 2010; Genç-Fuhrman et al. 2007; Johansson Westholm 2006; Kietlińska and Renman 2005; Wantanaphong et al. 2005). These permeable reactive barriers are able to remove dissolved inorganic and organic pollutants through ion exchange and/or sorption to the media surface (Genç-Fuhrman et al. 2008; Jaradat et al. 2009; Srinivasan et al. 2008). One material that has been proposed for the use in

reactive barriers are zeolites (Färm 2002; Knox et al. 2008), which are naturally occurring aluminosilicates made up of a repeating three-dimensional framework of $[\text{SiO}_4]^{-4}$ and $[\text{AlO}_4]^{-5}$ polyhedra. The zeolitic framework contains channels and cavities that are filled with water molecules and highly mobile cations that enforce electroneutrality on what would otherwise be a negatively charged structure (Dyer 1988). Natural zeolites such as clinoptilolite are very common and readily available (Gottardi and Galli 1985) and are seen by many as an effective and inexpensive alternative to other sorbents when used to remove various heavy metals, radionuclides, and ammonium from water through ion exchange and surface complexation (Bailey et al. 1999; Park et al. 2002; Srinivasan et al. 2008). However, to date, very little research exists on the transport of colloids through natural zeolites. Gamerdinger and Kaplan (2001b) investigated the potential transport of colloids carrying radionuclides through saturated Yucca mountain zeolitic tuff and concluded that at the high ionic strengths expected in the field that it was unlikely that colloids would be transported through tuff material. This is due to the low isoelectric point of zeolites ($\text{pH}_{\text{ZC}} = 2\text{-}3$ (Ersoy and Çelik 2002)), which creates a negative surface charge under typical groundwater conditions, which is unfavorable to most colloid deposition. Further transport studies through unsaturated tuff demonstrated that the tuff material will retain larger numbers of colloids at low ionic strengths and low moisture contents than clean sand due to the increased roughness and larger specific surface area of the zeolite (Gamerdinger and Kaplan 2001a).

Another common component of many permeable reactive barriers are various iron oxide coated media. While some barrier materials are created by coating natural silica sand with iron oxides (Benjamin et al. 1996), often iron oxide coated sands are a byproduct from steel manufacturing (Lee et al. 2004). Iron oxides are able to remove a wide variety of uncomplexed and ligand-complexed heavy metals through coprecipitation and adsorption to the mineral surface under a wide range of pH and ionic strengths (Benjamin

et al. 1996; Genç-Fuhrman et al. 2008; Sansalone 1999). Iron oxides have proven effective at removing dissolved forms of nitrogen and phosphates (Erickson et al. 2006; Kietlińska and Renman 2005). Certain forms of mineral iron sorbents, such as zero valent iron, can mediate degradation of many organic contaminants (e.g., trichloroethylene through reductive dechlorination) (Henderson and Demond 2007). Additionally, iron oxide coated sands have been used to remove bacterial colloids from drinking water, as well as stormwater runoff (Ahammed and Davra 2011; Mohanty et al. 2013; Park et al. 2012; L. Zhang et al. 2010).

The transport of colloids through iron oxide coated media is often inhibited in the natural environment due to the relatively high isoelectric pH of iron oxides ($pH_{ZC}=5-9$ (Parks 1965)) that leads to a positive surface charge under typical groundwater conditions (favorable to colloid deposition). Early research focused on the role of natural surface iron oxides play in transport of in-situ clay colloids through aquifers and highlighted the complex interplay between ionic strength, redox conditions, and pH on their fate (Ryan and Gschwend 1992). The same group found that electrostatic charge reversal through pH changes was more effective at mobilizing in-situ colloids than double layer suppression through ionic strength changes or dissolution of iron oxides through reductant (Ryan and Gschwend 1994). Despite the fact that most iron oxides exhibit positive surface charge in the environment, their ability to immobilize colloids is often impaired by the presence of natural organic matter which will sorb to the mineral surface and effectively reverse the charge creating unfavorable conditions (Ryan et al. 1999).

A significant body of work has utilized flow cell systems at the laboratory scale to explore the influence of iron oxide media coatings, and geochemically heterogeneous porous media in general. Johnson et al. (1996) systematically studied the role of increasing iron-oxide coated sand content as well as ionic strength on the transport of silica colloids and demonstrated the strong influence of iron oxides. Additional studies

have found similar results, with relatively low fractions of coated media having an extremely large impact on colloid breakthrough curves, with iron oxide content linearly correlated with the overall colloid removal efficiency (Lin et al. 2011; D. Wang et al. 2012, 2013). Even the low levels of iron oxides found on Ottawa silica sand have been shown to affect the results of colloid transport experiments (Bradford and Kim 2012; Litton and Olson 1993; Shani et al. 2008). It is for this reason that the use of bulk measurements of porous media zeta potential can lead to unexpected retention of colloids (Elimelech et al. 2000). Several studies have highlighted the importance of pH in determining the fate of colloids in iron oxide coated media. While below the pH_{ZC} of iron oxide favorable deposition takes place, at higher pH values deposition tends to be unfavorable, yet more deposition will occur in the coated media due to the reduced energy barrier caused by the less electronegative iron oxide (Lin et al. 2011). Similarly, the effect of increasing ionic strength on colloid deposition is more pronounced in iron oxide coated media in both favorable and unfavorable conditions and can increase the maximum colloidal coverage of iron oxide coated media (Bolster et al. 2001; Johnson et al. 1996). Numerous other lab studies have focused on the important role played by organic matter. When deposited before transport, organic matter will reverse the surface charge of the iron oxides promoting transport of colloids, or when co-transported with colloids, will compete for attachment to iron oxides (Abudalo et al. 2010; Foppen et al. 2006; D. Wang et al. 2012, 2013; Yang et al. 2013)

Modeling of colloid transport and retention in iron oxide coated media typically relies on a linear combination of two-kinetic site models, which separately account for favorable deposition on iron oxide minerals and unfavorable deposition on silica minerals. The model proposed by Johnson et al.'s (1996) study has seen wide spread use in describing the transport of colloids in the lab and the field (Loveland et al. 2003; Sun et al. 2001; Yang et al. 2013). Briefly, this model consists of a heterogeneity parameter that

acts as a weighted average for the two kinetic sites and a blocking function to describe the relative decrease in attachment rate as colloid soil surface concentrations increase. While some researchers have found a Langmuirian blocking function to be sufficient to describe colloid deposition to favorable sites (El Badawy et al. 2013; Bolster et al. 2001), other researchers have favored Johnson and Elimelech's (1995) random sequential adsorption (RSA) nonlinear blocking function because it has an appropriate theoretical basis in the attachment of colloids to surfaces. In some cases, it has been found to better describe the deposition of colloids in iron oxide coated media (Bhattacharjee et al. 2002; D. Wang et al. 2013). Still other researchers have incorporated depth dependent blocking functions to describe the retention of colloids in geochemically heterogeneous columns (D. Wang et al. 2012).

Very little work has been done on the transport of colloids through unsaturated iron oxide coated sands. Chu et al. (2001) examined the transport of two model viruses through two different quartz sands at different moisture contents. The natural quartz sand was deemed reactive due to the presence of trace amounts of iron oxides, while the cleaned quartz sand had iron oxide impurities removed. Their results indicated that the removal of virus particles was more pronounced at lower moisture contents in the reactive sand due to the increased likelihood of interaction with the soil water interface inherent in the thin films surrounding granular media when subjected to unsaturated flow. Chu et al. (2003) examined the transport of viruses through five natural soils and found similar results with the soils with higher iron content having greater removal rates at lower moisture contents.

2.5 THE ROLE OF COLLOID SHAPE IN TRANSPORT AND RETENTION

Colloid shape is considered an important parameter in predicting the behavior of both organic and inorganic colloids in porous media. Biocolloids can have extremely

diverse shapes ranging from spherical coccus, ellipsoid rod-like bacillus, or spiral-like shapes (Madigan et al. 2010). While many studies and reviews often mention the importance of bacteria shape and its influence on processes taking place in the subsurface, it is often difficult to isolate the influence of shape factors from cell charge, hydrophobicity, and motility (Shein and Devin 2007; Stevik et al. 2004). Cell shape has also been a consideration in bioremediation, as it may be necessary for cells to travel long distances in the subsurface to reach contaminated zones in the soil (Díaz et al. 2010; Ginn et al. 2002). Additionally cell shape has been considered as a potentially important factor in the use of bacteria in microbial enhanced oil-recovery (Bossolan et al. 2005). Natural mineral colloids can have diverse shapes, ranging from spherical silica and hematite particles, to plate-like clays such as kaolinite, to rod-shaped goethite, to needle-like attapulgite (Mahmood et al. 2001; Mitchell and Soga 2005). Manufactured colloids have recently received attention due to the increasing production and use of nanoparticles, and their subsequent presence in the natural environment (Hotze et al. 2010; Ju-Nam and Lead 2008; Klaine et al. 2008; Nowack and Bucheli 2007). Many nanoparticles have diverse shapes that affect their toxicity (Liu et al. 2013; Shi et al. 2008; Simon-Deckers et al. 2009), as well as their transport and retention in the subsurface (Kasel et al. 2013; Lin et al. 2010). Single and multiwalled carbon nanotubes have received particular attention as the high aspect ratio of their needle-like shape has an impact on its transport in saturated and unsaturated porous media (Mekonen et al. 2014; Y. Wang et al. 2012).

The role colloid shape plays in transport and retention in porous media is poorly understood and experimental observations have at times been conflicting, especially in the case of biocolloids. An early study by Fontes et al. (1991) compared the transport of two bacterial strains of different shape and found a higher recovery rate for the more spherical bacteria. Weis et al (1995) observed the retention of several different strains of bacteria in a saturated column subject to drainage. Bacteria strains with increased aspect

ratio experienced increased retention over spherical bacteria for twelve of the fourteen bacteria strains investigated. Dong et al. (2002) compared the transport of two strains of bacteria with similar properties through intact soil cores and found that the higher aspect ratio bacteria were retained in larger amounts and had higher collision efficiency as compared to the more spherical strain. Becker et al. (2003) observed similar behavior in fractured crystalline rock as well as in sand (Becker et al. 2004), with spherical bacteria being more mobile, though in both studies the authors were hesitant to attribute this behavior to cell shape alone. Contrary to previous studies, Jacobs et al. (2007) found no significant correlation between cell shape and transport through saturated sand for twenty-one different bacteria strains, but interestingly did observe some correlation between bacteria shape and sorption in batch equilibrium experiments. Castro and Tufenkji (2008a) observed an inverse relationship between cell shape and filtration efficiency, with more spherical bacteria experiencing a higher filtration efficiency than rod-like bacteria. Bolster et al. (2009) found that for twelve different strains of *E. coli* of varying shape, size, and hydrophobicity, retention behavior most strongly correlated with shape, with spherical bacteria more mobile than more rod-like bacteria. In contrast, Nola et al. (2010) observed that rod-like bacteria were more mobile than spherical bacteria when traveling through undisturbed cores containing natural soils. Conflicting behavior regarding the role of bacteria shape has also been observed in microfiltration membranes. Wang et al. (2007, 2008) examined the filtration of bacteria through porous membranes and found that bacteria with high aspect ratio (spirillum shaped bacteria) were less likely to be retained than rods and spheres, suggesting that in some cases shape may enhance transport of colloids, while Baltus et al. (2009) observed that rod shaped bacteria were more likely to be filtered than spheres of a similar diameter.

The lack of consistent observations between bacteria shape and transport in porous media is in part a function of the inherent variability in cell size, hydrophobicity,

surface functional groups, motility, and surface structures between not only microbe strains but within individual populations of the same strain (Bolster et al. 2009; Bradford, Morales, et al. 2013; Ginn et al. 2002; Sen 2011). In-situ conditions such as dissolved oxygen or nutrients may directly influence the shape of cells present in soils as well (Bossolan et al. 2005; Wang et al. 2008). It is for these reasons, among others, that many researchers use polystyrene latex (PSL) spheres as a model colloid in transport experiments. Researchers have been able to modify the shape of polystyrene latex spheres into ellipsoids or rods using a method first proposed by Ho et al. (1993b) and later generalized by Champion et al. (2007). Briefly, this method consists of casting PSL microspheres in a thin film of polyvinyl alcohol (PVA), heating the films to a temperature that is above the glass transition phase of PSL, and then mechanically stretching the film to a desired aspect ratio. The PSL particles are recovered by dissolving the PVA film and removed from suspension via centrifugation.

Salerno et al. (2006) investigated the transport of rod-like of carboxylated PSL (CPSL) particles of varying aspect ratio (1:1, 1:2, 1:3) in saturated glass beads under conditions both favorable and unfavorable to attachment, and found that overall retention of colloids and collision efficiency increased proportionally with increasing aspect ratio. Xu et al. (2008) examined impact of shape on straining in saturated sands using peanut shaped colloids. These low aspect ratio particles (1:1.5 or 2:3) consist of smaller diameter and larger diameter spheres attached to each other. Their experimental data showed that colloid straining was controlled by the minor axis length (i.e. the diameter of the larger sphere) and additional pore-scale velocity simulations demonstrated the tendency of the major axis of eccentric colloids to align with streamlines as they approached pore throats. Similar behavior has been observed in silt-sized particles approaching pore throats. Valdes and Santamarina (2008) examined bridging at simulated pore openings for various silt sized mineral particles and found that platy, high aspect ratio, particles were less likely

to become trapped by bridging. Liu et al. (2010) examined the deposition and release of high aspect ratio (1:7) CPSL rods in saturated glass beads. Spheres were retained in larger amounts than high aspect ratio particles regardless of the ionic strength of the pore fluid, which is contrary to observations made by Salerno et al. (2006). The lower retention of rods under low ionic strength conditions was attributed to the smaller critical dimension associated with rods, similar to previous observations made by Xu et al. (2008). Deposited colloids were also mobilized by reducing the ionic strength to measure the kinetics of colloid release. While the release of spheres was instantaneous, the release of rods was rate limited, suggesting the possibility that rods were re-deposited during mobilization. Seymour et al. (2013) used various methods to measure the deposition of CPSL microspheres and rods of varying aspect ratio in channels as well as in porous media. Interestingly, they observed a ripening effect when rods were passed through the porous medium, suggesting that attached rods may enhance the roughness of the glass beads and serve as additional attachment locations.

The preceding discussion largely focused on the role of colloid shape in transport and retention in saturated porous media, and it is expected that colloid shape will likely play an interesting role in transport and retention in unsaturated porous media. Studies focusing on carbon nanotubes as well as graphene oxide have demonstrated that high aspect ratio nanoparticles are still mobile in unsaturated soil (Mekonen et al. 2014). Colloid shape, as well as mineralogy, have been shown theoretically and experimentally to impact the magnitude of capillary forces that particles would be subject to when passing through the air-water interface (Chatterjee and Flury 2013; Chatterjee et al. 2012a). A study by Gómez-Suárez et al. (2001) on the detachment of bacteria from a glass channel found that rod shaped bacteria were less likely to be detached by the passage of an air-water interface than spherical bacteria. In a similar experiment, Aramrak et al. (2013) examined detachment of carboxyl polystyrene latex spheres, rods, barrels, and oblong

disk shaped particles and found that rods were the least likely to be removed by an advancing air-water interface. This suggests that shape will likely play an interesting role in the transport and retention of colloids in unsaturated porous media.

CHAPTER 3:

PHYSICAL AND HYDRAULIC CHARACTERIZATION OF PERMEABLE REACTIVE MEDIA

3.1 INTRODUCTION

The physical and hydrological characteristics of soils are helpful in understanding and predicting colloid transport and retention under saturated and unsaturated conditions. In this chapter the three coarse grained soils that are characterized include graded silica sand (US Silica, IL), laboratory prepared iron oxide coated silica sand, and natural zeolite tuff (St. Cloud Zeolite, MN). These materials were characterized using scanning electron microscopy, electrophoretic measurements, and nitrogen gas adsorption. The saturated and unsaturated hydraulic properties of the three soils were measured using the multi-step outflow method to estimate soil water characteristic curves and hydraulic conductivity functions.

3.2.1 Porous Media Preparation and Index Properties

The three coarse grained soils that are characterized in this study include graded silica sand (US Silica, IL), laboratory prepared iron oxide coated silica sand, and natural zeolite tuff (St. Cloud Zeolite, MN). Soils were dry sieved to have the same grain size distribution ($d_{50} = 0.36$ mm, $C_u = 1.82$). The silica sand was repeatedly rinsed with deionized water, ultrasonicated (Branson 8510 Ultrasonic Cleaner) for 30 minutes, and rinsed again with deionized water over a #200 sieve. Iron oxide coated sands were prepared using the heterogeneous suspension method (Larrahondo et al. 2011; Scheidegger et al. 1993). Briefly, cleaned silica sand was added to a 40 mg/L suspension of hematite nanoparticles (approximately 90 nm in diameter) at a pH of 3 and an ionic strength of 10 mM NaNO_3 . The sand-iron slurry was agitated for five days and the pH was

repeatedly adjusted to 3 using nitric acid every 24 hours. The iron oxide coated sands were then repeatedly rinsed over a #200 sieve to remove excess residual iron oxide nanoparticles. The iron content of the coated sand was measured using optical emission spectroscopy (ICP-OES Optima 8000, Perkin Elmer) after removing the iron oxide coating using the citrate-dithionite-buffer method (Mehra 1958) and found to be 1.4 mg_{Fe}/g_{sand}.

The zeolite was confirmed to be composed primarily of clinoptilolite ((Na,K)₆(Al₆Si₃₀O₇₂)) via X-ray powder diffraction (PANalytical X'Pert PRO MPD). Clinoptilolite is a commonly occurring aluminosilicate zeolite typically found in semiarid regions that has found wide spread usage as a low cost ion exchanger (Dyer 1988; Gottardi and Galli 1985; Vaughan 1976). The specific gravity and limiting void ratios for all media were measured following ASTM D854-06, D4253, and D4254 and are summarized below in Table 3.1. The specific gravity of the iron oxide coated sand was slightly higher than that of clean sand due to the presence of the iron oxide coating (Larrahondo et al. 2011). The specific gravity of the zeolite was lower than either of the sands, and was similar to previously reported values for zeolitic tuff (Lee et al. 2010; Oren and Ozdamar 2013). Limiting void ratios were slightly lower in iron oxide coating sand in agreement with previous observations (Larrahondo et al. 2011). Zeolite limiting void ratios were significantly higher than either sand. This is reflective of the highly angular zeolite particles, which were derived from a crushed tuff material (Cho et al. 2006).

Table 3.1: Index Properties

Porous Media	d₅₀	C_u	G_s	e_{min}	e_{max}
Sand	0.36	1.82	2.65	0.50	0.77
Iron Oxide Sand	0.36	1.82	2.67	0.48	0.71
Zeolite	0.36	1.82	2.36	1.11	1.65

3.2.2 Media Surface Characterization

Scanning electron microscope (SEM LEO 1530) micrographs of the three different soil types are shown below in Figure 3.1-3. The silica sand particles were well rounded and exhibited relatively smooth planar surfaces. The iron oxide coating was discrete in nature, with rounded hematite nanoparticles (approximately 90 nm) typically clustered in patches of varying size on the sand surface. The iron oxide patches were more common near rough features on the sand surface; however, some patches were observed on smooth portions of the sand surface. The zeolite particles were highly angular and the surface was extremely irregular. Large patches of cuboid zeolite crystals of varying size were observed on the surface, resulting in microscale roughness on the zeolite surface that was not observed in either of the two sands.

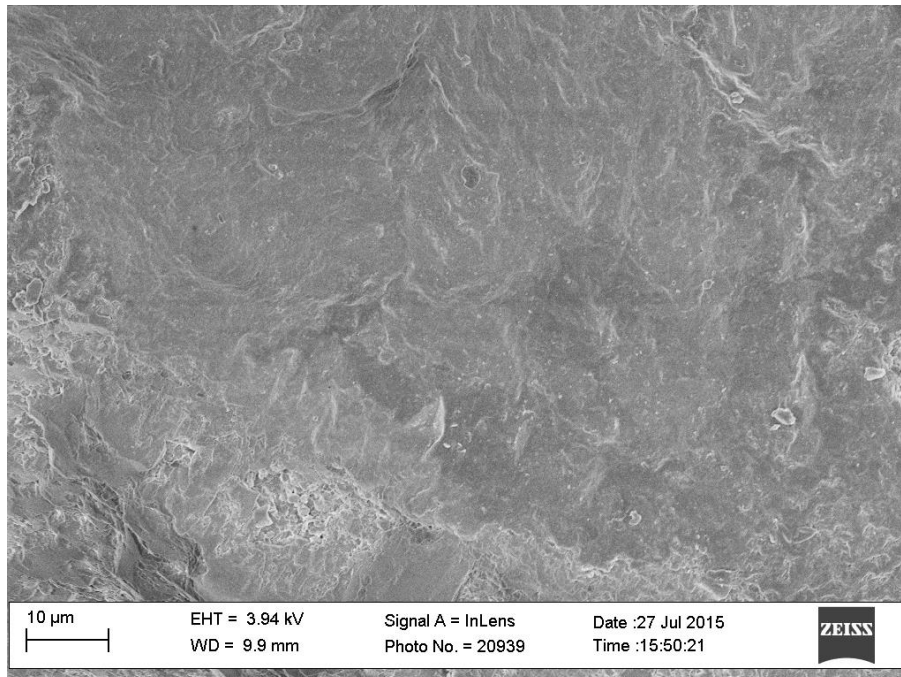


Figure 3.1: SEM micrograph of silica sand surface.

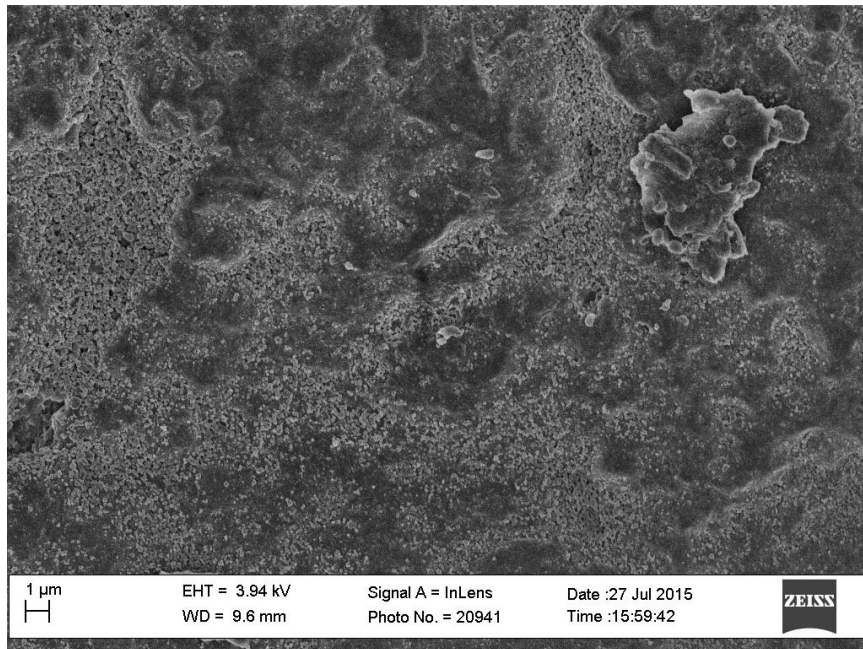


Figure 3.2: SEM micrograph of iron oxide coated sand surface. The hematite coating was discrete in nature and nanoparticles were typically grouped together in patches of varying size.

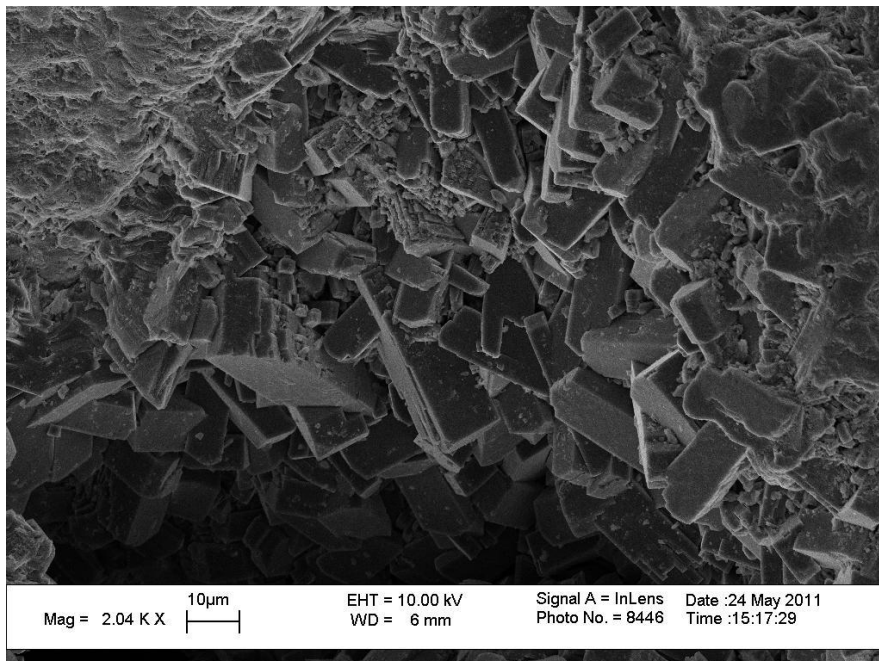


Figure 3.3: SEM micrograph of zeolite. Cuboid crystals occurred in patches of varying size and covered the majority zeolite surface.

The specific surface area of the zeolite was assessed using nitrogen gas adsorption (Micromeritics, ASAP 2020) and was found to be $11 \text{ m}^2/\text{g}$ as calculated by the Brunauer-Emmet-Teller (BET) isotherm. This value is on the lower end of the spectrum of reported specific surface areas reported for clinoptilolite, which typically ranges from 10 to $30 \text{ m}^2/\text{g}$ (Alvarez-Ayuso et al. 2003; Kowalczyk et al. 2006; Mockovčiaková et al. 2007; Sprynskyy et al. 2010). The silica and iron oxide coated sand specific surface areas were insufficiently large to be measured by nitrogen gas adsorption; specific surface areas for these materials was estimated to be on the order of $0.01 \text{ m}^2/\text{g}$ based on the grain size distribution and the assumption of spherical particles.

Silica sand and zeolite were crushed using a ball mill and the fraction of material passing the #400 sieve was retained in order to measure the electrophoretic properties of the different porous media. The hematite nanoparticles used to prepare iron oxide coated sand were used as is for electrophoretic measurements. Soil and hematite suspension at 10 g/L were prepared at varying pH (adjusted using HCl and NaOH) and a constant ionic strength of 1 mM (adjusted using NaCl). The electrophoretic mobilities of the soil suspensions were measured (Brookhaven Instruments Corporation, ZetaPALS) and converted to zeta potentials using the Smoluchowski equation. Zeta potential as a function of pH is shown below in Figure 3.4. The isoelectric point of the silica sand and zeolite is below pH 3, and the measured zeta potentials of the zeolite were lower in absolute value than the silica sand. The isoelectric point of the iron oxide coating was estimated to be approximately 6.3, similar to previously reported values for hematite (Parks 1965). The absolute values of the zeta potential of the hematite coating were lower than those of the silica sand and zeolite at pH greater than 6.3.

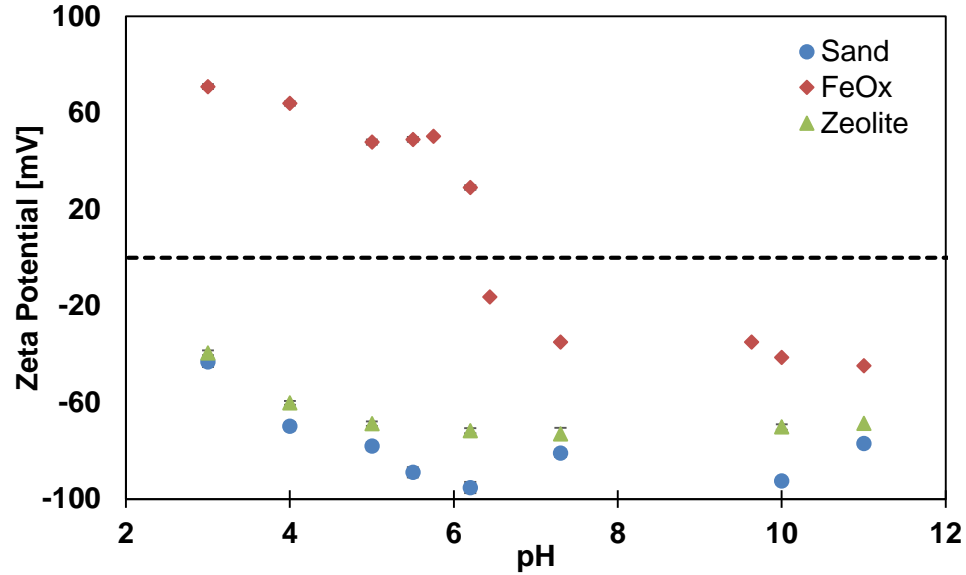


Figure 3.4: Zeta potential measurements at varying pH for milled sand and zeolite, and hematite nanoparticles used to prepare iron oxide coated sand. All measurements were made at a fixed ionic strength of 1 mM. Dashed line demarks positive and negative zeta potentials.

3.3 SATURATED AND UNSATURATED HYDRAULIC CHARACTERIZATION

The soil water characteristic curve (SWCC) is the relationship between soil water matric potential and volumetric moisture content and is a fundamental part of the hydraulic characterization of soil. Numerous SWCCs have been proposed in various forms, including empirical discontinuous power functions and S shaped functions such those of Brooks & Corey (1964) and van Genuchten (1980) (Assouline and Or 2013; Dane and Topp 2002). Others follow a more theoretical approach by linking the SWCC with the pore size distribution of the soil (Fredlund and Xing 1994; Kosugi 1994). Kosugi (1994) conceptualized the soil porosity as a bundle of capillary tubes with a lognormal pore radius distribution function linked to water retention by the height of capillary rise, yielding the following SWCC:

$$S_e = \frac{\theta - \theta_r}{\theta_s - \theta_r} = \frac{1}{2} \operatorname{erfc} \left[\frac{\ln(h/h_m)}{\sqrt{2}\sigma} \right] \quad (3.1)$$

where θ_s and θ_r are the dimensionless saturated and residual volumetric moisture contents respectively, h is the matric suction, h_m is related to the geometric mean pore radius, σ is the standard deviation of the pore size distribution, and $\text{erfc}[\]$ is the complimentary error function. Unlike the commonly used empirical SWCC of van Genuchten (1980), Kosugi's SWCC equation has a theoretical basis. Additionally, Kosugi's SWCC has been demonstrated to fit water retention data equally as well as van Genuchten's expression as measured by the mean square error of fitting the measured retention data for fifty soils (Kosugi 1994). It is for these reasons, and additional ones discussed below that Kosugi's SWCC was used in the following study.

Equally important in understanding the governing flow of water in unsaturated soils is the unsaturated hydraulic characteristic function (HCF) which describes the change in unsaturated hydraulic conductivity relative to the saturated hydraulic conductivity as a function of moisture content. Analytical expressions are typically derived using statistical models which integrate the contributions of individual pores according to Poiseuille's equation to yield macroscopic expressions for the unsaturated hydraulic conductivity (Mualem and Dagan 1978; Mualem 1976). The generalized form of the statistical model linking microscopic soil pores with and macroscopic hydraulic conductivity is given as (Kosugi 1999a; Mualem and Dagan 1978):

$$K_r = \frac{K_{unsat}}{K_{sat}} = S_e^\tau \left[\frac{\int_0^{S_e} h^{-\beta} dS_e}{\int_0^1 h^{-\beta} dS_e} \right]^\gamma \quad (3.2)$$

where K_{sat} and K_{unsat} are the saturated and unsaturated hydraulic conductivity respectively. The dimensionless fitting parameters τ and β relate to soil pore tortuosity and control the shape of the hydraulic conductivity function. Typically, β is fixed to a constant value to allow derivation of analytical expressions for the HCF from the SWCC, however this is unnecessary for Kosugi's SWCC (Burdine 1953; van Genuchten 1980; Kosugi 1999a; Mualem 1976). γ relates to how the effective pore radius is evaluated and is fixed to 1 or

2 (Burdine 1953; Mualem 1976). Inserting Equation 3.1 into Equation 3.2 and integrating yields the following HCF (Kosugi 1999a; b):

$$K_r = \frac{K_{unsat}}{K_{sat}} = S_e^\tau \left\{ \frac{1}{2} \operatorname{erfc} \left[\operatorname{erfc}^{-1}(2S_e) + \frac{\beta\sigma}{\sqrt{2}} \right] \right\}^\gamma \quad (3.3)$$

where $\operatorname{erfc}^{-1}[\cdot]$ is the inverse complimentary error function. γ has previously been demonstrated to have a similar effect on the shape of the Kosugi HCF as τ (Kosugi 1999a), thus γ was fixed to 2 after Mualem (1976). The major advantage of the above formulation of Kosugi's HCF over the HCF of van Genuchten is the additional free parameter β . Several studies have demonstrated that the inclusion of β as a free parameter in fitting directly measured unsaturated hydraulic conductivity data results in a substantial improvement in the fit of the HCF (Kosugi 1999a; b; Kutílek et al. 2009; Vervoort and Cattle 2003).

Together the SWCC and HCF form the constitutive relationship that describes the transport of water in unsaturated soils. Although direct measurement of water retention is relatively simple, the direct measurement of unsaturated hydraulic conductivity is extremely difficult (Dane and Topp 2002). This is due to the highly nonlinear nature of unsaturated hydraulic conductivity coupled with the lengthy time requirements to establish steady-state flow conditions in unsaturated porous media. For this reason researchers have increasingly turned to indirect, or inverse, methods to estimate unsaturated hydraulic parameters. This class of methods relies on simulating the measured response of a soil to changes in boundary conditions by solving Richard's equation coupled with the SWCC and HCF constitutive relationship, and iteratively changing the model SWCC and HCF parameters to minimize the difference between observed and simulated results (Dane and Topp 2002; Vrugt, Stauffer, et al. 2008). The multistep outflow (MSO) method is one such inverse method that has proven to be a robust and effective means of simultaneously

estimating the parameters of the SWCC and HCF (Eching and Hopmans 1993; Figueras and Gribb 2009; Nasta et al. 2011; Vrugt et al. 2003; Wayllace and Lu 2014).

The SWCC and HCF parameters of Equations 3.1 and 3.3 for clean sand, iron oxide coated sand, and zeolite were estimated using the extended MSO method (Durner and Iden 2011). It has already been demonstrated that MSO data yields unique and identifiable parameters for Equation 3.1 in sandy soils (Hwang and Powers 2003), however it is uncertain if the parameter β in the HCF is unique and identifiable. Thus, in addition characterizing the three permeable reactive media by fitting MSO data to Equations 3.1-3, the uniqueness and impact of fitting β from MSO data was assessed.

3.3.1 Experimental Setup

An acrylic flow cell (H=20 cm, D=5 cm) was used to conduct 1-D multi-step outflow experiments. Soil was contained in the bottom 10 cm half, while the top half was used to store ponded water for a falling head test to measure the saturated hydraulic conductivity prior to measuring unsaturated hydraulic properties. Soil suction was measured using three helically arranged tensiometers (652X03-B1M3, Soil Moisture Equipi. Corp) with pressure transducers (PX170-28DV, Omega Engineering) located at 2.5, 5, and 7.5 cm above the base and recorded every two seconds (CR3000, Campbell Scientific). An additional pressure transducer was used beneath the soil specimen to measure the suction applied to the specimen base. The cumulative mass of water extracted from the soil core was measured using a digital scale recording data every two seconds (4102 accuSeries, Fisher Scientific). The base of the soil specimen was supported using a hydrophilic nylon membrane (U-CMN-10, Component Supply Company) covering an aluminum disc and suction was applied to the soil by decreasing the elevation of the outlet tubing similar to a hanging column (Dane and Topp 2002). Preliminary tests confirmed that the bubbling pressure of the membrane was approximately 70 cm of H₂O and no

accumulated air was observed underneath the membrane over the course of the experiments.

Saturated samples were prepared using a modified form of slurry deposition which has been found to create specimens similar to those observed in alluvial deposits or hydraulic fills (Bandini and Sathiskumar 2009; Carraro et al. 2003; Wood et al. 2008). A known mass of dry material was introduced to a 55 cm long, 3.5 cm diameter acrylic cylinder half-filled with deaired deionized water and capped at the base using a rubber stopper. Entrapped air was minimized by adding additional deaired water to maintain a constant level of water above the soil slurry. The remaining headspace was filled with deaired water and then the cylinder was closed using a rubber stopper. Mixing of the slurry occurred by repeatedly inverting the cylinder end over end. Vacuum was then applied to the slurry for 12 hours to obtain a high level of saturation. After removal of vacuum, the specimen was repeatedly inverted for an additional 5 to 10 minutes to achieve a uniform mixture.

The rubber stopper was removed and replaced with an easily removed thin membrane. Prior to placement of the specimen, the acrylic flow cell was filled with deaired deionized water and the tensiometers were partially inserted into the column. The specimen was then inverted a final time and lowered to the bottom of the flow cell while simultaneously removing the end membrane. The end rubber stopper was carefully removed allowing the soil slurry to enter and fill the flow cell while the sides of the flow cell were tapped to densify the sample to a porosity of 0.37-0.38 for clean and iron oxide coated sand, and 0.59 for the zeolite.

Experiments followed the extended multistep outflow method proposed by Durner and Iden (2011). Water was initially ponded above the soil specimen to an approximate height of 9 cm, then allowed to drain as in a falling head experiment. This allowed for a very precise measurement of the saturated conductivity as well as an in-situ offset

correction for the pressure transducers and tensiometers (Durner and Iden 2011). After measuring the saturated hydraulic conductivity in the initial falling head portion of the test, suction at the lower boundary were increased as follows: -5,-10,-15,-22.5,-32.5, and -42.5 cm H₂O. The measurement time increased between subsequent increases in suction at the lower boundary of the soil. At the end of each experiment samples were weighed, dried at 105°C for 24 hours, and then weighed again to determine the moisture content at the end of the experiment. The initial saturated water content was calculated from the final moisture content and the measured cumulative outflow of water. Experiments typically ran approximately 12 hours.

3.3.2 Numerical Simulations

Uniform one-dimensional isothermal water flow in a partially saturated porous medium, assuming negligible vapor transport and rigid soil, can be simulated by Richard's equation:

$$\frac{\partial \theta}{\partial h} \frac{\partial h}{\partial t} = \nabla \cdot K(h) \nabla h \quad (3.4)$$

where θ is the volumetric water content, h [L] is the matric suction, t [T] is time, and $K(h)$ [LT⁻¹] is the unsaturated hydraulic conductivity. The nonlinear partial differential Equation 3.4, coupled with the constitutive relationships for the SWCC and HCF in Equations 3.1 and 3.3 were solved numerically using the finite element Hydrus-1D (Simunek et al. 2013) software package with the following initial and boundary conditions (Hopmans et al. 2002):

$$\begin{aligned} h(z, t = 0) &= z & 0 \leq z \leq L \\ q(z = L, t) &= 0 & 0 \leq t \leq t_{max} \\ h(z = 0, t) &= h_{LB} & 0 \leq t \leq t_{max} \end{aligned} \quad (3.5)$$

where q [LT⁻¹] is the hydraulic flux, L is the length of the flow cell, h_{LB} is the suction applied at the lower boundary.

Inversions were carried out by coupling the results of numerical simulations in Hydrus-1D with the Differential Evolution Adaptive Metropolis (DREAM) Markov Chain

Monte Carlo (MCMC) global optimization software package (Vrugt et al. 2009; Vrugt, ter Braak, Clark, et al. 2008). Briefly, DREAM builds upon the Metropolis-Hastings algorithm by combining differential evolution of multiple Markov chains with adaptive sampling to create an extremely robust and efficient means of global exploration in complex nonlinear and high dimensional problems. For a detailed description of the DREAM algorithm along with the principles behind it, see (Vrugt et al. 2009).

In a classical statistical based approach, unknown model parameters b are treated as fixed quantities, while in a Bayesian statistical approach model parameters are regarded as random variables with some known prior probability distribution $p(b)$. Bayesian theory provides a formal means of combining prior information about the system with information from observed data X to obtain the joint posterior probability density function for the parameter set, or $p(b|X)$. The posterior distribution of the model parameters in terms of the formal Bayes theorem is given below as:

$$p(b|X) = \frac{p(X|b)p(b)}{p(X)} \quad (3.6)$$

where $p(X|b)$ is the probability of observing X given model parameters b . The probability of producing the observed data $p(X)$ is typically removed from the denominator of equation $p(b|X) = \frac{p(X|b)p(b)}{p(X)}$ as it is impractical to calculate and not typically of interest (Wöhling and Vrugt 2011).

A common approach to inverse modeling is to aggregate the error residual, or the difference between N observed values X and simulated values \tilde{X} given parameters b , into a single residual vector:

$$\varepsilon_i(b) = X - \tilde{X}(b) \quad i = 1, \dots, N \quad (3.7)$$

Assuming that measurement errors are independent and uncorrelated, with a normally distributed and constant standard deviation σ_ε , the probability of observing data given the

model parameters b can be expressed by the following (Vrugt, ter Braak, Gupta, et al. 2008):

$$p(\mathbf{b}|\mathbf{X}) = c \cdot p(\mathbf{b}) \prod_{i=1}^N \frac{1}{\sqrt{2\pi\sigma_\varepsilon^2}} \exp\left(-\frac{1}{2\sigma_\varepsilon^2} \varepsilon_i(\mathbf{b})^2\right) \quad (3.8)$$

where c is a normalizing constant.

For reasons of convenience and numerical stability it is typical to maximize the logarithm of the likelihood function as the parameter values which maximize one will maximize the other. Thus the $p(\mathbf{b}|\mathbf{X})$ of Equation 3.8 becomes the log-likelihood of $l(\mathbf{b}|\mathbf{X})$ (Vrugt, ter Braak, Gupta, et al. 2008):

$$l(\mathbf{b}|\mathbf{X}) = -\frac{N}{2} \ln(2\pi) - \frac{N}{2} \ln(\sigma_\varepsilon^2) - \frac{1}{2\sigma_\varepsilon^2} \sum_{i=1}^N \varepsilon_i(\mathbf{b})^2 \quad (3.9)$$

The two different data types were included in a single objective function by summing the log-likelihood of each measurement type: (1) suction measured by the three tensiometers, and (2) the cumulative water flux, or outflow. Equation 3.9 is a function of both the error residual and the standard deviation of the residuals, σ_ε . Two typical approaches are to set σ_ε equal to the instrumental error variance a priori or to infer σ_ε posteriori from the quality of the fit by setting it equal to the root mean square error (RMSE) of the parameter set with the smallest error residual (Vrugt and Bouten 2002). Both of these approaches have an implicit assumption of zero model error. Preliminary tests found that the discrepancy in instrumental error variance for the different measurement types ($\sigma_\varepsilon = 0.0001$ cm for outflow and $\sigma_\varepsilon = 0.25$ cm H₂O for tensiometric measurements) led to the outflow measurements dominating the objective function. Therefore the latter approach was taken in setting σ_ε for the cumulative outflow and the individual tensiometric measurements equal to the RMSE from the optimum parameter set.

A uniform prior distribution for all model parameters was assumed as there was no independent information for parameter values. The boundaries for the various optimized parameters are shown in Table 3.2 and were selected to be sufficiently large enough to

ensure that optimum parameters were found while still maintaining consistent and correct values (Peters et al. 2011). The three parameters associated with the SWCC θ_r , h_m , and σ were estimated, however three different scenarios were considered for optimization of the HCF. In the first scenario, τ was estimated while β was fixed to one. In the second scenario, K_{sat} was treated as an additional fitting parameter, while τ was estimated as in scenario one. While there is no physical basis for including K_{sat} as fitting parameter, it is often treated as such in practice to improve the fitting of MSO data near saturation (Dane and Topp 2002; Eching and Hopmans 1993; Eching et al. 1994; Hwang and Powers 2003; Schaap and van Genuchten 2006; Vogel et al. 2000; Vrugt et al. 2001). In the third scenario both τ and β were optimized, while K_{sat} was fixed to the measured value.

Table 3.2: SWCC and HCF Parameter Prior Distribution

	$\theta_r^{*,+,x}$	$h_m^{*,+,x}$	$\sigma^{*,+,x}$	K_{sat}^+ [cm/min]	$\tau^{*,+,x}$	β^x
Min	0.01	-40	0.01	3	-2	0
Max	0.2	-1	1	0.05	4	12

Note: Superscripts (*), (+), (x) refer to whether a parameter was included in the optimization scenario. θ_r is the residual volumetric moisture content, h_m is a soil water characteristic (SWCC) parameter related to the geometric mean pore radius, and σ is an SWCC parameter related to the standard deviation of the pore size distribution. τ and β are hydraulic conductivity function (HCF) parameters related to the soil pore network tortuosity. In the first scenario (*) K_{sat} was fixed to the measured saturated value and β was fixed to 1. In the second scenario (+), τ and K_{sat} were treated as fitting parameters, while β was fixed to unity. In the third scenario (x) K_{sat} was fixed to the measured saturated value.

3.3.3 Results and Discussion

The directly measured hydraulic parameters for the three soil types are summarized in Table 3.3. The measured saturated hydraulic conductivity of both sands was higher than previously reported values for ASTM graded sand; however, this is likely an artifact of using a rigid wall permeameter versus a flexible wall device (Bandini and

Sathiskumar 2009). Interestingly, the greater void ratio associated with the zeolite did not result in a higher saturated hydraulic conductivity than the two sands.

Table 3.3: Directly estimated soil properties

Porous Media	θ_{Sat}	$\theta_{Termination}$	K_{sat} [cm/min]
Sand	0.382	0.0404	2.77
FeOx Sand	0.373	0.0390	2.44
Zeolite	0.594	0.1586	2.53

Note: $\theta_{Termination}$ refers to the moisture content that was measured at the termination of the MSO experiment and was used to calculate θ_{Sat} .

Tensiometric measurements of matric suction and cumulative outflow measurements for the three different porous media types are shown in Figures 3.5-7. The measured cumulative outflow initially increased rapidly in response to changes in the suction boundary condition. Indeed, the step changes in suction at the lower boundary are readily identified by the rapid increase in the cumulative outflow. After the initial large volume of water was extracted from the soil, cumulative outflows increased more gradually over time. A relatively small volume of water was extracted from the soils in response to the final increase in soil suction as compared to earlier step increases in the soil suction. The measured soil suction along the soil axis rapidly reached constant values for the first four increases to the boundary suction. However, the last two step increases to the boundary suction resulted in a much slower increase in the measured matric suction. Only in the case of the tensiometer located closest to the outlet at the base of the soil specimen is the final step increase in the boundary suction evident. This suggests that at the termination of MSO experiments, the majority of the capillary water had been extracted from the soil.

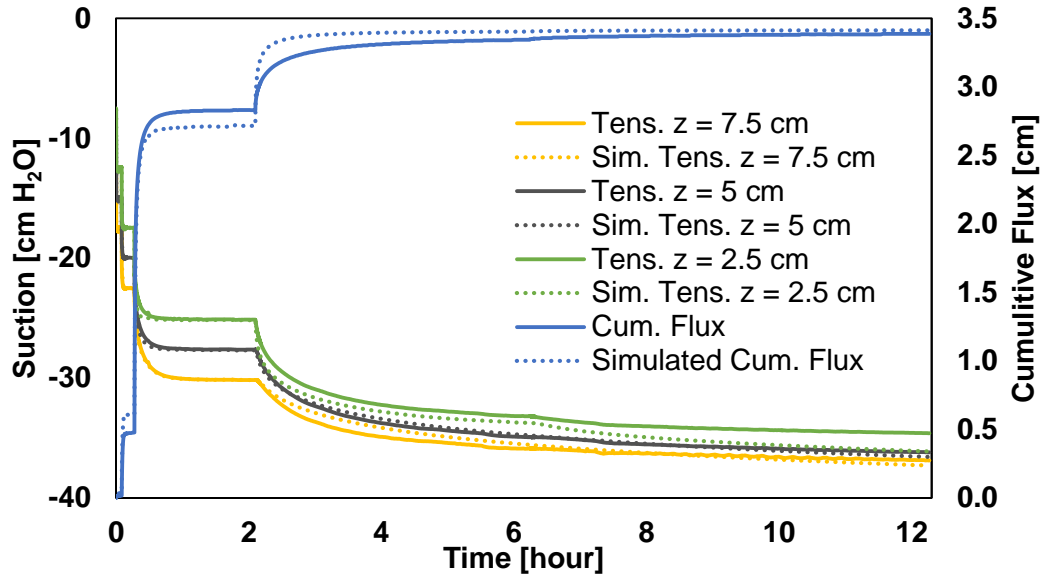


Figure 3.5: Suction measurements from top ($z = 7.5$ cm), middle ($z = 5$ cm), and bottom ($z = 2.5$ cm) tensiometers for clean sand MSO experiment (left axis). Cumulative flux (outflow) measurements (right axis). Simulated data was calculated in Hydrus using the average parameter values estimated from including β in the optimization.

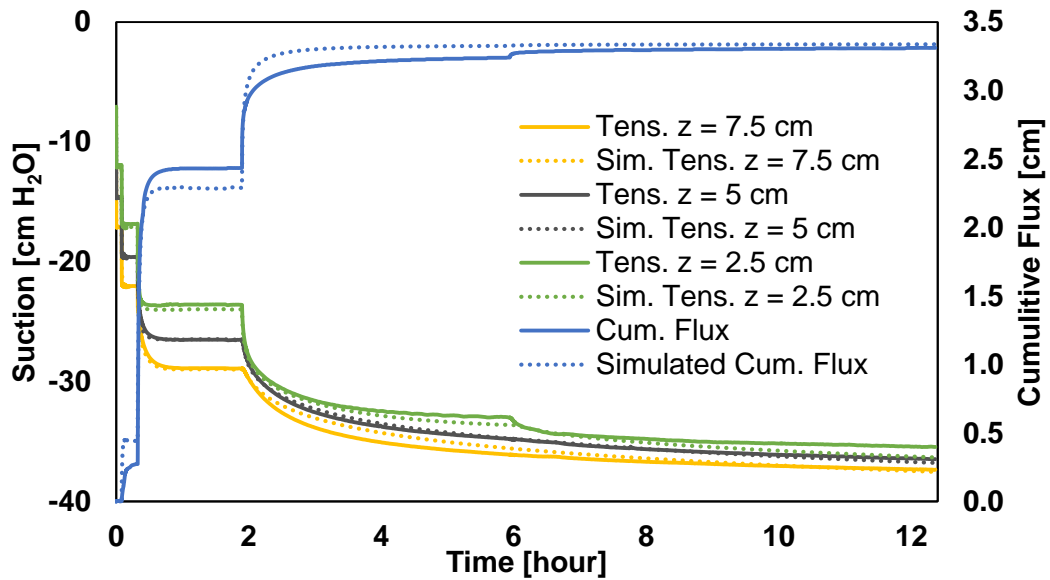


Figure 3.6: Suction measurements from top ($z = 7.5$ cm), middle ($z = 5$ cm), and bottom ($z = 2.5$ cm) tensiometers for iron oxide coated sand MSO experiment (left axis). Cumulative flux (outflow) measurements from scale (right axis).

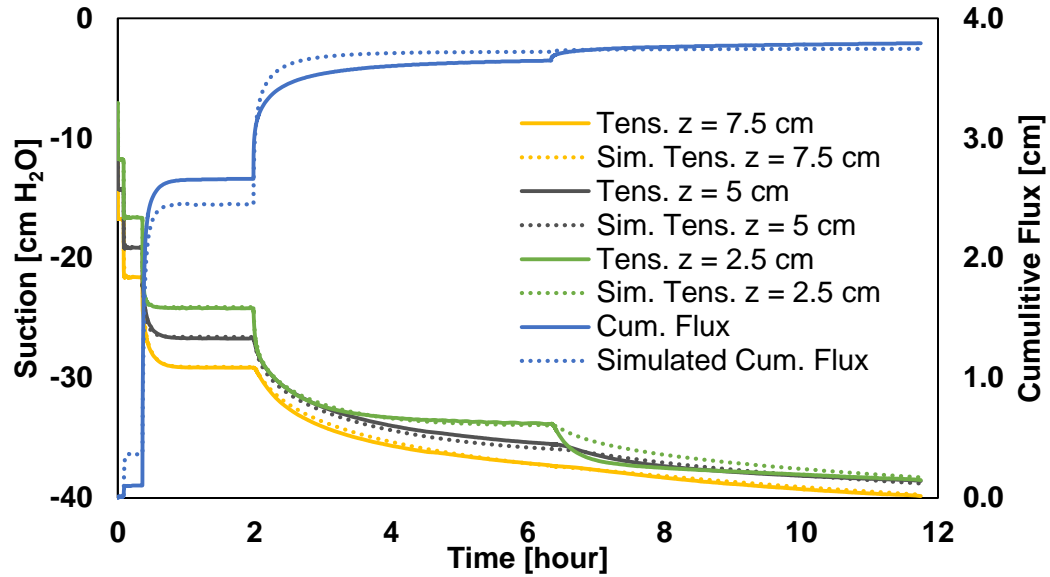


Figure 3.7: Suction measurements from top ($z = 7.5$ cm), middle ($z = 5$ cm), and bottom ($z = 2.5$ cm) tensiometers for zeolite MSO experiment (left axis). Cumulative flux (outflow) measurements from scale (right axis).

3.3.3.1 Hydraulic Conductivity Function Parameterization

The SWCC and HCF parameters are summarized in Table 3.4 and calculated coefficients of variation are summarized in Table 3.5. Coefficients of variation for θ_r and h_m were less than 1% for all parameter optimization scenarios, and typically decreased when K_{sat} or β were included in the optimization. The coefficients of variation of σ were higher than those of the other SWCC parameters, however were in all cases $\leq 2\%$. The coefficients of variation for τ were typically greater than other parameters and varied from 1% to 11%. The coefficients of variation associated K_{sat} and β were approximately 1% for all materials. This strongly suggests that β is unique and identifiable from MSO data for sandy soils. Additionally, the inclusion of β significantly improved the uniqueness of τ without reducing the uniqueness of other estimated parameters.

Table 3.4: SWCC and HCF Measured and Estimated Parameters

Porous Media	θ_{Sat}	θ_r	h_m	σ	K_{sat} [cm/min]	τ	β
Sand	0.382*	0.0392 (0.001)	-23.49 (0.03)	0.172 (0.001)	2.77*	0.20 (0.01)	1*
Sand	0.382*	0.0404 (0.0001)	-23.88 (0.04)	0.109 (0.001)	1.42 (0.02)	-0.48 (0.01)	1*
Sand	0.382*	0.0392 (0.0001)	-23.90 (0.02)	0.130 (0.001)	2.77*	-0.62 (0.01)	3.99 (0.06)
FeOx	0.373*	0.0359 (0.0001)	-23.51 (0.03)	0.190 (0.001)	2.44*	0.34 (0.02)	1*
FeOx	0.373*	0.0390 (0.0001)	-24.21 (0.02)	0.105 (0.001)	1.15 (0.01)	-0.51 (0.02)	1*
FeOx	0.373*	0.0389 (0.0001)	-24.22 (0.02)	0.126 (0.001)	2.44*	-0.70 (0.01)	4.49 (0.05)
Zeolite	0.594*	0.1467 (0.0001)	-23.91 (0.06)	0.262 (0.004)	2.53*	0.73 (0.04)	1*
Zeolite	0.594*	0.1577 (0.0001)	-24.36 (0.03)	0.165 (0.002)	1.31 (0.02)	-0.17 (0.02)	1*
Zeolite	0.594*	0.1666 (0.0001)	-24.64 (0.03)	0.137 (0.003)	2.53*	-0.98 (0.01)	5.49 (0.05)

Note: (*) refers to values fixed during optimization. Values in parenthesis are one standard deviation of the estimated parameter.

Table 3.5: Coefficient of Variation (COV) of Estimated Parameters

Porous Media	θ_r cov (%)	h_m cov (%)	σ cov (%)	K_{sat} cov (%)	τ cov (%)	β cov (%)
Sand	0.26	0.12	0.75	N/A	7.34	N/A
Sand	0.03	0.16	0.92	1.27	2.29	N/A
Sand	0.03	0.07	0.84	N/A	2.01	1.45
FeOx	0.56	0.14	1.05	N/A	6.76	N/A
FeOx	0.26	0.08	2.01	1.05	3.60	N/A
FeOx	0.26	0.08	0.95	N/A	1.51	1.22
Zeolite	0.68	0.24	1.34	N/A	5.14	N/A
Zeolite	0.06	0.12	1.33	1.37	11.09	N/A
Zeolite	0.36	0.13	0.22	N/A	0.82	0.97

Calculated root mean squared errors (RMSE) for the cumulative outflow and matrix suction are reported in Table 3.6. Additionally a total RMSE was reported, which is the combined RMSE for all three tensiometers and the cumulative outflow. The calculated

RMSE for cumulative outflow was significantly higher than the approximate variance associated with the outflow measurement (0.001 cm) in all experiments. The calculated RMSE associated with tensiometric measurements was similar to the approximate variance associated with the tensiometers and pressure transducers (0.25 cm of H₂O). The RMSE varied between the different axial tensiometers with no clear pattern. The inclusion of K_{sat} or β decreased the RMSE associated with the outflow measurement, and in most cases decreased the RMSE associated with the middle tensiometers. The total RMSE decreased for all materials with the inclusion of β in the optimization, while the total RMSE only improved for the two sands when K_{sat} was included in the optimization. Thus the inclusion of β resulted in the greatest reduction of the root mean squared error.

Table 3.6: Calculated RMSE and AIC

Porous Media	Estim. Param.	RMSE Q	RMSE T _{Top}	RMSE T _{Middle}	RMSE T _{Bottom}	RMSE Total	AIC
Sand	τ	0.121	0.310	0.332	0.887	0.502	3425
Sand	K_{sat}, τ	0.108	0.308	0.246	0.820	0.458	1972
Sand	β, τ	0.088	0.320	0.251	0.795	0.449	1451
FeOx	τ	0.188	0.431	0.264	0.450	0.351	3046
FeOx	K_{sat}, τ	0.117	0.433	0.195	0.430	0.325	635
FeOx	β, τ	0.110	0.403	0.206	0.432	0.318	415
Zeolite	τ	0.253	0.445	0.515	0.391	0.412	2709
Zeolite	K_{sat}, τ	0.160	0.455	0.549	0.426	0.423	2303
Zeolite	β, τ	0.139	0.286	0.302	0.431	0.308	596

Many different indirect metrics have been proposed to assess and compare models (Bennett et al. 2013). One such metric is the Akaike Information Criterion (AIC) which assesses the relative goodness of fit between models while taking into account the model complexity (Akaike 1974). The AIC is calculated by the following:

$$AIC = 2k - \ln(l)$$

where k is the number of fitted parameters (four in the case of fixed K_{sat} and β , otherwise 5) and $\ln(l)$ is the maximum value of the log-likelihood function (calculated from Equation 3.9 with the best fit parameters). Calculated AIC's associated with the different HCF parameterizations are included in Table 3.6. For all materials the AIC was highest when K_{sat} and β were fixed, and lowest when β was included in the optimization for the HCF. Thus the inclusion of β as a free parameter in the HCF minimized information loss as compared to the base scenario of only fitting τ , or treating K_{sat} as a free parameter (Akaike 1974). However, it should be noted that fitting β still resulted in systematic error in the cumulative outflow despite minimizing information loss (Figures 3.5-7).

The inclusion of β in the HCF versus treating K_{sat} as a fitting parameter offers additional advantages which are not easily quantified. Only the silica sand data is considered in the following discussion; however, the observations were similar for all soil types. The inclusion of either K_{sat} or β in the estimation of unsaturated parameters yielded very similar SWCC's as shown in the top of Figure 3.8. The inclusion of an additional fitting parameter in the HCF resulted in a slightly higher air entry value and a significantly narrower curve as compared to the base case in which only τ was fit. Fitting β and K_{sat} yielded very different HCF curves as shown in the bottom of Figure 3.8. Although HCFs were similar at high suctions and low moisture contents, including K_{sat} as an estimated parameter resulted in estimating significantly lower conductivities near saturation. This is in part because K_{sat} scales over the entire range of the MSO experiment and not simply near saturation where its physically relevant (Durner and Iden 2011; Vrugt et al. 2001, 2003). Additionally fitting K_{sat} results in a discontinuity in hydraulic conductivity between the unsaturated and saturated condition (Schaap and van Genuchten 2006; Vogel et al. 2000). The inclusion of β improves the fit of the HCF near saturation and avoids a discontinuity between saturated and unsaturated hydraulic conductivity.

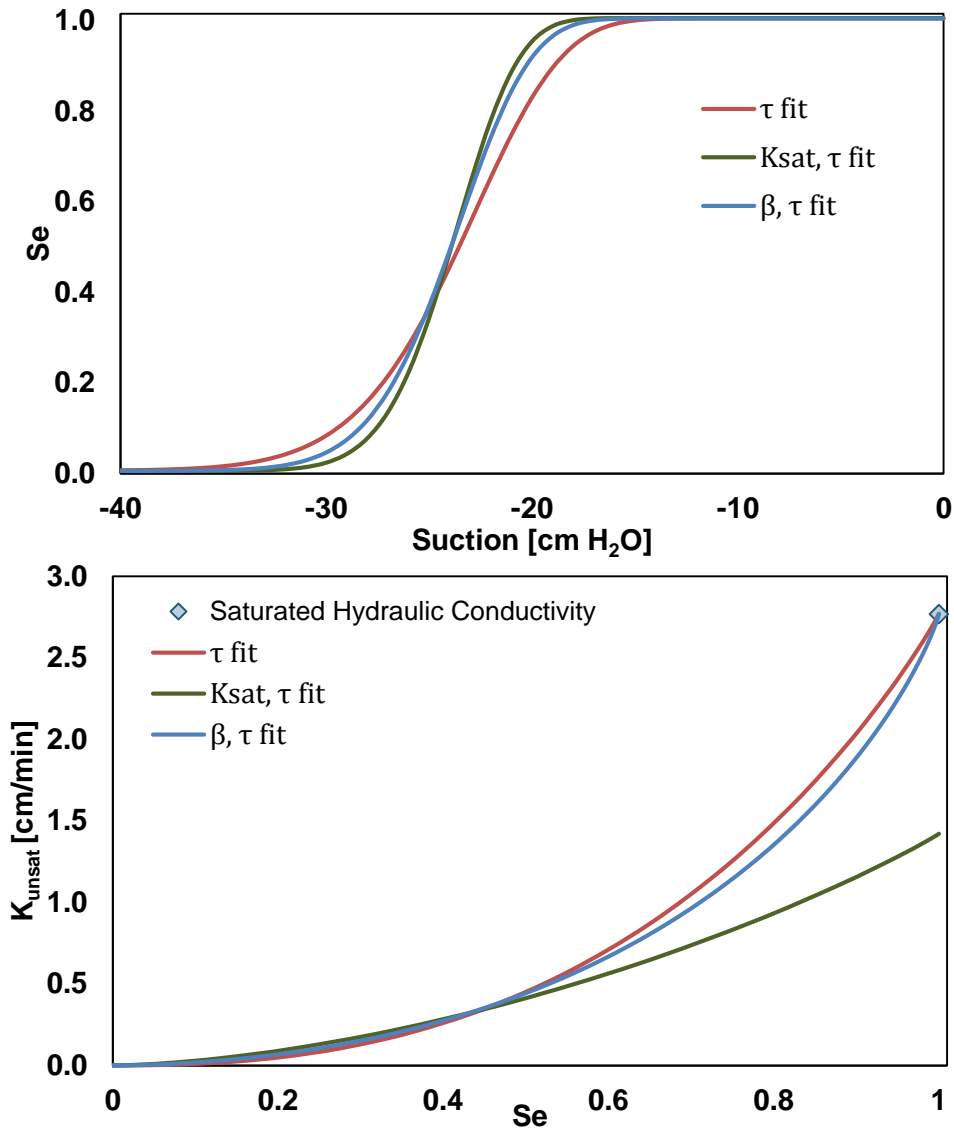


Figure 3.8: The effect of including β or K_{sat} as fitted parameters on the SWCC (top) and HCF (bottom) for clean sand.

3.3.3.2 SWCC and HCF of Permeable Reactive Media

The previous section demonstrated that the inclusion of β in the optimization resulted in the best fit to the MSO data, thus this formulation of the SWCC and HCF was adopted for comparing the results of the different soil types. The estimated soil water characteristic curves for the three different materials are shown in Figure 3.9 both in terms

of volumetric moisture content and effective saturation. The saturated moisture content and residual moisture contents for the two sands were nearly identical and significantly lower than the zeolite. This results in an offset in the zeolite SWCC when expressed in terms of volumetric moisture content; however, the SWCC's for the three materials were very similar when expressed in terms of effective saturation.

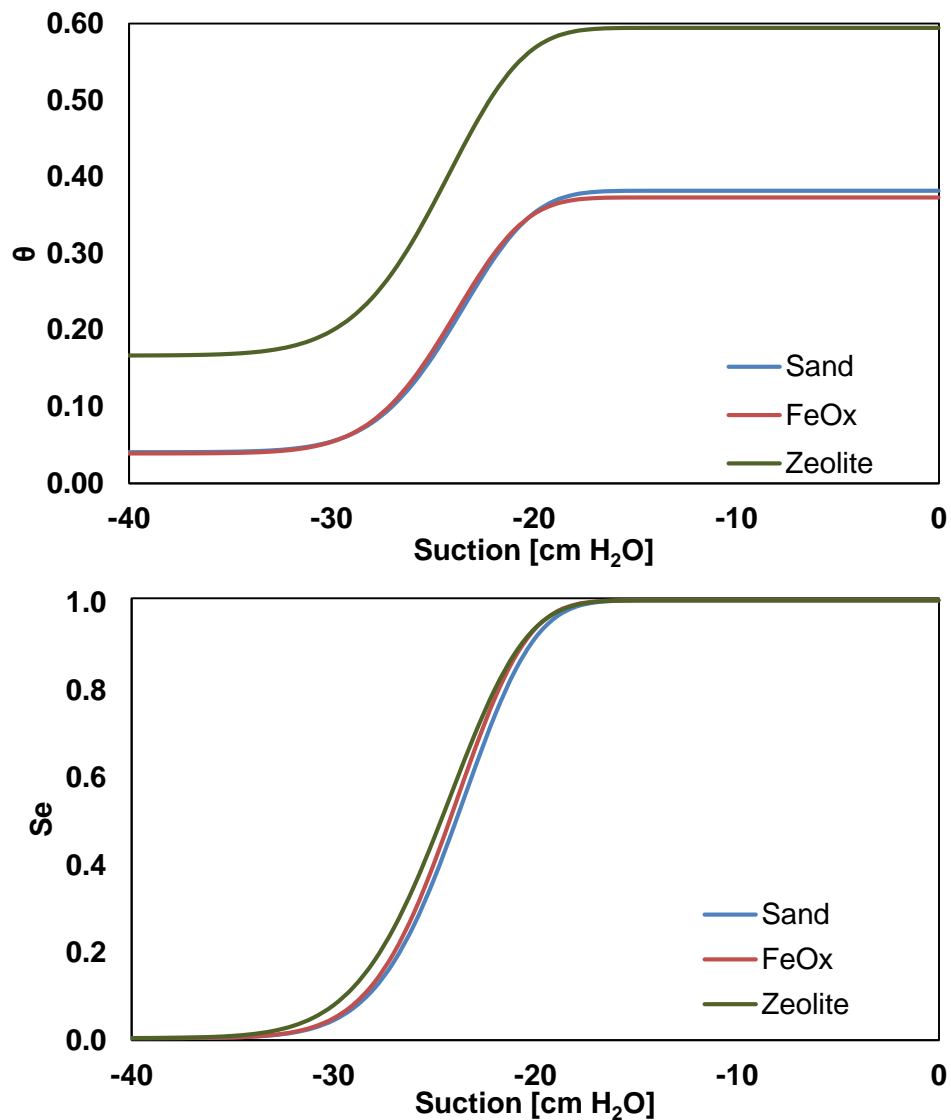


Figure 3.9: SWCC for sand, iron oxide coated sand, and zeolite expressed in terms of volumetric moisture content (top) and effective saturation (bottom). Note SWCC is calculated from the average estimated parameters from the optimization that included β .

The air entry value corresponded to approximately -17 cm of H₂O for all materials. Both sand SWCCs exhibited a very similar steep decrease in moisture content with increases in suction above the air entry value and are nearly indistinguishable at higher suctions where soil water is tightly bound to the surface of the soil. The parameter h_m , which is directly related to the geometric mean pore radius, was -23.90, -24.22, and -24.65 cm H₂O for silica sand, iron oxide coated sand and zeolite respectively. The slightly higher value for iron oxide coated sand may be due to the iron oxide coating constricting pores, or it may simply be the result of a slightly denser sample, as measured by the lower saturated porosity. The higher suction associated with the mean pore size in the zeolite may reflect broader pore size distribution. The parameter σ is the standard deviation of the log-transformed pore radius distribution, and was 0.130, 0.126, and 0.137 for the silica sand, iron oxide coated sand and zeolite respectively. The higher value estimated for zeolite is directly related to the higher saturated porosity of the zeolite, and likely reflects the greater limiting void ratios.

The transition from capillary water to water tightly bound to the surface was estimated to occur at an effective saturation of 0.1. This corresponded to a suction of -28 cm of H₂O for the two sands and -30 cm of H₂O for the zeolite. The residual moisture contents estimated for the two sands were similar to values previously reported (Hwang and Powers 2003). The estimated residual moisture content of the zeolite was significantly higher, similar to previous observations (Githinji et al. 2010). Despite having a higher residual moisture content than the two sands, the absolute volume of extracted from the zeolite was greater. The high residual moisture content suggests that a large fraction of the water retained in the zeolite is tightly bound to the soil surface and is possibly trapped in mesopores (Korkuna et al. 2006; Kowalczyk et al. 2006; Mockovčiaková et al. 2007). It is unclear how readily this water can be extracted from the zeolite by changes in suction. The SWCC estimated for the materials is only valid in the range of the MSO experiment

which is -43 cm of H₂O (Vrugt et al. 2003). This is in part why the estimated residual moisture content is equal to the moisture content measured at the termination of the experiment for the two sands (Table 3.4). The estimated residual moisture content was slightly lower than the moisture content measured at the termination of the zeolite experiment. Significantly greater suctions than the ones applied in this study are likely necessary to extract additional water from the zeolite (Githinji et al. 2010).

The unsaturated hydraulic conductivity function for the three media is shown in Figure 3.10. As was observed with the SWCC, the HCF for the zeolite is offset from the two sands due to the higher saturated and residual moisture content. All HCFs exhibited a sharp decrease in hydraulic conductivity at moisture contents below saturation, with the unsaturated hydraulic conductivity approximately half the saturated hydraulic conductivity at an effective saturation of 0.8, and one tenth the saturated hydraulic conductivity at an effective saturation of 0.5. The decrease in hydraulic conductivity with respect to volumetric moisture content was slightly steeper for iron oxide coated sand than in clean sand. This may be due to the greater density of the iron oxide coated sand flow cell as measured by the lower saturated volumetric moisture content at the start of the experiment. The decrease in hydraulic conductivity was steepest in the zeolite, possibly due to greater drag associated with the high specific surface area of the zeolite.

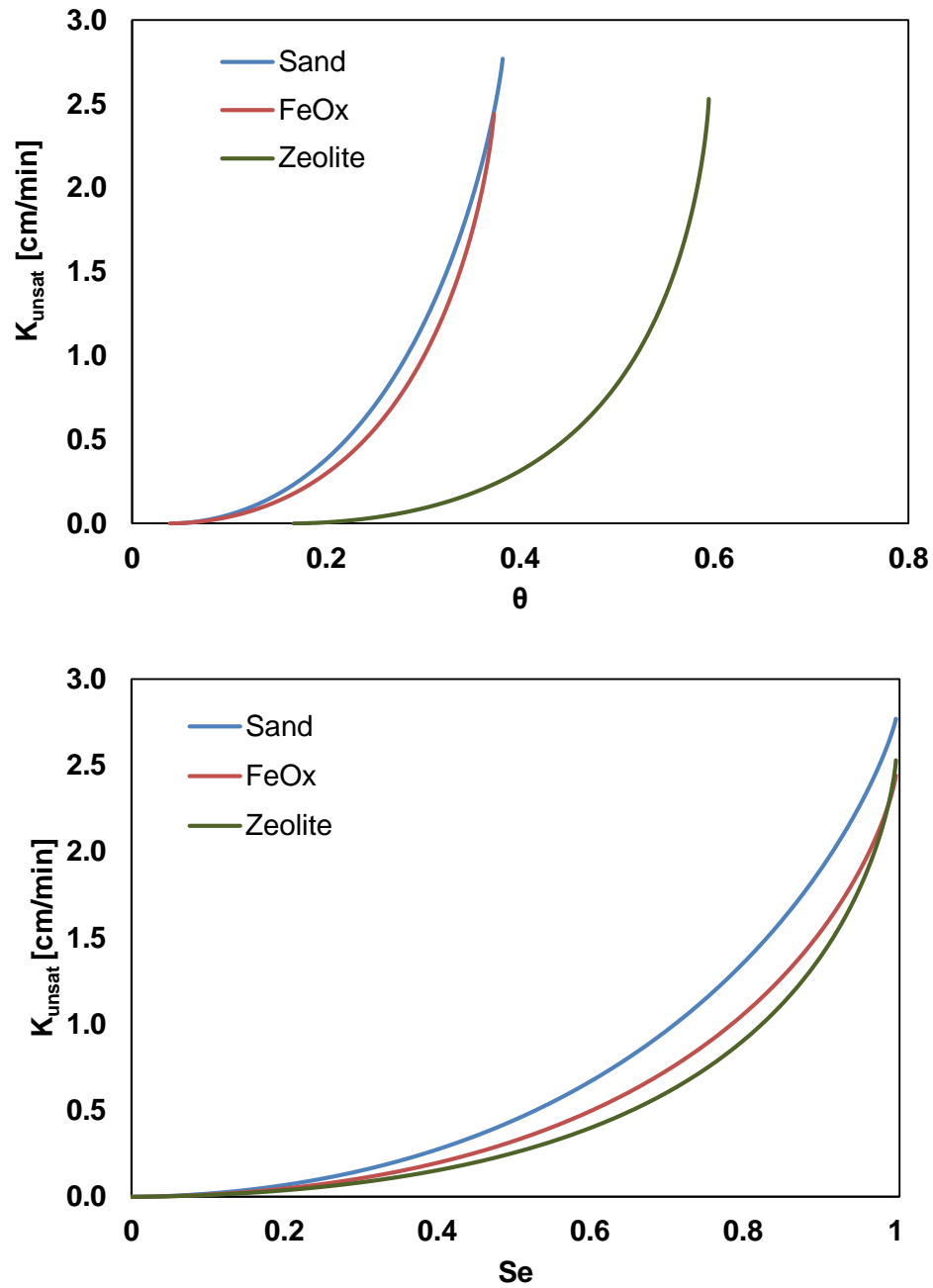


Figure 3.10: HCF for sand, iron oxide coated sand, and zeolite expressed in terms of volumetric moisture content (top) and effective saturation (bottom). Note HCF is calculated from the average estimated parameters from the optimization that included β .

3.4 CONCLUSIONS

The measured index properties of the clean and iron oxide coated sand were very similar; however, characterizations of the surface of these two materials revealed significant differences that are likely to affect the transport and retention of colloids. SEM micrographs of the silica sand showed the grains to be smooth, while the iron oxide coated sand surface was found to be heterogeneous and contain nodules of hematite that add nanoscale roughness to the soil surface which may enhance the retention of colloids. Electrokinetic measurements of the hematite nanoparticles demonstrate that the rough patches of iron oxide coating are positively charged for pHs below 6.3. Thus, it is expected that colloid transport through iron oxide coated sand will be sensitive to pH, and may be significantly retarded under pH conditions where the colloid and iron oxide coating are oppositely charged.

The measured limiting void ratios for the zeolite were significantly higher than for either of the two sands. This is in part due to the highly angular zeolite particles which were derived from a crushed tuff. SEM micrographs of the zeolite revealed a heterogeneous soil surface characterized by large patches of crystalline cuboid structures which contribute significantly to micro and nanoscale surface roughness and will likely affect the retention of colloids. These crystalline patches contribute significantly to the specific surface area of the zeolite, which was calculated to be 11 m²/g.

Multistep outflow data for the three soils were well described by Kosugi's (1994) soil water characteristic curve and hydraulic characteristic function. The HCF parameter β was determined to be unique and identifiable from MSO data, and its inclusion in the optimization of the SWCC and HCF improved the fit between the simulated and observed data. The SWCC and HCF was similar for the three soil types in the range of applied boundary suctions in MSO experiment. This is as expected as the unsaturated properties

of coarse grained soils are largely controlled by the grain size distribution (Cho and Santamarina 2001; Jaafar and Likos 2014).

CHAPTER 4:
THE TRANSPORT AND RETENTION OF COLLOIDS IN SATURATED PERMEABLE
REACTIVE MEDIA: THE ROLE OF PH AND IONIC STRENGTH

4.1 INTRODUCTION

Reactive porous media is a common component in many water treatment systems due to its ability to enhance treatment of a wide variety of contaminants found in stormwater runoff, acid mine drainage, landfill leachate, and wastewater (Chang et al. 2010; Genç-Fuhrman et al. 2007; Johansson Westholm 2006; Kietlińska and Renman 2005; Wantanaphong et al. 2005). Permeable reactive materials are able to remove dissolved inorganic and organic pollutants through ion exchange and/or sorption on the media surface (Genç-Fuhrman et al. 2008; Jaradat et al. 2009; Srinivasan et al. 2008). A material that has been commonly used in permeable reactive barriers are zeolites, which are naturally occurring aluminosilicates made up of a repeating three-dimensional framework of $[\text{SiO}_4]^{-4}$ and $[\text{AlO}_4]^{-5}$ polyhedra (Färm 2002; Knox et al. 2008). The zeolitic framework contains channels and cavities that are filled with water molecules and highly mobile cations that satisfy electroneutrality on a negatively charged structure (Dyer 1988). Natural zeolites such as clinoptilolite are very common and readily available (Gottardi and Galli 1985) and are seen by many as an effective and inexpensive alternative to other sorbents when used to remove various heavy metals, radionuclides, and ammonium from water through ion exchange and surface complexation (Bailey et al. 1999; Park et al. 2002; Srinivasan et al. 2008).

To date, very little research exists on the transport of colloids through natural zeolites. Gamerdinger and Kaplan (2001b) investigated the transport of colloids through saturated clean sand and zeolitic tuff at various ionic strengths. Colloids were retained in

greater numbers in zeolites, and furthermore, colloid retention in zeolites was more sensitive to increasing ionic strength than in clean sand. The reduced mobility of colloids in zeolite versus clean sand was attributed increased roughness and larger specific surface area of the zeolite (Gamerding and Kaplan 2001a). The coupled effects of pH and ionic strength colloid retention in zeolite have not been examined, though the relatively low isoelectric point of zeolites ($pH_{IEP} = 2-3$ (Ersoy and Çelik 2002)) suggests that colloid attachment will likely be unfavorable, with colloid retention occurring in the secondary minimum, at most environmentally relevant pHs.

Another common material in many permeable reactive barriers are iron oxides in various forms, including iron oxide coated sand (Benjamin et al. 1996). Iron oxides coated media have been used to treat a wide variety of contaminants including nitrogen and phosphates (Erickson et al. 2006; Kietlińska and Renman 2005), heavy metals (Benjamin et al. 1996; Genç-Fuhrman et al. 2008; Sansalone 1999), organic contaminants (Henderson and Demond 2007), and bacteria (Ahammed and Davra 2011; Mohanty et al. 2013; Park et al. 2012; L. Zhang et al. 2010). The transport of colloids through iron oxide coated sands has received much attention over the years, in large part as a means of understanding the role of geochemical heterogeneity in the transport of colloids through natural systems (Ryan and Gschwend 1992, 1994; Ryan et al. 1999).

Colloid retention in iron oxide coated media is very sensitive to pH, as the isoelectric point of most iron oxides is close to neutral pH (Parks 1965). The positive charge associated with the iron oxide coatings below the pH_{ZC} will result in conditions favorable to attachment of negatively charge colloids, with no energy barrier preventing colloid deposition, while at higher pHs colloid attachment will be unfavorable (Abudalo et al. 2005; Foppen et al. 2006). However, colloid retention at higher pHs is typically enhanced by the iron oxide coating due to the reduced energy barrier and deeper secondary minimum caused by the less electronegative iron oxide (Lin et al. 2011).

Similarly, the effect of increasing ionic strength on colloid deposition is more pronounced in iron oxide coated media in both favorable and unfavorable conditions and can increase the maximum colloidal coverage of iron oxide coated media (Bolster et al. 2001; Johnson et al. 1996).

The current study examines the mobility of carboxylate polystyrene latex microsphere in soil types that have traditionally been used in permeable reactive barrier systems to treat dissolved contaminants, including iron oxide coated sand and zeolite. Colloid mobility in iron oxide coated sand and natural zeolite were compared to clean silica sand under a wide range of pore water chemistries to assess colloid transport in these materials under a wide range of pore water chemistries. The impact of ionic strength and pH on the transport and retention of colloids in these permeable reactive soils was investigated using theoretical DLVO calculations and by conducting saturated column transport experiments. Colloid retention mechanisms are elucidated in the various soils by examining colloid mobility under varying solution chemistry.

4.2 MATERIALS AND METHODS

4.2.1 Theoretical Considerations

4.2.1.1 DLVO Interaction Potential Energy

The calculation of interaction potential energies from DLVO theory, which simply states that the interaction energy between two surfaces is the sum of the electrical double layer and London-van der Waals interaction energies, has proven an extremely valuable tool in understanding and predicting colloidal phenomena in porous media (Adamczyk and Weroński 1999; Elimelech et al. 1995). Interaction potentials as a function of separation distance between the colloid and soil surface allow researchers to predict how colloids are attached to the soil surface, and under what chemical conditions this attachment is likely

to occur (Elimelech et al. 1995). Interaction potential energies between colloid and soil surfaces were calculated under the different ionic strengths and pHs relevant to this study to understand colloid retention mechanisms.

The interaction potential energy due to the electrostatic double layer, Φ_{EDL} , between a sphere (colloid) and infinite plate (soil surface) with constant surface potential was calculated using the expression (Hogg et al. 1966):

$$\Phi_{EDL}(h) = \frac{\pi\epsilon_0\epsilon_r r_c}{2} (\psi_s^2 + \psi_p^2) \left(2\psi_s\psi_p \ln\left(\frac{1 + \exp(-\kappa h)}{1 - \exp(-\kappa h)}\right) + (\psi_s^2 + \psi_p^2) \ln(1 - \exp(-2\kappa h)) \right)$$

where h is the separation distance between colloid and surface, ϵ_0 is the vacuum permittivity ($8.85 \times 10^{-12} \text{ C}^2 \text{ N}^{-1} \text{ m}^{-2}$), and ϵ_r is the dimensionless dielectric constant of the medium (80 for water). ψ_s and ψ_p are the surface potentials of the colloid and soil surface, and were taken to be equal to the measured zeta potentials for the colloid and sand (Elimelech et al. 1995). The Debye-Hückel parameter, κ , is related to the double layer thickness and was calculated using the expression:

$$\kappa = \left(\frac{1000e^2 N_A I_s}{\epsilon_0 \epsilon_r k_b T} \right)^{0.5}$$

where e is the charge of an electron ($1.60 \times 10^{-19} \text{ C}$), N_A is Avogadro's number ($6.02 \times 10^{23} \text{ molecules mole}^{-1}$), I_s is the ionic strength of the aqueous phase [mol L^{-1}], k_b is Boltzmann's constant ($1.38 \times 10^{-23} \text{ J K}^{-1}$), and T is the absolute temperature [K].

The interaction energy due to retarded van der Waals forces, Φ_{VDW} , between a sphere and infinite plate was calculated after Gregory (1981):

$$\Phi_{VDW}(h) = -\frac{A_H r_c}{6h} \left(\frac{1}{1 + \frac{14h}{\lambda}} \right)$$

where A_H is the Hamaker constant, and λ is the characteristic wavelength and is typically assumed to be 100 nm. The Hamaker constant for polystyrene and quartz separated by water is $4.04 \times 10^{-21} \text{ J}$ and was assumed to be the same for the zeolite. The Hamaker

constant for polystyrene and iron oxide separated by water is 7.16×10^{-21} J (Israelachvili 2011). Due to the patchy nature of the iron oxide coating, only interaction between colloids and raw hematite was considered for iron oxide coated sand.

4.2.1.2 Transport Modeling

Colloid breakthrough curves were modeled using the 1-D advection dispersion equation (ADE) with one kinetic retention site to assess the retention of colloidal microspheres in saturated media. The mass balance for colloids passing through porous media with one retention sites is given as:

$$\frac{\partial \theta C}{\partial t} + \rho \frac{\partial S}{\partial t} = \frac{\partial}{\partial x} \left(\theta D_L \frac{\partial C}{\partial x} \right) - \frac{\partial qC}{\partial x} \quad (4.1)$$

where C is the colloid concentration in the aqueous phase, θ is volumetric moisture content, D is the hydrodynamic dispersion coefficient in the direction of flow, q is the Darcy flux in the direction of flow, ρ is the bulk density of the sand, S is the concentration of colloids immobilized in the soil column, x is the spatial coordinate in the direction parallel to flow, and t is time.

The single kinetic retention site was used to describe the mass transfer of colloids in both saturated and unsaturated porous media. The retention of colloids in porous media was described as an irreversible process:

$$\rho \frac{\partial S_1}{\partial t} = \theta \psi_s k_a C \quad (4.2)$$

where k_a is the rate coefficients for attachment and detachment respectively, and ψ_s is the dimensionless blocking function. The dimensionless concentration dependent blocking term takes the following form:

$$\psi_s = \left(1 - \frac{S}{S_{max}} \right) \quad (4.3)$$

where S_{max} is the retention capacity of immobilized colloids per unit mass of soil. The above blocking function has been used in saturated porous media to represent the

occupation and blocking of finite sites retention by colloids (Adamczyk et al. 1994; El Badawy et al. 2013; Bolster et al. 2001).

Equations 4.1-4.3 were solved using HYDRUS-1D, a finite element code used for one dimensional transport processes in variably saturated soils (Simunek et al. 2013). HYDRUS 1-D includes a weighted non-linear parameter estimation routine based on the Marquardt-Levenberg least squares algorithm, which combines the Newton and steepest descent method. The dispersion coefficient and porosity were fit to the conservative tracer portion of the experiment, and were kept fixed for the estimation of colloid transport parameters. Colloid transport parameters were estimated by simultaneously fitting measured colloid breakthrough curves and retention profiles. The breakthrough and retention profile data were weighted by the standard deviation of the two data sets using internal calculations in the Hydrus 1-D optimization algorithm; however, individual data points were uniformly weighted to unity.

Two optimization scenarios were considered. In the first scenario no blocking was assumed, thus ψ_s was fixed to unity while k_a was estimated. In the second scenario blocking was considered by simultaneously fitting k_a and s_{max} . Three trial optimizations, each with differing initial estimates of parameter values, yielded the same optimized parameters, thus all reported parameters are considered unique (Eching et al. 1994). Only the best fit optimization scenario as assessed by R^2 are reported.

4.2.2 Experimental

4.2.2.1. Colloid and Porous Media Preparation

Manufactured carboxylated polystyrene microspheres (Bang Laboratories, Inc. Fishers, IN) 1 μm in diameter were used in all experiments. Residual surfactant from the colloid manufacturer was removed by triple rinsing the microspheres before suspending them in deionized water. Colloid electrophoretic mobilities were measured (Brookhaven

Instruments Corporation, ZetaPALS) at varying ionic strengths and pHs and were converted to zeta potentials using the Smoluchowski equation.

All soils were sieved beforehand to have the same median grain size ($d_{50} = 0.36$ mm) and coefficient of uniformity ($C_u = 1.82$). Silica sand (US Silica) was used as an unreactive media for comparison purposes, and underwent a rigorous cleaning procedure to minimize any geochemical heterogeneity present on the surface using a procedure similar to Elimelech et al. (2000). Sands were rinsed in deionized water, then ultrasonicated (Branson 8510 Ultrasonic Cleaner) for 30 minutes then rinsed again with deionized water over a #200 sieve for 1 hour. Surface impurities in the form of metal oxides were removed by soaking sands in 0.1 M sodium dithionite solution, followed by rinsing with deionized water for 1 hour over a #200 sieve. The sand was next soaked in a 3% hydrogen peroxide while being ultrasonicated for 3 hours to remove any organics on the sand surface followed by 1 hour of rinsing with deionized water over a #200 sieve. The last major step in the cleaning process involved soaking the sand in 8 M nitric acid overnight. Sands were then soaked in deionized water and ultrasonicated for an additional hour, then rinsed over a #200 sieve until the effluent conductivity equilibrated with the inlet conductivity and finally oven dried at 105°C. The electrophoretic mobility and zeta potential of milled sand was measured under the same chemical conditions as the colloids.

Iron oxide coated sands were prepared using the heterogeneous suspension method (Larrahondo et al. 2011; Scheidegger et al. 1993). Briefly, cleaned sands were added to a 40 mg/L suspension of hematite nanoparticles (approximately 90 nm in diameter) at a pH of 3 and an ionic strength of 10 mM NaNO_3 . The sand-iron slurry was agitated for several days and the pH was repeatedly adjusted to 3 using nitric acid. The iron oxide coated sands were then repeatedly rinsed over a #200 sieve to remove excess residual iron oxide nanoparticles. The iron content of the coated sand was measured by using optical emission spectroscopy (ICP-OES Optima 8000, Perkin Elmer) after removing

the iron oxide coating using the citrate-dithionite-buffer method (Mehra 1958) and found to be $1.4 \text{ mg}_{\text{Fe}}/\text{g}_{\text{sand}}$. The electrophoretic mobility of the hematite coating before attachment to the soil was measured under the same chemical conditions of the colloids. Scanning electron microscopy (LEO 1530 SEM) revealed the iron oxide coating was patchy in nature, with more iron oxide nanoparticles occurring near rough portions of the sand surface. In addition to occurring in large patches, the discrete nature of the iron oxide nanoparticles used to coat the surface contribute to the nanoscale roughness of iron oxide coated sands.

Crushed natural zeolitic tuff (St. Cloud Zeolite, MN) was sieved to obtain a similar grain size distribution as the clean and iron oxide coated sand. The zeolite was confirmed to be composed primarily of clinoptilolite via X-ray powder diffraction (PANalytical X'Pert PRO MPD) while the specific surface area of the material was measured using nitrogen adsorption (BET-Micromeritics, ASAP 2020) and found to be $11 \text{ m}^2/\text{g}$. SEM micrographs revealed a high degree of physical heterogeneity on the surface of the zeolite, with large rough patches characterized by fractal crystal like structures. Additionally SEM micrographs confirmed the highly angular nature of the zeolite soil grains. Zeolites were ultrasonicated in deionized water for an hour, then repeatedly rinsed over a #200 sieve.

4.2.2.2 Column Transport Experiments

Transport experiments were conducted in an acrylic flow cell (L=10 cm, ID=5 cm) capped by stainless steel plates with 1 mm holes and supported by hydrophilic nylon mesh membranes with $10 \text{ }\mu\text{m}$ openings (U-CMN-10, Component Supply Company) on both ends. Saturated samples of soil were prepared using a modified form of slurry deposition (Bandini and Sathiskumar 2009; Carraro et al. 2003; Wood et al. 2008). A known mass of dry soil was introduced to a 55 cm long, 3.5 cm interior diameter acrylic cylinder partially filled with deaired and deionized water and capped on the bottom with a rubber stopper.

The remaining headspace was eliminated by filling the remaining volume with deionized deaired water, and the top capped by a rubber stopper. The soil slurry was mixed for several minutes by repeatedly inverting the cylinder, then vacuum (19 in Hg) was applied for approximately 8-12 hours. After removal of the vacuum, the specimen was repeatedly inverted for 1 minute to obtain a uniform mixture. The rubber end stopper was then removed and replaced with an easily removable nylon membrane. Prior to introducing the sand to the flow cell, the flow cell was filled with deionized water. The cylinder used to saturate the sand was slowly inverted and then lowered to the bottom of the flow cell while carefully removing the end membrane. The end rubber stopper was carefully removed allowing the soil slurry to enter and fill the flow cell while the sides of the flow cell were tapped to densify the sample to a porosity of 0.37-0.38 for clean and iron oxide coated sand, and 0.58-0.60 for zeolite.

The transport experiments were carried out at pH 4, 5.5, 7, and 10 with ionic strength adjusted to 1 mM using NaCl. The pH of the pore fluid was lowered to pH 4 and 5.5 using HCl. 0.16 mM NaHCO_3 was used for pH 7 experiments, and 0.2 mM Na_2CO_3 was used for pH 10 experiments. Experiments investigating the role of ionic strength at pH 5.5 were conducted by adjusting the ionic strength to 1, 2, and 5 mM using NaCl, while at pH 10 was adjusted to 1, 10, and 20 mM using NaCl. The aqueous phase was pumped (Cole Parmer Masterflex L/S) downward through the column at a Darcy velocity of 0.24 cm/min. Columns were pre-equilibrated by first passing 5 solutions of background solution. A 0.1 mM NaNO_3 conservative tracer was passed through the column to measure dispersion, followed by an additional 10 pore volumes of background solution. Three pore volumes of colloids at a concentration of 30 mg/L (5.6×10^7 particles/L) were passed through the column followed by an additional two pore volumes of colloid free background electrolyte solution to assess any colloid re-entrainment. Effluent samples were collected using a fraction collector (ISCO Retriever II) and tracer and colloid

concentrations were measured by UV-Vis spectrophotometry (Shimadzu UV/1800) at wavelengths of 204 nm and 435 nm respectively.

At the end of each experiment, the column was carefully dissected to measure the spatial distribution of colloid concentrations as a function of soil depth. Soil from each column was extruded into 1 cm sections and then placed in 60 mL of 0.2 mM Na_2CO_3 , and gently agitated for five minutes. The supernatant colloid concentrations were measured with UV/Vis spectrophotometry and used to construct the concentration profiles.

4.3 RESULTS AND DISCUSSION

Transport experiments were carried under various pHs and ionic strengths. Conservative NO_3 tracer breakthrough curves were measured prior to injecting colloids. In all experiments the tracer was conservative and tracer breakthrough curves were well described by the advection diffusion equation. Measured dispersion coefficients had no dependency on ionic strength or pH and breakthrough curves did not indicate the presence of immobile regions in the soil pore space (Cherrey et al. 2003). Clean and iron oxide coated sands had similar levels of dispersion and Peclet numbers (Table 4.1). This is expected, given that all sand experiments were conducted at the same porosity and pore water velocity (Compère et al. 2001). Additionally, the iron-oxide coating did not cause any observable retardation of the tracer at pH below the isoelectric point ($\text{pH}_{\text{IEP}} \sim 6$) of the iron oxide coating. Tracer breakthrough curves were similarly shaped for the zeolite, but estimated dispersion coefficients were consistently higher than those measured in sand. This is likely a function of the higher porosity and lower velocities in zeolite experiments allowing for additional mechanical dispersion to take place (Ewing et al. 2010). However, lower average porewater velocities in zeolite yielded lower Peclet numbers than were observed in either of the clean sands which agrees with previous

observations made in zeolitic tuff (Gamerdinger and Kaplan 2001b). The large Peclet numbers observed in the three soil types suggests that advection is likely more important than dispersion in describing the mass transfer of colloids to the soil surface.

Table 4.1: Experimental conditions and mass balance information

Porous Media	pH	IS [mM]	θ	q [cm/min]	D [cm]	Pe	M_{Eff}	M_{Soil}	M_{Total}
Sand	4	1	0.378	0.241	0.164	39	0.363	0.484	0.847
Sand	5.5	1	0.367	0.240	0.147	44	0.945	0.043	0.988
Sand	5.5	2	0.379	0.240	0.140	45	0.836	0.126	0.962
Sand	5.5	5	0.375	0.239	0.136	47	0.168	0.796	0.964
Sand	7	1	0.373	0.240	0.139	46	0.994	0.012	1.006
Sand	10	1	0.373	0.241	0.188	34	0.995	0.003	0.998
Sand	10	10	0.371	0.239	0.152	42	0.801	0.150	0.951
Sand	10	20	0.377	0.240	0.203	31	0.432	0.478	0.909
FeOx	4	1	0.373	0.242	0.176	37	0.035	0.655	0.690
FeOx	5.5	1	0.375	0.241	0.132	49	0.753	0.198	0.951
FeOx	5.5	2	0.377	0.241	0.138	46	0.145	0.640	0.785
FeOx	5.5	5	0.378	0.239	0.155	41	0.039	0.735	0.774
FeOx	7	1	0.377	0.240	0.151	42	0.977	0.027	1.004
FeOx	10	1	0.370	0.242	0.201	33	0.988	0.023	1.011
FeOx	10	10	0.372	0.241	0.152	43	0.661	0.284	0.946
FeOx	10	20	0.376	0.239	0.148	43	0.331	0.593	0.924
Zeolite	4	1	0.594	0.240	0.283	14	0.368	0.465	0.833
Zeolite	5.5	1	0.595	0.241	0.306	13	0.757	0.212	0.968
Zeolite	5.5	2	0.602	0.243	0.313	13	0.387	0.475	0.862
Zeolite	5.5	5	0.588	0.239	0.279	15	0.100	0.741	0.841
Zeolite	7	1	0.597	0.238	0.270	15	0.802	0.168	0.970
Zeolite	10	1	0.582	0.241	0.271	15	0.814	0.171	0.986
Zeolite	10	10	0.594	0.241	0.322	13	0.201	0.709	0.910
Zeolite	10	20	0.598	0.241	0.247	16	0.145	0.786	0.931

NOTE: θ is the porosity, q is the Darcy velocity, D is the dispersion coefficient, and Pe is the Peclet coefficient. All masses, M, are fraction of the total injected mass of colloids. M_{Eff} refers to mass eluted as measured by the effluent curve, M_{Soil} refers to mass of colloids attached to soil, and M_{Total} refers to total mass balance.

4.3.1 Effect of pH

Colloid transport experiments were carried out at a constant ionic strength of 1 mM to investigate the effect of pH on retention in permeable reactive media. Normalized concentration of colloids measured at the outlet of the flow cell are shown in the dimensionless breakthrough curves in Figure 4.1 for clean sand at various pHs. Effluent concentrations increased rapidly to a constant concentration, then decreased back to zero in a symmetrical fashion with no reentrainment of colloids observed. Identically shaped colloid breakthrough curves were observed for iron oxide coated sands as shown in Figure 4.2. Minimal colloid retention in clean sand was observed (<1%) at pH 10 and 7 and peak effluent concentrations were similar, while a small increase in retention (from 1% to 2%) was observed in iron oxide coated sands. A sharp increase in colloid retention in iron oxide coated sand was observed at pHs less than 7, with peak effluent concentrations decreasing. 25% of colloids were retained at a pH of 5.5 and 97% were retained at a pH of 4 in iron oxide coated sand. Although some colloids were retained in clean sand at a pH of 5.5, decreasing the pH to 4 resulted in an increase in retention from 6% to 64%.

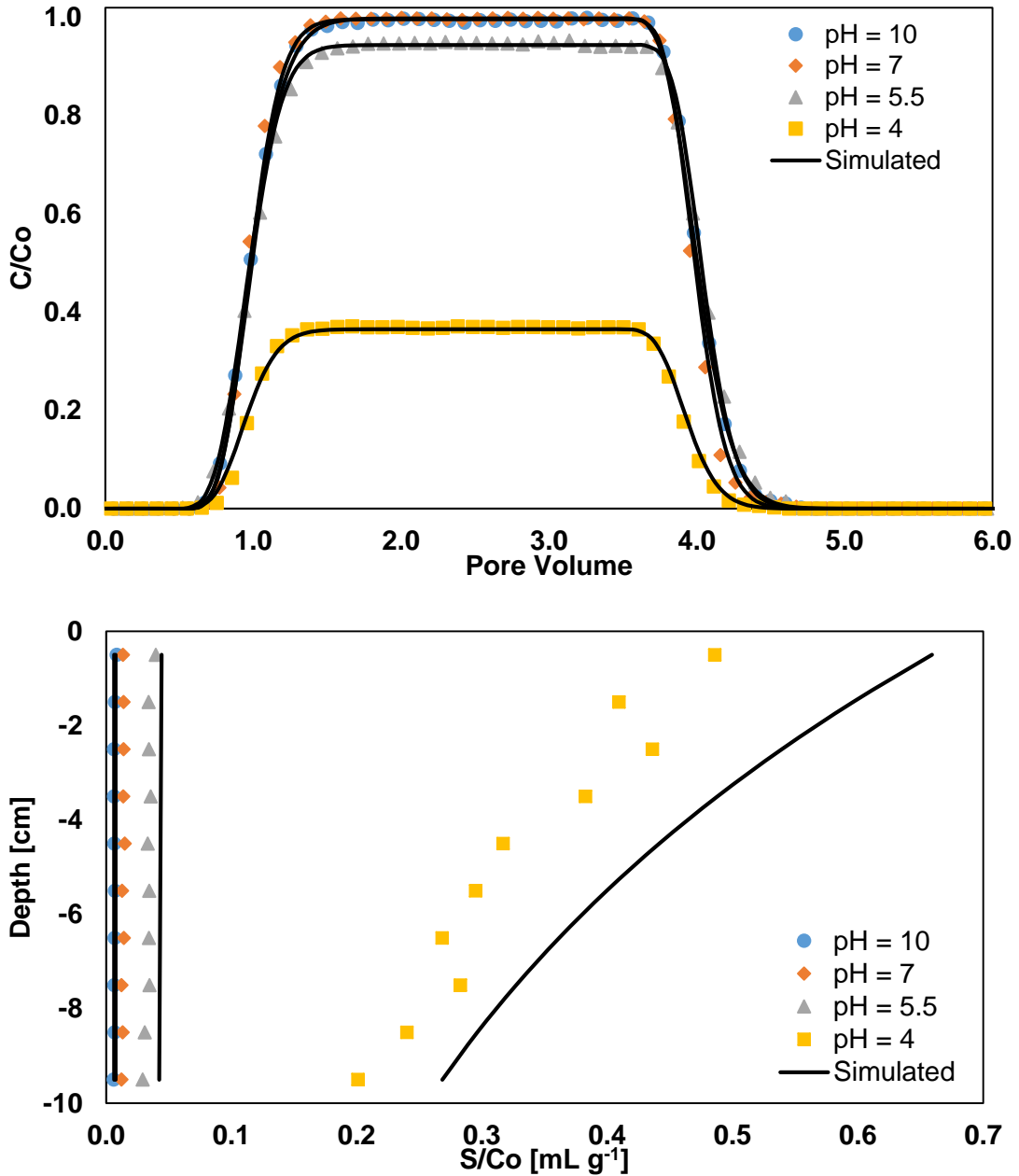


Figure 4.1: Colloid transport results for clean sand at various pHs and constant ionic strength of 1 mM. Top: measured and simulated normalized effluent concentration breakthrough curves for colloids. Effluent concentration is normalized by influent concentration C_0 . Bottom: measured and simulated normalized soil surface concentrations as a function of depth (distance from outlet). Surface concentration, S , refers to the mass of colloids retained per mass of soil. Simulated curves are shown as solid lines.

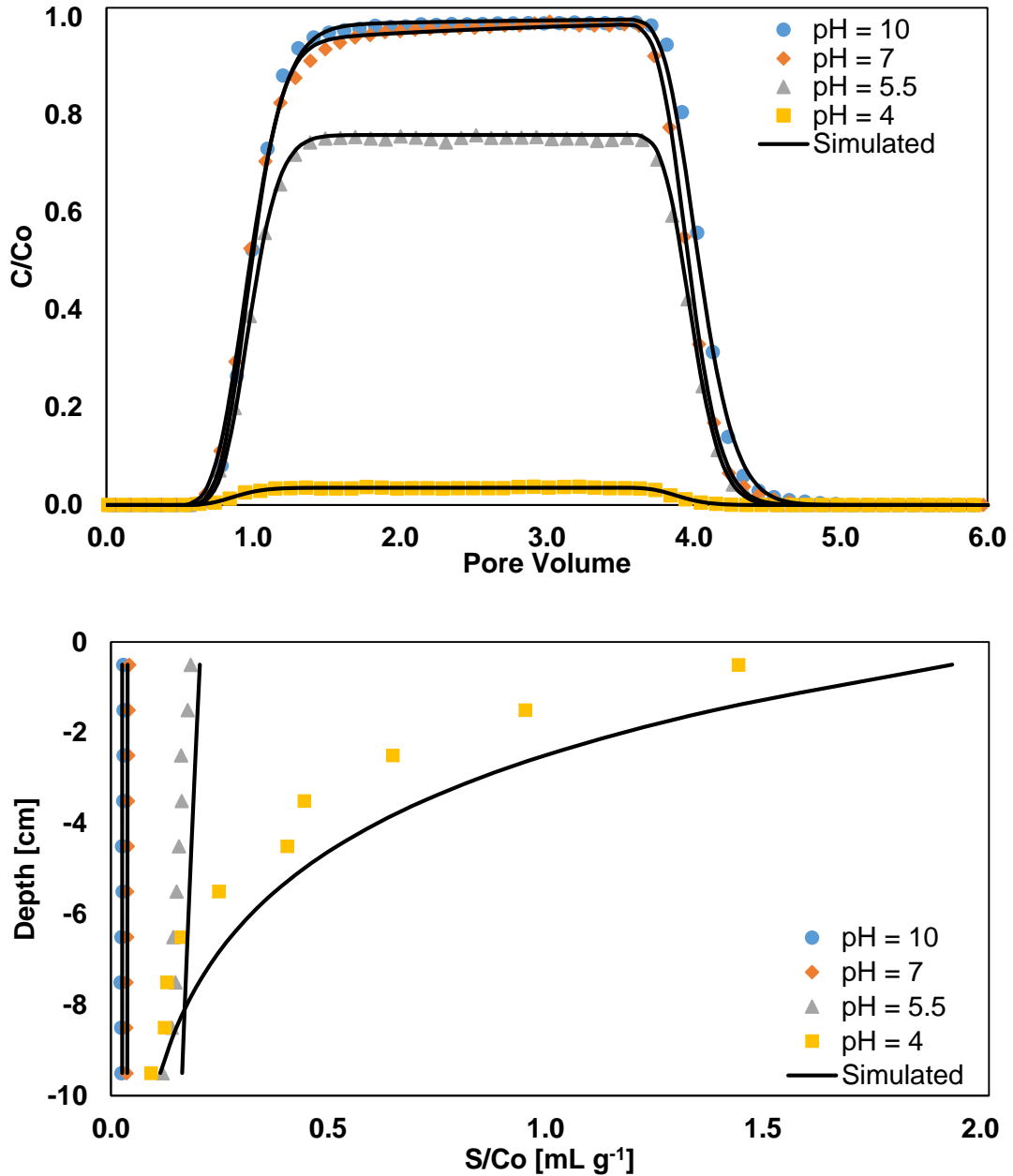


Figure 4.2: Colloid transport results for iron oxide coated sand at various pHs and constant ionic strength of 1 mM. Top: measured and simulated normalized effluent concentration breakthrough curves for colloids. Bottom: measured and simulated normalized soil surface concentrations as a function of depth.

Colloid breakthrough curves in zeolites differed in shape from clean and iron oxide coated sand breakthrough curves at all pHs as shown in Figure 4.3. Colloid effluent concentrations increased gradually, almost linearly, with time and lacked the symmetry in shape that was observed in breakthrough curves in clean and coated sands. In saturated porous media, breakthrough curves similarly shaped to the observed zeolite behavior have been associated with retained colloids blocking preferential retention sites on the soil surface, thus resulting in an overall decreasing attachment rate with time (Adamczyk et al. 1994; El Badawy et al. 2013; Bolster et al. 2001). As with clean and iron oxide coated sands, peak effluent concentrations decreased as pH decreased. Significant colloid retention in zeolite occurred at higher pHs, with approximately 20% of injected colloids retained at pH 7 and 10. As with clean sand, decreasing pH to 5.5 resulted in a small increase in colloid retention, while at pH 4 retention increased sharply from 24% to 63%.

The low levels in retention observed in clean and iron oxide coated sand at high pH values is supported by the DLVO calculations summarized in Table 4.2. At both pH 7 and 10, soil surface and colloids are oppositely charged, and thus are unfavorable to deposition. This is as expected as DLVO calculations predict a large barrier to deposition with no secondary minimum, and the ratio of the colloid to the mean soil grain size diameter (~ 0.003) is below the 0.005-0.008 ratio that has been typically associated with physical filtration or straining (Bradford et al. 2002, 2006; Sang et al. 2013; Xu and Saiers 2009). DLVO calculations predict a smaller barrier to deposition in the primary minimum and a shallow secondary minimum associated with the iron oxide coating at pH 7 and 10. However given the heterogeneous nature of the iron oxide coating observed in micrographs, only larger patches of iron oxide would likely serve as retention locations as uncoated portions of the sand are repulsive to colloids and impair retention (Bendersky and Davis 2011).

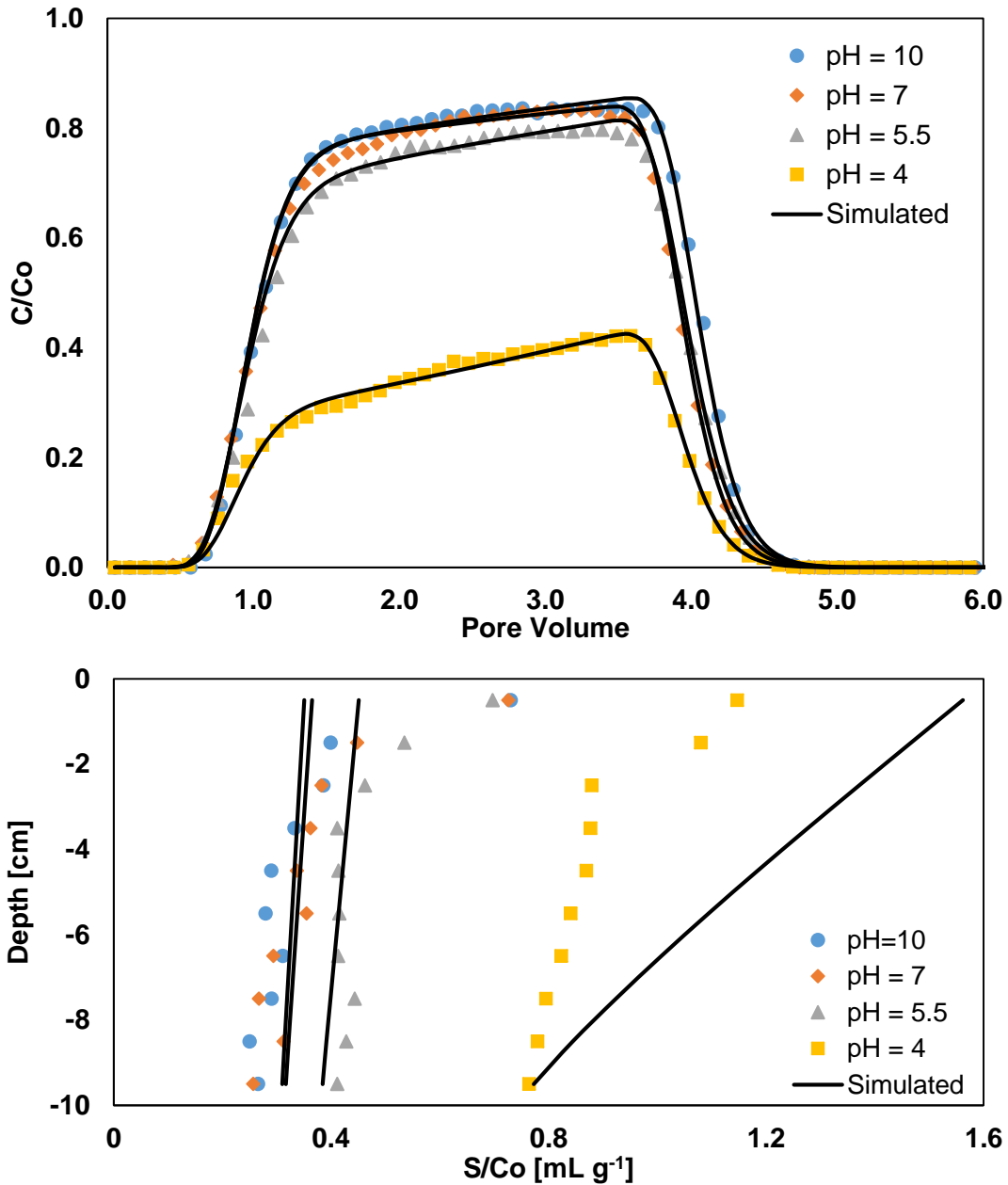


Figure 4.3: Colloid transport results for zeolite at various pHs and constant ionic strength of 1 mM. Top: measured and simulated normalized effluent concentration breakthrough curves for colloids. Bottom: measured and simulated normalized soil surface concentrations as a function of depth.

Table 4.2: DLVO Calculation Results

Porous Media	pH	IS [mM]	Zeta Potential, Colloid (mV)	Zeta Potential Soil (mV)	Energy Barrier Height (kT)	Secondary Minimum Depth (kT)
Sand	4	1	- 48	- 70	2026	-0.03
Sand	5.5	1	- 62	- 78	3150	-0.03
Sand	5.5	2	- 62	- 78	3120	-0.06
Sand	5.5	5	- 51	- 67	2073	-0.17
Sand	7	1	- 54	- 81	2640	-0.03
Sand	10	1	- 49	- 92	2330.1	-0.03
Sand	10	10	- 40	- 83	1513	-0.36
Sand	10	20	- 38	- 53	1060	-0.86
FeOx	4	1	- 48	64	none	none
FeOx	5.5	1	- 62	49	none	none
FeOx	5.5	2	- 62	49	none	none
FeOx	5.5	5	- 51	30	none	none
FeOx	7	1	- 54	- 35	1056	-0.06
FeOx	10	1	- 49	- 41	1243	-0.06
FeOx	10	10	- 40	- 31	586	-0.93
FeOx	10	20	- 38	- 26	376	-2.1
Zeolite	4	1	- 48	- 60	1850	-0.03
Zeolite	5.5	1	- 62	- 69	2878	-0.03
Zeolite	5.5	2	- 62	- 69	2836	-0.06
Zeolite	5.5	5	- 51	- 61	1930	-0.17
Zeolite	7	1	- 54	- 72	2586	-0.03
Zeolite	10	1	- 49	- 70	2114.5	-0.03
Zeolite	10	10	- 40	- 57	1270	-0.39
Zeolite	10	20	- 38	- 44	895	-0.9

An increase in colloid retention in all porous media was observed as pH dropped below 7, however the largest increase was observed in the iron oxide coated sand. This increase in retention with decreasing pH corresponds to dropping below the isoelectric point of the hematite coating, which was estimated to be approximately 6. At pHs below the isoelectric point of the hematite, the positively charged iron oxide coating acts as a favorable deposition site to the negatively charged colloids (Abudalo et al. 2005; Ryan and

Gschwend 1994). As pH decreased from 5.5 to 4 colloid retention in iron oxide coated sand increased from 25% to 97%. The positive zeta potential of the iron oxide coating increased at pH 4, resulting in colloid-soil attraction occurring at greater distances from the soil surface, and patchy iron oxide regions have a larger influence on colloid retention (Bendersky and Davis 2011). Observed colloid retention as a function of depth in iron oxide coated sand are shown in Figure 4.3 and matched the simulated log-linear retention profile at pH 5.5 and 4. Similar colloid retention profiles have been observed by others in iron oxide coated media (Han et al. 2014), and a log-linear decrease in retention with depth is indicative of favorable attachment of colloids in the primary minimum according to classical filtration theory (Elimelech et al. 1995; Tufenkji and Elimelech 2005).

The high levels of colloid retention observed in zeolite at pH 5.5, 7 and 10 cannot be readily explained by DLVO calculations, as demonstrated by the large barriers to deposition in the primary minimum and no secondary minimum present at all pHs in Table 4.2. As zeolite did not undergo a rigorous cleaning process to remove metal oxides or organic material from the surface, it is possible that the increased retention is due to the presence of geochemical heterogeneity. Several studies have highlighted the disproportionate effect that small levels of geochemical heterogeneity can have on colloid retention in porous media (Bradford and Kim 2012; Litton and Olson 1993; Shani et al. 2008). However, colloid retention in zeolite as function of pH exhibited similar behavior to clean sands in which geochemical heterogeneity was minimized as shown in Figure 4.4. This suggests that retention in zeolites cannot be explained entirely by geochemical heterogeneity.

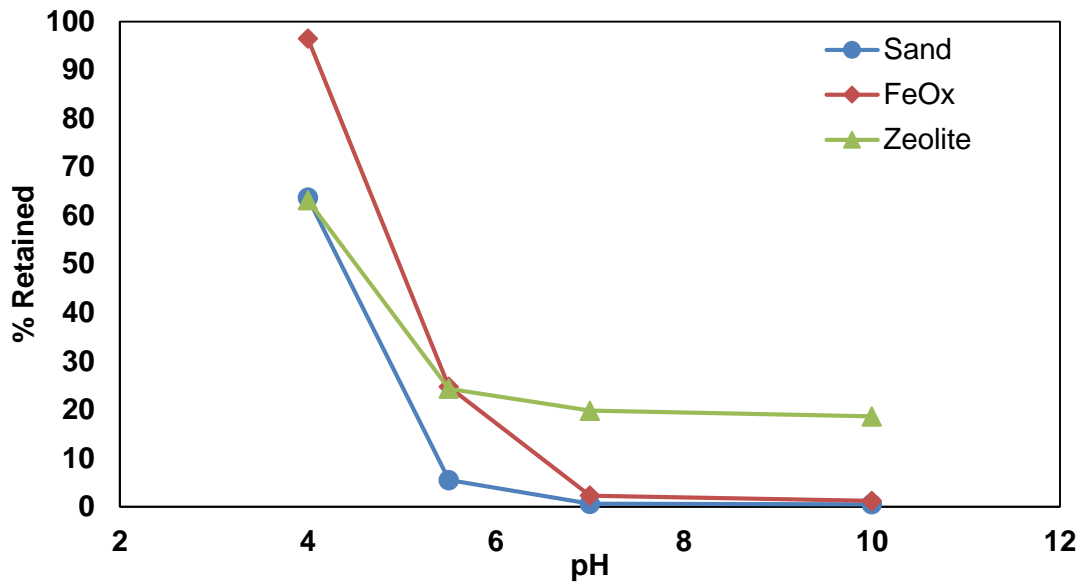


Figure 4.4: Mass of retained colloids as measured by integration of the breakthrough curve for all permeable reactive materials at varying pH.

Media roughness at various scales has been recognized as an important factor in colloid retention under conditions favorable to attachment (Tong and Johnson 2006). SEM micrographs of the zeolite revealed a high degree of microscale roughness present that likely served as retention sites for colloids under unfavorable conditions. The range of van der Waals forces increases at rough asperities, allowing colloids to be retained in the secondary minimum (Adamczyk and Weroński 1999). In addition to high levels of roughness observed on the surface, the angularity of the zeolites likely contributed to the retention of colloids. Grain angularity increases the number of contacts between soil grains and results in greater retention by straining at granular contact points (Barton and Buchberger 2007; Basha and Culligan 2010; Tong et al. 2008). Straining may explain the shape of the mass of retained colloids as a function of depth observed in zeolites shown in Figure 4.3. Whereas the mass of retained colloids in clean and iron oxide coated sands showed a linear or log-linear decrease with depth, zeolite retention profiles exhibited hyperexponential behavior, with increased retention in the top 1-2 cm of the soil profile.

Similarly shaped profiles have previously been attributed to colloid straining in sands and is associated with colloid retention at granular contacts (Bradford et al. 2003, 2006).

As pH decreased from 5.5 to 4, a large increase in colloid retention was observed for both clean sand and zeolite. In clean sands, colloid retention increased from 6% to 64%, and in zeolites retention increased from 24% to 63% despite DLVO calculations predicting a large barrier to deposition in the primary minimum and no secondary minimum for both materials. Numerous studies have cautioned against the use bulk measurements of soil zeta potentials in predicting colloid retention, as even small levels of geochemical heterogeneity will affect the retention of colloids (Elimelech et al. 2000). Although the increased retention in zeolites may be explained by the presence of positively charged metal oxides, the rigorous cleaning procedure minimized any metal oxides or organic material present on the sand surface. Another possibility is that colloid hydrophobic interactions may have played a greater role as pH decreased. During the course of the experiments colloids were constantly stirred using a magnetic stir-bar. However, at pH 4 colloid aggregation at the air-water interface was observed after stirring of the colloid suspension was stopped at the termination of experiments. According to the manufacturer, colloidal stability decreases at pHs lower than 6 (Bangs Laboratories 2013). Indeed, extensions to DLVO theory that include non-electrostatic interactions have demonstrated hydrophobicity can contribute significantly to colloidal interactions with surfaces (Bradford and Torkzaban 2008; Grasso et al. 2002).

4.3.2 Effect of Ionic Strength

The effect of increasing ionic strength on colloid retention in the reactive porous media was investigated at pH 5.5 and 10. At both pH 5.5 (Figures 4.5-7) and pH 10 (Figures 4.8-10) increasing ionic strength resulted lower peak effluent concentrations and greater colloid retention in all soil types. However, smaller ionic strength increases were

sufficient to increase colloid retention at pH 5.5 than at pH 10. Colloid immobilization in clean sand likely occurred in the secondary minimum at high and low pH, as indicated by DLVO calculations in Table 4.2. The secondary minimum depth increased as ionic strength increased, mirroring the observed increased retention in clean sands (Hahn and O'Melia 2004; Torkzaban et al. 2010). While overall mass retention of colloids as a function of ionic strength was similar in clean sand at high and low pH, minor differences in retention profile shapes were observed. At pH 10 colloid retention was relatively constant at all depths similar to retention profiles observed previously under unfavorable colloid attachment conditions (Liu et al. 2010). Interestingly, as ionic strength increased at pH 5.5, colloid retention profiles in clean sand resembled the log-linear shape associated with favorable retention conditions (Abudalo et al. 2005; Han et al. 2014). Although it is possible that colloids were able to cross the energy barrier and become immobilized in the primary minimum, this is a relatively slow process and would not entirely explain the shape of the retention profile (Hahn and O'Melia 2004; Tufenkji and Elimelech 2004a, 2005). Alternatively, increased hydrophobic interactions at pH 5.5 may have contributed the observed decrease in retention with depth in clean sand (Gargiulo et al. 2008).

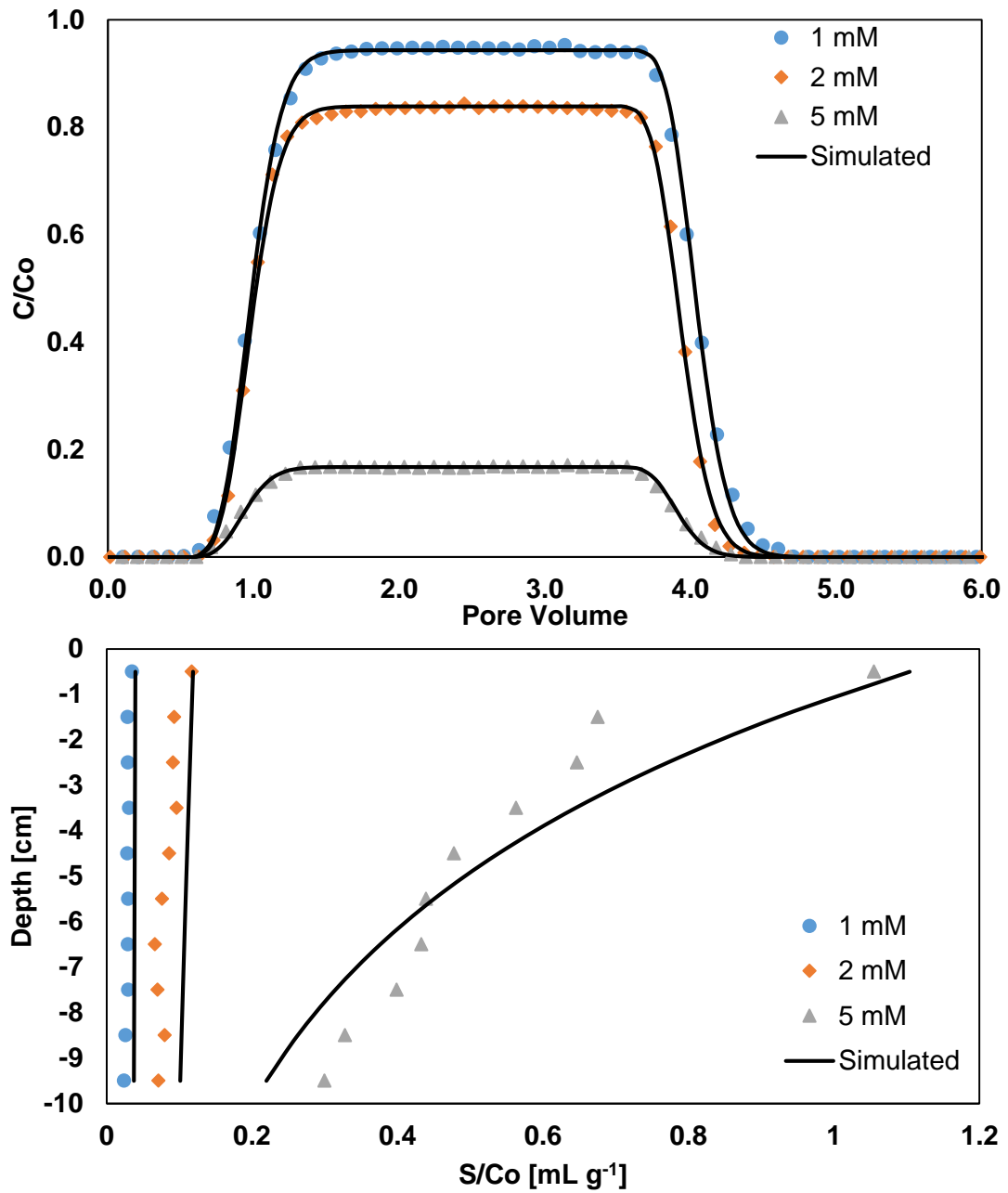


Figure 4.5: Colloid transport results for clean sand at various ionic strengths and a constant pH of 5.5. Top: measured and simulated normalized effluent concentration breakthrough curves for colloids. Bottom: measured and simulated normalized soil surface concentrations as a function of depth.

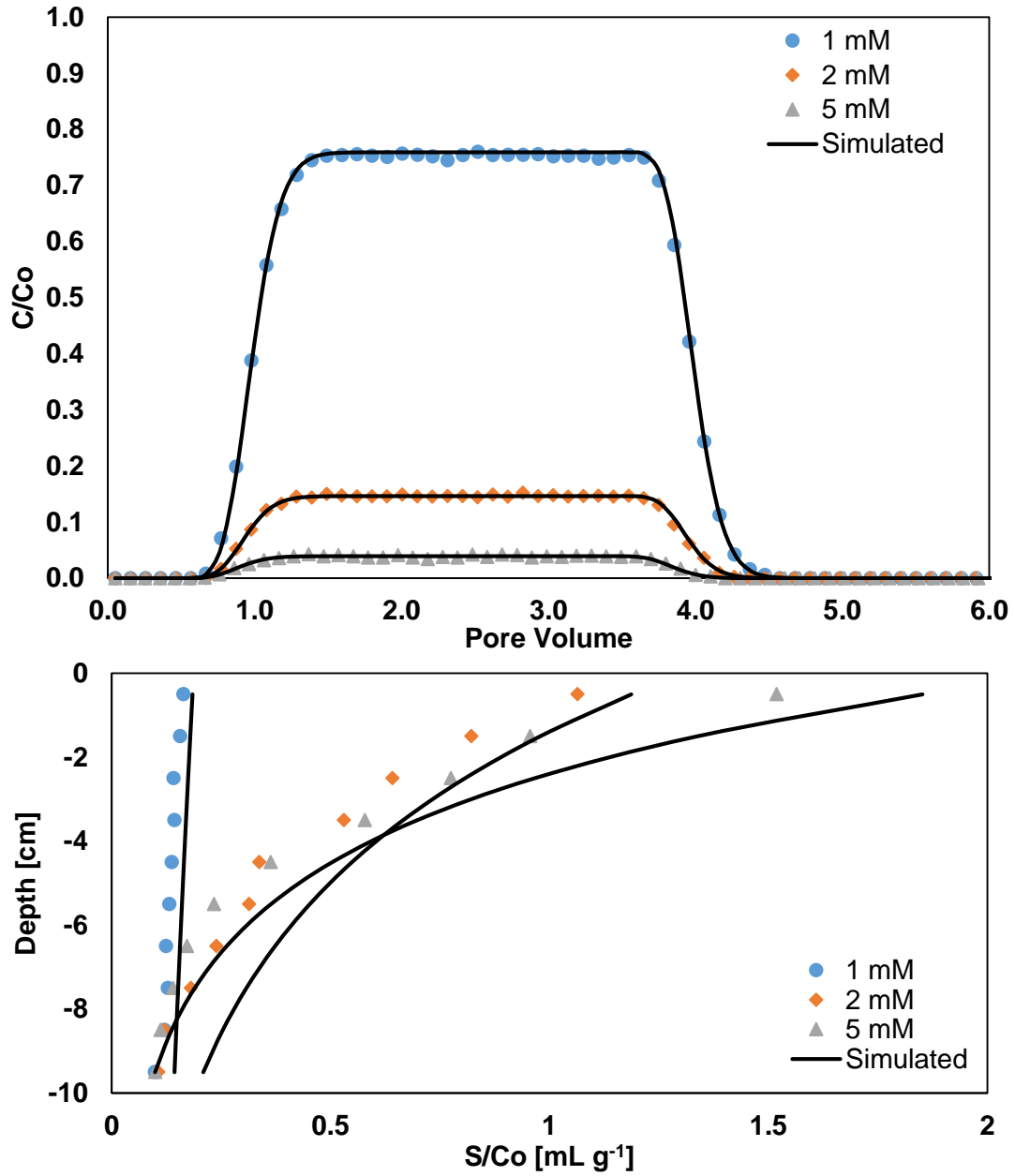


Figure 4.6: Colloid transport results for iron oxide coated sand at various ionic strengths and a constant pH of 5.5. Top: measured and simulated normalized effluent concentration breakthrough curves for colloids. Bottom: measured and simulated normalized soil surface concentrations as a function of depth.

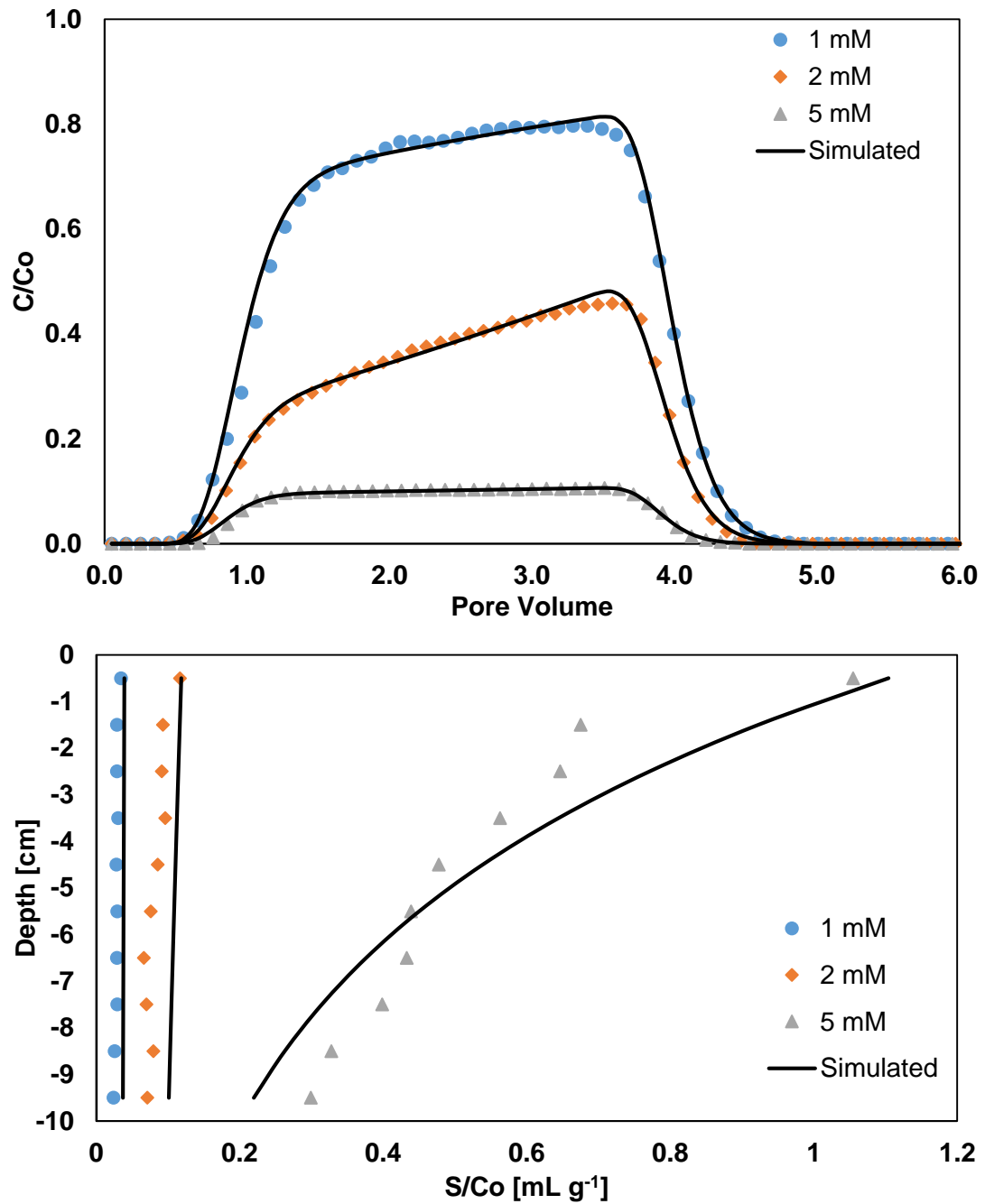


Figure 4.7: Colloid transport results for zeolite at various ionic strengths and a constant pH of 5.5. Top: measured and simulated normalized effluent concentration breakthrough curves for colloids. Bottom: measured and simulated normalized soil surface concentrations as a function of depth.

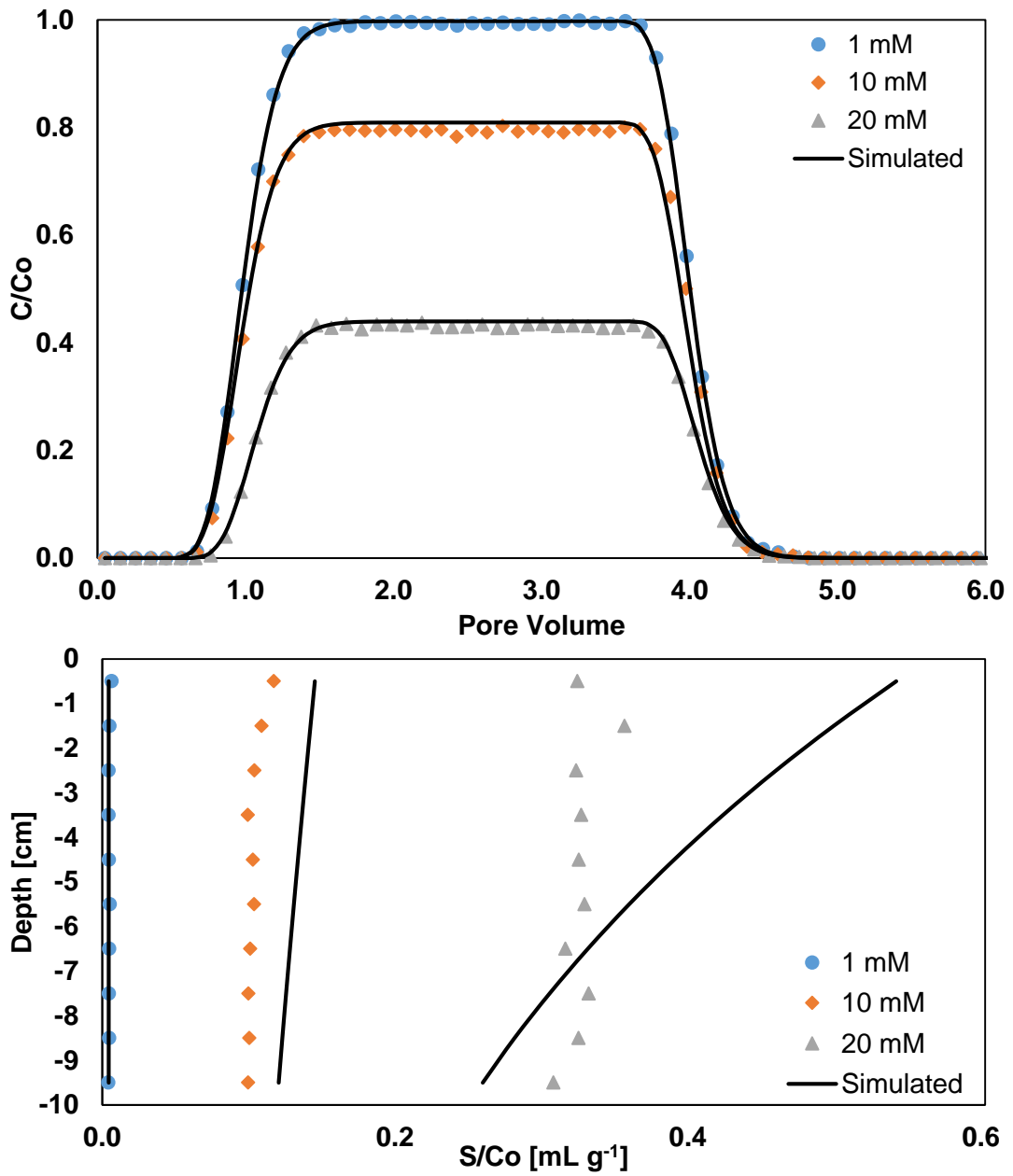


Figure 4.8: Colloid transport results for clean sand at various ionic strengths and a constant pH of 10. Top: measured and simulated normalized effluent concentration breakthrough curves for colloids. Bottom: measured and simulated normalized soil surface concentrations as a function of depth.

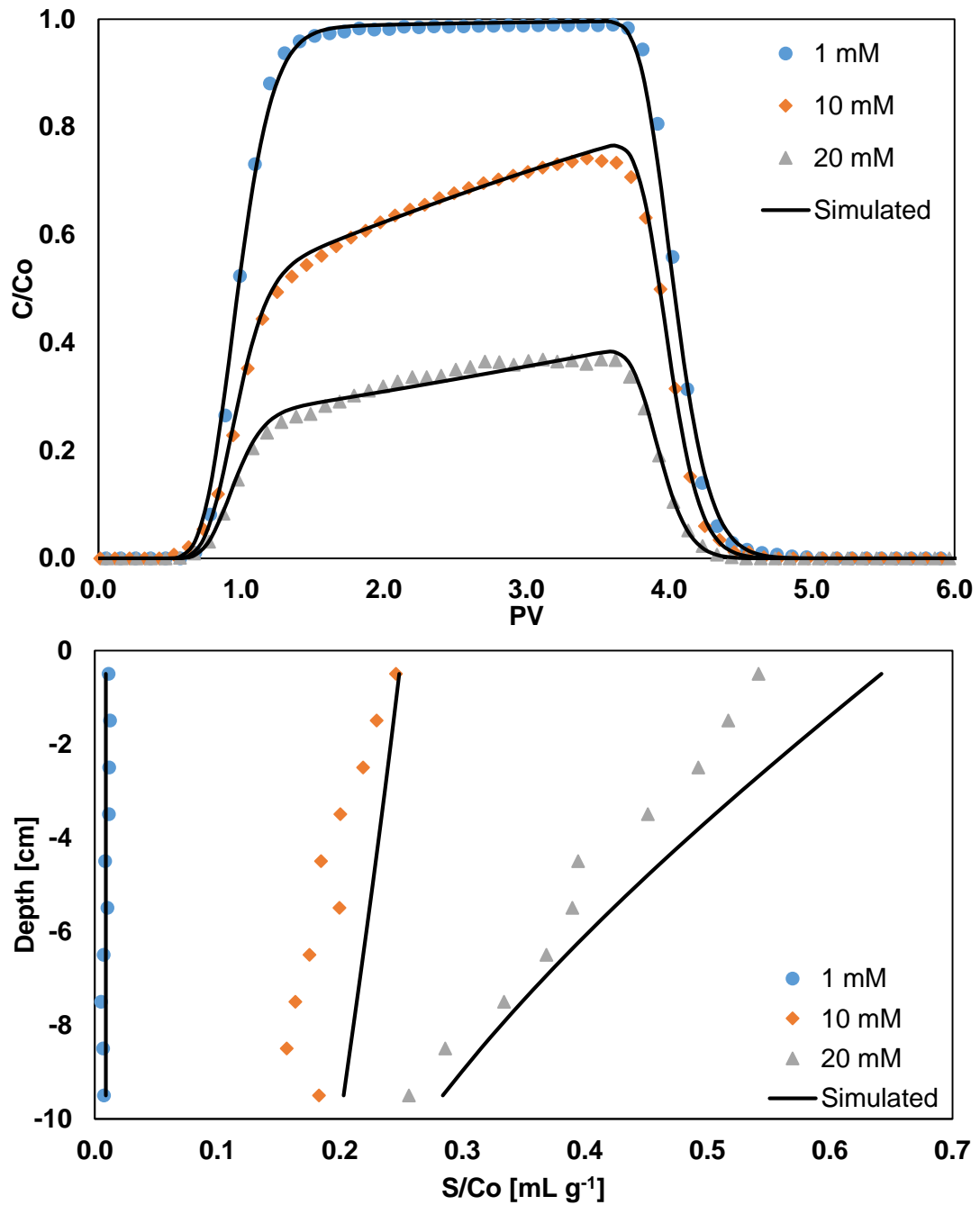


Figure 4.9: Colloid transport results for iron oxide coated sand at various ionic strengths and a constant pH of 10. Top: measured and simulated normalized effluent concentration breakthrough curves for colloids. Bottom: measured and simulated normalized soil surface concentrations as a function of depth.

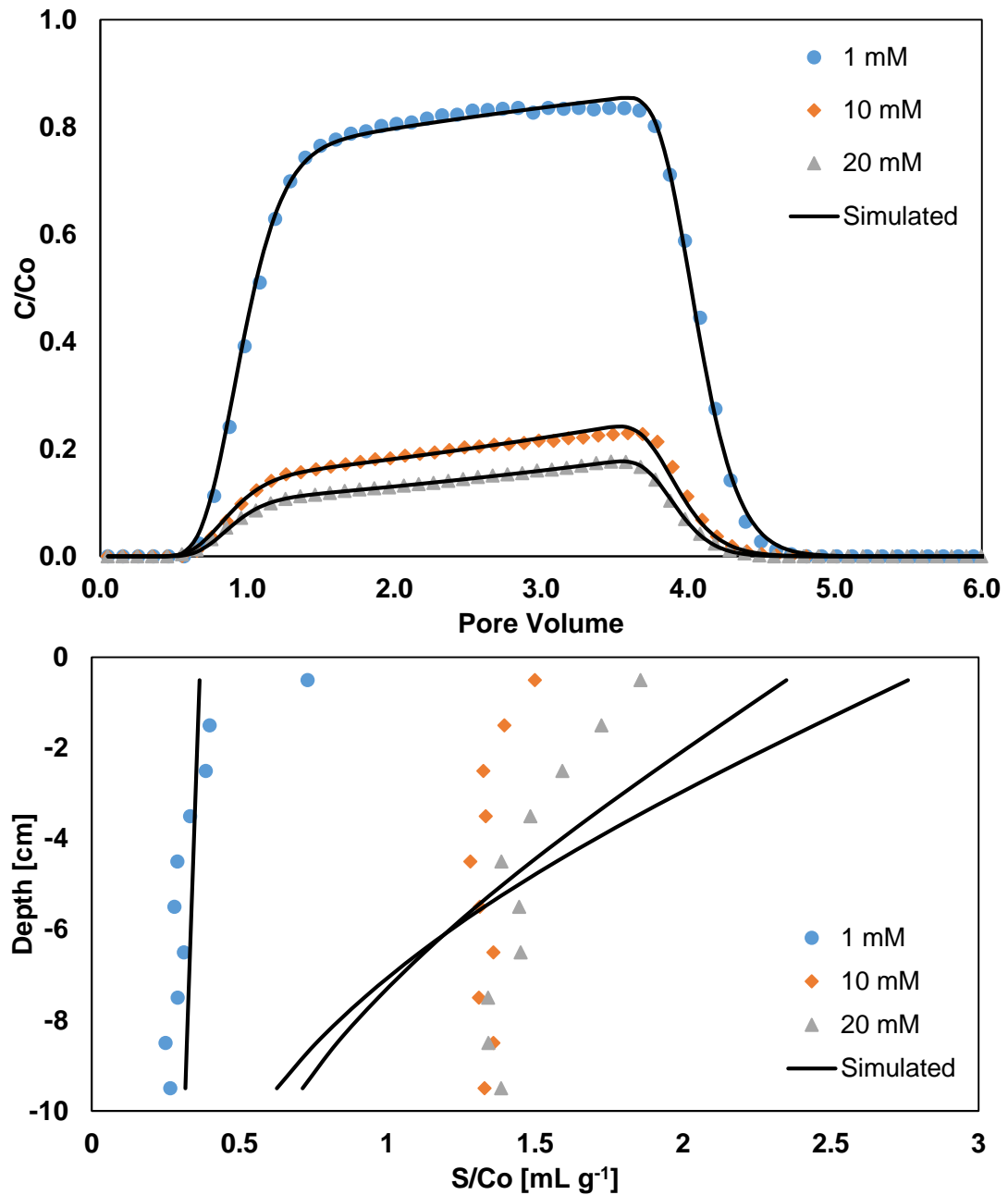


Figure 4.10: Colloid transport results zeolite at various ionic strengths and a constant pH of 10. Top: measured and simulated normalized effluent concentration breakthrough curves for colloids. Bottom: measured and simulated normalized soil surface concentrations as a function of depth.

Classical filtration theory predicts a reduced sensitivity to changes in ionic strength in terms of colloid retention under completely favorable conditions, such as in the case of oppositely charged colloid and media (Elimelech et al. 1995). Yet colloid retention in the iron oxide coated sand increased significantly as ionic strength was increased from 1 mM to 2 mM at pH 5.5. The positively charged patchy iron oxide coating served as favorable collector sites for colloids in coated sands at pH 5.5; however, the negatively charged uncoated portions of the sand likely masked smaller patches of the hematite coating. The large increase in colloid retention with ionic strength in the iron oxide-coated media is indicative of high degree of variability in iron-oxide patch size and suggests that as the ionic strength increased, retention occurred in the primary minimum on coated portions of the grain surface and in the secondary minimum on uncoated areas (Shen et al. 2007; Song et al. 1994). This may explain the less dramatic increase in retention as ionic strength was increased from 2 mM to 5 mM, as the intermediate ionic strength was sufficient to inhibit the effect of uncoated sand repulsion on smaller iron oxide patches. Indeed, the log-linear decrease in colloid retention with (Figure 4.6) is indicative of conditions favorable to colloid attachment, with colloid immobilization occurring in the primary energy well (Abudalo et al. 2005; Han et al. 2014).

The heterogeneous nature of the iron oxide coating is reflected in the difference in breakthrough curve shape that was observed at intermediate and high ionic strength at pH 5.5 and 10 as well (Figures 4.6 and 4.9). Clean sands exhibited similarly shaped breakthrough curves regardless of pH or ionic strength, with a rapid rise in effluent concentration that remained constant before decreasing to zero in a symmetrical fashion (Figure 4.1 and 4.5). At pH 5.5, iron oxide exhibited similarly shaped colloid breakthrough curves, with peak effluent concentration decreasing as ionic strength increased. However at pH 10, breakthrough curves observed in iron oxide coated sands changed in shape as ionic strength was increased. At pH 10, as ionic strength was increased above 1 mM,

breakthrough curves exhibited a gradual increase in effluent concentration with time, comparable in shape to the breakthrough curves observed in all zeolite experiments. Similarly shaped breakthrough curves have been previously observed in iron-oxide coated sands and has been attributed to the blocking of preferential retention sites by immobilized colloids causing a decrease in retention with time (El Badawy et al. 2013; Bolster et al. 2001; Johnson et al. 1996; D. Wang et al. 2013). Although DLVO calculations predict colloid retention occurred in the secondary minimum on both coated and uncoated portions of the sand surface, the lower primary energy barrier and deeper secondary minimum associated with the iron oxide coating suggest that iron oxide patches acted as preferential colloid collector sites. Despite overall unfavorable attachment conditions at pH 10, retention profiles in iron oxide coated sands differed from those observed in clean sand. At pH 10, iron oxide coated sand colloid retention profiles exhibited the same log-linear depth dependence that was observed at lower pHs. This suggests some iron oxide patches may have acted as favorable deposition sites due to the diminished barrier to deposition in the primary minimum (Tufenkji and Elimelech 2005).

Colloid retention in zeolite was sensitive to increases in ionic strength at both high and low pH (Figure 4.7 and 4.10), agreeing with previous work on colloid transport in zeolites (Gamerding and Kaplan 2001a). Relatively small increases in ionic strength resulted in greater retention at pH 5.5 than at pH 10 despite DLVO calculations predicting larger energy barriers and shallower secondary minimums (Table 4.2). In contrast to the heightened response to small ionic strength changes at low pH, the overall retention increased in an almost linear fashion with ionic strength as shown in Figure 4.11. That is, doubling the ionic strength from 1 mM to 2 mM and from 2 mM to 5 mM resulted comparably large increases in colloid retention (28% and 36% respectively). At pH 10, increasing ionic strength above the intermediate 10 mM resulted in a much smaller

increase in retention, though with nearly 80% of injected colloids retained there is significantly less opportunity for increased retention at higher ionic strengths.

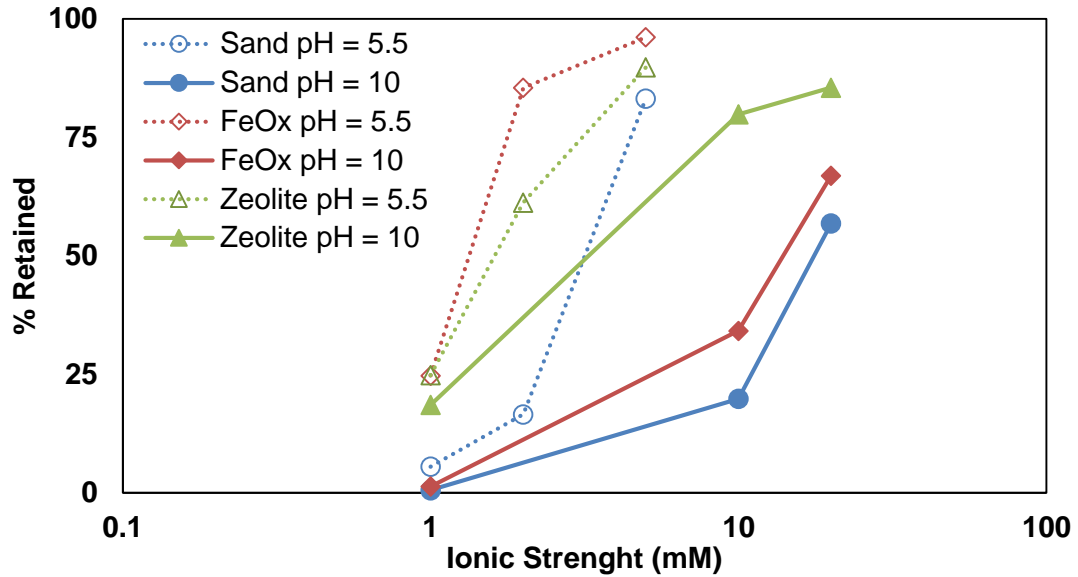


Figure 4.11: Mass of retained colloids as measured by integration of the breakthrough curve for all permeable reactive materials at varying ionic strength at pH 5.5 and 10.

Colloid retention profiles in zeolite did not vary significantly with increasing ionic strength at pH 5.5 and 10. In all experiments, observed retention profiles were relatively uniform with depth, with a slight increase in immobilized colloids at the soil surface. The similarity in colloid breakthrough curves and retention profiles at all ionic strengths and pHs suggests that colloid retention mechanisms did not differ at pH 5.5 and 10. Although geochemical heterogeneity may have played a role in retention at pH 5.5, as this is below the isoelectric point of many metal oxides (Parks 1965), the high levels of retention that were observed at pH 10 supports the idea that colloid retention occurred around rough asperities on the surface of the zeolite. Extended DLVO interaction calculations for colloid

interaction at rough surfaces have demonstrated that colloids can become immobilized in the secondary and primary minimum near asperities, and that the retention of colloids near rough features is increased by higher ionic strengths (Huang et al. 2010; Shen, F. Wang, Li, et al. 2012). Hyperexponential profiles have often been attributed to straining in sands, and previous work has shown that increases in ionic strength result in a more pronounced increase in retention at the surface of the soil specimen (Bradford et al. 2007). As increasing ionic strength did not result in greater retention near the soil surface, colloid retention in zeolites wasn't limited to granular contacts as ionic strength increased.

4.3.3 Modeling Results

Simulated breakthrough curves and retention profiles matched observed results for all materials; however, simulated curves for clean and iron oxide coated sand were closer to observed results than for zeolites as indicated by the smaller calculated R^2 values for zeolites (Table 4.3). Estimated kinetic attachment coefficients for the advection diffusion equation are shown below as a function of pH (Figure 4.12), and matched trends in retained mass as measured by colloid breakthrough curves in the different soil types (Figure 4.4). In all soil types the kinetic attachment coefficient increased as pH decreased, with the greatest increase in all soils occurring as pH dropped below pH 5.5 (Figure 4.12). At pH 7 and 10 zeolite exhibited the greatest attachment coefficient, followed by coated and uncoated sand, while at pH 5.5 the kinetic attachment coefficient was slightly larger for iron oxide coated sands. As discussed previously, this corresponds to dropping below the isoelectric point of the iron oxide coating. At pH 4, iron oxide coated sand had by far the highest kinetic attachment coefficient, followed by clean sand and zeolite. The similarity in trends of estimated kinetic attachment as a function of pH between zeolite and clean sand reinforces the limited role of geochemical heterogeneity in colloid retention in zeolites.

Table 4.3: ADE Model Results

Porous Media	pH	IS [mM]	K_{att} [min^{-1}]	Standard Error K_{att}	S_{max} [$N_T/N_i \text{ g}^{-1}$]	Standard Error S_{max}	R^2
Sand	4	1	0.065	4.5E-04	NA	NA	0.940
Sand	5.5	1	0.004	1.7E-04	NA	NA	0.999
Sand	5.5	2	0.011	2.0E-04	NA	NA	0.999
Sand	5.5	5	0.117	4.6E-04	NA	NA	0.970
Sand	7	1	2.5E-04	1.9E-04	NA	NA	0.998
Sand	10	1	1.3E-04	7.0E-05	NA	NA	1.000
Sand	10	10	0.014	3.0E-04	NA	NA	0.997
Sand	10	20	0.054	6.3E-04	NA	NA	0.954
FeOx	4	1	0.230	6.0E-04	NA	NA	0.994
FeOx	5.5	1	0.018	2.0E-04	NA	NA	0.999
FeOx	5.5	2	0.127	5.7E-04	NA	NA	0.971
FeOx	5.5	5	0.217	5.6E-04	NA	NA	0.994
FeOx	7	1	0.003	4.7E-04	0.023	0.003	0.999
FeOx	10	1	0.001	7.7E-04	0.007	0.004	0.998
FeOx	10	10	0.043	9.9E-04	0.340	0.010	0.997
FeOx	10	20	0.086	9.5E-04	1.41	0.061	0.984
Zeolite	4	1	0.053	5.8E-04	2.95	0.097	0.964
Zeolite	5.5	1	0.015	9.3E-04	0.803	0.100	0.987
Zeolite	5.5	2	0.056	8.2E-04	2.06	0.053	0.960
Zeolite	5.5	5	0.102	6.1E-04	27.8	4.7	0.858
Zeolite	7	1	0.011	1.2E-03	0.803	0.245	0.976
Zeolite	10	1	0.012	3.3E-04	0.639	0.038	0.976
Zeolite	10	10	0.083	7.6E-04	4.52	0.159	0.861
Zeolite	10	20	0.096	4.3E-04	5.48	0.108	0.872

Note: N_T refers to recovered colloids in the sand, N_i refers to number of colloids in a unit volume of injected colloid suspension.

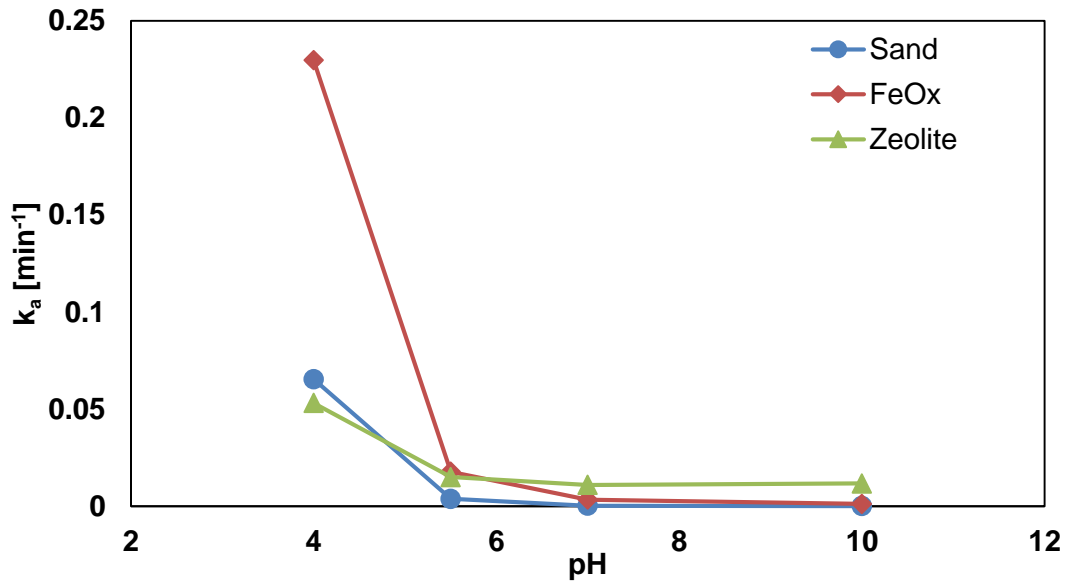


Figure 4.12: Estimated kinetic attachment coefficients for permeable reactive materials at varying pH.

Kinetic attachment as a function of ionic strength at pH 5.5 and 10 are shown in Figure 4.13. At both high and low pH, increasing ionic strength resulted in larger attachment coefficients for all soils. Attachment coefficients were greatest in zeolite, followed by iron oxide coated sand and clean sand at pH 10. At pH 5.5, results between the different media types were more mixed and the relative difference in magnitude of the attachment coefficients did not match overall trends in the mass of retained colloids as measured by effluent curves (Figure 4.11). Estimated attachment coefficients for iron oxide coated sand were greatest at all ionic strengths at pH 5.5. Estimated attachment coefficients for Zeolite were larger than those for clean sand at low and intermediate ionic strength, while the reverse was true at the highest ionic strength in the pH 5.5 experimental group.

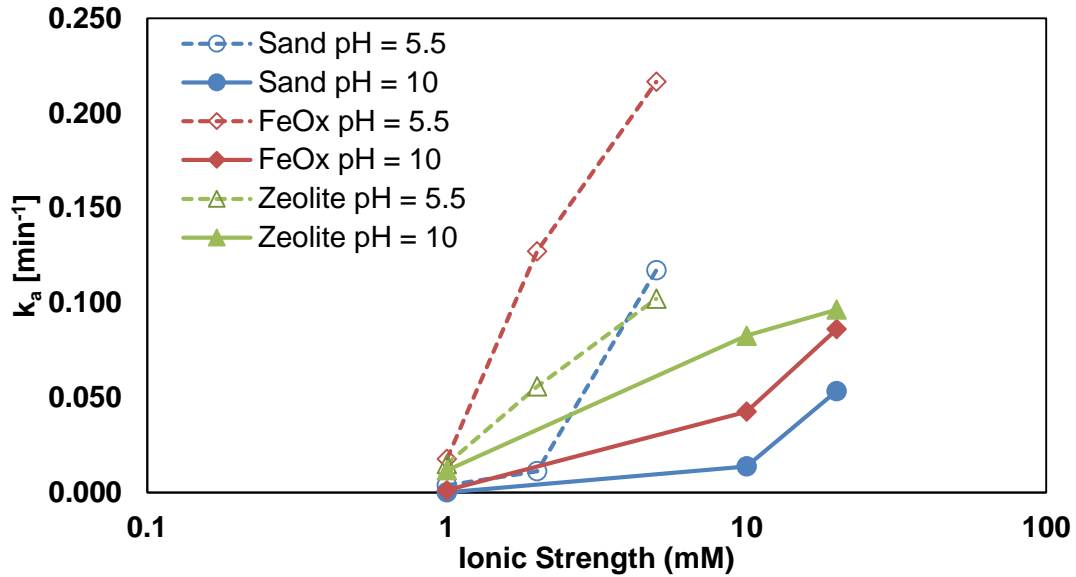


Figure 4.13: Estimated kinetic attachment coefficients for permeable reactive materials at varying ionic strength at pH 5.5 and 10.

Although clean sand colloid breakthrough curves were well characterized by first order kinetic attachment, breakthrough curves for zeolites exhibited a decrease in the overall kinetic attachment rate with time at all pHs and ionic strengths, while iron oxide coated sand only exhibited this behavior at pH 10. The estimated parameter S_{max} represents the maximum mass of colloids that can be attached to soil surface per unit mass of the soil, and partially controls the rate at which colloid attachment decreases with time (Adamczyk et al. 1994). For both zeolite and iron oxide coated sand, estimated S_{max} increased as ionic strength increased, an observation that agrees with the work of other researchers (Bolster et al. 2001; Bradford and Torkzaban 2012; Bradford, Torkzaban, et al. 2013; Johnson et al. 1996; Torkzaban et al. 2007). In iron oxide coated media under unfavorable attachment conditions, the maximum surface concentration increases with ionic strength as uncoated regions become less repulsive, allowing colloid attachment to occur in increasingly smaller iron oxide patches (Bradford, Torkzaban, et al. 2013; Song et al. 1994). Estimated S_{max} for zeolite was significantly larger than for iron oxide coated

sand at all ionic strengths. This is due both to the increased roughness and angularity of the zeolite, as well as its much larger specific surface area (Barton and Buchberger 2007; Ko and Elimelech 2000). Trends in S_{\max} differed at pH 10 and 5.5 for zeolite. At high pH, increasing ionic strength from intermediate ionic strength to high ionic strength resulted in a much smaller increase in S_{\max} at pH 10 than it did at pH 5.5. The large standard error associated with the S_{\max} at 5 mM at pH 5.5 suggests a high degree of uncertainty associated with the estimated parameter (Dane and Topp 2002). Estimated S_{\max} in zeolite experiments as a function of pH are shown in Figure 4.14. As with estimated attachment coefficients, S_{\max} was relatively constant at pH 5.5, 7, and 10, but increased significantly as pH dropped to 4.

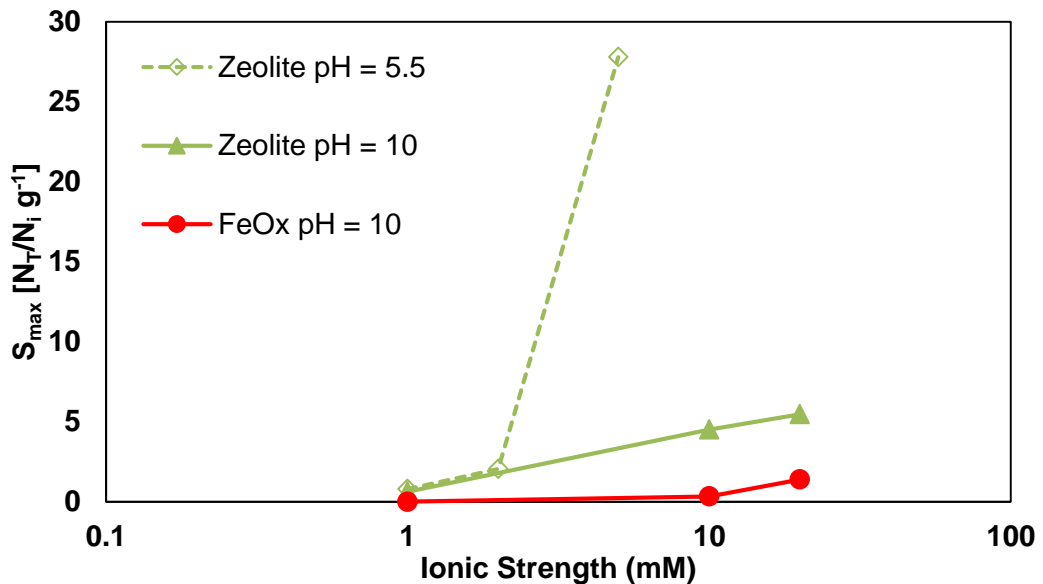


Figure 4.14: Estimated S_{\max} coefficients for iron oxide coated sand and zeolite at varying ionic strength at pH 5.5 and 10. N_T refers to recovered colloids in the sand, N_i refers to number of colloids in a unit volume of injected colloid suspension.

4.4 CONCLUSIONS

This study highlights the colloid mobility of materials that have traditionally been used in permeable reactive barriers to treat dissolved contaminants. Theoretical DLVO calculations and column transport experiments were conducted to assess the effect of pore water ionic strength and pH on the transport and retention of colloids in clean and iron oxide coated sand and zeolite. Colloid mobility decreased as pH decreased, with a sharp rise in retention at pH 4 for all porous media types. At pH 7 and 10 colloid mobility was lowest in zeolite. However, colloid retention was greater in iron oxide coated sand at pH 5.5 and 4, which corresponded to dropping below the isoelectric point of the hematite coating and resulting in conditions favorable for colloid attachment. Significant colloid retention in clean sand was only observed at pH 4. Colloid mobility in zeolite as a function of pH closely resembled that of clean sand, suggesting that the high levels of retention in zeolite were the result of surface roughness and not geochemical heterogeneity.

Increasing ionic strength resulted in greater retention in all soils at both low and high pH. However, colloid retention was more sensitive to changes in ionic strength at pH 5.5 than at pH 10. At pH 5.5, colloid retention was highest in iron oxide coated sands at all ionic strengths due to the positively charged iron oxide patches on the surface of the soil. While less colloid retention was observed in zeolites, colloid mobility was lower than in sands at all ionic strengths. At pH 10, colloid removal was greatest in zeolite at all ionic strengths, followed by iron oxide coated and clean sand. Although greater retention was observed in iron oxide coated sands at low pHs, large levels of colloid retention in zeolites at both low and high ionic strength. Additionally, colloid mobility was lowest in zeolites at intermediate and high pHs. This suggests that zeolite may be an ideal reactive barrier component in situations where the mobility of colloids is of concern, such as in the case

of pathogenic biocolloids, or when as colloids act as a vector for otherwise low mobility contaminants.

CHAPTER 5:
THE TRANSPORT AND RETENTION OF COLLOIDS IN UNSATURATED
PERMEABLE REACTIVE MEDIA

5.1 INTRODUCTION

Permeable reactive barrier technology has become ubiquitous in the treatment of a variety of dissolved contaminants. Iron oxide coated media and natural zeolites are two commonly used components in reactive barrier systems (Benjamin et al. 1996; Färm 2002; Knox et al. 2008). In many cases these reactive treatment systems operate under unsaturated conditions at least part of the time, such as in the case of storm water infiltration and filtering, bioinfiltration, and ground water recharge systems, as well as in horizontal permeable reactive barriers in the vadose zone (Gaber et al. 2002; Mohanty et al. 2013; Pitcher et al. 2004; Yi et al. 2010; L. Zhang et al. 2010). Previous studies have demonstrated that colloids can be extremely mobile in unsaturated soils and act as a vector in the transport of dissolved contaminants (de Jonge, Kjaergaard, et al. 2004; Sprague et al. 2000; Utsunomiya et al. 2009). However, to date very little research has been conducted on the transport of colloids through unsaturated iron oxide coated sand and natural zeolite.

Chu et al. (2001) compared the transport of virus colloids through unsaturated clean sand and sand with trace metal oxides present. Viruses were retained in greater numbers in the sand with metal oxides present, and this effect increased with decreasing moisture content due to the colloids coming closer to the favorable deposition sites on the soil surface under unsaturated conditions. Similar observations have been made in natural soils, where increased iron oxide content decreases mobility in unsaturated soils (Chu et al. 2003). Gamedainger and Kaplan (2001) compared the transport of

carboxylated microspheres in unsaturated sands and a tuff material containing some zeolite common to the Yucca Mountain geology. Colloids were less mobile in unsaturated zeolite than in sand, and this disparity increased as saturation decreased.

This current study examines the mobility of carboxylate polystyrene latex microspheres in saturated and unsaturated soil media that have traditionally been used in permeable reactive barrier systems to treat dissolved contaminants. Colloid mobility in iron oxide coated sand and natural zeolite were compared to clean silica sand under varying degrees of saturation to assess colloid retention under saturated and unsaturated conditions using column transport experiments to assess the suitability of these media to retain colloids in the vadose zone.

5.2 MATERIALS AND METHOD

5.2.1 Colloid and Porous Media Preparation

Manufactured carboxylated polystyrene microspheres (Bang Laboratories, Inc. Fishers, IN) 1 μm in diameter were used in all experiments. Residual surfactant from the colloid manufacturer was removed by triple rinsing the microspheres before suspending them in deionized water. All soils were sieved beforehand to have the same median grain size ($d_{50} = 0.36 \text{ mm}$) and coefficient of uniformity ($C_u = 1.82$). Silica sand (US Silica) was used as an unreactive media for comparison purposes. As in previous chapters, the sand was subject a rigorous cleaning procedure which included repeated ultrasonification, soaking in sodium dithionite, hydrogen peroxide, and nitric acid, and rinsing with DI over a #200 sieve to minimize any effects of geochemical heterogeneity on colloid mobility. Iron oxide coated sands were prepared from cleaned silica using the heterogeneous suspension method, and had an iron oxide coated content of 1.4 mg/g (Larrahondo et al. 2011; Scheidegger et al. 1993). Crushed clinoptilolite zeolitic tuff (St. Cloud Zeolite, MN)

composed was used for all zeolite experiments. Zeolites were ultrasonicated in deionized water for an hour, then repeatedly rinsed over a #200 sieve.

The soil water characteristic curves and hydraulic conductivity functions for all materials were previously measured using the multistep outflow method (Eching and Hopmans 1993; Eching et al. 1994; Hopmans et al. 2002) and were parameterized using the expressions of Kosugi (1994, 1996):

$$S_e = \frac{\theta - \theta_r}{\theta_s - \theta_r} = \frac{1}{2} \operatorname{erfc} \left[\frac{\ln \left(\frac{h}{h_m} \right)}{\sqrt{2}\sigma} \right]$$

$$K_r = \frac{K_{unsat}}{K_{sat}} = S_e^\tau \left\{ \frac{1}{2} \operatorname{erfc} \left[\operatorname{erfc}^{-1}(2S_e) + \frac{\beta\sigma}{\sqrt{2}} \right] \right\}^2$$

where S_e is the effective saturation, θ_s and θ_r are the dimensionless saturated and residual volumetric water contents, h is the matric suction in cm of H_2O , h_m is related to the geometric mean pore radius and, σ is the standard deviation of the pore size distribution, and $\operatorname{erfc}[\]$ and $\operatorname{erfc}^{-1}[\]$ are the complimentary error function and inverse complementary error function respectively. The hydraulic conductivity function describes the unsaturated hydraulic conductivity, K_{unsat} , relative to the saturated hydraulic conductivity, K_{sat} . The dimensionless fitting parameters τ and β are relate to soil pore tortuosity and control the shape of the hydraulic conductivity function in the dry and wet regime respectively (Kosugi 1999b; Mualem and Dagan 1978). Soil water characteristic curve and hydraulic conductivity function parameters are summarized in Table 5.1.

Table 5.1: Soil water characteristic curve and hydraulic conductivity parameters

Soil	θ_s	θ_r	h_m [cm H_2O]	σ	K_{sat} [cm/min]	τ	β
Sand	0.375	0.04	24	0.13	2.5	- 0.6	4.0
FeOx	0.375	0.04	24	0.13	2.5	- 0.6	4.5
Zeolite	0.6	0.17	24.6	0.14	2.4	- 1	5.5

5.2.2 Column Transport Experiments

All transport experiments were conducted in acrylic flow cells (L=10 cm, ID=5 cm). For all saturated experiments, both ends of the flow cell were initially capped with stainless steel plates with 1 mm holes and supported by hydrophilic nylon mesh membranes with 10 μm openings (U-CMN-10, Component Supply Company). Saturated soil samples were prepared using the modified slurry deposition procedure described in previous chapters (Bandini and Sathiskumar 2009; Carraro et al. 2003; Wood et al. 2008). For unsaturated experiments, tensiometers (652X03-B1M3, Soil Moisture Equip. Corp) arranged helically and located 2.5, 5, and 7.5 cm above the base plate were inserted during the slurry deposition of the soil, and pressure transducers (PX170-28DV, Omega Engineering) were used to measure matric suction. The average gravimetric moisture content of the unsaturated soil sample was monitored using a digital balance (4102 accuSeries, Fisher Scientific).

The pore fluid consisted a pH=10 buffer (0.2 mM Na_2CO_3) with sufficient sodium chloride to raise the ionic strength to 1 mM. These chemical conditions were selected to minimize colloid deposition at the soil water interface. For saturated experiments, the aqueous phase was pumped (Cole Parmer Masterflex L/S) downward through the column at a Darcy velocity of 0.24 cm/min. The soil samples were first pre-equilibrated by passing five pore volumes of the background electrolyte followed by 0.2 mM NaNO_3 conservative tracer to measure dispersion. This was followed by an additional ten pore volumes of background solution. Three pore volumes of colloids at 30 mg/L (5.6×10^7 particles/L) were passed through the column followed by an additional two pore volumes of colloid free background electrolyte solution.

Unsaturated transport experiments followed a modified protocol. Samples were initially pre-equilibrated by fifteen pore volumes of background electrolyte passed upward

through the porous media. After the initial pre-equilibration, the acrylic top cap of the flow cell and membrane were removed to expose the top of the soil surface to the atmosphere. Inlet flow to unsaturated experiments was applied using an acrylic sprinkling apparatus with seven stainless steel needles to evenly distribute flow over the top of the sand surface. Additionally, the stainless steel endcap was left in place on the top soil surface to minimize erosion caused by the sprinkler.

For unsaturated experiments, the lower boundary was controlled using a hanging water column to apply suction to the base of the soil sample (Cherrey et al. 2003). The desired saturation was achieved by simultaneously reducing the inlet flow rate while increasing the suction at the lower boundary condition by changing the elevation of the column outlet. A uniform hydraulic gradient was achieved when all tensiometers measured the same constant value, implying a constant level of saturation along the length of the column (Chen et al. 2007; Gargiulo et al. 2008; Torkzaban et al. 2008). Once uniform flow conditions were achieved, a 0.2 mM NaNO₃ conservative tracer was passed through the column to measure dispersion, followed by three pore volumes of background electrolyte. Three pore volumes of colloids at 30 mg/L were then passed through the column followed by an additional two pore volumes of colloid free background solution. At the termination of unsaturated experiments, the sprinkler at the inlet was shut off while simultaneously closing the valve at the end of the hanging column.

At the end of both saturated and unsaturated experiments, columns were extruded into 1 cm sections and mixed with 60 mL of 0.2 mM Na₂CO₃ to measure retention profiles as described in previous chapters. For unsaturated experiments, the dissected soil samples were massed before the addition of the 0.2 mM Na₂CO₃ to assess the moisture content at the end of the experiment. All effluent concentrations and soil-colloid concentrations were measured using UV-Vis spectrophotometry (Shimadzu UV/1800).

5.2.3 Transport Modeling

Colloid breakthrough curves were modeled using the 1-D advection dispersion equation (ADE) with one kinetic retention sites to assess the retention of ellipsoids and spheres in saturated and unsaturated porous media. The mass balance for colloids passing through porous media with one retention site is given as:

$$\frac{\partial \theta C}{\partial t} + \rho \frac{\partial S}{\partial t} = \frac{\partial}{\partial x} \left(\theta D_L \frac{\partial C}{\partial x} \right) - \frac{\partial qC}{\partial x} \quad (5.1)$$

where C is the colloid concentration in the aqueous phase, θ is volumetric moisture content, D is the hydrodynamic dispersion coefficient in the direction of flow, q is the Darcy flux in the direction of flow, ρ is the bulk density of the sand, S is the concentration of colloids immobilized in the soil column, x is the spatial coordinate in the direction parallel to flow, and t is time.

A single kinetic retention site was used to describe the mass transfer of colloids in both saturated and unsaturated porous media. The retention of colloids in porous media was described as a reversible process with a blocking function:

$$\rho \frac{\partial S_1}{\partial t} = \theta \psi_s k_a C - k_d \rho k_d \quad (5.2)$$

where k_a and k_d are the rate coefficients for attachment and detachment respectively, and ψ_s is the dimensionless blocking function. The dimensionless blocking function combines depth dependent retention with concentration dependent blocking and takes the following form:

$$\psi_s = \left(1 - \frac{S_1}{S_{max}} \right) \left(1 + \frac{x}{d_s} \right)^{-\mu} \quad (5.3)$$

where in the first term S_{max} is the retention capacity of immobilized colloids for the soil. The concentration dependent first term in the above blocking function has been used in saturated porous media to represent the occupation of finite preferential attachment sites (Adamczyk et al. 1994; El Badawy et al. 2013; Bolster et al. 2001), while in unsaturated porous media it has typically been used to represent the accumulation of colloids at the

air-water interface (Chu et al. 2001; Corapcioglu and Choi 1996; Lenhart and Sayers 2002). The second term in the above formulation controls depth dependent retention behavior. μ is an empirical factor that controls the shape of the retention profile. Following the approach of Kasel et al. (2013), μ was estimated by initially fitting breakthrough curves and retention profiles for individual experiments, then fixed to the average value for all experiments for a given soil type. μ was only fit for unsaturated experiments for sands and was found to be equal to 0.7, while μ was fit to both saturated and unsaturated zeolite experiments and found to be 0.44. It is extremely difficult to infer pore scale retention mechanisms from fitting macroscopic data from column breakthrough experiments (Goldberg et al. 2014; Johnson et al. 2011; Pazmino et al. 2011). The above formulation of the ADE has been shown to be extremely flexible in its ability to describe both colloid breakthrough curves and retention profiles in saturated and unsaturated porous media, and was adopted for simplicity (Gargiulo et al. 2008; Goebel et al. 2013; Kasel et al. 2013; Torkzaban et al. 2008).

Equations 5.1-3 were solved using HYDRUS-1D, a finite element code used for one dimensional transport processes in variably saturated soils (Simunek et al. 2013). HYDRUS 1-D includes a weighted non-linear parameter estimation routine based on the Marquardt-Levenberg least squares algorithm, and was used to estimate unknown coefficients. The dispersion coefficient was fit to the conservative tracer portion of the experiment and fixed for the colloid transport portion of the experiment. For saturated sand experiments, ψ_s was set equal to 1, and k_d was set equal to zero, thus simplifying the ADE to a conventional attachment model with k_a as the sole estimated parameter. Following the approach of Kasel et al. (2013), μ was estimated by initially fitting breakthrough curves and retention profiles for individual experiments, while simultaneously fitting k_a , k_d , and s_{max} . μ was then fixed to the average value for all experiments for a given soil type. μ was only fit for unsaturated experiments for sands

and the average value was found to be equal to 0.7, while μ was fit to both saturated and unsaturated zeolite experiments and the average value found to be 0.44. k_a , k_d , and S_{max} were then estimated again by simultaneously fitting measured colloid breakthrough curves and retention profiles, with μ fixed to the average value. Volumetric moisture content was determined independently during column dissection.

5.3 RESULTS AND DISCUSSION

Unsaturated flow conditions were assessed by several means, and demonstrate that a uniform hydraulic gradient was achieved in all experiments. The average gravimetric moisture content as measured by the digital scale remained constant throughout experiments (all standard deviations in moisture content < 0.001). Gravimetric moisture content along the length of the specimen were measured at the termination of experiments and converted into volumetric moisture contents. Saturation as a function of depth exhibited some variability, as shown in Figure 5.1, and in all experiments effective saturation showed an overall decrease with depth. Tensiometric measurements of soil suction were constant along the length of the soil column, and did not reflect the decrease in saturation with depth. This is likely due to the disparity in precision and accuracy between moisture content measurements and tensiometric measurements (Dane and Topp 2002).

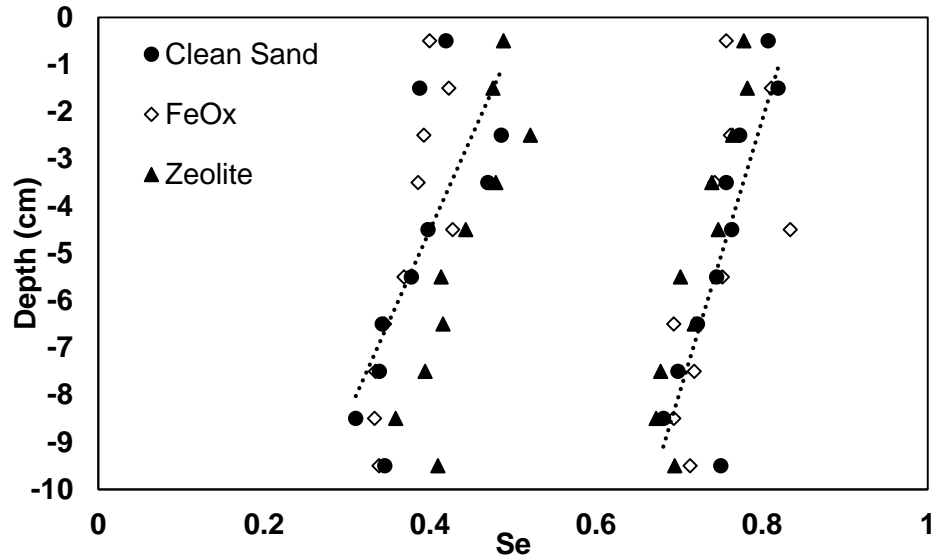


Figure 5.1: Effective saturation profiles for unsaturated experiments measured at termination of experiments. Dashed lines show the general trend of decreasing saturation with depth.

Breakthrough curves for the conservative tracer were conducted for all experiments and were well described by the 1-D advection dispersion equation. Observed tracer breakthrough curves did not exhibit any tailing and did not indicate the presence of low flow or immobile pore water present in the soil matrix of any of the permeable reactive media (Cherrey et al. 2003; Gao et al. 2006; W. Zhang et al. 2010). Estimated dispersion coefficients were similar for clean and iron oxide coated sand, while dispersion coefficients were slightly larger in zeolite experiments (Table 5.2). The larger estimated dispersion coefficients for zeolite experiments is likely due to the smaller velocities and higher porosities, allowing for additional mechanical dispersion to take place (Ewing et al. 2010). Estimated dispersion coefficients for clean and iron oxide coated sand were slightly higher for fully saturated experiments than for intermediate saturation levels, but increased significantly at the lowest saturation level. Zeolite dispersion coefficients were similar between full and intermediate saturation, and increased slightly for the lowest saturation

level. Dispersion coefficients typically increase as saturation decreases due to the higher tortuosity in unsaturated soils media (Cherrey et al. 2003; Knappenberger et al. 2014). Although the effective saturation values were similar for all materials, the higher volumetric moisture content in zeolite experiments may explain the smaller increase in dispersion with decreasing saturation than was observed in clean and iron oxide coated sand. The relatively large Peclet numbers observed in the soil types suggests that dispersion may play a less important role in mass transfer of colloids to the soil surfaces than advection at all saturation levels.

Table 5.2: Experimental conditions and mass balance information

Soil	S_e	θ	h_{avg} [cm H ₂ O]	q [cm/m in]	D [cm]	Pe	M_{Eff}	M_{Soil}	M_{Total}
Sand	1.0	0.373	na	0.241	0.148	44	0.993	0.009	1.002
FeOx	1.0	0.370	na	0.242	0.201	33	0.988	0.023	1.011
Zeolite	1.0	0.582	na	0.241	0.271	15	0.814	0.171	0.986
Sand	0.74	0.292 ± 0.014	21.9 ± 0.2	0.928	0.127	250	0.949	0.030	0.979
FeOx	0.75	0.290 ± 0.015	21.7 ± 0.4	0.927	0.113	283	0.931	0.055	0.987
Zeolite	0.73	0.483 ± 0.017	21.4 ± 0.1	0.948	0.262	75	0.773	0.198	0.971
Sand	0.38	0.169 ± 0.018	24.8 ± 0.3	0.252	0.319	47	0.824	0.093	0.917
FeOx	0.37	0.166 ± 0.012	24.7 ± 0.1	0.251	0.329	46	0.762	0.186	0.948
Zeolite	0.44	0.359 ± 0.021	25.1 ± 0.2	0.244	0.372	18	0.561	0.392	0.953

NOTE: θ is the volumetric moisture content as measured by dissection at the termination of unsaturated experiments, h_{avg} refers to the average measured matric suction, and the standard deviation is calculated between the three axial tensiometers, q is the Darcy flux, D is the dispersion coefficient, and Pe is the Peclet number. All masses, M, are fraction of the total injected mass of colloids. M_{Eff} refers to mass eluted as measured by the effluent curve, M_{Soil} refers to mass of colloids attached to soil, and M_{Total} refers to total mass balance.

Saturated colloid breakthrough curves for clean and iron oxide coated sand were identically shaped, with a rapid increase in effluent colloid concentration to a constant value that decreased back to zero in a symmetrical fashion with no observable tailing

(Figure 5.2 and 5.3). Minimal colloid retention was observed in clean (0.7%) and iron oxide coated sand at full saturation (1.2%). The low levels of retention observed in clean and iron oxide coated sand agree with previous DVLO calculations. Both clean sand and the hematite coating of the iron oxide coated sand surface are largely repulsive to colloids for the given pore water chemistry, though the energy barrier for the hematite coating is reduced as compared to the clean sand surface, and a small secondary minimum is present. The ratio between colloid and mean grain size for both of these materials is sufficiently small to limit physical filtration or straining (Bradford et al. 2002; Sang et al. 2013; Xu and Saiers 2009). The limited colloid retention in these two materials likely occurred in low velocity regions around granular contacts, or near rough asperities (Johnson et al. 2007; Ko and Elimelech 2000; Saiers and Ryan 2005; Shen, L.-P. Wang, Li, et al. 2012). Additionally, some colloid immobilization may have occurred near larger iron oxide coated patches as DLVO calculations predict a small secondary minimum.

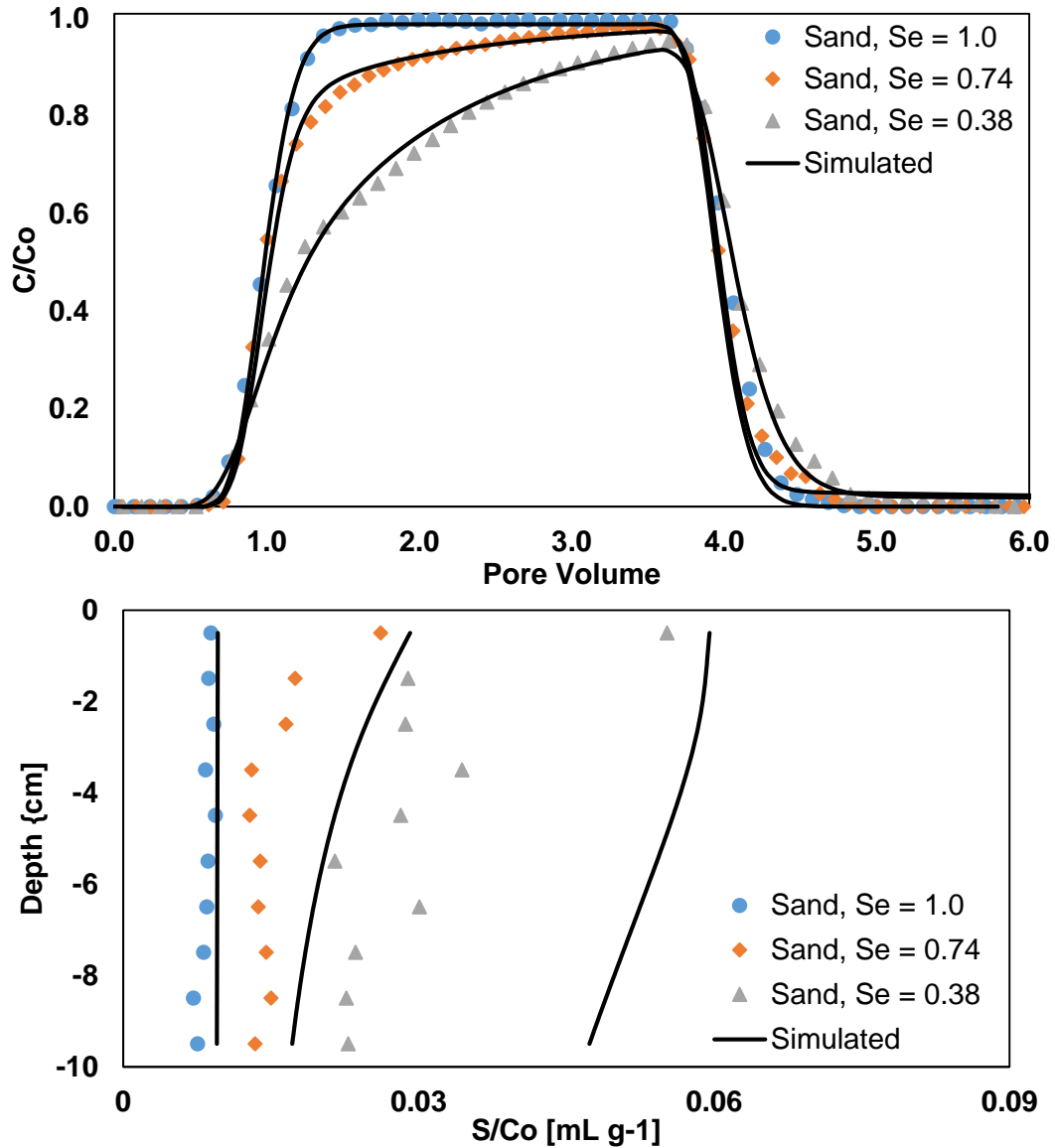


Figure 5.2: Colloid transport results for sand under varying degrees of saturation. Top: measured and simulated normalized effluent concentration breakthrough curves for colloids. C_o is the concentration of the injected colloids. Bottom: measured and simulated normalized soil surface concentrations as a function of depth (distance from outlet). Surface concentration, S , refers to the mass of colloids retained per mass of soil. Simulated curves are shown as solid lines.

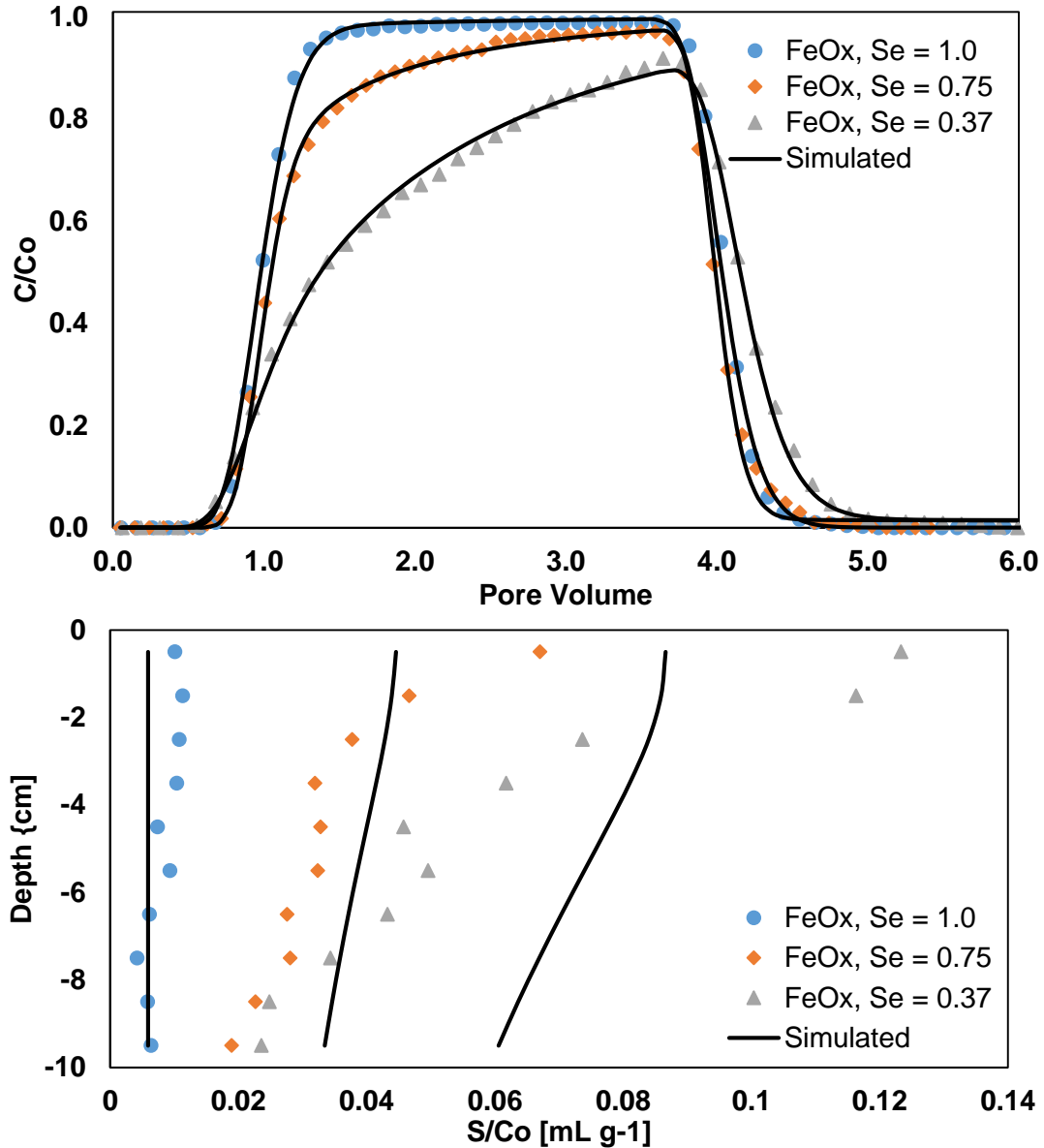


Figure 5.3: Colloid transport results for iron oxide coated sand under varying degrees of saturation. Top: measured and simulated normalized effluent concentration breakthrough curves for colloids. Bottom: measured and simulated normalized soil surface concentrations as a function of depth.

Retention in saturated zeolite was significantly higher (18.6%) than in clean and iron oxide coated sand, and the colloid breakthrough curve differed in shape (Figure 5.4). Colloid effluent concentrations in saturated zeolite increased gradually with time, instead of remaining at a constant peak value as was observed in saturated sands. The greater

levels of colloid retention observed in saturated zeolite is likely due to the high degree of roughness present on the soil surface as well as grain angularity. Although DLVO calculations for colloid and zeolite predict a large energy barrier to immobilization in the primary minimum, and no secondary minimum, similar to clean sand, researchers have demonstrated that colloids can become immobilized in the primary and secondary minimum near rough asperities under conditions otherwise unfavorable to colloid attachment (Shen, F. Wang, Li, et al. 2012). The gradual increase in colloid effluent concentration is indicative of an overall decrease in attachment with time. This may be due to colloids occupying preferential retention locations near rough features. Additionally, the retention profile observed in saturated zeolite was hyperexponential, with increased colloid retention near the inlet of the soil column. This behavior has typically been associated with straining in sands, and suggests that increased retention may have occurred near granular contacts in the zeolite (Barton and Buchberger 2007; Bradford et al. 2006; Li et al. 2006). The greater number of intergranular contacts associated with the high angularity of the zeolite likely contributed to this phenomena (Barton and Buchberger 2007).

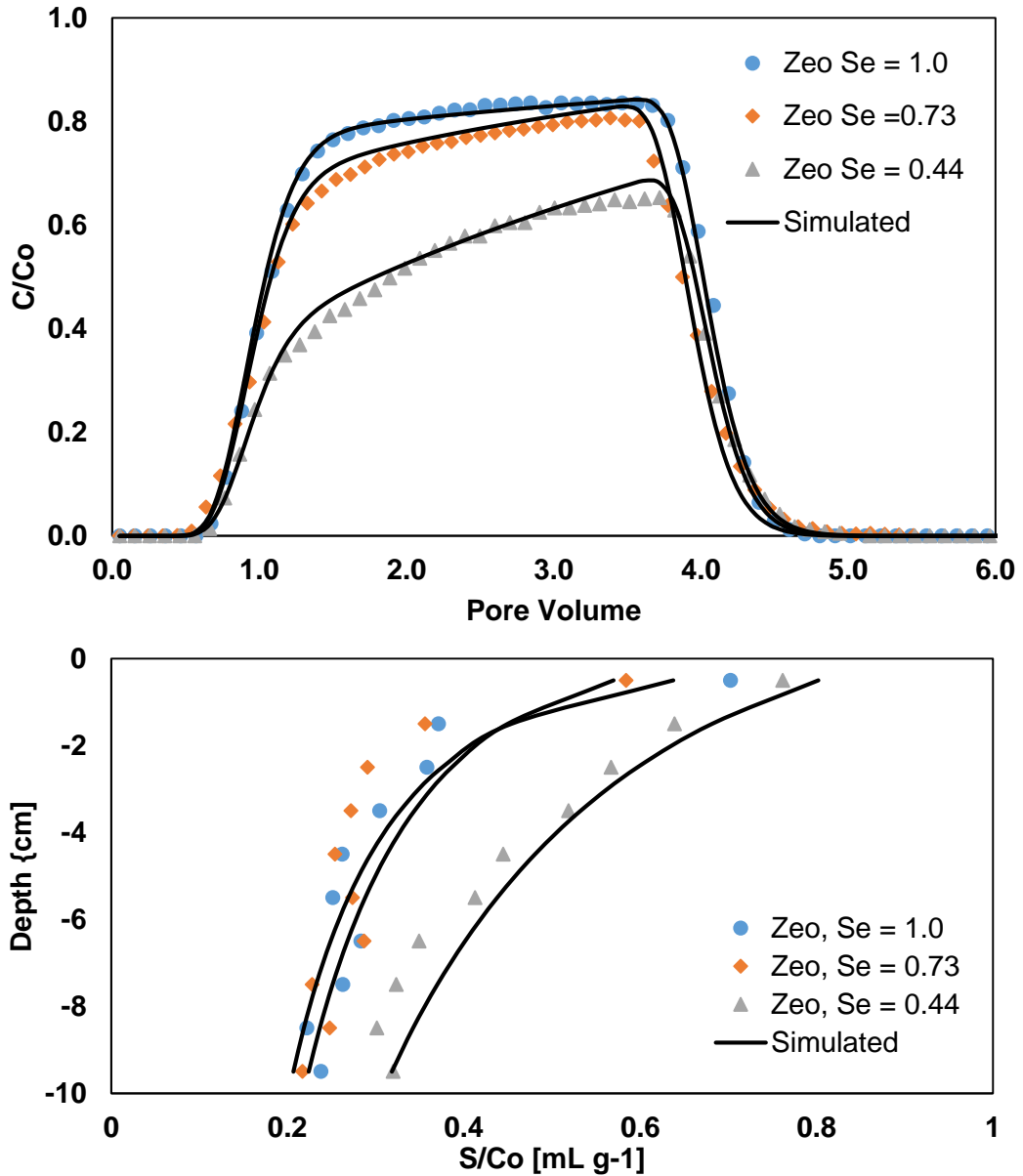


Figure 5.4: Colloid transport results for zeolite under varying degrees of saturation. Top: measured and simulated normalized effluent concentration breakthrough curves for colloids. Bottom: measured and simulated normalized soil surface concentrations as a function of depth.

Colloid mobility was reduced in all unsaturated experiments compared to the saturated condition (Figure 5.5), and the mass fraction of immobilized colloid increased as effective saturation decreased for all soil types, a phenomena commonly observed in

unsaturated porous media (Lenhart and Saiers 2002; Wan and Wilson 1994b; Zevi et al. 2009). Colloid breakthrough curves differed in shape in unsaturated clean and coated sand and exhibited a gradual increase in effluent concentration over time, similar to the breakthrough curves observed in zeolite experiments. However, effluent concentration increases were steeper in clean and coated sand than in zeolite, and some tailing was observed in sand breakthrough curves. Clean and iron oxide coated sands had similar mass fractions of colloids retained at the intermediate effective saturation, with 5% of colloids retained in clean sand, and 7% in iron oxide coated sand. The disparity in colloid retention between clean and iron oxide coated sand increased for the lowest effective saturation, with 18% of colloids retained in clean sand versus 24% in iron oxide coated sand. This observation agrees with previous research which has shown increased colloid retention in unsaturated soils with metal oxides naturally present (Chu et al. 2001, 2003). Colloids were less mobile in unsaturated zeolite than in both sands, with 27% of injected colloids retained at an effective saturation of 0.75 and 56% at an effective saturation of 0.44, which agrees with previous work on colloid transport in unsaturated zeolitic tuff (Gamerding and Kaplan 2001a). Interestingly, the increase in mass retention in the zeolite between the saturated and intermediate saturation was similar in magnitude to that of either of the two sands. However, the mass retention increased significantly for the zeolite at the lowest saturation level.

Water flow in unsaturated soils is significantly constrained, and as a result transported colloids come in closer proximity to the soil-water and air-water interface. The air-water interface increases in area as moisture content decreases for soils undergoing drainage, and colloids may become immobilized at this interface (Chen et al. 2008; Saiers and Lenhart 2003a). Classic DLVO calculations predict repulsion between polystyrene microspheres and the air-water interface at all separation distances with no secondary minimum present due to the negative charge associated with the air-water interface

coupled with the negative Hamaker constant for polystyrene-air-water. However, the inclusion of hydrophobic interactions in extended DLVO theory have demonstrated that colloids can overcome electrostatic repulsion and become attached to the air-water interface (Bradford and Torkzaban 2008; Chen and Flury 2006; Grasso et al. 2002; Zevi et al. 2005). Although carboxylated polystyrene-latex microspheres are considered hydrophilic, a wide range of non-zero contact angles have been reported (Bradford et al. 2004; Sharma, Flury, et al. 2008; Wan and Wilson 1994b; Zevi et al. 2005). Additionally, pore scale visualization experiments in capillary channels have observed carboxylate microsphere attachment to the air-water interface (Lazouskaya and Jin 2008). Colloid immobilization at the air-water interface may in part explain the observed increase in effluent concentration in breakthrough curves in unsaturated experiments. Similarly shaped breakthrough curves have previously been attributed to attachment and blocking or filling of the air-water interface by colloids (Gargiulo et al. 2008; Lenhart and Saiers 2002; Zhuang et al. 2005).

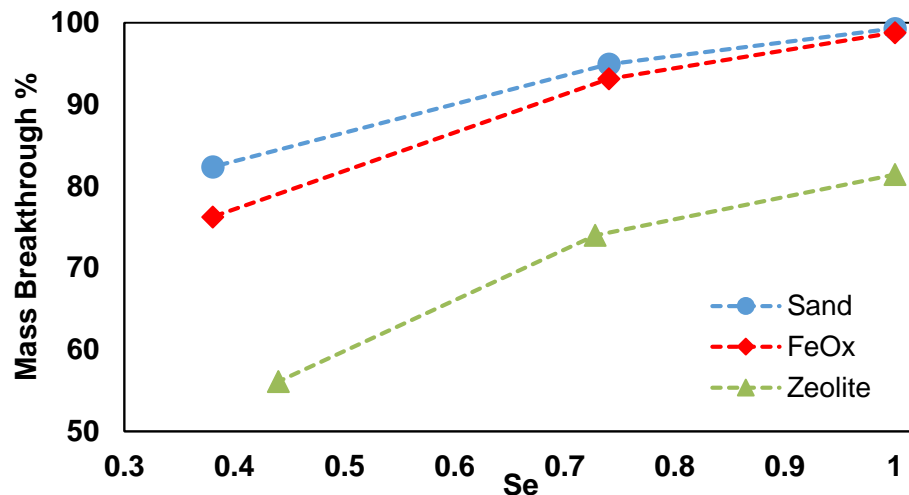


Figure 5.5: Mass of eluted colloids as measured by integration of the breakthrough curve at varying degrees of saturation.

Colloid transport in unsaturated porous media is significantly constrained, and immobilization can be the result of a wide range of mechanisms absent in saturated porous media (Bradford and Torkzaban 2008; DeNovio et al. 2004; Wan and Wilson 1994b). At suctions greater than the air entry value, water is increasingly constrained to pendular water and thin films surrounding soil grains. Colloids that are too large to pass through these thin films become immobilized. Straining in thin films surrounding the porous media becomes significant in the retention of colloids when the moisture content drops below a critical value and pendular water no longer connects (Tokunaga 2011). For close packed uniform spheres with a zero contact angle, the Laplace-Young equation shows that the critical suction at which pendular water connects is given as:

$$h_{critical} = \frac{B\gamma}{d_s}$$

where γ is the surface tension of water, and B is a constant related to the wetting conditions and soil wettability, and is equal to 12-18 for drying media (Fisher 1926; Tokunaga 2011; Wan and Tokunaga 1997). This corresponds to matric suctions well above 25 cm H₂O and effective saturations below 0.2 for sands, and 0.25 for zeolites. Although the non-uniformity of the soil grain size distribution of the soils as well as non-zero contact angles may have led to some localized film straining in the low saturation experiments, it is unlikely film straining played a critical role in colloid retention in any of the soils (Knappenberger et al. 2014). Researchers have observed that colloids can become trapped in hydrodynamic vortices in pendular water, where they can undergo aggregation or become immobilized near the air-water meniscus in a process that is similar in nature to film straining (Crist et al. 2004; Wan and Tokunaga 2005; Zevi et al. 2005, 2012). Temporary immobilization in pendular vortices may explain some of the tailing observed in unsaturated clean and iron oxide coated sand.

The increased tortuosity and constrained flow paths associated with unsaturated media will result in colloids coming in closer proximity to the soil surface and granular contacts (Mishurov et al. 2008; Torkzaban et al. 2008). Thus there is an increased likelihood of retention at granular contact points, rough asperities, or other locations that may be favorable to retention in unsaturated soils (Morales et al. 2009). This likely explains the increasing retention observed in iron oxide coated sands with decreasing saturation. The likelihood of immobilization near iron oxide coated portions of the soil surface increases under unsaturated conditions, as colloids pass in closer proximity to the soil water interface. Previous DLVO calculations demonstrated colloids may become immobilized in the secondary minimum under the pore water chemical conditions. Constrained flow paths in unsaturated zeolite likely drove increased retention in a similar fashion, with colloids becoming immobilized in the primary and secondary minimum as they come in close proximity to rough asperities on zeolite surface (Huang et al. 2010; Shen, F. Wang, Li, et al. 2012; Shen, Lazouskaya, et al. 2012).

Retention profiles for clean and iron oxide coated sand changed in a similar fashion as moisture content decreased. Attached colloid concentrations were relatively uniform under saturated conditions in both sands; however, retention profiles changed in shape as saturation decreased. At the intermediate saturation levels, retention profiles show increased retention near the top of the column before becoming relatively constant with depth. This effect is even more pronounced at the lower saturation level, with retained concentrations decreasing with depth. This stands in contrast with the observed decrease in moisture content with depth Figure 5.1, which would suggest that colloid retention would increase with depth as hydraulic flow becomes more constrained at lower depths. Higher levels of colloid retention near the inlet of sand experiments suggest that colloid retention near granular contacts may have been significant. Similarly shaped hyperexponential retention profiles in saturated sand have been attributed to colloid retention at granular

contacts, and this phenomena likely persists in unsaturated porous media (Bradford and Torkzaban 2008; Bradford et al. 2006; Fang et al. 2013). Although the colloid diameter to mean grain size ratio was smaller than values typically associated with straining, these straining ratios were estimated for colloid straining in saturated sand (Bradford et al. 2002; Knappenberger et al. 2014; Sang et al. 2013; Xu and Saiers 2009). Hyperexponential retention profiles were observed in all zeolite experiments, suggesting that colloid retention at granular contacts was important at all saturation levels. Indeed the immobilized colloid concentrations near the inlet at the lowest saturation experiment increased, suggests that retention near granular contacts became more important as saturation decreased in zeolite experiments, and may explain the large increase in retention as saturation decreases from the intermediate to low saturation level.

Visually identifiable systematic deviations occurred between observed and simulated breakthrough curves and retention profiles, despite R^2 values close to unity for modeled results (Table 5.3). Simulated breakthrough curves did not exhibit the same tailing behavior observed in clean and iron oxide coated sand; however, the inclusion of colloid detachment improved the fit visually and increased R^2 . Simulated retention profiles for both sands failed to capture the hyperexponential behavior observed, in part due to underestimating S_{max} . Nonetheless, estimated parameters can provide insight into processes taking place in the different soils (Goldberg et al. 2014). Estimated attachment coefficients increased with decreasing moisture content for sands, and were greater in iron oxide coated sand experiments. Greater attachment coefficients in iron oxide coated sand likely reflect increased colloid retention occurring in the secondary minimum near large iron oxide patches and at granular contacts (Shen et al. 2007). Estimated attachment coefficients for zeolite experiments were lower than in sands despite retaining greater mass fractions of injected colloids. This is likely do to the lower pore water velocity associated with unsaturated zeolite experiments (Tong and Johnson 2006).

Table 5.3: Fitted model parameters and calculated standard errors

Soil	S_e	K_a [min ⁻¹]	K_d [min ⁻¹]	S_{max} [N_T/N_i g ⁻¹]	R^2
Sand	1.0	0.0004 ± 0.0001	na	na	0.999
FeOx	1.0	0.0010 ± 0.0002	na	na	0.998
Zeolite	1.0	0.085 ± 0.003	na	0.76 ± 0.05	0.996
Sand	0.74	1.5 ± 0.19	0.05 ± 0.01	0.055 ± 0.008	0.997
FeOx	0.75	2.5 ± 0.15	0.02 ± 0.005	0.054 ± 0.003	0.999
Zeolite	0.73	0.58 ± 0.02	na	0.77 ± 0.04	0.995
Sand	0.38	3.1 ± 0.14	0.005 ± 0.001	0.068 ± 0.002	0.997
FeOx	0.37	3.6 ± 0.13	0.003 ± 0.001	0.090 ± 0.002	0.997
Zeolite	0.44	0.46 ± 0.02	na	0.86 ± 0.02	0.996

Note: N_T refers to recovered colloids in the sand, N_i refers to number of colloids in a unit volume of injected colloid suspension.

Tailing in the unsaturated sand breakthrough curves as well as estimated detachment coefficients suggest colloid retention was reversible (Torkzaban et al. 2006). Colloids may become temporarily retained in hydrodynamic vortices in pendular water, though tracer tests did not indicate the presence of immobile zones (Zevi et al. 2012; W. Zhang et al. 2010). More likely, the larger velocities in unsaturated sand experiments resulted in sufficient hydrodynamic drag to mobilize colloids retained at the soil water interface in the secondary minimum (Bergendahl and Grasso 2000; Pazmino et al. 2014; Sharma et al. 1992). Smaller detachment coefficients were estimated for the lowest saturation for both sands, which may be due to the lower pore water velocity associated with these experiments. No tailing was observed in unsaturated zeolite experiments, and estimated detachment coefficients did not improve agreement between simulated and observed breakthrough curves as assessed by R^2 . Less particle detachment occurred in zeolites due in part to the smaller pore water velocities, which in turn did not cause sufficient hydrodynamic drag to mobilize colloids (Bergendahl and Grasso 2000; Pazmino

et al. 2014). Higher hydrodynamic drag is required to detach colloids retained at rough asperities (Darbha et al. 2012; Shen et al. 2011).

The maximum amount of retained colloids, as measured by the fitted parameter S_{max} increased as saturation decreased for sands. Similar S_{max} values were estimated for clean and iron oxide coated sand at the intermediate saturation, while the estimated S_{max} was greater for iron oxide coated sand at the lowest saturation. This suggests that the number of preferential retention sites in sands increased as saturation decreased, and that at the lowest saturation level, a greater number of preferential retention sites were present in iron oxide coated sands. The increase in S_{max} associated with the iron oxide coated sand is presumably due to increased colloid retention at the soil water interface or near the air-water soil meniscus, as the air-water interface and pendular water configurations were very similar between clean and iron oxide coated sand. Estimated S_{max} values were significantly higher for all zeolite experiments than for any of the sand experiments. Large S_{max} values estimated for zeolite experiments are likely a function of the large specific surface area associated with the zeolite (Barton and Buchberger 2007; Ko and Elimelech 2000). Estimated S_{max} were similar for fully saturated zeolite and zeolite at the intermediate saturation level, but were higher for the lowest saturation level. This increase in S_{max} is likely due colloid flow paths becoming increasingly constrained as moisture content decreased, leading to greater retention at rough asperities (Mishurov et al. 2008; Torkzaban et al. 2008).

5.4 CONCLUSIONS

This chapter investigated the transport and retention of colloids in unsaturated soils that have traditionally been used in permeable reactive barriers to treat dissolved contaminants. Column transport experiments were conducted to assess the impact of saturation level on transport and retention of colloids in clean and iron oxide coated sand

and zeolite. Colloid mobility decreased in all soil types as saturation decreased. Retention of colloids most likely occurred at the soil water interface near granular contacts and the soil water meniscus, as saturation levels were insufficiently low for film straining to be significant. Colloid transport in clean and iron oxide coated sand was similar, although retention was slightly increased in iron oxide coated sand. The disparity in colloid retention between the two sand types became larger as saturation decreased and hydraulic flow brought colloids in closer proximity to the soil surface. Soil angularity and roughness likely contributed to colloid immobilization in zeolite, which retained significantly higher mass fractions of colloids at all saturation levels. This study demonstrates the potential benefit of including reactive media in water treatment systems operating in the vadose zone, where colloid mobility may be of concern.

CHAPTER 6:
THE MOBILIZATION OF COLLOIDS FROM PERMEABLE REACTIVE MEDIA
DURING DRAINAGE

6.1 INTRODUCTION

Iron oxide coated media and natural zeolites are used in reactive barrier systems to treat a wide range of dissolved contaminants (Benjamin et al. 1996; Färm 2002; Knox et al. 2008). In many instances these reactive barrier systems are subject to infiltration and drainage as in the case of storm water infiltration and filtering and bioinfiltration (Genç-Fuhrman et al. 2007; Mohanty et al. 2013; Pitcher et al. 2004; L. Zhang et al. 2010). While previous chapters have demonstrated that these materials are effective at retaining colloids under saturated and unsaturated steady-state flow conditions, in-situ retained colloids are readily mobilized by dynamic changes in saturation (Cheng and Saiers 2009; Lenhart and Saiers 2003; Shang et al. 2008). During such transient flow conditions, colloids can become attached to and mobilized by the air-water interface (Saiers et al. 2003).

Measurements of in-situ colloids mobilized from sands suggests that drainage may be more effective than wetting in mobilizing colloids (Cheng and Saiers 2009). Saiers et al. (2003) found that the amount of colloids scoured from sand by drying increased with the decreasing ionic strength of the porewater. It was found that as the discharge rate was increased, the probability of remobilization increased, an observation made by others (Chen et al. 2008; Zhuang et al. 2009). Bridge et al. (2009) used a flat 2D flow cell to observe the transport of colloids during drainage of sand and found that at low ionic strengths or drainage rate that particles tended to accumulate at the drying front, while at higher ionic strengths or drainage rate that mobilized particles were deposited over increasingly shorter distances. Aramrak et al. (2014) used confocal microscopy to observe

colloid transport in glass beads in response to wetting and drying front and observed similar behavior, with colloids retained in the secondary minimum being transported across the SWI. Mohanty et al. (2013) examined the effect of including iron oxide coated sand in bioinfiltration columns on bacteria transport during imbibition and found iron oxide sand greatly inhibited bacteria mobilization. However, their study was limited to a fixed ionic strength, pH, and hydraulic conditions.

The objective of this study is to examine the effect of porewater chemistry on the mobilization of retained colloids from iron oxide coated sand and zeolite columns by drainage. Colloid mobilization in these materials is compared to clean sand under varying ionic strength and pH. Additional experiments assess the impact of hydraulic flux, or drainage rate, on colloid mobilization from permeable reactive media under constant ionic strength and pH.

6.2 MATERIALS AND METHOD

6.2.1 Theoretical Considerations

For colloids to become mobilized from the soil-water interface during drainage it is necessary to overcome the force of attachment between the colloid and soil surface. The force of attachment due to DLVO interactions is given as:

$$F_{Attachment} = \frac{\partial \Phi_{DLVO}}{\partial h} \Big|_{1^{st}/2^{nd} minimum}$$

where Φ_{DLVO} was calculated using the expressions of Hogg et al. (1966) and Gregory (1981) for a spherical colloid and infinite flat plate as in previous chapters. The primary minimum was assumed to occur at 0.1 nm from the surface, while the location of the secondary minimum was taken directly from calculated interaction potential energies (Bradford and Torkzaban 2008; Bradford, Torkzaban, et al. 2013; Elimelech et al. 1995).

The driving force for colloid mobilization during drainage is attachment to the air-water interface. The maximum detachment force due to capillary forces associated with the air-water interface for a spherical colloid attached to a flat surface is given as (Lazouskaya et al. 2013; Noordmans et al. 1997; Sharma, Flury, et al. 2008):

$$F_{Detachment} = 2\pi\gamma r_c \sin^2\left(\frac{\theta}{2}\right) \cos \alpha$$

where γ is the water surface tension, r_c is the radius of the colloid, and θ and α are the colloid and soil surface contact angle respectively. The colloids were assumed to be hydrophilic and have an estimated contact angle of 30°, which is similar to values measured by others (Aramrak et al. 2013; Sharma, Flury, et al. 2008). The contact angle of the soils was assumed to be zero for all materials, which is conservative.

Table 6.1: DLVO Interaction Energies and Attachment Force Calculations

Media	pH	IS [mM]	ZP Colloid (mV)	ZP Soil (mV)	Primary Barrier (kT)	F _{Primary} (nN)	2 nd Min. location (nm)	F _{2nd-Min} (nN)
Sand	5.5	1	-62	-78	3150	35	113	1E-06
Sand	5.5	2	-62	-78	3120	35	75	3E-06
FeOx	5.5	1	-62	49	none	196	N/A	N/A
FeOx	5.5	2	-62	49	none	196	N/A	N/A
Zeolite	5.5	1	-62	-69	2878	33	112	1E-06
Zeolite	5.5	2	-62	-69	2836	33	74	3E-06
Sand	10	1	-49	-92	2330.1	38	114	1E-06
Sand	10	10	-40	-83	1513	35	33	5E-05
FeOx	10	1	-49	-41	1243	53	98	2E-06
FeOx	10	10	-40	-31	586	60	26	1E-04
Zeolite	10	1	-49	-70	2114.5	60	110	1E-06
Zeolite	10	10	-40	-57	1270	51	31	5E-05

6.2.2 Colloid and Porous Media Preparation

Manufactured carboxylated polystyrene microspheres (Bang Laboratories, Inc. Fishers, IN) 1 μm in diameter were used in all experiments. Residual surfactant from the colloid manufacturer was removed by triple rinsing the microspheres before suspending them in deionized water. All soils were sieved beforehand to have the same median grain size ($d_{50} = 0.36 \text{ mm}$) and coefficient of uniformity ($C_u = 1.82$). Silica sand (US Silica) was used as an unreactive media for comparison purposes. As in previous chapters, the sand was subject a rigorous cleaning procedure which included repeated ultrasonification, soaking in sodium dithionite, hydrogen peroxide, and nitric acid, and rinsing with DI over a #200 sieve to minimize any effects of geochemical heterogeneity on colloid mobility. Iron oxide coated sands were prepared from cleaned silica using the heterogeneous suspension method, and had an iron oxide coated content of 1.4 mg/g (Larrahondo et al. 2011; Scheidegger et al. 1993). Crushed clinoptilolite zeolitic tuff (St. Cloud Zeolite, MN) composed was used for all zeolite experiments. Zeolites were ultrasonicated in deionized water for an hour, then repeatedly rinsed over a #200 sieve.

6.2.3 Column Mobilization Experiments

Experiments consisted of two stages, with the first stage involving injecting colloids into a saturated soil specimen under varying ionic strength and pH, and the second stage involved draining the soil specimen at constant hydraulic flux to mobilize retained colloids. Saturated soil samples were introduced to an acrylic flow cell ($L=10 \text{ cm}$, $ID=5 \text{ cm}$) using the modified slurry deposition procedure described in previous chapters and densified to 0.37-38 porosity for sands and 0.58-0.6 for zeolites (Bandini and Sathiskumar 2009; Carraro et al. 2003; Wood et al. 2008). Both ends of the flow cell were capped with stainless steel plates with 1 mm holes and supported by hydrophilic nylon mesh membranes with 10 μm openings (U-CMN-10, Component Supply Company).

In the first stage of the experiment the pore fluid was pumped (Cole Parmer Masterflex L/S) downward through the column at a Darcy velocity of 0.24 cm/min. Experiments were carried to assess the impact ionic strength (IS) and pH on colloid mobilization. pH 5.5 solutions were prepared with HCl, and NaCl was used to increase the ionic strength to 1 and 2 mM. pH 10 solutions were prepared with 0.2 mM Na₂CO₃ and NaCl was used to adjust the ionic strength to 1 and 10 mM. Columns were pre-equilibrated by first passing 15 solutions of background electrolyte. Columns were seeded with colloids by injecting the equivalent of 6.7 mg of colloids at a concentration of 30 mg/L (5.6×10^7 particles/L). Note that this differs from previous saturated and unsaturated steady-state experiments where the absolute mass of injected colloids varied due to the different porosities of zeolite and sands. An additional three pore volumes of background electrolyte were passed through the column to assess any colloid detachment or tailing.

The second stage of the experiment consisted of draining the saturated soil column to mobilize colloids retained during the transport stage of the experiment. The top end cap and nylon membrane were removed from the flow cell, exposing the soil surface to the atmosphere. Flow cells were drained from the bottom using a peristaltic pump at a constant hydraulic flux of 0.24 cm/min. Additional experiments were carried out at a high and low hydraulic flux to assess the impact of drainage rate on colloid mobilization. These experiments involved seeding the soil column with colloids at pH 10 and 10 mM IS. Columns were drained at 0.36 cm/min for high flux experiments and 0.08 cm/min for low flux experiments. The experimental matrix along with measured masses of colloids are summarized in Table 6.2. Effluent samples during both stages of the experiments were collected using a fraction collector (ISCO Retriever II) and colloid concentrations were measured by UV-Vis spectrophotometry (Shimadzu UV/1800) at 435 nm.

Table 6.2: Experimental Conditions

Media	pH	IS [mM]	q_{Drain} [cm/min]	M_{Injected} (mg)	$M_{\text{Deposited}}$ (mg)	$M_{\text{Mobilized}}$ (mg)
Sand	5.5	1	0.24	6.61	0.39	0.019
Sand	5.5	2	0.24	6.65	1.09	0.030
Sand	10	1	0.24	6.75	0.06	0.033
Sand	10	10	0.08	6.71	1.38	0.027
Sand	10	10	0.24	6.66	1.39	0.047
Sand	10	10	0.36	6.75	1.36	0.093
FeOx	5.5	1	0.24	6.73	1.68	0.017
FeOx	5.5	2	0.24	6.73	5.76	0.007
FeOx	10	1	0.24	6.61	0.12	0.039
FeOx	10	10	0.08	6.72	2.30	0.016
FeOx	10	10	0.24	6.69	2.26	0.043
FeOx	10	10	0.36	6.74	2.23	0.102
Zeolite	5.5	1	0.24	6.69	1.66	0.015
Zeolite	5.5	2	0.24	6.69	4.37	0.013
Zeolite	10	1	0.24	6.69	1.26	0.027
Zeolite	10	10	0.08	6.66	5.47	0.008
Zeolite	10	10	0.24	6.73	5.52	0.010
Zeolite	10	10	0.36	6.71	5.48	0.021

NOTE: IS refers to ionic strength and q_{Drain} is the drainage rate or flux. M_{inj} refers to mass of colloids injected during the first stage of the experiment as measured by the effluent curve, $M_{\text{Deposited}}$ refers to mass of colloids attached to soil as measured by integration of the effluent curve, and $M_{\text{Mobilized}}$ refers to the mass of mobilized colloids during the second stage of the experiment.

6.3 RESULTS AND DISCUSSION

In the first stage of the experiment, colloids were injected into saturated soil columns at a constant Darcy velocity of 0.24 cm/min at varying pH and ionic strength. Clean sand colloid breakthrough curves were similar in shape under all conditions, with a rapid rise in effluent concentration to a constant peak value, before declining back to zero in a symmetrical fashion (Figure 6.1). No tailing was observed in colloid effluent curves in sands suggesting that hydrodynamic drag was insufficient to detach and reentrain colloids during the saturated portion of the experiment. Peak effluent concentrations in sand

experiments decreased with ionic strength at low and high pH. DLVO calculations demonstrate that colloid retention occurred in the secondary minimum, and that the depth of the secondary minimum increased with ionic strength. The breakthrough curve for high pH and high ionic strength include error bars demarking the standard deviation between the low, medium and high flux experiments. Although some variability was observed in the rising and tailing section of the breakthrough curve between replicates, peak effluent concentrations were constant indicating a high degree of repeatability in experiments.

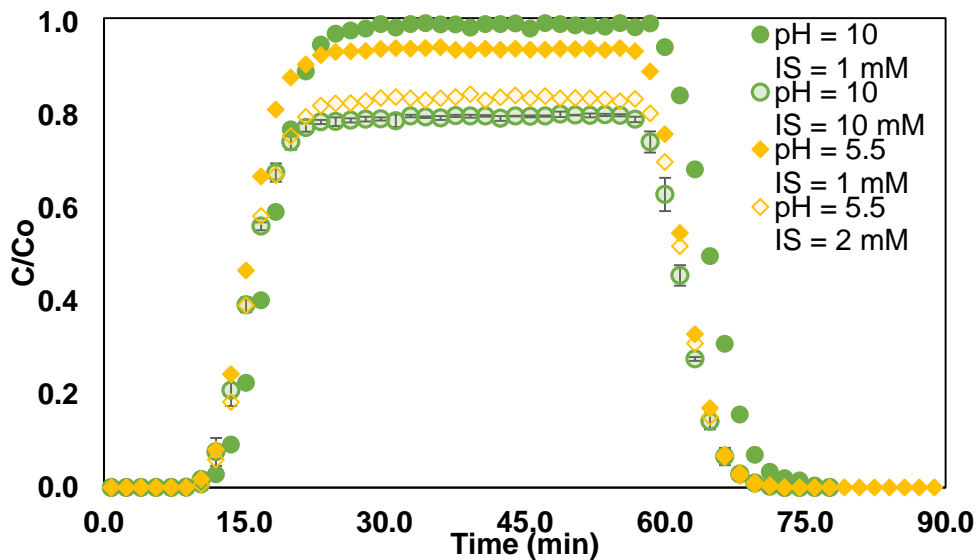


Figure 6.1: Measured effluent colloid concentration breakthrough curves in saturated clean sand under varying ionic strength and pH during first stage of experiment. Error bars are the standard deviations from three replicates. C_o is the concentration of the injected colloids.

Colloid breakthrough curves in iron oxide coated sand at low pH were similarly shaped to those of clean sand, though peak effluent concentrations were lower in iron oxide coated sand (Figure 6.2). Colloids are attracted to the oppositely charged iron oxide coating in low pH experiments resulting colloid attachment in the primary minimum.

Additional colloid attachment likely occurred on uncoated portions of the iron oxide sand in the secondary minimum, as colloid retention was observed in clean sands at low pH (Shen et al. 2007; Song et al. 1994). Breakthrough curves in iron oxide coated sand differed at high pH with effluent concentrations gradually increasing over time. The effluent concentration increased more rapidly in the iron oxide sand experiment at pH 10 and high IS. The difference of colloid retention behavior in iron oxide coated sand at high and low pH is likely reflective of the heterogeneous, patchy nature of the iron oxide coated sand (Bendersky and Davis 2011). DLVO calculations demonstrate that in high pH experiments colloid attachment occurred in the secondary minimum at both iron oxide patches and on uncoated portions of the soil surface; however, the primary energy barrier is smaller and the secondary minimum is deeper for colloids approaching iron oxide patches. Similarly shaped breakthrough curves have often been associated with blocking behavior, suggesting that a portion of the iron oxide patches may have acted as preferential colloid attachment sites in high pH experiments (El Badawy et al. 2013; Bolster et al. 2001; Johnson et al. 1996; D. Wang et al. 2013).

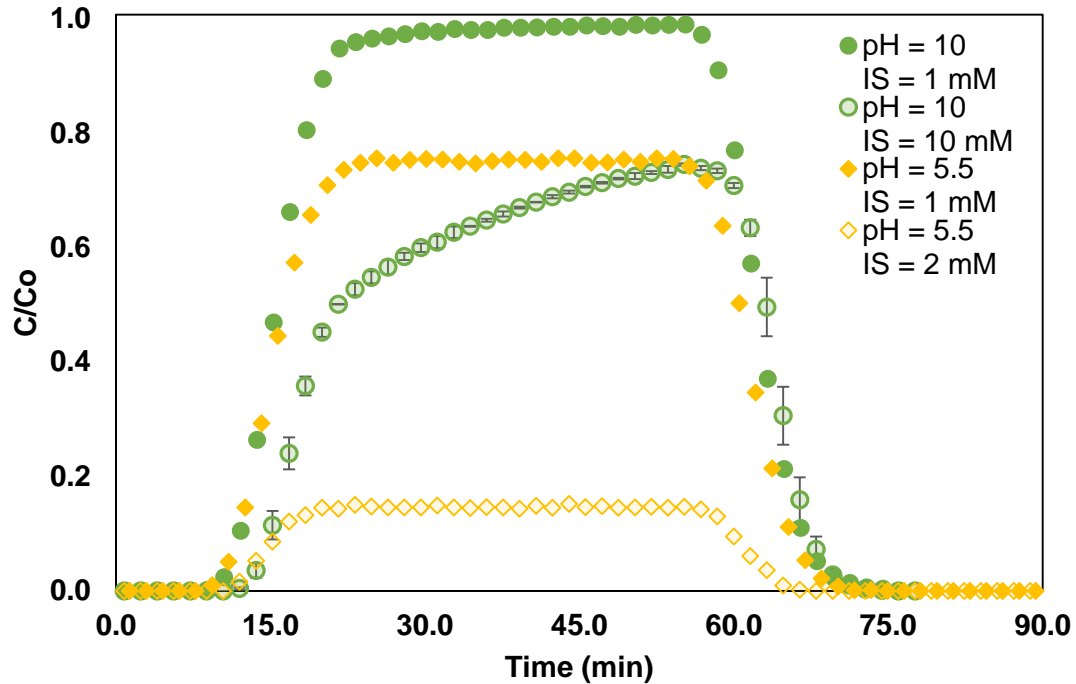


Figure 6.2: Measured effluent colloid concentration breakthrough curves in saturated iron oxide coated sand under varying ionic strength and pH during first stage of experiment. Error bars are the standard deviations from three replicates.

Colloid breakthrough occurred later in time in zeolite experiments due to the greater porosity and smaller average velocities, and breakthrough curves differed in shape from most sand experiments (Figure 6.3). Greater mechanical dispersion is evident in both the first arrival of colloids and the tailing section of the breakthrough curve. In the middle portion of the breakthrough curves, effluents increase in a nearly linear fashion, similar to the colloid breakthrough curve observed in iron oxide coated sand under high pH and high ionic strength. DLVO calculations suggest colloid interaction with the zeolite should be similar to that of clean sands, with a large barrier to deposition in the primary minimum, and a shallow secondary minimum. Colloid retention in zeolite at lower pH experiments may have occurred in the primary minimum near any metal oxides present on the zeolite surface, as pH 5.5 is below the isoelectric point of many minerals, and

zeolites were not chemically cleaned like sands (Parks 1965). However, as was discussed in the previous chapters, the high angularity of the zeolite grain and the micro and nanoscale roughness associated with crystalline structures present on the soil surface likely contributed significantly to colloid retention in zeolite experiments.

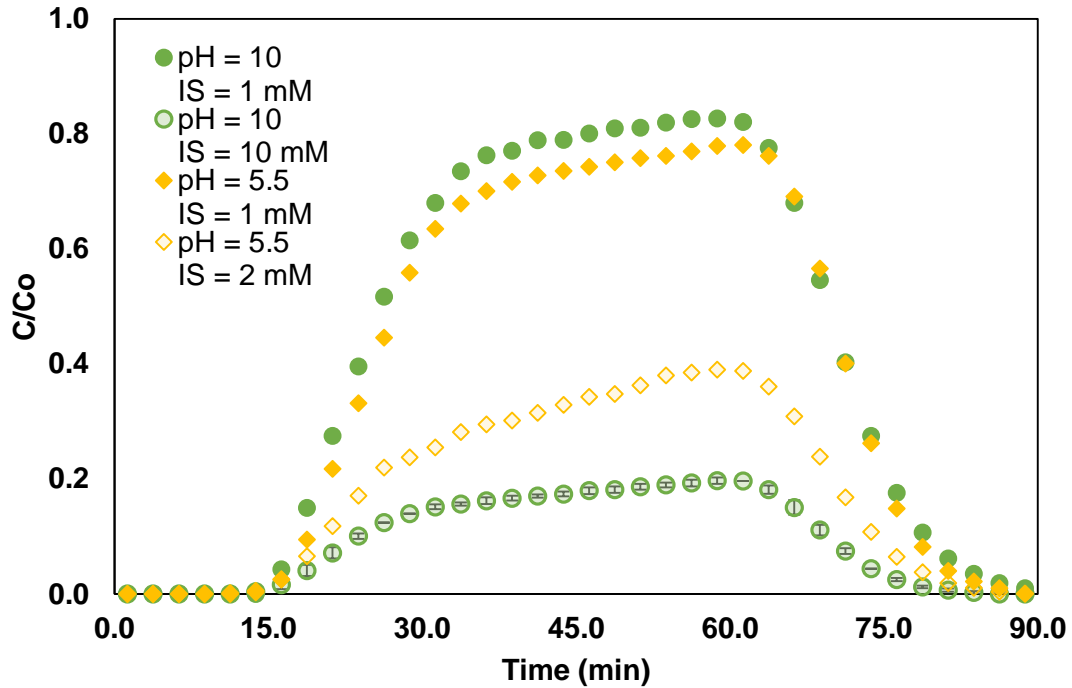


Figure 6.3: Measured effluent colloid concentration breakthrough curves in zeolite under varying ionic strength and pH during first stage of experiment. Error bars are the standard deviations from three replicates.

Colloid retention between the three soil types under the varying porewater chemistries is summarized in Figure 6.4. At low pH and low IS zeolite and iron oxide coated sand retained similar quantities of colloids. Colloid retention for both materials increased as ionic strength increased in low pH experiments, with greater attachment taking place in iron oxide coated sand. Colloid retention in clean sand was significantly lower than in zeolite and iron oxide coated sand in low pH experiments, and this disparity

increased as ionic strength increased. Colloid retention in high pH, low IS experiments was extremely low in both sands, while retention in zeolites was significantly greater. As in the case of low pH experiments, increasing ionic strength resulted in greater colloid retention in all materials, with the highest retention occurring in zeolite experiments, followed by iron oxide coated sand and clean sand.

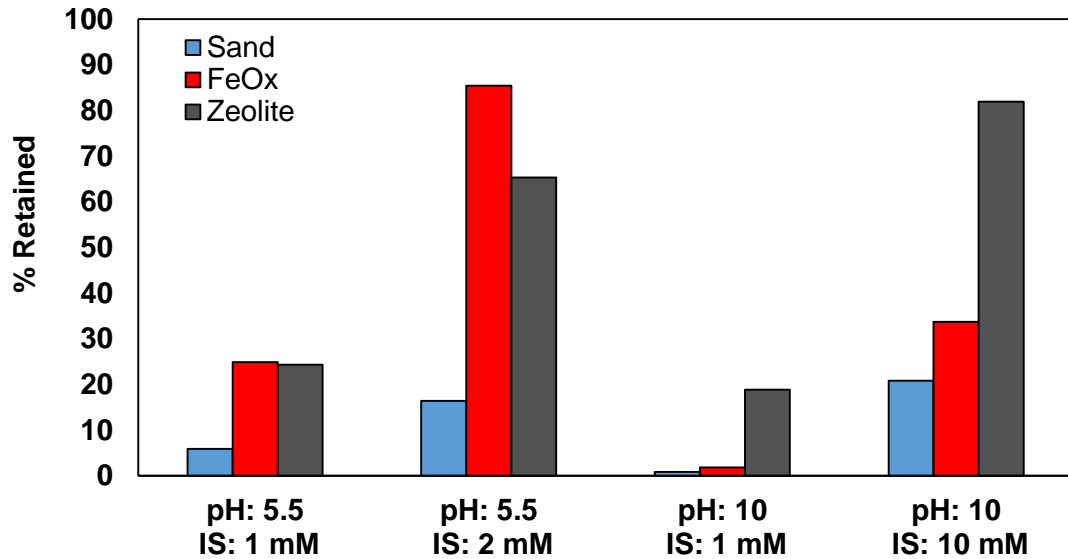


Figure 6.4: Percent mass of retained colloids (mass of retained colloids as measured by integration of the breakthrough curve divided by the injected mass of colloids) for all soil types under varying ionic strength and pH. Retained mass calculated from integration of the breakthrough curve.

Appreciable quantities of colloids were mobilized from all soil types during the drainage portion of the experiment. Effluent colloid concentrations curves measured during the drainage portion were qualitatively similar in all experiments across all material types (Figure 6.5-7). Effluent concentrations were below detectable limits until after the 6.5 minute mark in most sand experiments and around the 8 minute mark in zeolite experiments. The later arrival in zeolite drainage experiments is consistent with

observations in the saturated transport portion of the experiment and is due to the smaller average porewater velocities. After the first arrival of colloids at the outlet, concentrations increased continuously and rapidly before reaching a peak values between 3% and 27% of the injected colloid concentration.

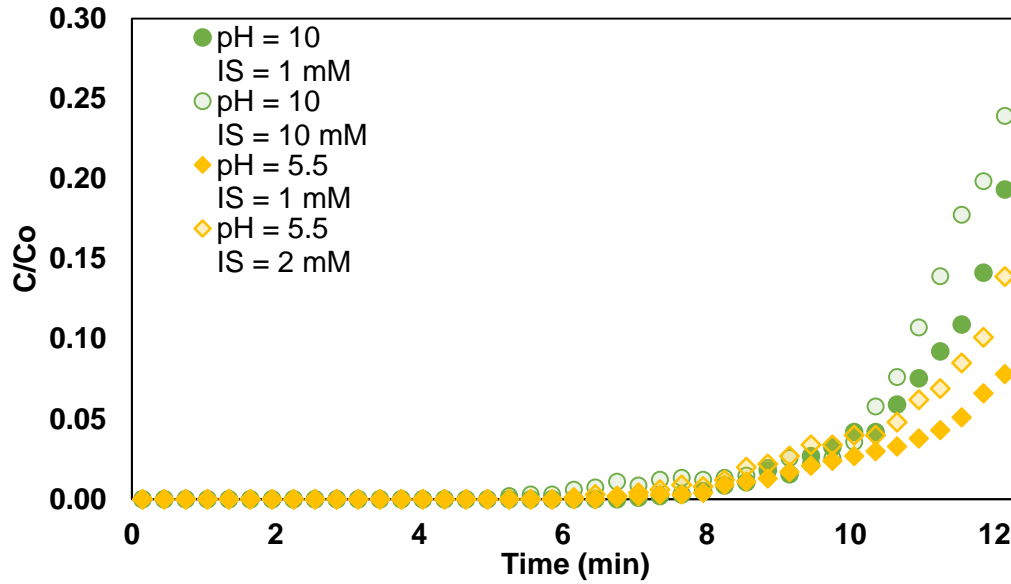


Figure 6.5: Measured drainage effluent colloid concentrations in clean sand under varying ionic strength and pH during second stage of experiment.

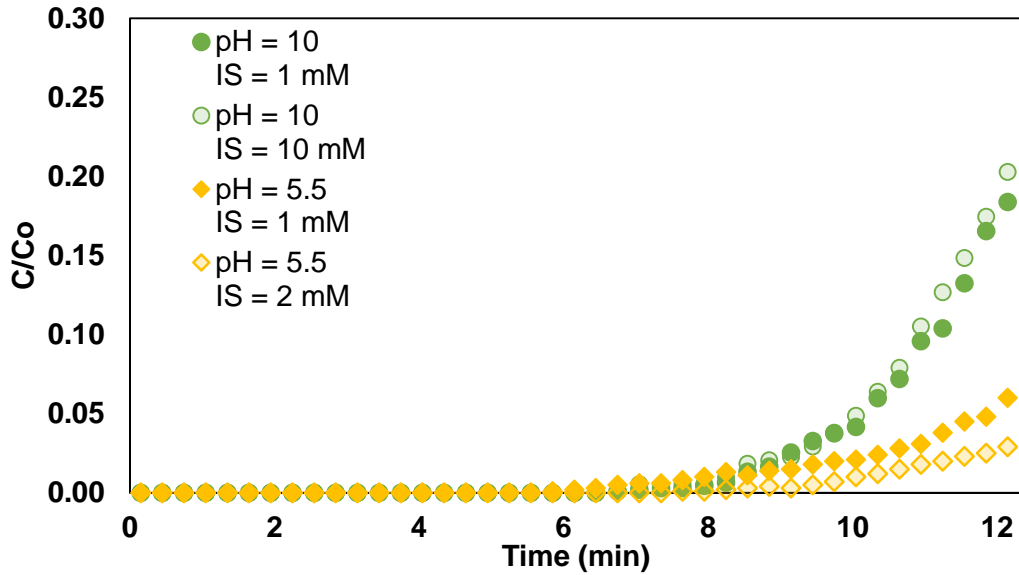


Figure 6.6: Measured drainage effluent colloid concentrations in iron oxide coated sand under varying ionic strength and pH during second stage of experiment.

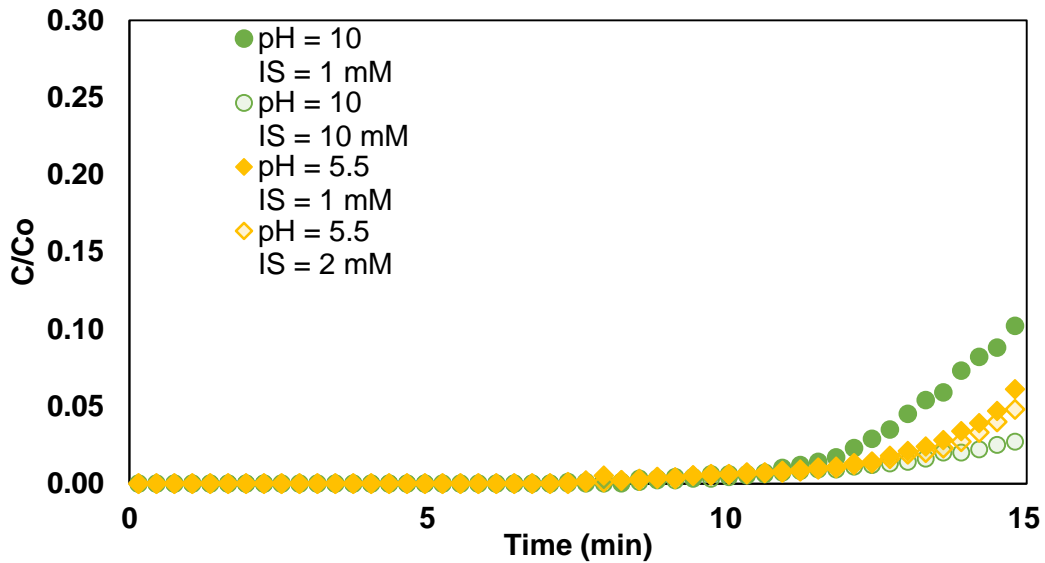


Figure 6.7: Measured drainage effluent colloid concentrations in zeolite under varying ionic strength and pH during second stage of experiment.

The absolute mass of mobilized colloids along with mass fractions of mobilized colloids for varying porewater chemistries are shown in Figure 6.8. The mass fraction of mobilized colloids in the low pH, low IS experiment set was highest in clean sand, followed

by iron oxide coated sand and zeolite. This stands in contrast to the similar absolute masses of colloids mobilized in all materials. The fraction of mobilized colloids decreased with increasing ionic strength for low pH experiments in all materials, with clean sand having the greatest fraction mobilized followed by zeolite and iron oxide coated sand in the high IS experiment set. The absolute mass mobilized increased in clean sand for the higher IS experiment set, while the mobilized mass decreased slightly in zeolite and dropped significantly in iron oxide coated sands.

The absolute mass of mobilized colloids was higher for all materials in the low IS, high pH experiment set, with the greatest mobilization taking place in iron oxide coated sand followed by clean sand and zeolite. Coupled with the relatively low colloid retention in the saturated portion of the experiment, this led to extremely high mobilized fractions in both sands, with 60% of retained colloids mobilized from clean sand and 32% of colloids mobilized from iron oxide coated sand. The absolute mass and mass fraction for zeolite was greatest under this porewater chemistry; however, colloid mobilization was still significantly lower in zeolite than either sand. The mass fraction of mobilized colloids decreased for all materials with increasing IS in high pH experiments, similar to observations in the low pH experimental set. The absolute mass of mobilized colloids increased in clean sand, but this was offset by greater retention in the saturated transport stage of the experiment. This agrees with previous observations of kaolinite mobilization from drained sands (Saiers et al. 2003). Unlike in low pH experiments, the mass of mobilized colloids in iron oxide coated sand increased at the higher IS, similar to observations made in clean sand. The absolute mass of mobilized colloids decreased sharply with increasing IS in high pH experiments.

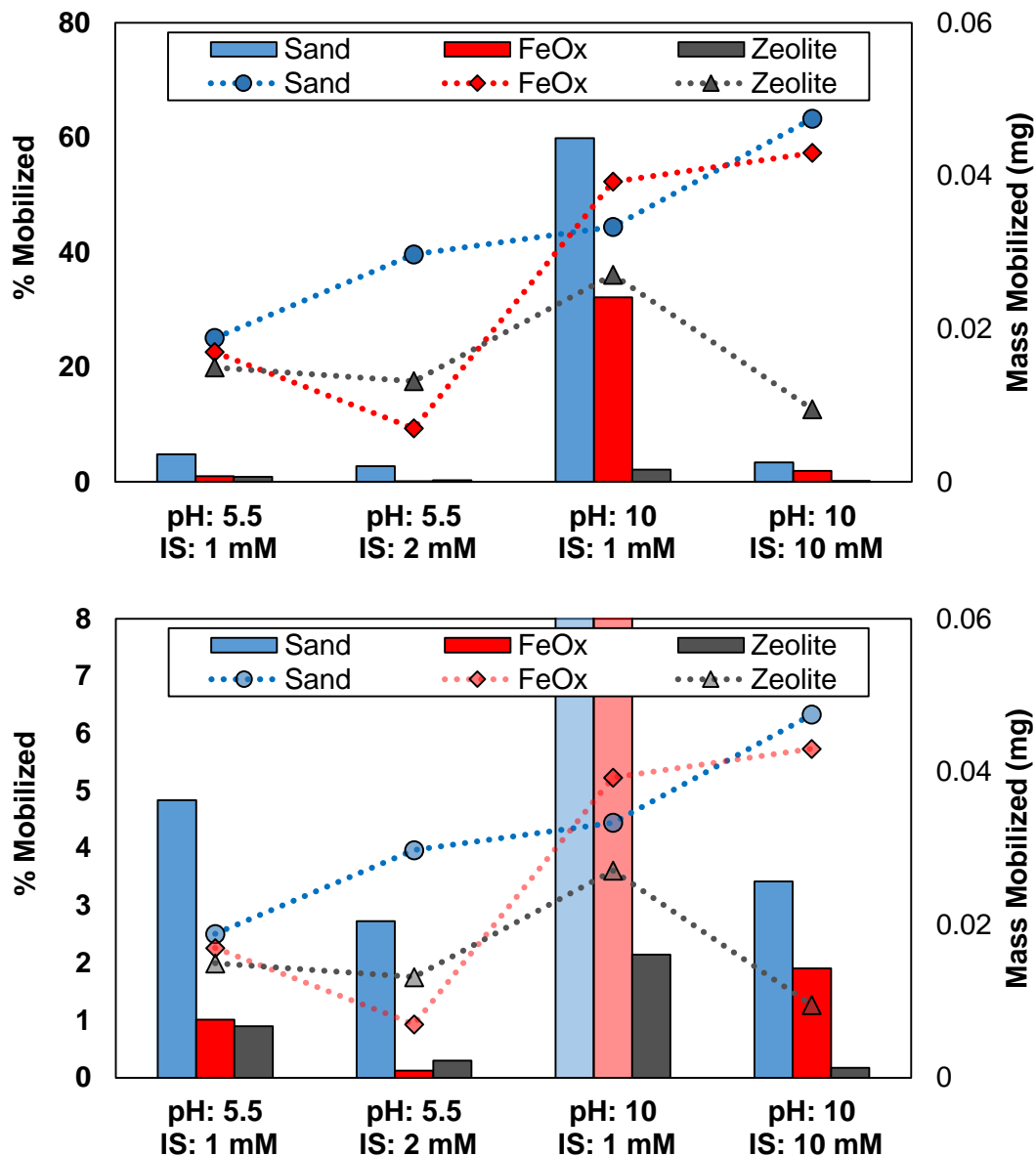


Figure 6.8: Top and Bottom: Percent mass of mobilized colloids (bars, left axis) compared with actual mass of mobilized colloids (lines, right axis) for all soil types under varying pH and ionic strength. Bottom portion of figure has cropped percent mobilized (left) axis to allow for easier comparison in low mobilization experiments.

The maximum detachment force exerted on a colloid deposited on the soil surface by an air-water interface was calculated to be approximately 15 nN. Attachment forces for colloids retained in the primary and secondary minimum are summarized in Table 6.2. The attachment force for colloids retained in the secondary minimum is 4-6 orders of magnitude smaller than the estimated capillary force. This explains the greater masses of mobilized colloids in clean sands, as colloids were retained in the secondary minimum for all porewater chemistries. Colloids attached to the soil surface in the primary minimum were unlikely to be detached by the capillary force associated with air-water interface as the attachment force is greater than the detachment force. The colloids mobilized from iron oxide coated sands in low pH experiments were likely initially attached to smaller iron oxide patches as well as uncoated portions of the sand surface. Increasing IS in low pH experiments likely resulted in greater retention in the primary minimum for iron oxide coated sands, thus explaining the large decrease in colloid mobilization. Interestingly, although colloids were mobilized from iron oxide coated sand in greater quantities in high pH experiments than compared to low pH experiments, it still out performed clean sand in terms of retention during drainage in high IS experiments. That is, the absolute mass mobilized from iron oxide coated sand was lower than clean sand despite DLVO calculations predict retention in the secondary minimum for both materials. The smaller energy barrier coupled with the rough nature of the iron oxide coating may have resulted in some colloid retention in the primary minimum in high pH/IS experiments, thus decreasing the absolute mass of mobilized colloids from iron oxides.

The absolute mass of mobilized colloids in zeolites was lower than all other materials except for in the low pH, high IS experiment set in which less colloids were mobilized from iron oxide coated sand. This suggests that some colloids may have been retained in the primary minimum in zeolite. Colloid retention may have occurred under low pH conditions in the primary minimum near any metal oxides present on the surface,

however these interactions would be significantly reduced in high pH experiments. Extended DLVO interaction calculations for colloid interaction at rough surfaces have demonstrated that colloids can become immobilized in the secondary and primary minimum near asperities, and that the retention of colloids near rough features is increased at higher ionic strengths (Huang et al. 2010; Shen, F. Wang, Li, et al. 2012). Colloids retained near rough asperities are less prone to detachment by perturbations in porewater IS and velocity (Bradford, Torkzaban, et al. 2013; Shen et al. 2011). Colloids deposited at rough asperities may be less prone to detachment by an air-water interface during drying as well. Colloids retained near granular contacts in zeolite may have been less prone to mobilization during drying as it is unlikely that the air-water interface would come in contact with colloids in this region before film straining inhibited colloid transport (Wan and Tokunaga 1997).

Colloid concentration curves measured during the second stage of the experiment in all soil types for varying drainage flux are shown in Figure 6.9 for high pH/IS porewater chemistry. Colloids arrived at the outlet earlier in time for high flux experiments and significantly later in time for low flux experiments as expected. Colloid arrival at the outlet occurred slightly later in time for all zeolite drainage concentration curves due to the higher porosity of the soil, similar to colloid breakthrough curves in the saturated transport stage. Drainage concentration curves were similar in shape for high and medium flux experiments, however peak concentrations were lower in medium flux experiments. Low flux experiments exhibited a much more gradual increase in drainage concentrations and significantly lower peak concentrations were observed than in high and medium flux experiments.

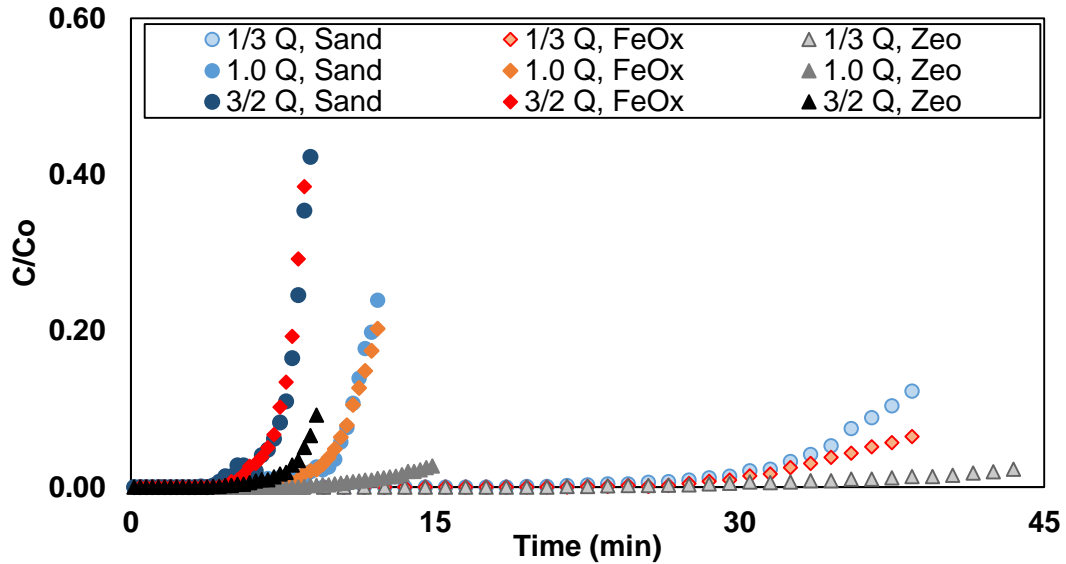


Figure 6.9: Effluent colloid concentrations measured during drainage at varying hydraulic flux. Q is normalized flux, $Q = q_{\text{experiment}}/q$, where q is the hydraulic flux (0.24 cm/min) during the saturated portion of the experiment. All experiments were carried out at IS = 10 mM and pH = 10.

The absolute mass of mobilized colloids along with mass fractions of mobilized colloids for varying flux are shown in Figure 6.10. The mass fraction of mobilized colloids increased with increasing flux for all materials, and was highest in clean sand and lowest in zeolites by a large margin. Colloid mobilization by increased hydraulic fluxes have been observed by others (Bridge et al. 2009; Chen et al. 2008; Saiers et al. 2003; Zhuang et al. 2009). The absolute mass of colloids mobilized increased with flux for both sands, and was smaller in iron oxide coated sands at low flux and greater at high flux as compared to clean sand. The mass of colloids mobilized from zeolite was nearly constant at low and medium flux, but increased slightly in the high flux experiment.

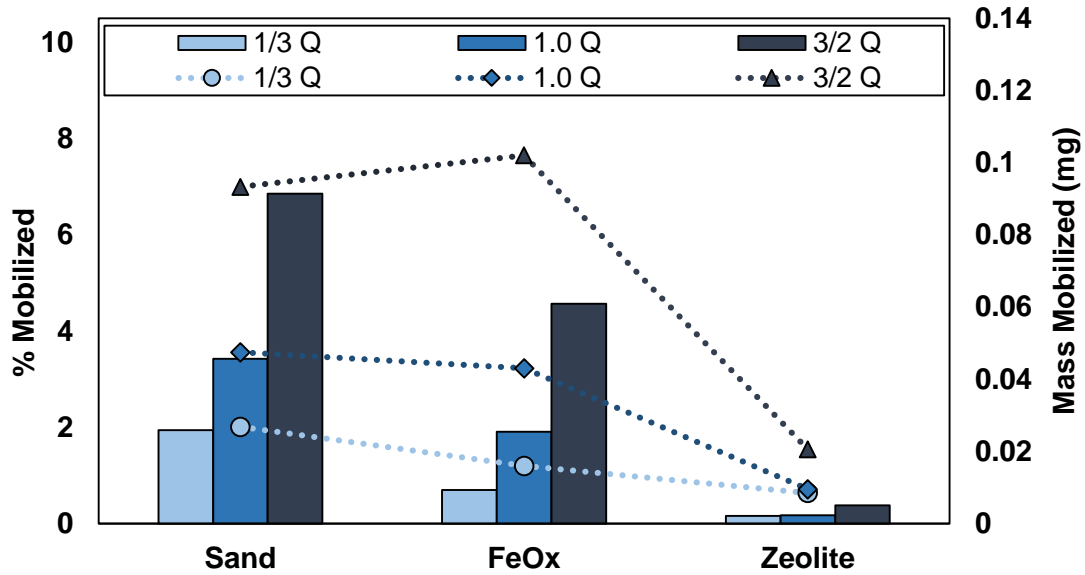


Figure 6.10: Percent mass of mobilized colloids (bars, left axis) compared with actual mass of mobilized colloids (lines, right axis) for all soil types under varying hydraulic flux. Q is normalized hydraulic flux, $Q = q_{\text{experiment}}/q$, where q is the hydraulic flux (0.24 cm/min) during the saturated portion of the experiment. All experiments carried out at IS = 10 mM, pH = 10.

The sensitivity of colloid mobilization to flux suggests that in addition to detachment by capillary forces associated with the air-water interface, colloid detachment may have been caused by hydrodynamic drag during drainage. Various porescale visualization experiments have observed that colloids are transported along the soil surface during drainage and can undergo multiple attachment/detachment cycles (Aramrak et al. 2014; Bridge et al. 2009). Although no hydrodynamic detachment was observed during the saturated stage of experiments, in the drainage stage of the experiment the average porewater velocity increased significantly over time as the moisture content decreased. Spherical colloids mobilized by hydrodynamic drag will roll on a collector surface (Sharma et al. 1992). This may explain the smaller masses mobilized in iron oxide coated sand in low flux experiments, as colloids retained in high shear zones may have been transported

to more favorable retention sites such as near large iron oxide patches or granular contacts, thus limiting further mobilization during drainage. High flux experiments may have yielded sufficient hydrodynamic drag to negate this advantage for iron oxide coated sands, resulting in greater mobilization than was observed in clean sand.

Despite similar fluxes in all experiments, average porewater velocities were lower in zeolite than in other materials. This may explain the small increase in colloid mobilization in the high flux experiment. The lower sensitivity to colloid mobilization by changes in hydraulic flux in zeolite experiments is in line with colloid attachment near rough asperities. As has been discussed previously, colloids initially attached to rough asperities may be retained in the primary minimum even under unfavorable conditions (Shen et al. 2011; Shen, Lazouskaya, et al. 2012). Similar to the mechanism proposed in iron oxide coated sands, colloids mobilized by hydrodynamic drag may have rolled to rough locations where they were less likely to be mobilized by the air-water interface.

6.4 CONCLUSIONS

This study highlights the effect of porewater chemistry and hydraulic flux on the mobilization of colloids from permeable reactive media during drainage. Colloid mobilization was lower for all materials during drainage in low pH experiments, and the absolute mass of mobilized colloids decreased with increasing IS for iron oxide coated sand and zeolite. Low colloid retention during high pH, high IS experiments resulted in large mass fractions of mobilization taking place in clean and iron oxide coated sand. The absolute mass of mobilized colloids increased with IS in high pH clean and iron oxide coated sand, but the greater retention in the saturated stage of the experiment led to a decrease in the mass fraction mobilized. The mass fraction of mobilized colloids was highest in clean sand for all porewater chemistries, and the absolute mass mobilized highest in all but the high pH, low IS experiment set. The absolute mass and mass fraction

of colloids mobilized was lowest in zeolite under all porewater chemistries except in the low pH, low IS experiment set.

Colloid mobilization in all materials increased with hydraulic flux. The mobilized mass fraction for the varying hydraulic fluxes was greatest in clean sand, followed by iron oxide coated sand and zeolite. Smaller quantities of colloids were mobilized from iron oxide coated sand than in clean sand for low flux experiments; however this was reversed in high flux experiments, with a greater mass mobilized from iron oxide coated sands. Colloid mobilization in zeolites was less sensitive to changes in hydraulic flux, and the absolute mass and mass fraction of mobilized colloids was significantly lower than in clean and iron oxide coated sand.

The work in this chapter highlights the potential benefit of including reactive media in filters subject to drainage, such as in the case of bioinfiltration systems and stormwater filters. The reduced mobilization of colloids by drainage in iron oxide coated sand and zeolites suggests that these materials are more likely to act as a colloid sink during intermittent flow than clean sand. Additionally the low sensitivity to pH suggest that zeolite is a particularly suitable material for this purpose.

CHAPTER 7:

THE EFFECT OF IONIC STRENGTH ON THE TRANSPORT AND RETENTION OF SPHERICAL AND ELLIPSOIDAL COLLOIDS IN SATURATED POROUS MEDIA

7.1 INTRODUCTION

Engineers and scientists typically use spherical colloids as model particles in bench scale experiments (e.g. Auset and Keller 2006; Elimelech and O'Melia 1990; Pazmino et al. 2014; Ramachandran and Fogler 1999; Tufenkji et al. 2006). Despite the valuable information that can be gained from the use of model particles, most natural and engineered colloids have distinctly non-spherical diverse shapes and geometries that can affect their behavior in the subsurface. Mineral colloids such as clays are often plate-like, while precipitated metal oxides such as goethite can be needle-like (Mitchell and Soga 2005). Single and multiwall carbon nanotubes are nonspherical, high aspect ratio colloids that have received recent attention and have been shown to be mobile in porous media (Mekonen et al. 2014; Y. Wang et al. 2012). Bacteria and viruses are ubiquitous in the subsurface, and come in varied shapes including spherical coccus, ellipsoidal bacillus, and high aspect ratio spirillum (Bradford, Morales, et al. 2013; Madigan et al. 2010; Sen 2011).

Despite the numerous studies citing the importance of colloid shape in explaining results of column transport experiments, very few studies have explicitly investigated its significance in natural systems (Baltus et al. 2009; Becker et al. 2003, 2004; Castro and Tufenkji 2008; Dong et al. 2002; Fontes et al. 1991). Several studies have examined the role of colloid shape in transport and retention by using shape modified polystyrene-latex microparticles, which allow for easy control of colloid surface properties. Salerno et al. (2006) investigated the transport of spherical and ellipsoidal carboxylate polystyrene-latex particles (aspect ratio of 1:2; 1:3) and found that as the aspect ratio of the colloid

increased, overall retention and collision efficiency increased proportionally under both favorable and unfavorable conditions. Liu et al. (2010) examined the retention and subsequent release by perturbations in ionic strength of high aspect ratio (1:7) rods in saturated glass beads. Spheres were retained in greater quantities than the rod shaped colloids, which stands in contrast to the observations of Salerno et al. (2006). Xu et al. (2008) utilized peanut shaped colloids under unfavorable conditions to investigate the role of colloid shape in straining in saturated sand. Their experimental observations, coupled with pore scale hydrodynamic simulations, demonstrated that the minor axis length of elongated colloids controlled size based retention behavior. Seymour et al. (2013) measured the kinetics of attachment of spheres and ellipsoids (1:2 and 1:4) to a silica collector using a quartz crystal microbalance under varying ionic strengths and found that the attachment rate of spheres was higher than that of the ellipsoidal particles. However, when transported through glass beads, the higher aspect ratio colloids were retained in greater numbers than spherical colloids.

The preceding discussion demonstrates that even when colloid shape is controlled in the lab, its role in the transport and retention porous media is not entirely understood. In this study, the effect of colloid shape on retention in saturated graded sand was examined using column transport experiments with spherical and ellipsoidal colloids. This study examines the effect of ionic strength on the interaction energies at the colloidal scale as well as its impact on the retention of spheres and ellipsoids in sand at the bench scale.

7.2 MATERIALS AND METHOD

7.2.1 Colloid and Porous Media Preparation

Manufactured carboxylated polystyrene microspheres (Bang Laboratories, Inc. Fishers, IN) 1 μm in diameter were used in this study. These uniform spherical particles were modified into ellipsoidal rods using the method proposed by Ho et al. (1993) and

later generalized by Champion et al. (2007). A 10% (wt/vol) solution of polyvinyl alcohol (PVA) was created by dissolving PVA in deionized water at 85°C. Colloids were added to the PVA solution, resulting in a concentration of 0.1% (wt/vol) spheres. The resulting mixture was then poured onto a flat 20 cm square glass surface and the excess water was allowed to evaporate (12-18 hours to dry) resulting in an approximately 70 μm thick film of colloid impregnated polyvinyl alcohol. The dried film was then cut into 3 cm x 6 cm sections and placed on a mechanical stretcher. The films were submerged in a mineral oil bath at 125°C for five minutes, then mechanically stretched while submerged in mineral oil. This temperature is above the glass transition temperature of polystyrene latex, allowing the colloids to deform into the desired shape during the stretching process.

The shape modified colloids were recovered from the middle 4 cm of the stretched films. Films were first washed in isopropanol to remove excess oil, then dissolved in a mixture of 30% isopropanol and deionized water at 65°C. The ellipsoids were then recovered by centrifugation (Eppendorf Centrifuge 5430), and resuspended in a 30% isopropanol/DI water and washed 10 times to clean the particles to remove any excess PVA from their surface. The cleaned colloids were centrifuged to remove the wash solution then suspended in deionized water and stored at 4°C. To minimize any differences in the surface properties caused by heating and washing of the shape modified colloids, spherical colloids were also subjected to a similar treatment without the stretching (Aramrak et al. 2013; Salerno et al. 2006). Scanning Electron Microscopy (LEO 1530) was used to measure the characteristic dimensions of the ellipsoidal particles and confirm uniformity in shape. Electrophoretic mobilities of the spherical and ellipsoidal colloids were measured using dynamic light scattering (Brookhaven Instruments Corporation, ZetaPALS) at pH=10 in varying concentrations of NaCl (1-20 mM) and were converted to zeta potentials using the Smoluchowski equation (Ho et al. 1997).

Graded silica sand (US Silica) with an average grain size of 0.36 mm and a coefficient of uniformity of 1.82 was used in all experiments. The sand was subjected to a rigorous cleaning procedure to minimize any geochemical heterogeneity present on the surface using a procedure similar to Elimelech et al. (2000). Sands were rinsed, then ultrasonicated (Branson 8510 Ultrasonic Cleaner) for 30 minutes then rinsed again with deionized water over a #200 sieve for 1 hour. Surface impurities in the form of metal oxides were removed by soaking sands in 0.1 M sodium dithionite solution, followed by rinsing with deionized water for 1 hour over a #200 sieve. The sand was next soaked in a 3% hydrogen peroxide while being ultrasonicated for 3 hours to remove any organics on the sand surface followed by 1 hour of rinsing with deionized water over a #200 sieve. The last major step in the cleaning process involved soaking the sand in 8 M nitric acid overnight. Sands were then soaked in deionized water and ultrasonicated for an additional hour, then rinsed over a #200 sieve until the effluent conductivity equilibrated with the inlet conductivity and finally oven dried at 105°C. The electrophoretic mobility and zeta potential of milled sand was measured under the same conditions as the colloids.

7.2.2 Column Transport Experiments

Transport experiments were conducted in an acrylic flow cell (L=10 cm, ID=5 cm) capped by stainless steel plates with 1 mm holes and supported by hydrophilic nylon mesh membranes with 10 μm openings (U-CMN-10, Component Supply Company) on both ends. Saturated samples of sand were prepared using a modified form of slurry deposition (Bandini and Sathiskumar 2009; Carraro et al. 2003; Wood et al. 2008). A known mass of dry sand was introduced to a 55 cm long, 3.5 cm interior diameter acrylic cylinder partially filled with deaired and deionized water and capped on the bottom with a rubber stopper. The remaining headspace was eliminated by filling the remaining volume with deionized deaired water, and the top capped by a rubber stopper. The slurry was mixed

for several minutes by repeatedly inverting the cylinder, then vacuum (19 in Hg) was applied for approximately 8-12 hours. After removal of the vacuum, the specimen was repeatedly inverted for 1 minute to obtain a uniform mixture. The rubber end stopper was then removed and replaced with an easily removable nylon membrane. Prior to introducing the sand to the flow cell, the flow cell was filled with deionized water. The cylinder used to saturate the sand was slowly inverted and then lowered to the bottom of the flow cell while carefully removing the end membrane. The end rubber stopper was slowly removed allowing the soil slurry to enter and fill the flow cell while the sides of the flow cell were tapped to densify the sample to a porosity of 0.37-0.38.

The transport experiments were carried out at three different ionic strengths (IS=1, 10, and 20 mM NaCl) buffered to pH=10 (0.2 mM Na₂CO₃). The aqueous phase was pumped (Cole Parmer Masterflex L/S) downward through the column at a Darcy velocity of 0.24 cm/min. Columns were pre-equilibrated by first passing 5 solutions of background solution. A 0.1 mM NaNO₃ conservative tracer was passed through the column to measure dispersion, followed by an additional 10 pore volumes of background solution. Three pore volumes of either spherical or ellipsoidal colloids at a concentration of 10 mg/L (1.9×10^7 particles/L) were passed through the column followed by an additional two pore volumes of colloid free background electrolyte solution to assess any colloid re-entrainment. Effluent samples were collected using a fraction collector (ISCO Retriever II) and tracer and colloid concentrations were measured by UV-Vis spectrophotometry (Shimadzu UV/1800) at wavelengths of 204 nm and 435 nm respectively.

At the end of each experiment, the column was carefully dissected to measure the spatial distribution of colloid concentrations along the length of the column. Sand from each column was extruded into 1 cm sections and then placed in 60 mL of 0.2 mM Na₂CO₃, and gently agitated for five minutes. The supernatant concentrations were measured with UV/Vis spectrophotometry and used to construct the concentration profiles.

7.2.3 Theoretical Considerations

7.2.3.1 DLVO and Surface Element Integration

The calculation of interaction energies from DLVO theory, which simply states that the interaction energy between two surfaces is the sum of the electrical double layer and London-van der Waals interaction energies, has proven an extremely effective means of understanding and predicting colloidal phenomena (Adamczyk and Weroński 1999; Elimelech et al. 1995). Interaction potentials as a function of separation distance between the colloid and soil surface allow researchers to predict how colloids are attached to the soil surface, and under what chemical conditions this attachment is likely (Elimelech et al. 1995). Interaction potentials for colloids in porous media are typically calculated by treating colloids as spheres and the porous media as an infinite plate or half space. This simplification provides a facile means of evaluating interaction potential energies analytically. However more advanced techniques are necessary to calculate the interaction potential between non-spherical colloids and porous media. Interaction energies were evaluated numerically using Surface Element Integration (SEI), a novel method that allows interaction potentials in more complex systems, such as between particles of any shape and infinite flat plates to be calculated by scaling the interaction energy between two infinite plates (Bhattacharjee and Elimelech 1997; Bhattacharjee et al. 1998).

Interaction potential energies of spherical and ellipsoidal colloids was investigated using SEI to better understand the role colloid shape plays in retention in porous media. The non-spherical colloids used in this study are reasonably well approximated as a prolate ellipsoid (Aramrak et al. 2013; Salerno et al. 2006; Seymour et al. 2013). The equation for spheroid in spherical coordinates is given as (Bhattacharjee et al. 2000):

$$r^2 = \frac{1}{\frac{\sin^2 \theta \cos^2 \phi}{a^2} + \frac{\sin^2 \theta \sin^2 \phi}{b^2} + \frac{\cos^2 \theta}{c^2}} \quad (7.1)$$

where a , b , and c are the semi-axis of the spheroid. In the case of a prolate ellipsoid, a is equal to b and are the semi-minor axis, while c is the semi-major axis. For a spherical particle, a , b , and c are equal to the radii of the particle. r , θ , and ϕ are the radial and angular coordinates in a spherical coordinate system.

In the case of a spheroidal particle, the total interaction energy, U , between the particle surface and an infinite plate is given as (Bhattacharjee et al. 2000):

$$U(D) = \int_0^{2\pi} \int_0^\pi \hat{\mathbf{n}} \cdot \hat{\mathbf{k}} E(h) r^2 \sin \theta \, d\theta d\phi \quad (7.2)$$

where $\hat{\mathbf{n}}$ is the unit vector normal to the surface element, $\hat{\mathbf{k}}$ is the unit vector normal to the plate, E is the interaction energy per unit area between two infinite plates, and h is the distance between a surface element and the infinite flat plate as shown in Figure 7.1.

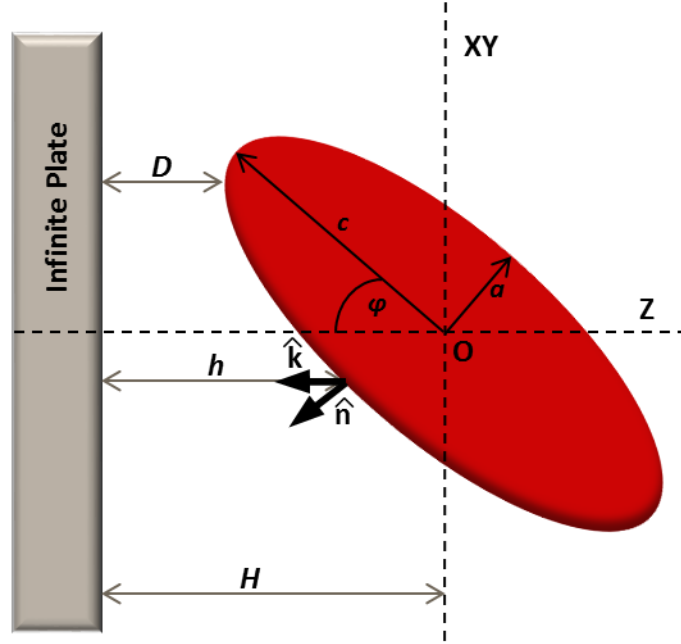


Figure 7.1: Illustrated representation of the geometrical considerations when modeling an ellipsoidal particle and an infinite flat plate using surface element integration. In the case of a prolate ellipsoid, a and c are the semi-minor and semi-major axis respectively. \hat{n} is the unit vector normal to the surface element. \hat{k} is the unit vector normal to the plate. h is the distance between a surface element and the infinite flat plate. r , θ , and ϕ are the radial and angular coordinates in a spherical coordinate system. ϕ is the orientation of the ellipsoid relative to the surface. Only the two limiting cases for particle orientation were considered, that is $\phi = 0$ for an end-on configuration and $\phi = 90^\circ$ for a side-on configuration.

The interaction energy per unit area between two infinite plates due to the electrostatic double layer between two infinite plates with constant surface potential was calculated using the expression (Hogg et al. 1966):

$$E_{EDL}(h) = \frac{\epsilon_0 \epsilon_r \kappa}{2} (\psi_s^2 + \psi_p^2) \left(1 - \coth(\kappa h) + \frac{2 \psi_s \psi_p}{(\psi_s^2 + \psi_p^2)} \operatorname{cosech}(\kappa h) \right) \quad (7.3)$$

where ψ_s and ψ_p are the surface potentials of the particle and plate and were taken to be equal to the measured zeta potentials for the colloid and sand (Elimelech et al. 1995), ϵ_0

is the vacuum permittivity ($8.85 \times 10^{-12} \text{ C}^2 \text{ N}^{-1} \text{ m}^{-2}$), and ϵ_r is the dimensionless dielectric constant of the medium (80 for water). The Debye-Hückel parameter, κ , is related to the double layer thickness and was calculated using the expression:

$$\kappa = \left(\frac{1000e^2 N_A I_s}{\epsilon_0 \epsilon_r k_b T} \right)^{0.5} \quad (7.4)$$

where e is the charge of an electron ($1.60 \times 10^{-19} \text{ C}$), N_A is Avogadro's number (6.02×10^{23} molecules mole⁻¹), I_s is the ionic strength of the aqueous phase [mol L⁻¹], k_b is Boltzmann's constant ($1.38 \times 10^{-23} \text{ J K}^{-1}$), and T is the absolute temperature [K].

The retarded interaction energy per unit area between two infinite plates due to van der Waals interactions was calculated after Gregory (1981):

$$E_{vdw} = -\frac{A_H}{12\pi h^2} \left(\frac{1}{1 + \frac{5.32h}{\lambda}} \right) \quad (7.5)$$

where A_H is the Hamaker constant ($4.04 \times 10^{-21} \text{ J}$ for polystyrene and quartz separated by water (Israelachvili 2011)), and λ is the characteristic wavelength and is typically assumed to be 100 nm. Equations 7.1-7.5 were combined and solved numerically using Mathematica to generate interaction potential energies under the ionic strengths relevant to the experiments in this chapter for both spherical and ellipsoidal colloids.

In addition to calculating interaction potentials, the surface area of spherical and ellipsoidal colloids were calculated. The surface area, S , for an ellipsoid is given as:

$$S = 2\pi a^2 \left(1 + \frac{c}{a \sqrt{1 - \frac{a^2}{c^2}}} \sin^{-1} \left(\sqrt{1 - \frac{a^2}{c^2}} \right) \right)$$

where a and c are the semi-minor and semi-major axis respectively.

7.2.3.2 Transport Modeling

Colloid break through curves were modeled using the 1-D advection dispersion equation (ADE) to assess the kinetic rates of attachment for ellipsoids and spheres. The mass balance for colloids passing through saturated sand is given by the following:

$$\frac{\partial nC}{\partial t} + \rho \frac{\partial S}{\partial t} = \frac{\partial}{\partial x} \left(nD_L \frac{\partial C}{\partial x} \right) - \frac{\partial qC}{\partial x} \quad (7.6)$$

where C is the colloid concentration in the aqueous phase, n is porosity, D is the hydrodynamic dispersion coefficient in the direction of flow, q is the Darcy flux in the direction of flow, ρ is the bulk density of the sand, S is the concentration of colloids attached to the sand surface, x is the spatial coordinate in the direction parallel to flow, and t is time. The transfer of colloids to the surface of the porous media was modeled as an irreversible attachment process:

$$\rho \frac{\partial S}{\partial t} = nk_a C \quad (7.7)$$

where k_a is a first-order kinetic term. Equations 7.6-7.7 were solved using HYDRUS-1D, a finite element code used for one dimensional transport processes in variably saturated soils (Simunek et al. 2013). HYDRUS 1-D includes a non-linear parameter estimation routine based on the Marquardt-Levenberg least squares algorithm, and was used to estimate the dispersion coefficient and porosity from the tracer break through curve, and the first order kinetic attachment from the colloid break through curve. While retention profiles were simulated, the measured colloid concentrations retained in the sand were not included in the fitting.

7.3 RESULTS AND DISCUSSION

7.3.1 Characterization of Colloids and DLVO Interaction Energies

SEM micrographs of colloids before and after the shape modification process are shown below in Figure 7.2. The shape modification process resulted in a controlled ellipsoid colloid population as indicated by the relatively low standard deviations of major and minor axis length (Table 7.1). The ellipsoids used in this study had an average aspect ratio of 2.30. The casting of particles in PVA films and heating in oil resulted in a small drop in electrophoretic mobility, a commonly observed phenomena that has been attributed to the deactivation of surface carboxyl groups and residual PVA remaining on

the surface of the particles (Aramrak et al. 2013; Ho et al. 1997; Ho, Keller, et al. 1993). However, the difference in measured zeta potential for treated spheres and ellipsoids was minimal.

Table 7.1: Geometric dimensions of spherical and ellipsoidal particles

Shape	Semi-Major Axis (μm)	Minor Axis (μm)	Ellipticity (e)	Surface Area (μm^2)	Zeta Potential in 1 mM NaCl pH=10 (mV)
Sphere (untreated)	0.5	-	0	3.14	-49.0 (2.4)
Sphere (treated)	0.5	-	0	3.14	-47.3 (2.4)
Ellipsoid	0.880 (0.09)	0.380 (0.03)	0.90	3.52	-45.4 (2.3)

Note: values in parenthesis are one standard deviation

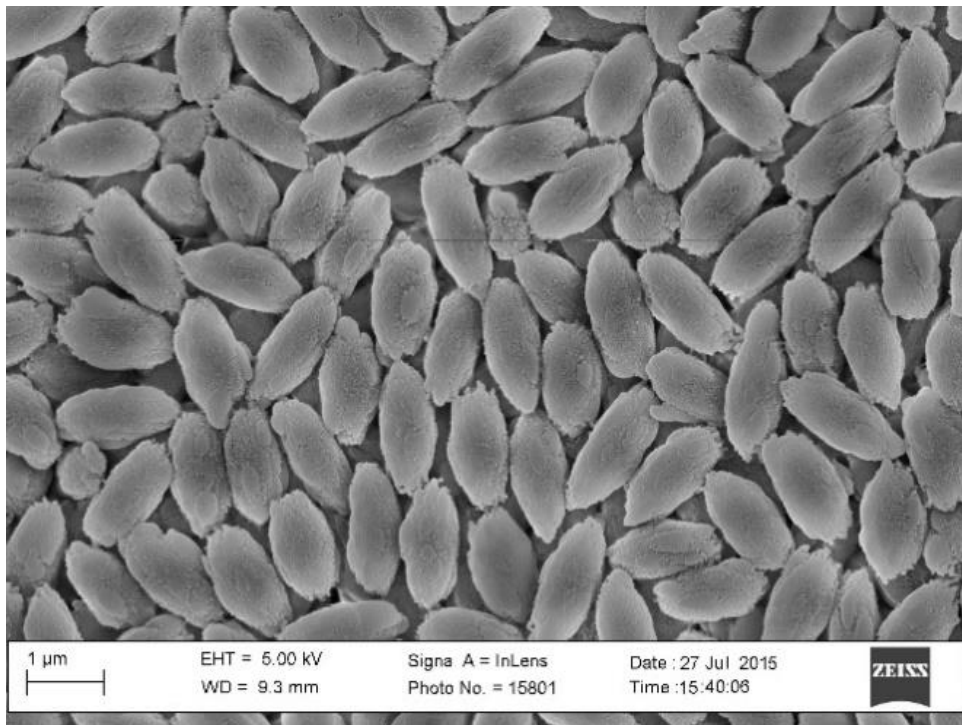
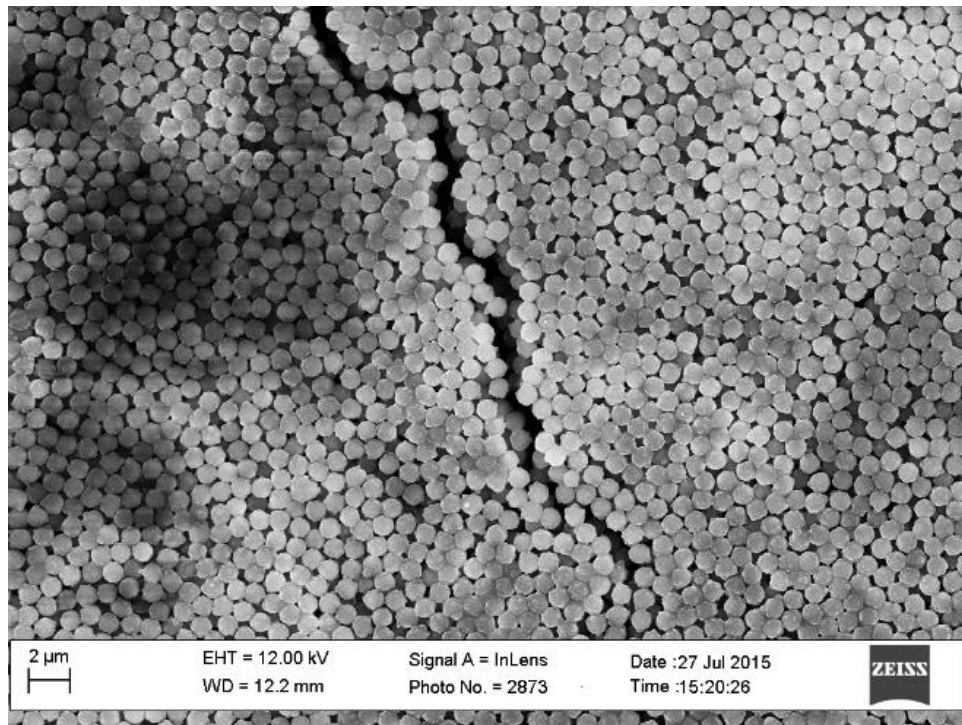


Figure 7.2: SEM micrograph of spherical (top) and ellipsoidal (bottom) colloids.

The interaction energy as a function of separation distance for spherical and ellipsoidal colloids near the surface of the porous media at an ionic strength of 10 mM calculated using surface element integration are shown in Figure 7.3 and are demonstrative of the effect of both shape and colloid orientation. For ellipsoidal particles, only the two limiting cases were considered. In the side-on orientation, the major semi-axis is parallel to the soil surface, while in the end-on configuration the major semi-axis is perpendicular to the soil surface. The colloid-soil interaction energy profiles demonstrate that colloids are unlikely to be deposited in the primary energy well as indicated by the height of the energy barrier. For ellipsoidal colloids, the energy barrier for the side-on configuration was consistently higher than that of the end-on configuration, while the barrier for spherical particles fell in between those of the ellipsoidal colloids under all ionic strength conditions.

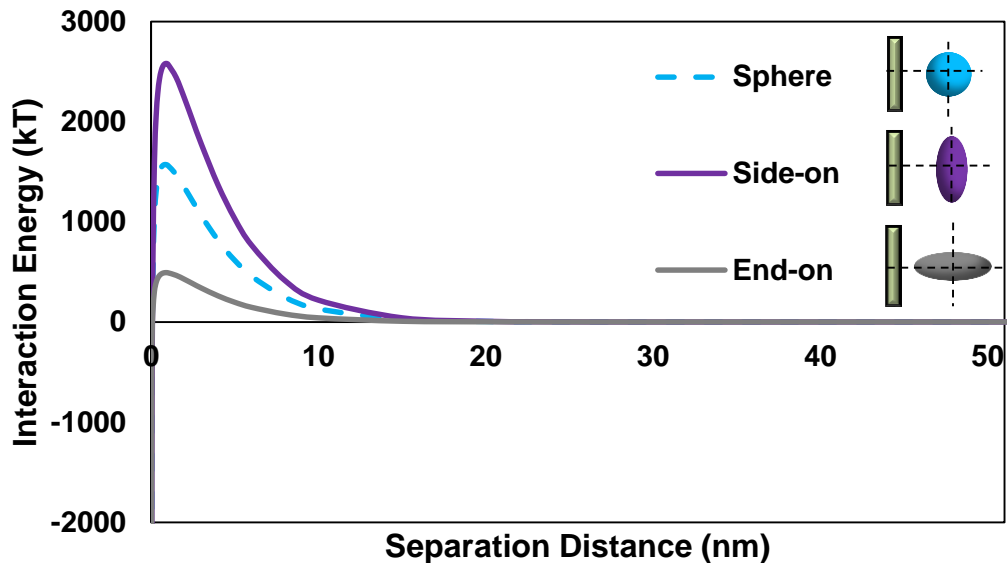


Figure 7.3: DLVO Interaction energy as a function of separation distance for spheres and ellipsoids at an ionic strength of 10 mM. For the ellipsoidal particles, only the limiting configurations were considered. That is, side-on, with the major semi-axis parallel to the soil surface, and end-on, with the major semi-axis perpendicular to the soil surface.

Table 7.2 summarizes the relevant DLVO parameters for the different experimental conditions examined in this study. The relatively large energy barrier to deposition in the primary energy well suggests that any observed retention took place due to colloids becoming trapped in the secondary minimum (Shen et al. 2007). As the ionic strength of the pore fluid is increased, the height of the energy barrier decreases and the absolute depth of the secondary minimum increases (Li and Johnson 2005; Torkzaban et al. 2010). Interestingly, despite the consistently larger primary energy barrier of ellipsoids in the side-on orientation, the absolute depth of the secondary minimum is consistently deeper than that of spherical colloids. The effect of colloid shape and orientation on the secondary minimum is illustrated in Figure 7.4. The secondary minimum for the side-on ellipsoid is deeper and extends to greater separation distances as compared to that of the spherical colloid. The depth of the secondary minimum for ellipsoids in the end-on configuration is consistently smaller than that of spheres and ellipsoids in the side-on configuration. At the highest ionic strength (20 mM), the end-on secondary minimum is a fifth as deep as in the side-on configuration, and shallower than that of spherical colloids at a lower ionic strength of 10 mM.

Table 7.2: DLVO Interaction Potential Energy Results

IS (mM)	Colloid	Zeta Potential, Colloid (mV)	Zeta Potential, Sand (mV)	Energy Barrier Height (kT)	Secondary Minimum Depth (kT)
1	Sphere	- 47	- 92	2100	- 0.01
1	Ellipsoid Side-on	- 45	- 92	3230	- 0.04
1	Ellipsoid End-on	- 45	- 92	625	- 0.01
10	Sphere	- 41	- 82	1570	- 0.41
10	Ellipsoid Side-on	- 40	- 82	2580	- 0.65
10	Ellipsoid End-on	- 40	- 82	492	- 0.13
20	Sphere	- 37	- 53	1020	- 0.95
20	Ellipsoid Side-on	- 34	- 53	1540	- 1.57
20	Ellipsoid End-on	- 34	- 53	293	- 0.31

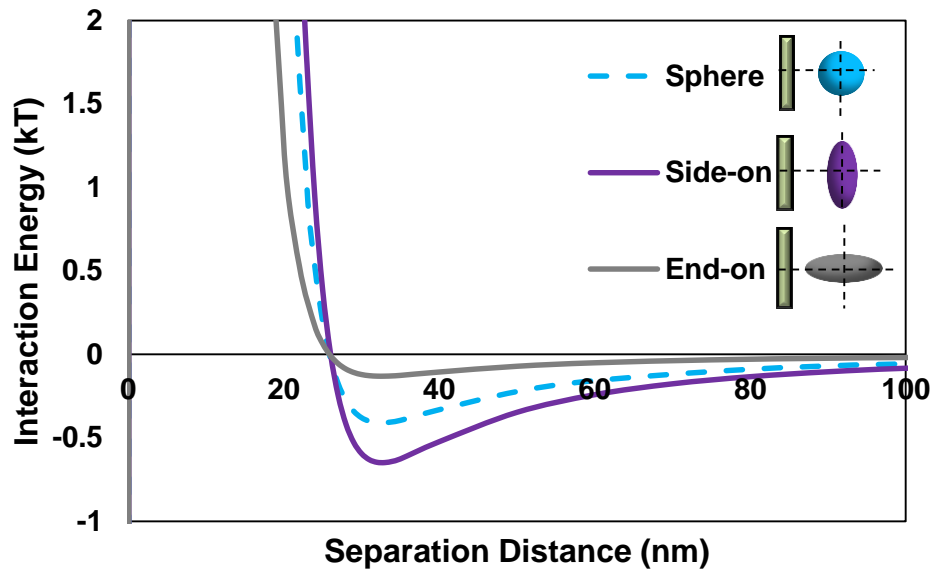


Figure 7.4: Expanded view of DLVO Interaction energies for spheres and ellipsoids at an ionic strength of 10 mM. The secondary minimum for ellipsoids in the side-on orientation is both deeper and broader than that of spherical colloids.

7.3.2 Column Transport Experiments

Normalized concentration of colloids measured at the outlet of the flow cell are shown in the dimensionless breakthrough curves in Figure 7.5. In all experiments, the effluent colloid concentration rapidly reached constant value, then decreased to zero in a symmetrical fashion as the step function of injected colloids passed through the sand. At an IS of 1 mM, low levels of retention of spherical and ellipsoidal colloids were observed. This is expected as DLVO interaction energies predict an extremely shallow secondary minimum, and thus repulsion occurs between colloids and the porous media at all separation distances. Additionally, the ratio of colloid to mean grain size diameter (~ 0.003) is below the 0.005-0.008 ratio that has been typically associated with physical filtration or straining (Bradford et al. 2002, 2006; Sang et al. 2013; Xu and Saiers 2009). The fact that ellipsoids were retained in similar amounts as spheres under these same conditions reinforces the observations of other researchers that the smallest dimension is controlling in the straining of nonspherical colloids (Liu et al. 2010; Xu et al. 2008). Despite the larger barrier to deposition in the primary minimum predicted in interaction energy profiles, the breakthrough curves in Figure 7.5 and the mass balances in Table 7.3, demonstrate that increasing the ionic strength of the pore fluid results in increased retention of colloids, similar to other studies (Bradford and Kim 2012; Hajra et al. 2002; Saiers and Lenhart 2003a). The tailing end of the colloid breakthrough curves show that re-entrainment of colloids was negligible under the timescale of the transport experiments.

Table 7.3: Experimental conditions and mass balance information

IS (mM)	Colloid	D [cm]	q [cm/min]	Porosity	M_{Eff}	M_{Soil}	M_{Total}
1	Sphere	0.144	0.242	0.373	0.994	0.011	1.005
1	Ellipsoid	0.141	0.240	0.378	0.990	0.024	1.014
10	Sphere	0.155	0.240	0.371	0.772	0.215	0.987
10	Ellipsoid	0.138	0.240	0.374	0.709	0.205	0.914
20	Sphere	0.202	0.240	0.375	0.417	0.516	0.933
20	Ellipsoid	0.164	0.239	0.375	0.319	0.580	0.899

NOTE: θ is the porosity, q is the Darcy velocity, and D is the dispersion coefficient. All masses, M , are fraction of the total injected mass of colloids. M_{Eff} refers to mass eluted as measured by the effluent curve, M_{Soil} refers to mass of colloids attached to soil, and M_{Total} refers to total mass balance.

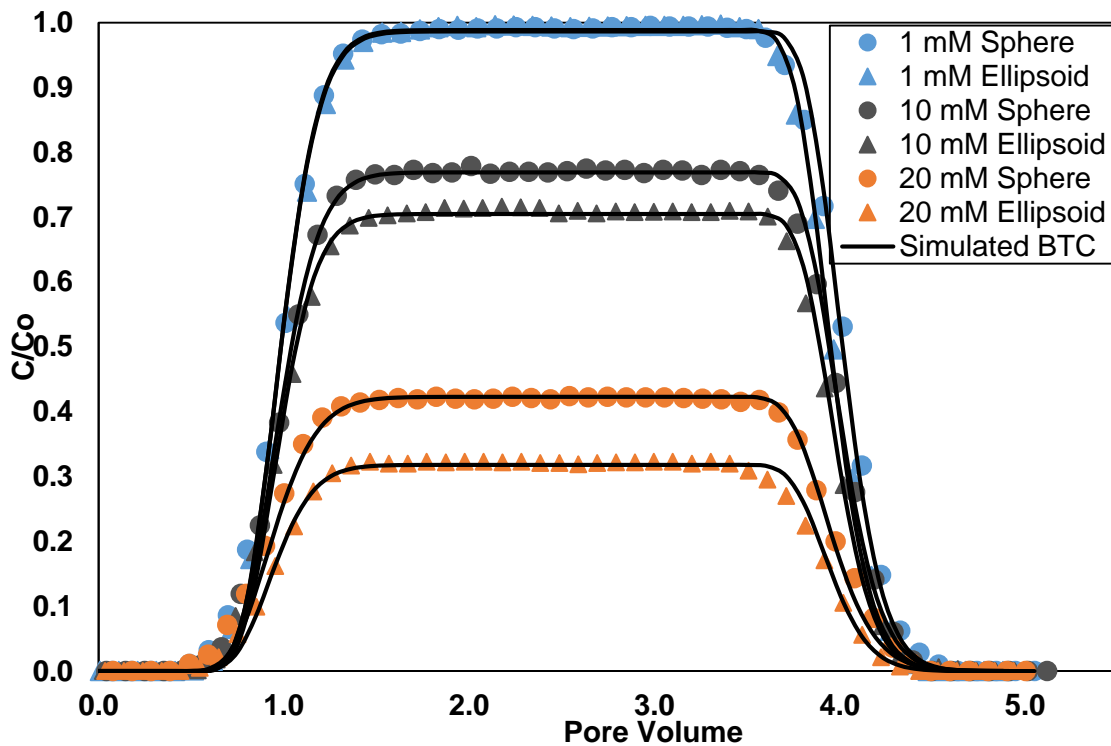


Figure 7.5: Measured and simulated normalized effluent concentration breakthrough curves for spherical and ellipsoidal colloids. Effluent concentration is normalized by influent concentration C_0 . Simulated breakthrough curves for each experiment are shown as solid lines.

The observation that some retention of colloids was observed under the lowest ionic strength could be due to the presence of low levels of geochemical heterogeneity still present on the surface of the cleaned sand (Litton and Olson 1993; Shani et al. 2008; Torkzaban et al. 2010). As has been pointed out by other researchers, bulk measurements of electrokinetic properties of soils are ineffective at measuring small heterogeneities: however, the rigorous cleaning procedure is expected to have greatly reduced the likelihood of this scenario (Elimelech et al. 2000). Another more likely scenario is that colloids may have been retained near rough locations on the soil surface. Asperities can decrease the energy barrier to deposition and deepen the secondary minimum, and retention in these locations is sensitive to the ionic strength of the pore fluid (Huang et al. 2010; Shen, L.-P. Wang, Li, et al. 2012). Similarly, colloids may have traveled along the soil surface and become immobilized in low velocity stagnation points, or in valleys sheltered between asperities (Johnson et al. 2007; Krishna Darbha et al. 2012; Shen et al. 2011; Tong and Johnson 2006)

The difference in retention of spheres and ellipsoids becomes increasingly evident as ionic strength is increased. At an intermediate ionic strength of 10 mM, 23% of spherical colloids were retained versus 29% of ellipsoids retained, while at an ionic strength of 20 mM, 58% of spheres were retained versus 68% of ellipsoids retained. This trend agrees with the observations of Salerno et al. (2006) and Seymour et al. (2013) who found that increasing ionic strength resulted in an increased removal of ellipsoids over spherical colloids transported through glass beads. The increased retention of ellipsoids with ionic strength is mirrored by the increase in depth of the secondary minimum calculated for a side-on orientation calculated using interaction energy profiles. This suggests that the major axis of the ellipsoid is parallel to the soil surface during transport experiments. Pore scale hydrodynamic simulations by (Xu et al. 2008) have shown that as non-spherical particles approach constrictions, viscous shear forces will align the major

axis parallel to streamlines and the soil surface. Ellipsoidal colloids deposited in an end-on configuration will be subject to increased torque due to viscous forces and will orient to a more energetically favorable side-on configuration (Bhattacharjee et al. 2000; Seymour et al. 2013).

The advective dispersion equation with first order kinetic retention provided an adequate fit to the observed effluent data, with an $R^2 > 0.99$ for all experiments. Colloid dispersion was similar to that of the conservative tracer. Increasing the ionic strength of the pore fluid resulted in higher kinetic removal rates for both spheres and ellipsoids as shown in Figure 7.6. The kinetic coefficients of removal for ellipsoids was consistently higher than that of spherical particles. While the absolute difference in the kinetic coefficient for spheres and ellipsoids increased as ionic strength was increased, the ratio of the kinetic attachment of ellipsoids to spheres was constant ($k_{\text{ellipsoid}}/k_{\text{sphere}} = 1.32$) for 10 and 20 mM IS. As with absolute retention, the increased kinetic rate of attachment agrees well with the calculated deeper secondary minimum associated with ellipsoidal colloids and is in agreement with the observations of Salerno et al. (2006) and Seymour et al. (2013) that ellipsoidal colloids are removed at higher rates.

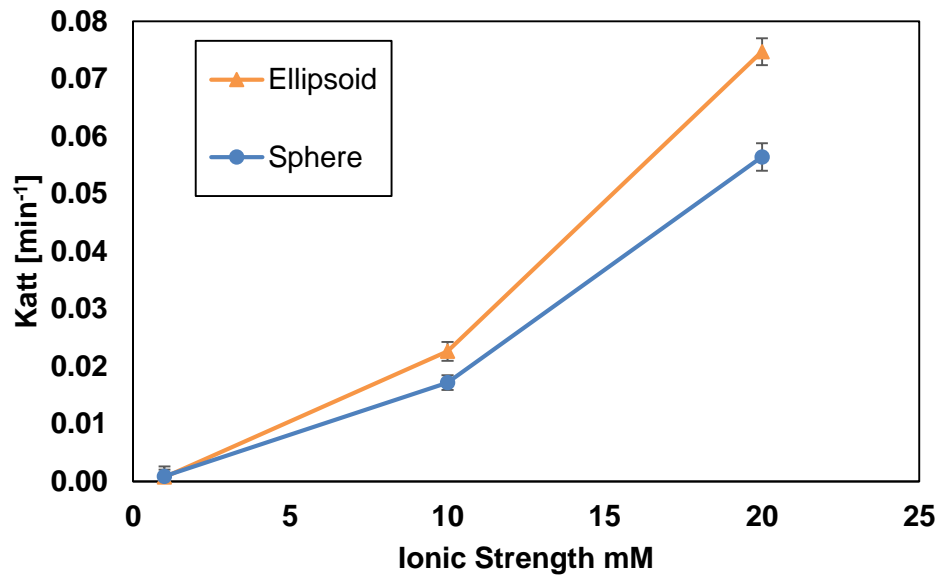


Figure 7.6: First order attachment coefficients from estimated from simulated break through curves. Error bars denote the standard deviation of the estimated parameters.

Retention profiles measured from experiments conducted under conditions unfavorable to deposition are often nonmonotonic or hyperexponential (Molnar et al. 2015; Tufenkji and Elimelech 2004a). This has been attributed to straining (Bradford et al. 2003), as well as heterogeneity in the soil surface or colloid population (Li et al. 2004). Measured colloid concentrations immobilized in the soil matrix in this study were relatively uniform with depth as shown in Figures 7.7 and 7.8, and did not vary significantly with the shape of the colloid or ionic strength. Similarly uniform retention profiles have been observed for spheres and low aspect ratio peanut shaped particle under unfavorable conditions (Xu et al. 2008). Liu et al. (2010) observed relatively uniform deposition profiles for high aspect rod-shaped colloids under both favorable and unfavorable conditions. Classic first-order kinetic attachment models yield a log linear decrease in retained colloids with depth (Elimelech 1994; Tufenkji and Elimelech 2004b). At lower ionic strengths, and thus less retention, simulated profiles did not differ in shape from the observed profiles.

However, at an ionic strength of 20 mM, the difference between simulated and observed retention profiles increases significantly.

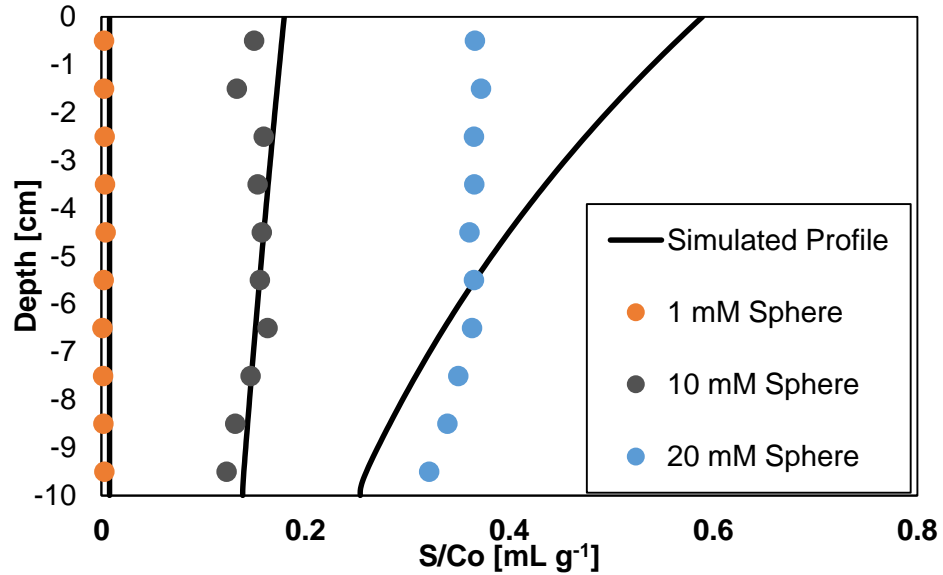


Figure 7.7: Measured normalized surface concentrations for spherical colloids as a function depth (distance from inlet). Surface concentration, S , has been normalized by influent concentration, C_o . Solid lines are simulated retention profiles.

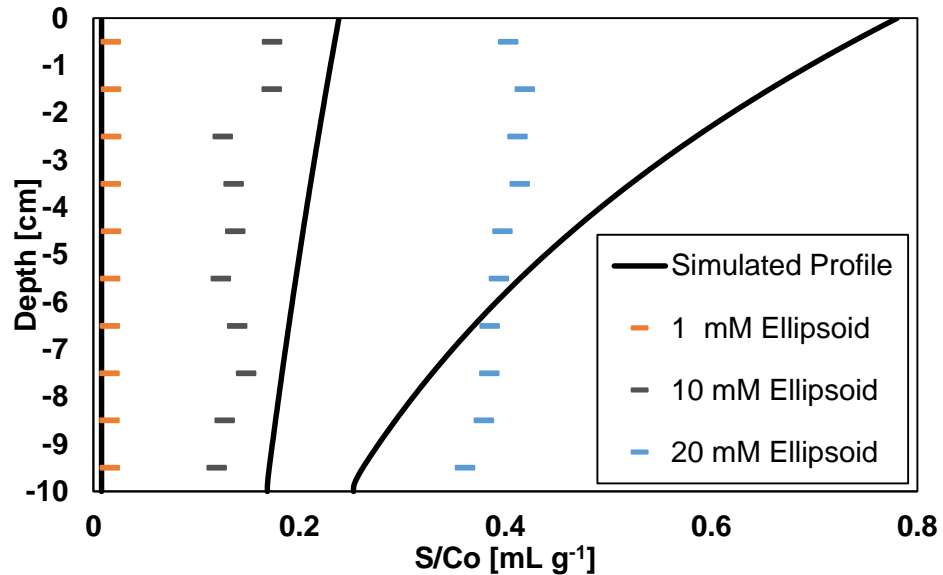


Figure 7.8: Measured and modeled normalized surface concentrations for ellipsoidal colloids as a function depth (distance from inlet).

7.4 CONCLUSIONS

The role of colloid shape and ionic strength in the transport and retention of colloids in saturated porous media was examined using column transport experiments with supporting DLVO interaction energy calculations. Calculated interaction potentials demonstrate that at the lowest ionic strength, both spherical and ellipsoidal colloids will experience repulsion with the soil surface at all separation distances. Under these conditions little retention of ellipsoidal and spherical colloids was observed in column transport experiments. This suggests that when repulsion between colloids and the soil surface is present at all separation distances, the minor-axis controls the retention of colloids. Greater amounts of spherical and ellipsoidal colloids were retained as the ionic strength of the pore fluid was increases. Interaction potential energies show that this retention was primarily in the secondary minimum for both spheres and ellipsoids. As ionic strength was increased, the depth of the secondary minimum increased for both spheres and ellipsoids. However, the depth of secondary minimum was consistently deeper for ellipsoids in the side-on configuration than in the end-on as well as spheres. The calculated interaction energies matched the observed increased retention rates of ellipsoids over spheres in transport experiments, and suggest that non-spherical particles align the major axis parallel to the direction of flow in porous media. As the ionic strength was increased, the difference in retention of spheres versus colloids increased, agreeing with the results of others (Liu et al. 2010; Salerno et al. 2006). This suggests that ellipsoidal colloids are more sensitive to changes in ionic strength than spherical colloids. The increased retention of ellipsoidal particles over spherical particles under the unfavorable conditions in these experiments demonstrate that colloid shape plays an important role in predicting the fate of colloids in porous media and suggests that ellipsoidal colloids may be less mobile in saturated porous media than spheres.

CHAPTER 8:
THE TRANSPORT AND RETENTION OF COLLOIDS IN UNSATURATED SAND:
THE ROLE OF COLLOID SHAPE AND MOISTURE CONTENT

8.1 INTRODUCTION

Typically, researchers utilize spherical colloids as model particles for transport in unsaturated soils (Crist et al. 2005; Keller and Sirivithayapakorn 2004; Sirivithayapakorn and Keller 2003a), and numerous studies have demonstrated the decreased mobility of these colloids in unsaturated porous media, when compared to transport through saturated media (Corapcioglu and Choi 1996; Wan and Wilson 1994b). While mineral, biological, and engineered colloids come in many diverse, nonspherical shapes, shape is rarely explicitly considered in colloid transport in unsaturated porous media (Bradford, Morales, et al. 2013; Madigan et al. 2010; Mitchell and Soga 2005; Sen and Khilar 2006; Tian et al. 2012; Y. Wang et al. 2012). Numerous studies have demonstrated that colloid shape affects interactions at the soil-water interface in saturated porous media, including the work in the previous chapter (Liu et al. 2010; Salerno et al. 2006; Seymour et al. 2013). In this chapter, the effect of shape on transport in unsaturated sand will be investigated.

Colloids transported through unsaturated soils are subject to additional interactions at the air-water interface that are not present in saturated porous media (Chen et al. 2009; Chu et al. 2001; Knappenberger et al. 2014; Zevi et al. 2005, 2012). While very few studies explicitly deal with the role of colloid shape in transport through unsaturated porous media, several have demonstrated the importance of colloid shape on interactions with the air-water interface. Shape has been found to affect the magnitude of capillary forces experienced by colloids at the air-water interface, and the capillary forces experienced by natural colloids is best approximated by a volume equivalent ellipsoid (Chatterjee and Flury 2013; Chatterjee et al. 2012b; Shang et al. 2009). Aramrak

et al. (2013) investigated the role of colloid shape on detachment from a glass substrate by a moving air-water interface. Their work demonstrated that rod-like colloids were less likely to be mobilized than spheres by both advancing and receding air-water interfaces. Similar observations for bacteria detachment from glass substrates by air-water interfaces have shown that rod-shaped bacteria were detached less than spherical bacteria (Gómez-Suárez et al. 2001). Although these systems were extremely different from porous media, they offer insight as to the importance colloid shape may play in transport through soils.

In this study, the role of colloid shape in the transport and retention in unsaturated porous media was investigated by conducting column transport experiments at varying levels of saturation, using spherical and ellipsoidal colloids. Additional transport experiments were conducted with spherical colloids that underwent the same film casting and heat treatment as the ellipsoidal colloids to determine if the shape modification procedure had any effect on colloid retention in unsaturated porous media.

8.2 MATERIALS AND METHOD

8.2.1 Colloid and Porous Media Preparation

Spherical and ellipsoidal colloids were used to investigate the role of colloid shape in the fate of colloids in unsaturated porous media. Carboxylated polystyrene-latex 1 μm microspheres (Bang Laboratories, Inc. Fishers, IN) and prolate ellipsoids (0.76 μm by 1.75 μm) prepared using the method of Ho et al. (1993b) and Champion et al. (2007) were used in all experiments and have been described in the previous chapter. Briefly, spherical colloids were cast in polyvinyl alcohol (PVA) films, heated to 125° C, and the films were mechanically stretched to the desired aspect ratio. Colloids were then recovered by dissolving the PVA films and cleaned by centrifuging and resuspending the colloids in 30% isopropanol water mixture 10 times before finally suspending in DI water. In addition to comparing the effect of colloid shape, experiments were carried out to assess the effect

of the shape modification procedure on the transport and retention of colloids. Untreated spherical colloids were triple rinsed and suspended in deionized water to remove residual surfactant from the manufacturer, while treated spheres underwent the same casting, heating, and rinsing procedure without mechanical stretching as the ellipsoids.

Graded silica sand ($d_{50} = 0.36$ mm, $C_u = 1.82$, US Silica) served as the porous media in all experiments. As in previous chapters, the sand was subject a rigorous cleaning procedure which included repeated ultrasonification, soaking in sodium dithionite, hydrogen peroxide, and nitric acid, and rinsing with DI over a #200 sieve to minimize any effects of geochemical heterogeneity on colloid retention. The soil water characteristic curve and hydraulic conductivity function were previously measured using the multistep outflow method (Eching and Hopmans 1993; Eching et al. 1994; Hopmans et al. 2002) and were parameterized using the expressions of Kosugi (1994, 1996):

$$S_e = \frac{\theta - \theta_r}{\theta_s - \theta_r} = \frac{1}{2} \operatorname{erfc} \left[\frac{\ln \left(\frac{h}{h_m} \right)}{\sqrt{2} \sigma} \right]$$

$$K_r = \frac{K_{unsat}}{K_{sat}} = S_e^\tau \left\{ \frac{1}{2} \operatorname{erfc} \left[\operatorname{erfc}^{-1}(2S_e) + \frac{\beta \sigma}{\sqrt{2}} \right] \right\}^2$$

where S_e is the effective saturation, $\theta_s = 0.375$ and $\theta_r = 0.04$ are the dimensionless saturated and residual volumetric water contents, h is the matric suction in cm of H_2O , $h_m = 24$ cm H_2O is related to the geometric mean pore radius, $\sigma = 0.13$ is the standard deviation of the pore size distribution, and $\operatorname{erfc}[\]$ and $\operatorname{erfc}^{-1}[\]$ are the complimentary error function and inverse complimentary error function respectively. The hydraulic conductivity function describes the hydraulic conductivity relative to the saturated hydraulic conductivity, $K_{sat} = 2.5$ cm/min. The dimensionless parameters fitting parameters $\tau = 0.33$ and $\beta = 4.5$ relate to soil pore tortuosity (Kosugi 1999b; Mualem and Dagan 1978).

8.2.2 Column Transport Experiments

All transport experiments were conducted in acrylic flow cells (L=10 cm, ID=5 cm). For all experiments, both ends of the flow cell were initially capped with stainless steel plates with 1 mm holes and supported by hydrophilic nylon mesh membranes with 10 μm openings (U-CMN-10, Component Supply Company). Saturated soil samples for all experiments were prepared using the modified slurry deposition procedure described in previous chapters (Bandini and Sathiskumar 2009; Carraro et al. 2003; Wood et al. 2008). For unsaturated experiments, tensiometers (652X03-B1M3, Soil Moisture Equip. Corp) arranged helically and located 2.5, 5, and 7.5 cm above the base plate were inserted during the slurry deposition of the soil, and pressure transducers (PX170-28DV, Omega Engineering) were used to measure matric suction. The average gravimetric moisture content of the unsaturated soil sample was monitored using a digital balance (4102 accuSeries, Fisher Scientific).

The pore fluid consisted a pH=10 buffer (0.2 mM Na_2CO_3) with sufficient sodium chloride to raise the ionic strength to 1 mM. These chemical conditions were selected to minimize colloid deposition at the soil water interface. For saturated experiments, the aqueous phase was pumped (Cole Parmer Masterflex L/S) downward through the column at a Darcy velocity of 0.24 cm/min. The soil samples were first pre-equilibrated by passing five pore volumes of the background electrolyte followed by 0.2 mM NaNO_3 conservative tracer to measure dispersion. This was followed by an additional ten pore volumes of background solution. Three pore volumes of colloids at 10 mg/L (1.9×10^7 particles/L) were passed through the column followed by an additional two pore volumes of colloid free background electrolyte solution.

Unsaturated transport experiments followed a modified protocol. Samples were initially pre-equilibrated by fifteen pore volumes of background electrolyte passed upward

through the porous media. After the initial pre-equilibration, the acrylic top cap of the flow cell and membrane were removed to expose the top of the soil surface to the atmosphere. Inlet flow to unsaturated experiments was applied using an acrylic sprinkling apparatus with seven stainless steel needles to evenly distribute flow over the top of the sand surface. Additionally, the stainless steel endcap was left in place on the top soil surface to minimize erosion caused by the sprinkler.

For unsaturated experiments, the lower boundary was controlled using a hanging water column to apply suction to the base of the soil sample (Cherrey et al. 2003). The desired saturation was achieved by simultaneously reducing the inlet flow rate while increasing the suction at the lower boundary condition by changing the elevation of the column outlet. A uniform hydraulic gradient was achieved when all tensiometers measured the same constant value, implying a constant level of saturation along the length of the column (Chen et al. 2007; Gargiulo et al. 2008; Torkzaban et al. 2008). Once uniform flow conditions were achieved, a 0.2 mM NaNO₃ conservative tracer was passed through the column to measure dispersion, followed by three pore volumes of background electrolyte. Three pore volumes of colloids at 10 mg/L were then passed through the column followed by an additional two pore volumes of colloid free background solution. At the termination of unsaturated experiments, the sprinkler at the inlet was shut off while simultaneously closing the valve at the end of the hanging column.

At the end of both saturated and unsaturated experiments, columns were extruded into 1 cm sections and mixed with 60 mL of 0.2 mM Na₂CO₃ to measure retention profiles as described in previous chapters. For unsaturated experiments, the dissected soil samples were massed before the addition of the 0.2 mM Na₂CO₃ to assess the moisture content at the end of the experiment. All effluent concentrations and soil-colloid concentrations were measured using UV-Vis spectrophotometry (Shimadzu UV/1800).

8.2.3 Transport Modeling

Colloid breakthrough curves were modeled using the 1-D advection dispersion equation (ADE) with one kinetic retention sites to assess the retention of ellipsoids and spheres in saturated and unsaturated porous media. The mass balance for colloids passing through porous media with one retention site is given as:

$$\frac{\partial \theta C}{\partial t} + \rho \frac{\partial S}{\partial t} = \frac{\partial}{\partial x} \left(\theta D_L \frac{\partial C}{\partial x} \right) - \frac{\partial qC}{\partial x} \quad (8.1)$$

where C is the colloid concentration in the aqueous phase, θ is volumetric moisture content, D is the hydrodynamic dispersion coefficient in the direction of flow, q is the Darcy flux in the direction of flow, ρ is the bulk density of the sand, S is the concentration of colloids immobilized in the soil column, x is the spatial coordinate in the direction parallel to flow, and t is time.

The single kinetic retention site was used to describe the mass transfer of colloids in both saturated and unsaturated porous media. The retention of colloids in porous media was described as a reversible process with a blocking function:

$$\rho \frac{\partial S_1}{\partial t} = \theta \psi_s k_a C - k_d \rho k_d \quad (8.2)$$

where k_a and k_d are the rate coefficients for attachment and detachment respectively, and ψ_s is the dimensionless blocking function. The dimensionless blocking function combines depth dependent retention with concentration dependent blocking and takes the following form:

$$\psi_s = \left(1 - \frac{S_1}{S_{max}} \right) \left(1 + \frac{x}{d_s} \right)^{-\mu} \quad (8.3)$$

where in the first term S_{max} is the retention capacity of immobilized colloids. The concentration dependent first term in the above blocking function has been used in saturated porous media to represent the occupation of finite sites favorable to deposition (Adamczyk et al. 1994; El Badawy et al. 2013; Bolster et al. 2001), while in unsaturated porous media it has typically been used to represent the accumulation of colloids at the

air-water interface (Chu et al. 2001; Corapcioglu and Choi 1996; Lenhart and Sayers 2002). The second term in the above formulation controls depth dependent behavior. μ is an empirical factor that controls the shape of the retention profile. It is extremely difficult to infer pore scale retention mechanisms from fitting macroscopic data from column breakthrough experiments (Goldberg et al. 2014; Johnson et al. 2011; Pazmino et al. 2011). The above formulation of the ADE has been shown to be extremely flexible in its ability to describe both colloid breakthrough curves and retention profiles in saturated and unsaturated porous media, and was adopted for simplicity (Gargiulo et al. 2008; Goebel et al. 2013; Kasel et al. 2013; Torkzaban et al. 2008).

Equations 8.1-8.3 were solved using HYDRUS-1D, a finite element code used for one dimensional transport processes in variably saturated soils (Simunek et al. 2013). HYDRUS 1-D includes a weighted non-linear parameter estimation routine based on the Marquardt-Levenberg least squares algorithm, and was used to estimate unknown coefficients. The dispersion coefficient was fit to the conservative tracer portion of the experiment and fixed for the colloid transport portion of the experiment. For saturated sand experiments, ψ_s was set equal to 1, and k_d was set equal to zero, thus simplifying the ADE to a conventional attachment model with k_a as the sole estimated parameter. Following the approach of Kasel et al. (2013), μ was estimated by initially fitting breakthrough curves and retention profiles for individual experiments, while simultaneously fitting k_a , k_d , and S_{max} . μ was only fit for unsaturated sand experiments and the average value was found to be equal to 0.7. k_a , k_d , and S_{max} were then estimated again by simultaneously fitting measured colloid breakthrough curves and retention profiles, with μ fixed to the average value. Volumetric moisture content was determined independently during column dissection.

8.3 RESULTS AND DISCUSSION

Unsaturated flow conditions were assessed by several means, and overall demonstrate that a uniform hydraulic gradient was achieved. The average gravimetric moisture content as measured by the digital scale remained constant throughout experiments (all standard deviations in moisture content < 0.005). Gravimetric moisture content along the length of the specimen were also measured at the termination of experiments. Moisture contents measured in this fashion show some variability, as shown in Figure 8.1. In all unsaturated experiments, measured moisture contents decreased with depth.

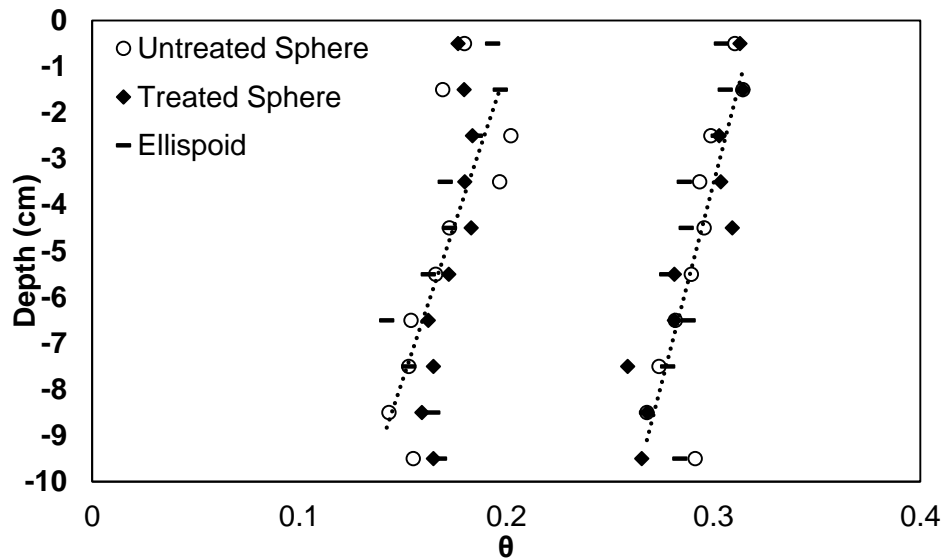


Figure 8.1: Moisture content profiles for unsaturated experiments measured during dissection. Dashed lines show the general trend of decreasing moisture content with depth.

In all unsaturated experiments the standard deviation in matric suction between the three tensiometers was less than 0.4 cm H₂O as shown in Table 8.1. Figure 8.2 shows example matric suction measurements for the untreated sphere unsaturated flow cell experiments. If tensiometers data were to follow the same trend as observed in the measured moisture content profiles, it would be expected that suction measurements would increase with depth. Suction at the lower boundary was increased until the tensiometers measurements were relatively constant and the average gravimetric moisture content stabilized. As such, no discernible trend between tensiometric measurements with depth was observed between the different unsaturated experiments.

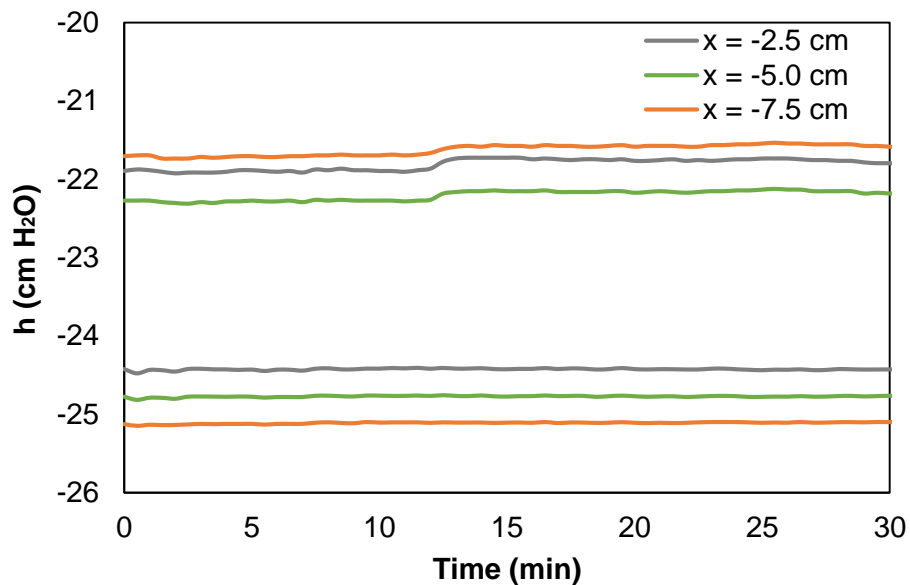


Figure 8.2: Matric suction measurements for untreated spherical colloids for both unsaturated flow cell tests. Upper data set is from the $\theta = 0.292$ experiment, lower data set is from the $\theta = 0.169$ experiment.

Table 8.1: Experimental conditions and mass balance

Colloid	S_e	θ	h_{avg} [cm H ₂ O]	q [cm/min]	D [cm]	M_{Eff}	M_{Soil}	M_{Total}
Sphere	1.0	0.373	na	0.241	0.148	0.993	0.009	1.002
Treated Sphere	1.0	0.373	na	0.242	0.144	0.994	0.011	1.005
Ellipsoid	1.0	0.378	na	0.240	0.141	0.990	0.024	1.014
Sphere	0.74	0.292 ± 0.014	21.9 ± 0.2	0.928	0.127	0.949	0.030	0.979
Treated Sphere	0.73	0.290 ± 0.020	21.7 ± 0.3	0.931	0.138	0.944	0.020	0.964
Ellipsoid	0.73	0.288 ± 0.012	21.6 ± 0.3	0.929	0.119	0.939	0.013	0.961
Sphere	0.38	0.169 ± 0.018	24.8 ± 0.3	0.252	0.319	0.824	0.093	0.917
Treated Sphere	0.39	0.173 ± 0.010	25.0 ± 0.4	0.253	0.305	0.833	0.107	0.940
Ellipsoid	0.39	0.171 ± 0.016	24.6 ± 0.1	0.255	0.317	0.796	0.130	0.926

NOTE: Treated sphere refers to colloids that underwent heating and rinsing without stretching. h_{avg} refers to the average measured matric suction, and the standard deviation is calculated between the three axial tensiometers. θ is the volumetric moisture content as measured by dissection at the termination of unsaturated experiments. q is the Darcy velocity, and D is the dispersion coefficient. All masses, M , are fraction of the total injected mass of colloids. M_{Eff} refers to mass eluted as measured by the effluent curve, M_{Soil} refers to mass of colloids attached to soil, and M_{Total} refers to total mass balance.

Breakthrough curves for the conservative tracer were conducted for all experiments, and were well described by the 1-D advection dispersion equation. Figure 8.3 shows example tracer breakthrough curves measured for saturated and unsaturated experiments involving untreated spherical colloids. In unsaturated porous media, breakthrough curves can sometimes exhibit extended tailing, indicating the presence of low flow, or immobile regions (Gao et al. 2006; W. Zhang et al. 2010). The lack of extended tailing observed in breakthrough curves suggests that immobile pore water did not play a significant role in transport and retention during saturated and unsaturated experiments. Dispersion, as measured by the conservative tracers, was slightly higher in the fully saturated tests than in the unsaturated tests with higher volumetric moisture contents. This is likely an artifact of the sprinkler versus a membrane at the top of the soil surface.

Estimated dispersion coefficients increased as moisture content decreased for all unsaturated experiments. This phenomena has been observed by others and is likely due to the increased tortuosity of flow paths in unsaturated porous media (Cherrey et al. 2003; Knappenberger et al. 2014).

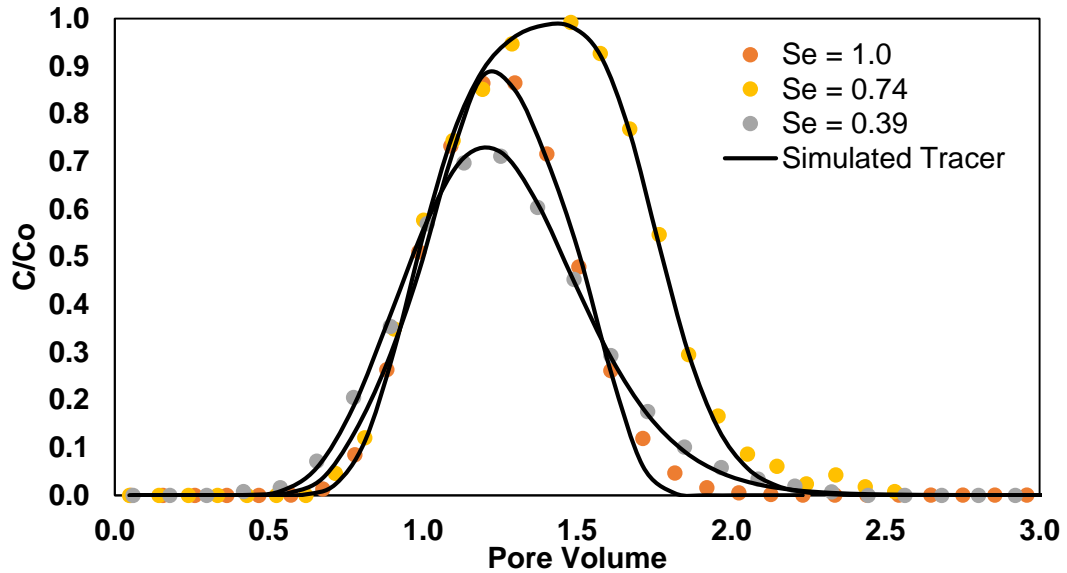


Figure 8.3: Measured and simulated conservative NaNO_3 tracer breakthrough curves for untreated spherical colloid transport experiments for saturated and unsaturated flow cells. C_o is the concentration of the injected tracer.

Colloid mass recoveries for all breakthrough experiments are presented in Table 8.1. At full saturation, only minor retention was observed in all experiments. The ratio of colloid to mean grain size diameter is ~ 0.003 , and is sufficiently low to largely rule out physical filtration or straining, which becomes important as size ratios increase to 0.005 to 0.008 (Bradford et al. 2002; Sang et al. 2013; Xu and Saiers 2009). Previous DLVO interaction potential calculations demonstrated that under the ionic strength and pH of experiments all colloids will experience repulsion with the soil water interface at all

separation distances. Thus, most likely retention in saturated experiments occurred around rough asperities, or in low velocity regions located between asperities and at granular contacts (Johnson et al. 2007; Ko and Elimelech 2000; Saiers and Ryan 2005; Shen, L.-P. Wang, Li, et al. 2012).

Greater levels of retention of colloids were observed in unsaturated experiments, with the mass of retained colloids increasing as moisture content decreased. At an effective saturation of 0.73, an average of 6% of injected colloids were retained, while at an effective saturation of 0.39, the average retained mass increased to 18%, a phenomena commonly observed in unsaturated porous media (Lenhart and Saiers 2002; Wan and Wilson 1994b; Zevi et al. 2009). In addition to increased retention, the unsaturated colloid breakthrough curves differed in shape from saturated breakthrough curves, as shown in Figures 8.4-8.6. For saturated breakthrough curves, the effluent concentrations rapidly increased to a constant value and then decreased to zero in a symmetric fashion. Unsaturated colloid breakthrough curves showed a gradual increase in effluent concentration over time, with a peak concentration that decreased with saturation level. Additionally, minor tailing of effluent concentrations was observed in unsaturated experiments.

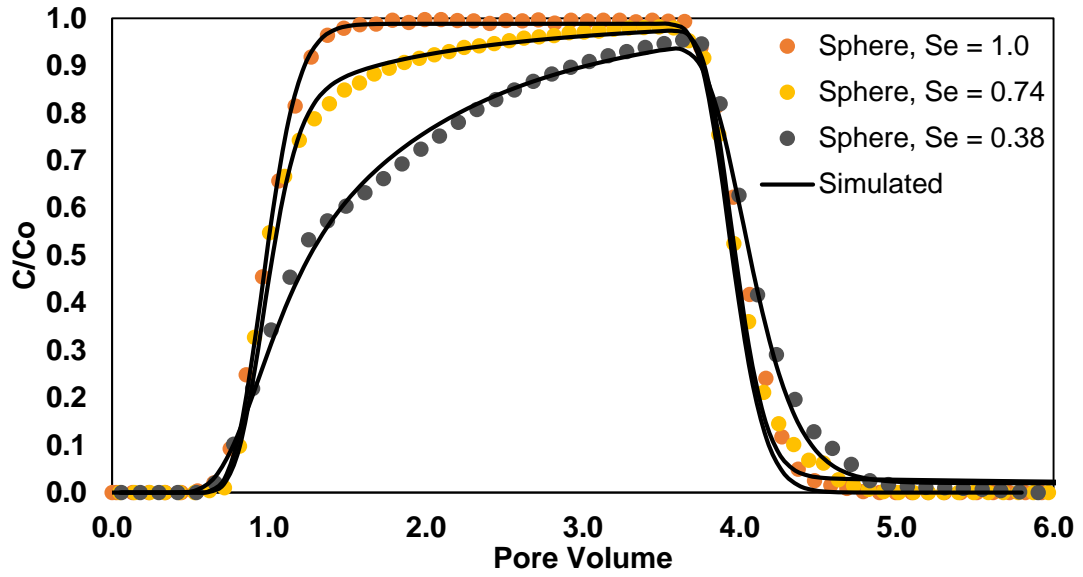


Figure 8.4: Measured and simulated normalized colloid breakthrough curves for untreated spherical colloids under varying degrees of saturation. C_o is the concentration of the injected colloids.

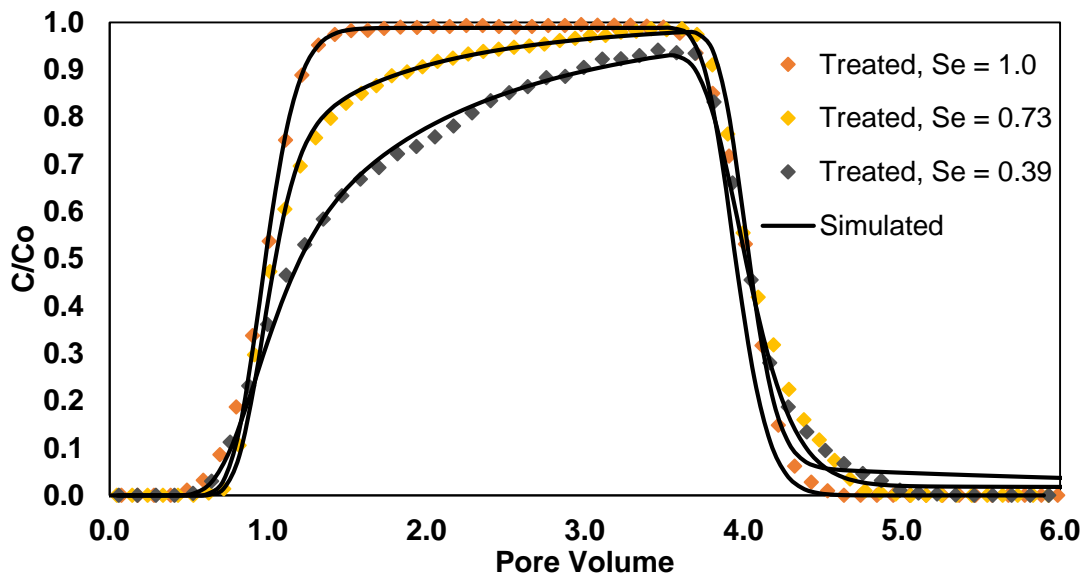


Figure 8.5: Measured and simulated normalized colloid breakthrough curves for treated spherical colloids under varying degrees of saturation.

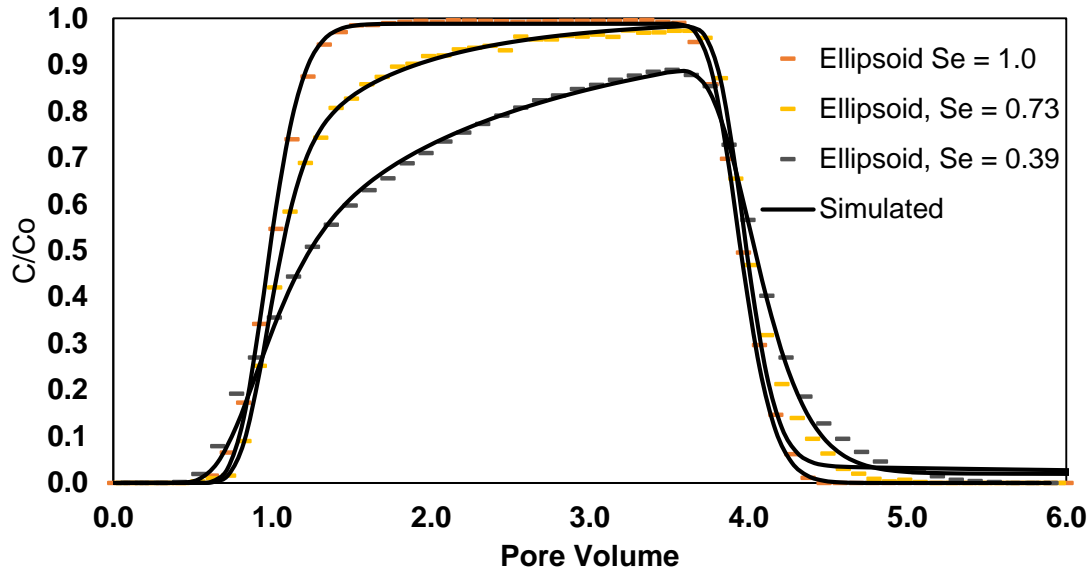


Figure 8.6: Measured and simulated breakthrough curves for ellipsoidal colloids under varying degrees of saturation.

The film casting and heating process had a negligible on the amount of retained colloids as measured by colloid breakthrough curves. As shown in Figure 8.7, retention of untreated and treated spheres were nearly identical, with slightly more treated spheres retained at the intermediate moisture content, and slightly less at the lowest moisture content. The close agreement between the untreated and treated spheres suggests that experiments were reasonably repeatable. At all levels of saturations greater amounts of ellipsoids were retained, though at both saturation and the intermediate saturation level the increase is minor. At the lowest saturation level, the difference in retention between spherical and ellipsoidal colloids becomes noticeable, with 20.4% of ellipsoids retained versus an average of 17.2% for spherical colloids.

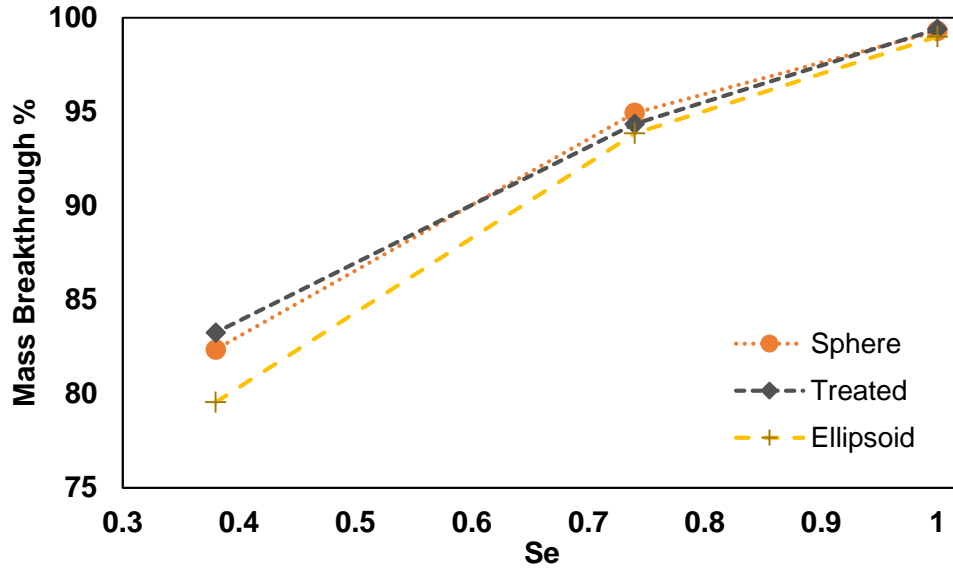


Figure 8.7: Mass of eluted colloids as measured by integration of the breakthrough curve.

At suctions greater than the air entry value, water is increasingly constrained to pendular water and films surrounding soil grains. Straining in thin films surrounding the porous media becomes significant in the retention of colloids when the moisture content drops below a critical value and pendular water no longer connects (Tokunaga 2011). For close packed uniform spheres with zero contact angle, the Laplace-Young equation shows that the critical suction at which pendular water connects is given as:

$$h_{critical} = \frac{B\gamma}{d_s}$$

where γ is the surface tension of water, and B is a constant related to the wetting conditions and soil wettability, and is equal to 12-18 for drying media (Fisher 1926; Tokunaga 2011; Wan and Tokunaga 1997). For the soil used in this study, this corresponds to a suction greater than -25 cm of H_2O , and an effective saturation less than 0.3. While the critical saturation increases for a non-zero contact angles, it is likely pendular water was not discontinuous in the soil and that thin film straining did not play an

important role in colloid retention (Knappenberger et al. 2014). Even at moisture contents above the threshold for film straining, colloid mobility in unsaturated soils typically increases with decreasing colloid size (Mitropoulou et al. 2013; Zhuang et al. 2005). Pore scale hydrodynamic simulations have shown that non-spherical particles will align their major axis parallel to the direction of flow as they approach constrictions (Xu et al. 2008). Ellipsoids, with their smaller minor axis (720 nm minor diameter), would therefore be expected to be more mobile than spherical colloids (1000 nm diameter) if retention were taking place based on size exclusion. This phenomena has been observed in saturated porous media, with the minor dimension of peanut shaped particles controlling size based retention (Xu et al. 2008).

Although film straining was an unlikely mechanism of retention, the increased tortuosity and constrained flow paths associated with unsaturated media will result in colloids coming in closer proximity to the soil surface and granular contacts (Mishurov et al. 2008; Torkzaban et al. 2008). Thus there is an increased likelihood of retention at granular contact points, rough asperities, or other locations that may be favorable to retention in unsaturated soils (Morales et al. 2009). In saturated media, this phenomena has been suggested as a possible cause for hyper-exponential retention profiles, and has been expanded to unsaturated media (Bradford and Torkzaban 2008; Bradford et al. 2006; Fang et al. 2013). This may explain the shape of the observed retention profiles shown Figures 8.8-8.10. As the saturation is decreased the retention profiles shift from relatively uniform with depth to increasingly nonlinear. At the intermediate saturation levels, retention profiles show increased retention near the top of the column before becoming relatively constant with depth. This effect is even more pronounced at the lower saturation level, with retained concentrations decreasing with depth. Interestingly, the decrease in retained colloids with depth stands in contrast to the decreasing moisture content with depth shown in Figure 8.1. The greater retention of ellipsoids may be explained by

increased retention at rough asperities in unsaturated media. The work in the previous chapter demonstrated the increased retention of ellipsoids in saturated porous media in terms of calculated DLVO secondary minimum depths. DLVO calculations between spheres and smooth and rough surfaces have demonstrated that the presence of asperities can create additional secondary minimum locations where particles can become immobilized (Huang et al. 2010; Shen, F. Wang, Li, et al. 2012; Shen, Lazouskaya, et al. 2012). Based on DLVO calculations in the previous chapter, it is expected that ellipsoids would be more susceptible to retention in rough locations than spherical colloids.

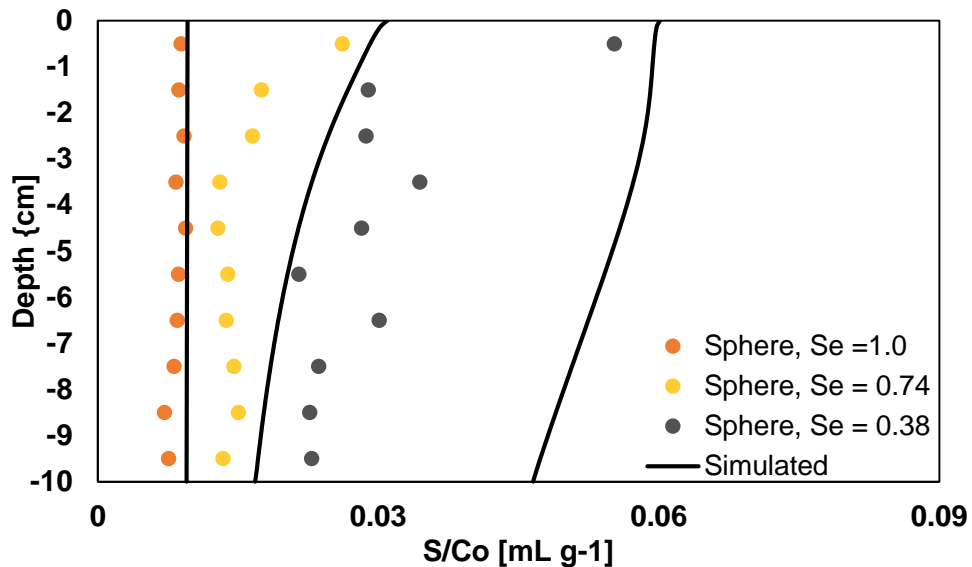


Figure 8.8: Measured and simulated normalized soil surface concentrations as a function of depth (distance from outlet) for untreated spherical colloids. Surface concentration, S , refers to the mass of colloids retained per mass of soil. Simulated curves are shown as solid lines.

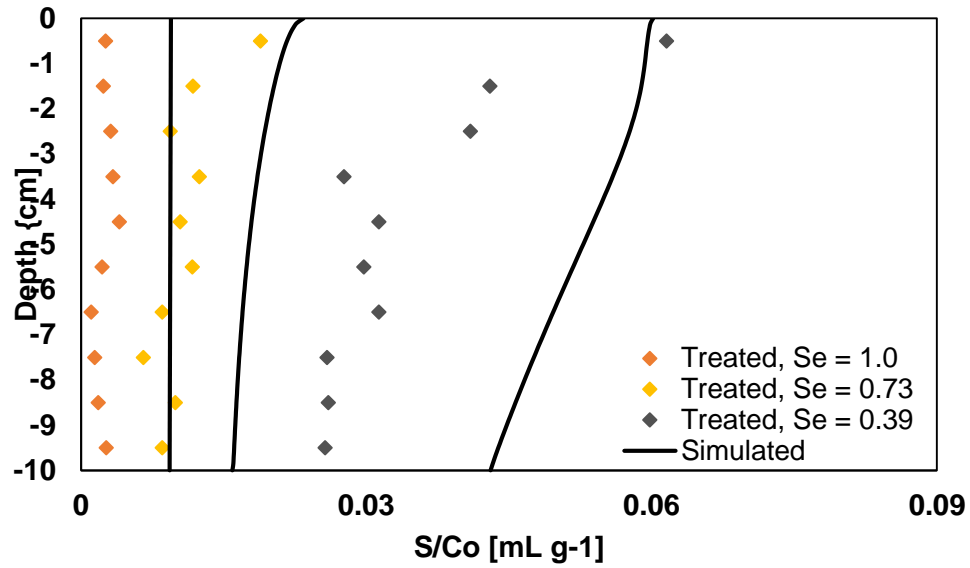


Figure 8.9: Measured and simulated normalized soil surface concentrations as a function of depth for treated spherical colloids.

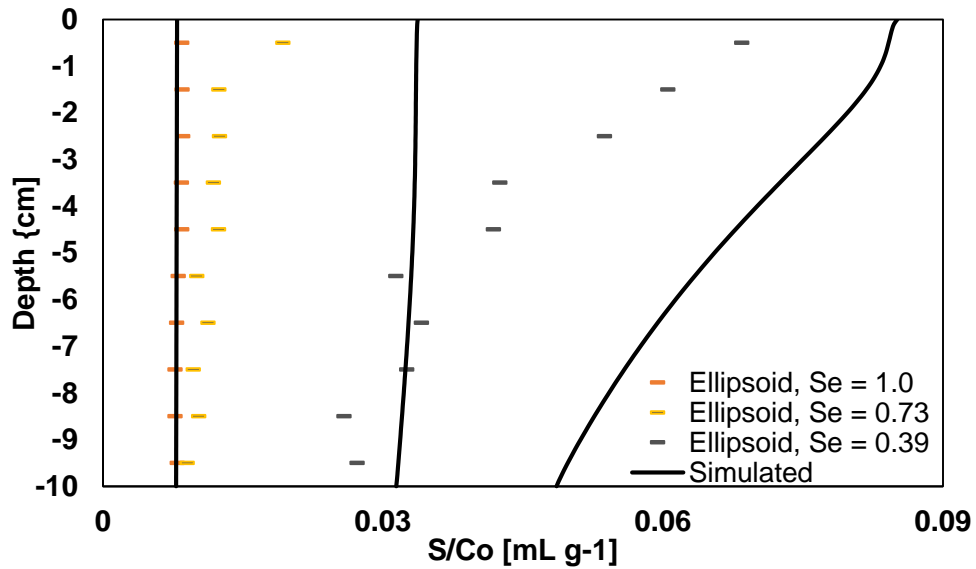


Figure 8.10: Measured and simulated normalized soil surface concentrations as a function of depth for ellipsoidal colloids.

In unsaturated porous media undergoing drainage, increasing suction reduces the soil moisture content and increases the area of the air-water interface (Chen et al. 2008; Saiers and Lenhart 2003a). The negative charge associated with the air-water interface coupled with the negative Hamaker constant for polystyrene-air-water system will result in DLVO calculations predicting repulsion at all distances to the air-water-interface for negatively charged colloids (Bradford and Torkzaban 2008; Israelachvili 2011). However, additional hydrophobic interactions can overcome electrostatic repulsion resulting in retention at the air-water interface (Bradford and Torkzaban 2008; Chen and Flury 2006; Zevi et al. 2005). While carboxylated polystyrene-latex microspheres are considered hydrophilic, a wide range of non-zero contact angles have been reported (Bradford et al. 2004; Sharma, Flury, et al. 2008; Wan and Wilson 1994b; Zevi et al. 2005), and porescale visualization experiments in capillary channels have demonstrated carboxylate microspheres can still attach to the air-water interface (Lazouskaya and Jin 2008). Similarly shaped breakthrough curves, with gradual increase in effluent concentration have previously been attributed to attachment and blocking or filling of the air-water interface (Gargiulo et al. 2008; Lenhart and Saiers 2002; Zhuang et al. 2005).

Colloid hydrophobicity has been demonstrated to be important in retention in unsaturated media, with hydrophilicity increasing mobility (Gargiulo et al. 2008; Zevi et al. 2005; Zhuang et al. 2005). Thus the increased retention of ellipsoids may be due to a difference in hydrophobicity. Aramrak et al. (2013) measured static contact angles of similarly treated spherical colloids and higher aspect ratio rod shaped colloids and observed an increase in hydrophobicity of the rod like colloids as measured by static sessile drop contact angles. Previous measurements have shown that both the heat treating process and stretching of colloids decreased the zeta potential of the colloids used in these experiments. If this decrease is due to the destruction of hydrophilic carboxyl groups, then it would be expected that both heat treatment and stretching would increase

the hydrophobicity of the colloids. Regardless of the absolute differences in hydrophobicity of the different colloids, it is expected that the increased surface area of the ellipsoids will result in greater exposure to contact with the air-water interface and may be the cause of greater retention of ellipsoids.

Although it is impractical to attribute retention mechanisms using simulated breakthrough curves and retention profiles, they can offer insight into the processes taking place. Estimated detachment coefficients for unsaturated experiments suggest that the retention was reversible, while reversibility was not observed in saturated experiments. This may in part be due to the larger velocities present in the unsaturated experiments leading to colloids at the soil water interface to become remobilized by hydrodynamic drag (Bergendahl and Grasso 2000; Sharma et al. 1992). Alternatively, colloids may become temporarily retained in pendular vortices, though tracer tests did not indicate the presence of immobile zones (Zevi et al. 2012; W. Zhang et al. 2010). Estimated detachment coefficients for the intermediate saturation level were an order of magnitude greater than at the lowest saturation level, suggesting that less detachment was taking place at the lower moisture content (Table 8.2). Attachment to the air-water interface is typically assumed to be irreversible, due to the large capillary forces acting on colloids though pore scale observations have shown particles can translate or slide along the interface (Chatterjee et al. 2012a; Lazouskaya and Jin 2008). The smaller detachment coefficients at the lowest moisture content suggest that more retention may be taking place at the air-water interface.

Table 8.2: Fitted model parameters and calculated standard errors.

Colloid	S_e	K_a [min ⁻¹]	K_d [min ⁻¹]	S_{max} [N_T/N_i g ⁻¹]	R^2
Sphere	1.0	0.0004 ± 0.0001	na	na	0.999
Treated Sphere	1.0	0.0009 ± 0.0002	na	na	0.998
Ellipsoid	1.0	0.0007 ± 0.0002	na	na	0.999
Sphere	0.74	1.5 ± 0.19	0.05 ± 0.01	0.055 ± 0.008	0.997
Treated Sphere	0.73	2.4 ± 0.34	0.08 ± 0.02	0.063 ± 0.009	0.994
Ellipsoid	0.73	3.1 ± 0.36	0.05 ± 0.01	0.053 ± 0.004	0.997
Sphere	0.38	3.1 ± 0.14	0.005 ± 0.001	0.068 ± 0.002	0.997
Treated Sphere	0.39	2.5 ± 0.11	0.005 ± 0.001	0.069 ± 0.002	0.998
Ellipsoid	0.39	2.5 ± 0.10	0.005 ± 0.001	0.093 ± 0.003	0.997

Note: N_T refers to recovered colloids in the sand, N_i refers to number of colloids in a unit volume of injected colloid suspension.

The maximum amount of retained colloids, as measured by the fitted parameter S_{max} increased as saturation decreased. This can be attributed the number of preferential retention sites increasing in saturated sand. These sites may include attachment at the soil-water interface, the air-water interface, and the air-water-meniscus (Karraker and Radke 2002; Wan and Tokunaga 1998; Zevi et al. 2005). S_{max} was relatively constant at the intermediate saturation level for the different colloid treatments and shape, while at the lower saturation maximum retained colloids was significantly larger for ellipsoids, suggesting greater capacity for retention of ellipsoidal colloids. Previous pore-scale visualization studies of rod-like colloids in saturated porous media have shown a ripening effect, whereby immobilized rods served as favorable retention sites for more rods (Seymour et al. 2013). This may explain the increased retention of ellipsoids at the lower moisture content, though no ripening was observed for ellipsoids in saturated sands in the previous chapter. The average fitted parameter k_a increased as saturation decreased. This suggests that as saturation decreased, the rate at which retention sites became occupied increased, though there was discernible trend in terms of colloid treatment or shape.

8.4 CONCLUSIONS

This chapter investigated the role of colloid shape on mobility in unsaturated porous media by examining the transport and retention of spherical and ellipsoidal colloids in sand at varying moisture contents. The mass of retained colloids increased as the saturation levels decreased, demonstrating the lower mobility of colloids in unsaturated porous media. In all unsaturated experiments, ellipsoidal colloids were retained in greater amounts and were less mobile than spherical colloids. This suggests that the previously observed lower mobility of ellipsoids in saturated porous media extends into the vadose zone. Particle shape became increasingly important in the fate of colloids in unsaturated porous media as saturation decreased, as evidenced by the observed difference in retention of spheres and ellipsoids that increased as moisture content decreased. Transport experiments conducted on spherical colloids that had undergone the same film casting and heating treatment as ellipsoids had similar breakthrough curves and levels of retention as untreated spherical colloids at all moisture contents. This suggests that the decreased mobility of ellipsoidal colloids in unsaturated sand was the result of the difference in colloid shape, and not simply an artifact of the shape modification process.

CHAPTER 9:
THE EFFECT OF IONIC STRENGTH AND HYDRAULIC FLUX ON THE
MOBILIZATION OF SPHERICAL AND ELLIPSOIDAL COLLOIDS FROM SAND
DURING DRAINAGE

9.1 INTRODUCTION

Soils in the vadose zone are routinely subject to imbibition and drainage. Numerous studies have demonstrated that in-situ colloids are readily mobilized by dynamic changes in saturation (Kjaergaard, Moldrup, et al. 2004; Kjaergaard, Poulsen, et al. 2004; Levin et al. 2006; Majdalani et al. 2008; Rousseau et al. 2004; Shang et al. 2008). The work of Cheng and Saiers (2009) suggests that drainage may be particularly effective in mobilizing colloids. As shown in a previous chapter, the mobilization of colloids by a drying front is affected by both porewater chemistry and the hydraulic conditions. Colloid mobility during drying has been found to decrease with ionic strength and increase with drainage rate (Bridge et al. 2009; Saiers et al. 2003; Zhuang et al. 2009).

The extent to which colloid shape affects mobilization during drying in porous media is unknown as previous studies have utilized either natural mineral colloids or synthetic spherical colloids. However, simple model experiments involving colloid detachment from flat substrates by air bubbles suggest that colloid shape may be important. Gómez-Suárez et al. (2001) examined the detachment of bacteria from hydrophilic and hydrophobic surfaces by the passage of an air bubble and found that spherical bacteria were detached in greater quantities than rod-shaped bacteria. In a similar study, Aramrak et al. (2013) examined the detachment of carboxylated polystyrene colloids of varying shape from a glass substrate by the passage of an air-bubble and found that spheres were detached in greater numbers than rod shaped colloids.

The objective of this study was to examine the role of colloid shape in mobilization by drainage in clean sand. Spherical and ellipsoidal colloids were attached to clean sand under varying ionic strength, then mobilized by draining of the soil column at constant flux. Additional experiments examine the impact of hydraulic flux, or drainage rate, on the mobilization of spherical and ellipsoidal colloids.

9.2 MATERIALS AND METHOD

9.2.1 Colloid and Porous Media Preparation

Spherical and ellipsoidal colloids were used to investigate the role of colloid shape in mobilization during drainage. Carboxylated polystyrene-latex 1 μm microspheres (Bang Laboratories, Inc. Fishers, IN) and prolate ellipsoids (0.76 μm by 1.75 μm) prepared using the method of Ho et al. (1993b) and Champion et al. (2007) were used in all experiments and have been described in a previous chapter. Briefly, spherical colloids were cast in polyvinyl alcohol (PVA) films, heated to 125° C, and the films were mechanically stretched to the desired aspect ratio. Colloids were then recovered by dissolving the PVA films and cleaned by centrifuging and resuspending the colloids in 30% isopropanol water mixture 10 times before finally suspending in DI water. Graded silica sand ($d_{50} = 0.36$ mm, $C_u = 1.82$, US Silica) served as the porous media in all experiments. As in previous chapters, the sand was subjected to a rigorous cleaning procedure which included repeated ultrasonification, soaking in sodium dithionite, hydrogen peroxide, and nitric acid, and rinsing with DI over a #200 sieve to minimize any effects of geochemical heterogeneity on colloid retention.

9.2.2 Column Mobilization Experiments

Experiments consisted of two stages, with the first stage involving injecting colloids into a saturated sand under varying ionic strength, and the second stage involved draining the soil specimen at constant hydraulic flux to mobilize retained spheres and ellipsoids.

Saturated soil samples were introduced to an acrylic flow cell (L=10 cm, ID=5 cm) using the modified slurry deposition procedure described in previous chapters and densified to 0.37-38 porosity (Bandini and Sathiskumar 2009; Carraro et al. 2003; Wood et al. 2008). Both ends of the flow cell were capped with stainless steel plates with 1 mm holes and supported by hydrophilic nylon mesh membranes with 10 μm openings (U-CMN-10, Component Supply Company).

In the first stage of the experiment the pore fluid was pumped (Cole Parmer Masterflex L/S) downward through the column at a Darcy velocity of 0.24 cm/min. Experiments were out carried to assess the impact ionic strength (IS) on colloid mobilization. pH 10 solutions were prepared with 0.2 mM Na_2CO_3 and NaCl was used to adjust the ionic strength to 1 and 10 mM. Columns were pre-equilibrated by first passing 15 solutions of background electrolyte. Columns were seeded with colloids by injecting three pore volumes of colloids at a concentration of 10 mg/L ($1. \times 10^7$ particles/L), which is the equivalent of 2.3 mg of spheres and ellipsoids.

The second stage of the experiment consisted of draining the saturated soil column to mobilize colloids retained during the transport stage of the experiment. The top end cap and nylon membrane were removed from the flow cell, exposing the soil surface to the atmosphere. Flow cells were drained from the bottom using a peristaltic pump at a constant hydraulic flux of 0.24 cm/min. Additional experiments were carried out at a high and low hydraulic flux to assess the impact of drainage rate on colloid mobilization. These experiments involved seeding the soil column with spheres or ellipsoids at 10 mM IS. Columns were drained at 0.36 cm/min for high flux experiments and 0.08 cm/min for low flux experiments. The experimental matrix along with measured masses of colloids are summarized in Table 9.1. Effluent samples during both stages of the experiments were collected using a fraction collector (ISCO Retriever II) and colloid concentrations were measured by UV-Vis spectrophotometry (Shimadzu UV/1800) at 435 nm.

Table 9.1: Experimental conditions and mass balance information

Colloid Shape	IS [mM]	q_{Drain} [cm/min]	M_{Injected} (mg)	$M_{\text{Deposited}}$ (mg)	$M_{\text{Mobilized}}$ (mg)
Sphere	1	0.24	2.228	0.015	0.012
Sphere	10	0.08	2.239	0.514	0.014
Sphere	10	0.24	2.222	0.514	0.021
Sphere	10	0.36	2.226	0.508	0.032
Ellipsoid	1	0.24	2.220	0.015	0.018
Ellipsoid	10	0.08	2.250	0.654	0.019
Ellipsoid	10	0.24	2.228	0.670	0.037
Ellipsoid	10	0.36	2.232	0.676	0.059

NOTE: IS refers to ionic strength and q_{Drain} is the drainage rate or flux. M_{inj} refers to mass of colloids injected during the first stage of the experiment as measured by the effluent curve, $M_{\text{Deposited}}$ refers to mass of colloids attached to soil as measured by integration of the effluent curve, and $M_{\text{Mobilized}}$ refers to the mass of mobilized colloids during the second stage of the experiment.

9.3 RESULTS AND DISCUSSION

Spherical and ellipsoidal colloid breakthrough curves measured during the saturated transport stage are shown in Figure 9.1. Breakthrough curves were similar in all experiments with colloid concentrations rising sharply to a constant value before decreasing to background levels in a symmetrical fashion. No tailing was observed for spherical and ellipsoidal colloids suggesting that no reentrainment took place during the saturated stage of the experiments. Very little colloid retention was observed in low ionic strength experiments, however a slightly greater mass of ellipsoids was retained. As discussed in previous chapters, the low levels of retention is expected as DLVO interaction energies predict an extremely shallow secondary minimum for both particle shapes at low ionic strength. The small amounts of spherical and ellipsoidal colloids retained in low ionic strength experiments likely took place near granular contacts and rough asperities on the sand surface, as the ratio of colloid to mean grain size diameter is below values typically associated with straining (Bradford et al. 2002, 2006; Sang et al. 2013; Xu and Saiers 2009).

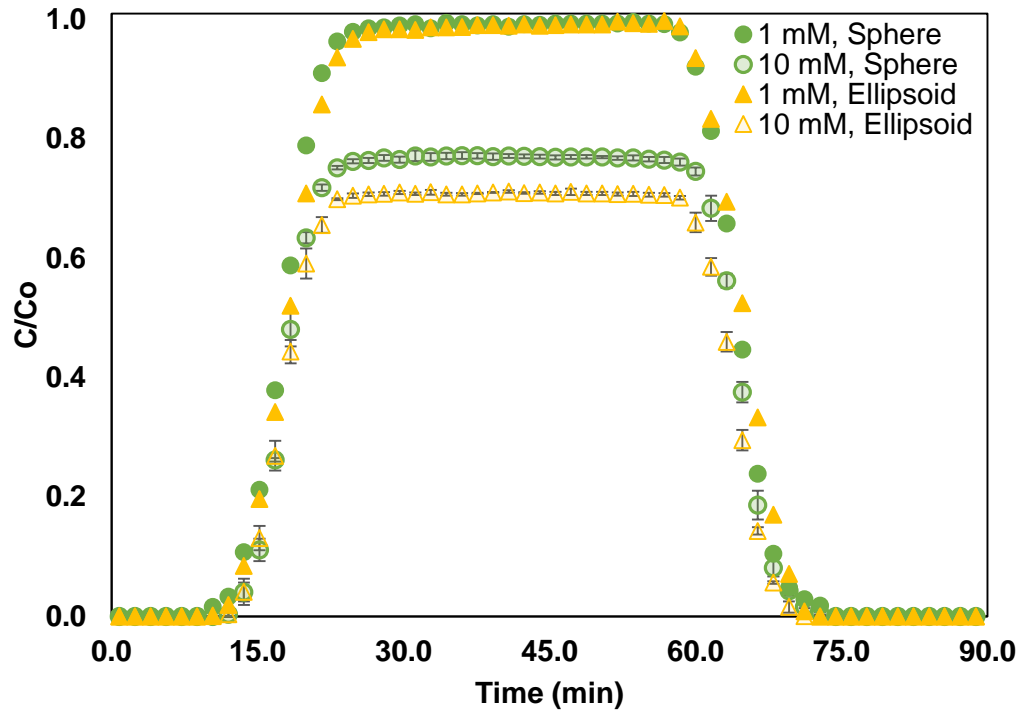


Figure 9.1: Measured effluent colloid concentration breakthrough curves for spherical and ellipsoidal colloids under varying ionic strength during first stage of experiment. Error bars are the standard deviations from three replicates. C_o is the concentration of the injected colloids.

Peak effluent concentrations decreased and the mass of retained colloid increased for high ionic strength experiments. Ellipsoidal colloids were retained in greater quantities and peak effluent concentrations were lower than spheres in high ionic strength experiments. 70% of injected ellipsoids were retained in high ionic strength experiments versus 77% of injected spheres. Calculated DLVO interaction energies between the colloids and the sand surface from a previous chapter demonstrate that the secondary minimum is deeper for ellipsoidal colloids. The shallower secondary minimum associated with spherical colloids led to less retention taking place in the saturated transport stage of the experiment (Shen et al. 2007; Torkzaban et al. 2008).

Appreciable quantities of spherical and ellipsoidal colloids were mobilized from the sand during the drainage portion of the experiment. Effluent colloid concentrations curves measured during the drainage stage of the experiment are shown in Figure 9.2. Colloids were below detectable limits until the seven minute mark and did not vary significantly with colloid shape. After the first arrival of colloids at the outlet, concentrations increased continuously and rapidly before reaching a peak values between 24% and 50% of the injected colloid concentration. Spherical colloid concentrations were lower in the early part of the curve for low ionic strength experiments, but peak values were similar for spheres and ellipsoids in low ionic strength experiments. In high ionic strength experiments, sphere concentrations increased less rapidly and reached a significantly lower peak value than ellipsoids.

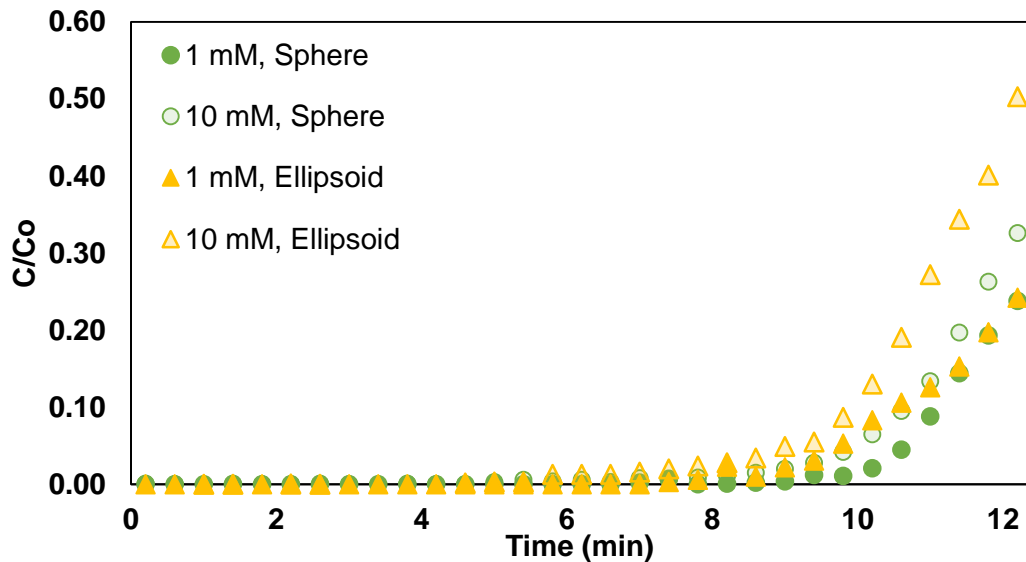


Figure 9.2: Measured drainage effluent colloid concentrations under varying ionic strength for spherical and ellipsoidal colloids during second stage of experiment.

The absolute mass of mobilized colloids along with mass fraction of mobilized spheres and ellipsoids for high and low ionic strength are shown in Figure 9.3. Relatively high mass fractions of colloids were mobilized in low ionic strength experiments, in large part due to the relatively small quantities of retained colloids during the saturated transport stage of the experiment. 82% of retained spherical colloids were mobilized while 76% of retained ellipsoids were mobilized in low ionic strength experiments. This stands in contrast to the lower absolute mass of spherical colloids mobilized. The mass fraction of mobilized spheres and ellipsoids decreased with ionic strength, similar to the observations Saiers et al. (2003) for kaolin mobilization from sand during drainage. The mass fraction of mobilized spherical colloids was 4% and 6% for ellipsoids in high ionic strength experiments. The absolute mass of mobilized colloids increased for both colloid shapes, however the absolute mass of ellipsoids more than doubled.

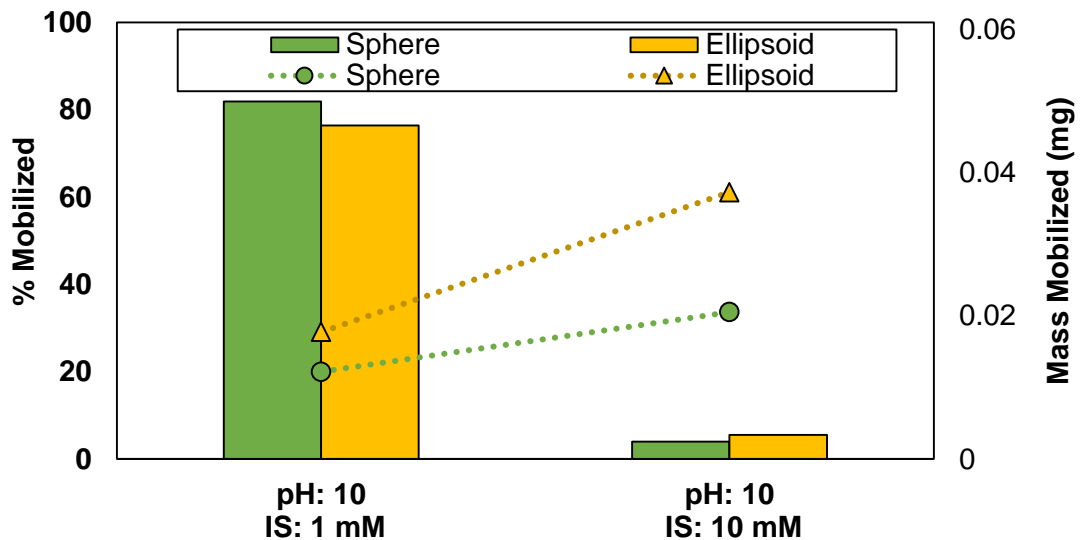


Figure 9.3: Percent mass of mobilized colloids (bars, left axis) compared with actual mass of mobilized colloids (lines, right axis) at high and low ionic strength.

Colloid concentration measured for varying drainage flux and constant high ionic strength are shown in Figure 9.4. Colloids arrived at the outlet earlier in time for high flux experiments and significantly later in time for low flux experiments as expected. Drainage concentration curves were similar in shape for high and medium flux experiments, however peak concentrations were lower in medium flux experiments. Low flux experiments exhibited a more gradual increase in drainage concentrations and slightly lower peak concentrations were observed than in medium flux experiments. Peak effluent concentrations were lower for spherical than ellipsoids for all drainage fluxes.

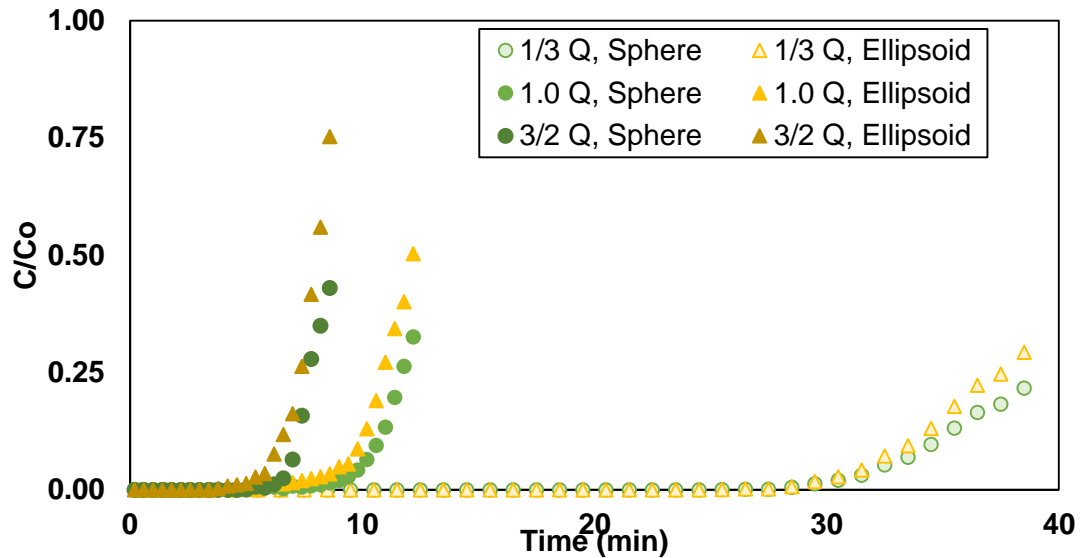


Figure 9.4: Spherical and ellipsoidal colloid effluent concentrations measured during drainage at varying hydraulic flux. Q is normalized flux, $Q = q_{\text{experiment}}/q$, where q is the hydraulic flux (0.24 cm/min) during the saturated portion of the experiment. All experiments carried out at IS = 10 mM.

The absolute mass and mass fractions of mobilized colloids for varying flux are shown in Figure 9.5. The mass fraction and absolute mass of mobilized colloids increased with flux for spherical and ellipsoidal colloids. This agrees with previous observations of higher colloid mobilization with increasing drainage flux in sands (Bridge et al. 2009; Chen et al. 2008; Saiers et al. 2003; Zhuang et al. 2009). The mobilization of spherical and ellipsoidal colloids was similar in low flux experiments, with slightly less spheres mobilized. However, the disparity in mobilization between spheres and ellipsoids increased with hydraulic flux, with consistently more ellipsoids mobilizing.

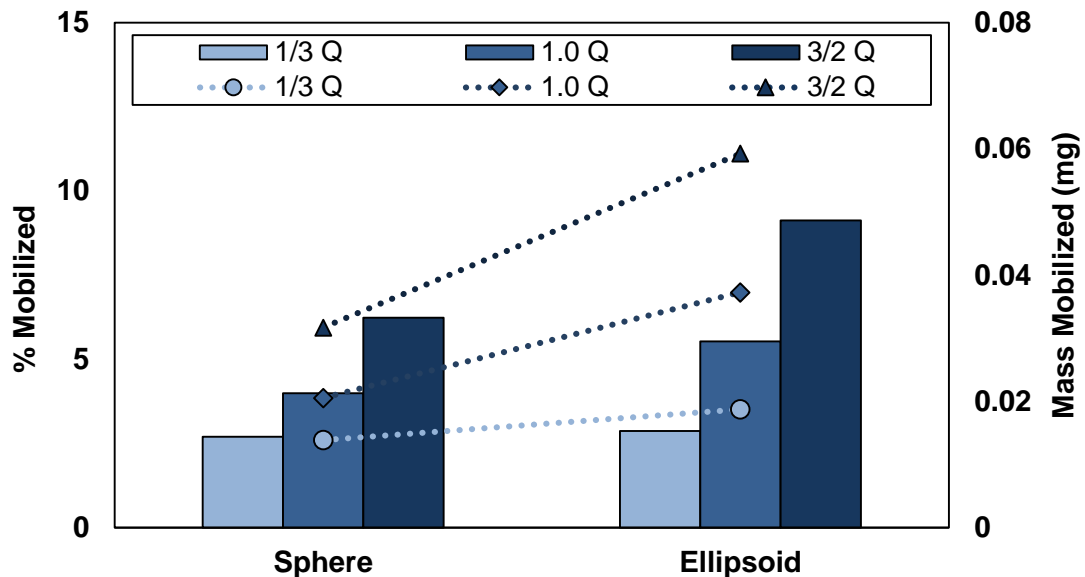


Figure 9.5: Percent mass of mobilized spheres and ellipsoids (bars, left axis) compared with actual mass of mobilized colloids (lines, right axis) under varying hydraulic flux. Q is normalized hydraulic flux, $Q = q_{\text{experiment}}/q$, where q is the hydraulic flux (0.24 cm/min) during the saturated portion of the experiment. All experiments were carried out at $IS = 10$ mM.

Spherical colloids were consistently mobilized in lower amounts than ellipsoidal colloids. Chatterjee and Flury (2013) assessed the impact of particle shape capillary forces associated with the air-water interface and found that the theoretical maximum force exerted on spherical particles is less than the force exerted on ellipsoidal colloids. This is unlikely to matter as the attachment force associated with colloid retention in the secondary minimum is 4-6 orders of magnitude smaller than the capillary mobilizing force, as was demonstrated in a previous chapter. Contrary to the observations made in this chapter, Aramrak et al. (2013) found that spherical colloids were more likely to be detached from a silica surface by a moving air-water interface than ellipsoidal colloids. (Aramrak et al. 2013). However, their experimental geometry differed significantly from porous media, and colloids were initially attached to the surface in the primary minimum.

The larger surface area and contact line associated with ellipsoidal colloids may have increased the chance of these particles coming in contact with the air-water interface and thus becoming mobilized. Additionally, it is possible that spherical colloids were more hydrophilic than ellipsoids. This is supported by the greater retention of ellipsoids in unsaturated steady-state experiments described in a previous chapter. Aramrak et al. (2013) measured static and dynamic contact angles of similarly treated spherical colloids and higher aspect ratio rod shaped colloids and observed greater static contact angles for rods, though dynamic contact angles were similar. Previous porescale studies have demonstrated hydrophobic colloids are more likely to be detached from surfaces by a dynamic passage of the air-water interface (Sharma, Flury, et al. 2008).

The sensitivity of colloid mobilization to flux suggests that in addition to detachment by capillary forces associated with the air-water interface, colloid detachment may have been caused by hydrodynamic drag during drainage. Although no hydrodynamic detachment was observed for spheres or ellipsoids during the saturated stage of experiments, in the drainage stage of the experiment the average porewater velocity

increased significantly over time as the moisture content decreased. Spherical colloids mobilized by hydrodynamic drag will roll on a collector surface (Sharma et al. 1992). It is possible that some spherical colloids may have been transported to granular contacts or to rough asperities on the sand surface where they were less likely to be mobilized further during drying. The impact of hydrodynamic shear on an ellipsoidal colloid attached to a surface is less clear. Hydrodynamic simulations of suspended ellipsoidal colloids have demonstrated that the longer axis will align parallel to the prominent stream line (Xu et al. 2008). This suggests that ellipsoids on the sand surface would be aligned with their long axis parallel to the direction of shear, and thus would be less likely to roll; though colloids in the secondary minimum may slide along the soil surface (Lazouskaya et al. 2013).

9.4 CONCLUSIONS

This study highlights the effect of porewater chemistry and hydraulic flux on the mobilization of spherical and ellipsoidal colloids in clean sand. The mass fraction of mobilized colloids decreased with ionic strength, while the absolute mass mobilized increased. Spherical colloids were mobilized in smaller quantities than ellipsoids at both low and high ionic strength. Colloid mobilization was also sensitive to hydraulic flux, with smaller quantities mobilized in low flux experiments and greater quantities mobilized in high flux experiments. Similar quantities of spherical and ellipsoidal colloids were mobilized in low flux experiments, however significantly more ellipsoids were mobilized in low and medium flux experiments. The work in this chapter suggests that ellipsoids are more readily mobilized than spherical colloids by drainage in sand under conditions unfavorable to colloid attachment at the soil-water interface.

CHAPTER 10: CONCLUSIONS AND FUTURE WORK

This dissertation investigated the transport, retention, and mobilization of colloids in non-idealized systems. The first part of the dissertation focused on the transport and retention of spherical colloids in iron oxide coated sand and zeolite, which have typically been used in permeable reactive systems to treat dissolved contaminants. In these experiments, clean silica sand was used as a baseline material for comparison of colloid transport and retention in the two reactive soils under saturated and unsaturated conditions. Some of the major lessons learned in these studies can be summarized as follows:

Colloid transport in saturated permeable reactive media

- Colloid transport through saturated permeable reactive soil is strongly affected by the porewater chemistry, including pH and ionic strength.
- Very little colloid retention was observed in clean sand at pHs greater than or equal to 5.5, however significant colloid retention occurred at pH 4. Theoretical DLVO interaction potential energies between the colloids and the silica surface indicated a significant energy barrier between colloids and the sand which limits colloid attachment to the soil surface. Thus non-DLVO forces such as hydrophobic interactions contributed to colloid retention in low pH experiments.
- Colloids were retained in significantly greater quantities in iron oxide coated sand at pHs below the isoelectric point of the hematite coating. Calculations of DLVO interaction potential energy between the colloids and the iron oxide coating demonstrate that there is no energy barrier to colloid attachment to the iron oxide surface. Thus colloid attachment is favorable in iron oxide coated sands at low pH. Greater colloid retention was observed in iron oxide coated sand than in clean

silica sand at pHs above the isoelectric point of the hematite coating as well. This is due to the smaller energy barrier and deeper secondary minimum in the interaction potential energy between the colloid and iron oxide surface.

- Colloid mobility in zeolites was significantly impaired at both low and high pH despite DLVO theory predicting a large energy barrier between the zeolite surface and colloid. The overall trend of colloid retention in zeolite as a function of pH closely resembled those observed in clean sand despite greater retention occurring in the zeolite. Although geochemical minerals not identified by bulk measurements such as XRD or electrophoretic measurements may have contributed to colloid retention in zeolite in low pH experiments, the similarity to clean sand suggest that geochemical heterogeneity is solely at work. However, it is very unlikely that geochemical heterogeneity is sufficient to explain the observed colloid retention in high pH experiments. SEM micrographs revealed highly angular particles with microscale roughness in the form of cuboid crystals which occurred in patches on the zeolite surface. The reduced sensitivity of colloid retention in zeolites to pH suggests that these rough crystalline patches on the zeolite significantly impaired the transport of colloids. Additionally, colloid retention profiles exhibited increased colloid soil surface concentrations near the inlet of zeolite experiments suggesting that colloid retention at granular contact points is an important colloid retention mechanism in zeolite.
- Colloid retention in all permeable reactive soils increased with ionic strength at low and high pH. Colloid retention was more sensitive to changes in ionic strength at low pH, with small changes in ionic strength significantly increasing colloid retention in all soil types. DLVO calculations of interaction energies demonstrate that increasing ionic strength reduces the energy barrier between the colloid and soil surface and increases the depth of the secondary minimum which in turn

results in greater colloid retention. Colloid retention in zeolite was more sensitive to ionic strength than silica sand, and greater colloid retention occurred at all ionic strengths.

- Colloid retention in iron oxide coated sand was sensitive to ionic strength in low pH experiments despite no energy barrier between the hematite coating and colloids. This is due in part to the heterogeneous, patchy nature of the iron oxide coating. Thus higher ionic strengths effectively enhanced colloid retention at iron oxide patches by reducing the energy barrier between colloids and bare silica portions of the soil surface. In high pH experiments, a large energy barrier existed for colloids and coated and uncoated portions of the iron oxide sand surface. However, the energy barrier was smaller and the secondary minimum deeper for colloid interactions with the iron oxide coating which enhanced colloid retention as compared to clean silica sands.
- Generally, at low pH colloid retention was greatest in iron oxide coated sand, followed by zeolite, and silica sand. At high pH colloid retention was greatest in zeolites, followed by iron oxide coated sand and clean silica sand.

Colloid transport in unsaturated permeable reactive media

- Hydraulic characterization utilizing the multistep outflow method demonstrated that the silica sand, iron oxide coated sand, and zeolite unsaturated properties are well described by Kosugi's soil water characteristic curve and hydraulic conductivity function. The water retention and unsaturated hydraulic conductivity of the three soils is similar in the range of suctions measured. However greater volumes of water were retained in the zeolite due to its greater porosity. Additionally, a significant fraction of zeolite pore water is tightly bound to the soil surface.

- Colloid mobility in all soils was significantly reduced under unsaturated conditions. Although unsaturated soil water characteristics were similar for silica and iron oxide coated sand, greater colloid retention was observed in iron oxide coated sands under unsaturated conditions. The difference in colloid retention between clean and iron oxide coated sand increased as the moisture content decreased because the greater tortuosity associated with unsaturated flow enhanced colloid interactions with the iron oxide patches.
- Colloid retention in zeolite was significantly greater in unsaturated zeolite than either of the two sands. As with iron oxide coated sand, the increased tortuosity associated with unsaturated flow enhanced colloid interactions with the rough zeolite surface. Additionally, colloid surface concentrations near the inlet of the zeolite flow cells increased as moisture content decreased. This suggests that colloid retention near granular contacts in zeolite were enhanced during unsaturated transport.

Colloid mobilization from permeable reactive media by drainage

- Colloids were readily mobilized from all soils by a downward propagating drying front during drainage. Colloid mobilization in the different soils was sensitive to pH, ionic strength, and drainage rate.
- Theoretical calculations of the mobilizing detachment force of colloid attachment to the air-water interface was smaller than the resisting force for colloids attached to soil surfaces in the primary minimum, but significantly larger than the resisting force for colloids attach to soil surfaces in the secondary minimum.
- Colloid mobilization in all soil types was reduced in low pH experiments. Colloid mobilization from iron oxide coated sands was significantly lower than in clean sands at low pHs because colloids were retained in the primary minimum near iron

oxide patches. Although the percent of mobilized colloids decreased with increasing ionic strength in low pH experiments for all soils, the absolute mass of mobilized colloids increased for clean sand. In iron oxide coated sand the mobilized mass of colloids decreased significantly. This suggests that higher ionic strength increased retention of colloids in the primary minimum at iron oxide coated patches.

- Low colloid retention during high pH, high ionic strength experiments resulted in large mass fractions of colloid mobilization occurring in clean and iron oxide coated sand. The absolute mass of mobilized colloids increased with IS in high pH clean and iron oxide coated sand experiments despite the mass fraction of mobilized colloids decreasing. This is because the mobilization driving force of the air-water interface is significantly greater than the resisting attachment force for colloids retained in the secondary minimum. Smaller quantities of colloids were mobilized from iron oxide coated sands than clean sands suggesting that a portion of the colloids may have been retained in the primary minimum despite the energy barrier to attachment at iron oxide patches.
- The absolute mass and mass fraction of colloids mobilized was lowest in zeolite under all porewater chemistries except in the low pH, low IS experiment set. This suggests that colloids may have been retained in the primary minimum near rough asperities. Additionally colloid retention near granular contacts in zeolite may be less susceptible to mobilization by drying fronts due to the low likelihood of the air-water interface coming in close proximity to the soil surface in this region.
- Colloid mobilization in all materials increased with drainage rate, suggesting that colloid mobilization may have been influenced by hydrodynamic drag. The mobilized mass fraction for the varying drainage rates was greatest in clean sand, followed by iron oxide coated sand and zeolite. Smaller quantities of colloids were

mobilized from iron oxide coated sand than in clean sand for low flux experiments; however this was reversed in high flux experiments, with a greater mass mobilized from iron oxide coated sands. Colloid mobilization in zeolites was less sensitive to changes in drainage rate, and the absolute mass and mass fraction of mobilized colloids was significantly lower than in clean and iron oxide coated sand.

Future work on colloid transport in permeable reactive media

- The saturated transport of colloids through permeable reactive soils was limited to steady-state porewater velocity and chemistry. Future work should focus on colloid retention and mobilization due to changes in ionic strength and pH to assess the reversibility of colloid retention in these materials. Similarly, previous studies have demonstrated that porewater velocity can affect colloid retention in clean sands (Tong and Johnson 2006). Future work should assess the impact of porewater velocity in colloid retention in iron oxide coated sand and zeolite.
- Experiments were conducted at a single porosity. The increased retention associated with granular contacts in zeolite suggest that this parameter may be extremely important in colloid retention, thus future work should investigate the effect of porosity on colloid retention in permeable reactive medias.
- Natural organic matter (NOM) is extremely common in the environment and has been shown to significantly affect the fate of colloids in saturated and unsaturated porous media (Franchi and O'Melia 2003; Petosa et al. 2010). NOM is particularly important in colloid transport through iron oxide coated sands because NOM can coat positively charged iron oxides and significantly inhibit colloid retention (D. Wang et al. 2013). It is important ascertain how colloid transport in zeolites is affected by the presence of NOM.

- The transport of colloids through unsaturated permeable reactive media was limited to constant pH and ionic strength. Future work should explore the coupled effects of porewater chemistry and saturation on colloid retention in unsaturated permeable reactive media.
- Investigations of the transport of colloids through permeable reactive materials at lower levels of saturation than the ones used in this study should be conducted. Specifically, colloid mobility in silica sand decreases significantly when pendular water becomes discontinuous due to colloid retention in thin films surrounding the soil grains (Wan and Tokunaga 1997). Observations in this thesis strongly suggest that colloid transport under these conditions would be significantly impaired in permeable reactive media.
- Drainage induced colloid mobilization was significant in all permeable reactive media. Several studies have investigated proposed of various numerical models to describe colloid mobilization by flow transients in clean sand and natural sediments (Russell et al. 2012; Shang et al. 2008; Q. Zhang et al. 2012). It is unclear however if these models are applicable in permeable reactive media.
- Soils in the natural environment routinely undergo cyclical imbibition and drainage which can increase colloid mobility (Aramrak et al. 2014). Future work should investigate colloid transport in permeable reactive soils during cyclical imbibition and drainage, as well as step changes in moisture content.

The second half of the dissertation investigated the role of colloid shape on transport, retention, and mobilization in saturated and unsaturated clean silica sand. Ellipsoidal, rod-like, colloids were fabricated from carboxyl microspheres by heating and physically stretching spherical colloids that were previously suspended in polyvinyl alcohol films. The

ellipsoidal colloid dimensions were measured using SEM micrographs and the colloid surface was characterized by electrophoretic mobility measurements.

Role of colloid shape in saturated transport

- Theoretical DLVO interaction potentials calculated by surface element integration demonstrate that colloid shape affects the magnitude and shape of the interaction potential energy between colloids and the sand surface. The orientation of ellipsoidal colloids with respect to the soil surface affects the shape and magnitude of the interaction potential energy. Ellipsoids oriented with the long axis parallel to the soil surface have a larger energy barrier to attachment to the soil surface in the primary minimum but a deeper secondary minimum than spherical colloids. Ellipsoids oriented with the long axis perpendicular to the soil surface have a significantly lower energy barrier to attachment to the soil surface in the primary minimum but a shallower secondary minimum than spherical colloids.
- The transport of spherical and ellipsoidal colloids in clean sand is affected by ionic strength. Spheres and ellipsoidal colloids were retained in extremely low quantities in low ionic strength experiments. Thus, the ellipsoidal colloids were not subject to sized based retention in saturated silica sand, suggesting that the major ellipsoid axis was parallel to the direction of flow.
- The retention of spherical and ellipsoidal colloids increased with ionic strength. DLVO calculations indicate that spheres and ellipsoids were attached to the soil surface in the secondary minimum. Ellipsoids were retained in greater quantities than spherical colloids in medium and high ionic strength experiments, and the difference in the retention between the two colloid shapes increased with ionic strength agreeing with the results of others. The lower retention of spherical colloids is due to the shallower secondary minimum in the interaction energy between the colloid and the sand surface. The increased retention of ellipsoids

supports the observation that ellipsoidal colloids are oriented with the long axis parallel to the direction of flow and the soil surface. Thus ellipsoids were less mobile in saturated silica sand due to the deeper secondary minimum between colloids and the sand surface.

Role of colloid shape in unsaturated transport

- Spherical and ellipsoidal colloids were less mobile in unsaturated silica sand than in saturated silica sand.
- At intermediate saturation levels spherical and ellipsoidal colloids were retained in similar quantities, although slightly more ellipsoidal colloids were retained. However, at the lowest saturation ellipsoids were retained in significantly greater quantities than spherical colloids. This suggests that colloid shape may affect interactions at the air-water interface and the air-water-meniscus in unsaturated sand, and that previous observations of the reduced mobility of ellipsoidal colloids in saturated porous media extends into the vadose zone.
- Additional experiments utilizing colloids that underwent the same heating and film casting procedure as ellipsoidal colloids were retained in similar quantities as untreated spheres at all saturation levels. This demonstrates that the lower mobility of ellipsoids in unsaturated sand is due to the particle shape and not an artifact of the shape modification procedure.

Role of colloid shape in mobilization from clean sand by drainage

- Spherical and ellipsoidal colloids were readily mobilized from sand by a downward propagating drying front during drainage. Colloid mobilization was sensitive to ionic strength and drainage rate.
- Similar mass fractions of spherical and ellipsoidal colloids were mobilized in low ionic strength experiments. In high ionic strength experiments the absolute mass

of mobilized spheres and ellipsoids increased while the mass fraction of mobilized colloids decreased. The absolute mass of mobilized spherical colloids was consistently lower than the mass of mobilized ellipsoids at low and high ionic strength. The mass fraction of mobilized ellipsoids was higher than spheres in high ionic strength experiments.

- Spherical and ellipsoidal mobilization increased with drainage rate. The mass fraction and absolute mass of mobilized spherical colloids was consistently lower than ellipsoidal colloids. Thus ellipsoidal colloids attached to the soil surface in the secondary minimum in clean sands are more readily mobilized by drying fronts than spherical colloids.
- This work demonstrated that particle shape affects the fate of colloids differently under steady state and transient flow conditions. Although ellipsoidal colloids are less mobile in porous media under saturated and unsaturated steady state conditions, they are more mobile than spherical colloids during flow transients.

Future work on the effect of colloid shape

- The coupled effects of colloid shape and porewater chemistry was limited to low and high ionic strength in clean sand, in large part due to the limited quantities of ellipsoids available for tests. Future work should investigate the effects of pH as well as ionic strength on the transport and retention of colloids of various shapes.
- Work in this dissertation demonstrated that colloid retention mechanisms were different in iron oxide coated sand and zeolite. Future work should explore how or if colloid shape impacts retention mechanism in these reactive soils.
- The work in this dissertation demonstrated that ellipsoidal colloids are less mobile in unsaturated clean sands that have been drained from an initially saturated state.

Future work should investigate the effects of unsaturated flow hysteresis on the transport of spherical and ellipsoidal colloids under steady state conditions.

- The work in this dissertation was limited to the transport and retention of spherical and ellipsoidal colloids. The method used to create ellipsoidal colloids can be extended to create colloids of many diverse and complex shapes (Champion et al. 2007). Future work should explore how other shapes affect colloid transport in saturated and unsaturated porous media.

REFERENCES

- Abudalo, R. A., Bogatsu, Y. G., Ryan, J., Harvey, R. W., Metge, D. W., and Elimelech, M. (2005). "Effect of ferric oxyhydroxide grain coatings on the transport of bacteriophage PRD1 and *Cryptosporidium parvum* oocysts in saturated porous media." *Environmental science & technology*, 39(17), 6412–9.
- Abudalo, R. A., Ryan, J. N., Harvey, R. W., Metge, D. W., and Landkamer, L. (2010). "Influence of organic matter on the transport of *Cryptosporidium parvum* oocysts in a ferric oxyhydroxide-coated quartz sand saturated porous medium." *Water Research*, Elsevier Ltd, 44(4), 1104–1113.
- Adamczyk, Z., Siwek, B., Zembala, M., and Belouschek, P. (1994). "Kinetics of localized adsorption of colloid particles." *Advances in Colloid and Interface Science*, 48, 151–280.
- Adamczyk, Z., and Weroński, P. (1999). "Application of the DLVO theory for particle deposition problems." *Advances in Colloid and Interface Science*, 83(1-3), 137–226.
- Ahammed, M. M., and Davra, K. (2011). "Performance evaluation of biosand filter modified with iron oxide-coated sand for household treatment of drinking water." *Desalination*, Elsevier B.V., 276(1-3), 287–293.
- Akaike, H. (1974). "A new look at the statistical model identification." *IEEE Transactions on Automatic Control*, 19(6), 716–723.
- Aramahi, B., Alshibli, K. A., and Fratta, D. (2010). "Effect of Fine Particle Migration on the Small-Strain Stiffness of Unsaturated Soils." *Journal of Geotechnical and Geoenvironmental Engineering*, 136(4), 620.
- Alvarez-Ayuso, E., García-Sánchez, A., and Querol, X. (2003). "Purification of metal electroplating waste waters using zeolites." *Water research*, Elsevier, 37(20), 4855–4862.
- Aramrak, S., Flury, M., Harsh, J. B., and Zollars, R. L. (2014). "Colloid mobilization and

- transport during capillary fringe fluctuations." *Environmental science & technology*, 48(13), 7272–9.
- Aramrak, S., Flury, M., Harsh, J. B., Zollars, R. L., and Davis, H. P. (2013). "Does colloid shape affect detachment of colloids by a moving air-water interface?" *Langmuir*, 29(19), 5770–5780.
- Assouline, S., and Or, D. (2013). "Conceptual and Parametric Representation of Soil Hydraulic Properties: A Review." *gsvadzone*, 12(4), -.
- Auset, M., and Keller, A. A. (2006). "Pore-scale visualization of colloid straining and filtration in saturated porous media using micromodels." *Water Resources Research*, 42(12), W12802.
- Baalousha, M., Lead, J. R., and Ju-Nam, Y. (2011). "Natural Colloids and Manufactured Nanoparticles in Aquatic and Terrestrial Systems." *Treatise on Water Science*, 89–129.
- El Badawy, A. M., Hassan, A. A., Scheckel, K. G., Suidan, M. T., and Tolaymat, T. M. (2013). "Key factors controlling the transport of silver nanoparticles in porous media." *Environmental science & technology*, 47, 4039–45.
- Bailey, S. E., Olin, T. J., Bricka, R. M., and Adrian, D. D. (1999). "A review of potentially low-cost sorbents for heavy metals." *Water Research*, Elsevier, 33(11), 2469–2479.
- Baltus, R. E., Badireddy, A. R., Xu, W., and Chellam, S. (2009). "Analysis of Configurational Effects on Hindered Convection of Nonspherical Bacteria and Viruses across Microfiltration Membranes." *Industrial & Engineering Chemistry Research*, 48(5), 2404–2413.
- Bandini, P., and Sathiskumar, S. (2009). "Effects of silt content and void ratio on the saturated hydraulic conductivity and compressibility of sand-silt mixtures." *Journal of Geotechnical and Geoenvironmental Engineering*, 135(12), 1976–1980.
- Bangs Laboratories, I. (2013). *Working with Microspheres*.

- Barton, J. M. H., and Buchberger, S. G. (2007). "Effect of Media Grain Shape on Particle Straining during Filtration." *Journal of Environmental Engineering*.
- Basha, H. A., and Culligan, P. J. (2010). "Modeling particle transport in downward and upward flows." *Water Resources Research*, 46(7), W07518.
- Bates, J. K., Bradley, J. P., Teetsov, A., Bradley, C. R., and Ten Brink, M. B. (1992). "Colloid formation during waste form reaction: implications for nuclear waste disposal." *Science*, 256(5057), 649–651.
- Baumann, T., Fruhstorfer, P., Klein, T., and Niessner, R. (2006). "Colloid and heavy metal transport at landfill sites in direct contact with groundwater." *Water Research*, 40, 2776–2786.
- Béchet, B., Durin, B., Legret, M., and Le Cloirec, P. (2006). "Colloidal speciation of heavy metals in runoff and interstitial waters of a retention/infiltration pond." *Water Science & Technology*, 54(6-7), 307.
- Becker, M. W., Collins, S. A., Metge, D. W., Harvey, R. W., and Shapiro, A. M. (2004). "Effect of cell physicochemical characteristics and motility on bacterial transport in groundwater." *Journal of Contaminant Hydrology*, 69(3-4), 195–213.
- Becker, M. W., Metge, D. W., Collins, S. A., Shapiro, A. M., and Harvey, R. W. (2003). "Bacterial Transport Experiments in Fractured Crystalline Bedrock." *Ground Water*, 41(5), 682–689.
- Bendersky, M., and Davis, J. M. (2011). "DLVO interaction of colloidal particles with topographically and chemically heterogeneous surfaces." *Journal of Colloid and Interface Science*, Elsevier Inc., 353(1), 87–97.
- Benjamin, M. M. (2002). *Water Chemistry*. McGraw-Hill, New York.
- Benjamin, M. M., Sletten, R. S., Bailey, R. P., and Bennett, T. (1996). "Sorption and filtration of metals using iron-oxide-coated sand." *Water Research*, 30(11), 2609–2620.

- Bennett, N. D., Croke, B. F. W., Guariso, G., Guillaume, J. H. ., Hamilton, S. H., Jakeman, A. J., Marsili-Libelli, S., Newham, L. T. H., Norton, J. P., Perrin, C., Pierce, S. A., Robson, B., Seppelt, R., Voinov, A. A., Fath, B. D., and Andreassian, V. (2013). "Characterising performance of environmental models." *Environmental Modelling & Software*, Elsevier Ltd, 40, 1–20.
- Bergendahl, J., and Grasso, D. (2000). "Prediction of colloid detachment in a model porous media: Hydrodynamics." *Chemical Engineering Science*, 55(9), 1523–1532.
- Bhattacharjee, S., Chen, J. Y., and Elimelech, M. (2000). "DLVO interaction energy between spheroidal particles and a flat surface." *Colloids and Surfaces A: Physicochemical and Engineering Aspects*, 165(1-3), 143–156.
- Bhattacharjee, S., and Elimelech, M. (1997). "Surface Element Integration: A Novel Technique for Evaluation of DLVO Interaction between a Particle and a Flat Plate." *Journal of colloid and interface science*, 193(2), 273–85.
- Bhattacharjee, S., Ko, C., and Elimelech, M. (1998). "DLVO Interaction between Rough Surfaces." *Langmuir*, 14(12), 3365–3375.
- Bhattacharjee, S., Ryan, J. N., and Elimelech, M. (2002). "Virus transport in physically and geochemically heterogeneous subsurface porous media." *Journal of Contaminant Hydrology*, 57, 161–187.
- Bin, G., Cao, X., Dong, Y., Luo, Y., and Ma, L. Q. (2011). "Colloid Deposition and Release in Soils and Their Association With Heavy Metals." *Critical Reviews in Environmental Science and Technology*.
- Bird, G. W., and Fyfe, W. S. (1982). "The nuclear waste disposal problem — An overview from a geological and geochemical perspective." *Chemical Geology*.
- Birkholzer, J., Houseworth, J., and Tsang, C.-F. (2012). "Geologic Disposal of High-Level Radioactive Waste: Status, Key Issues, and Trends." *Annual Review of Environment and Resources*.

- Bolster, C. H., Haznedaroglu, B. Z., and Walker, S. L. (2009). "Diversity in cell properties and transport behavior among 12 different environmental *Escherichia coli* isolates." *Journal of environmental quality*, 38(2), 465–472.
- Bolster, C. H., Mills, A. L., Hornberger, G. M., and Herman, J. S. (2001). "Effect of surface coatings, grain size, and ionic strength on the maximum attainable coverage of bacteria on sand surfaces." *Journal of contaminant hydrology*, 50(3-4), 287–305.
- Bossolan, N. R. S., Godinho, M. J. L., and Volpon, A. G. T. (2005). "Growth and Starvation of a Strain of *Klebsiella pneumoniae* Isolated from a Brazilian Oil Formation." *World Journal of Microbiology and Biotechnology*, 21(8-9), 1471–1475.
- Bradford, S. A. (2005). "Straining of colloids at textural interfaces." *Water Resources Research*, 41(10), 1–18.
- Bradford, S. A., and Bettahar, M. (2006). "Concentration dependent transport of colloids in saturated porous media." *Journal of contaminant hydrology*, 82(1-2), 99–117.
- Bradford, S. A., Bettahar, M., Simunek, J., and van Genuchten, M. T. (2004). "Straining and Attachment of Colloids in Physically Heterogeneous Porous Media." *Vadose Zone Journal*, 3(2), 384–394.
- Bradford, S. A., and Kim, H. (2012). "Causes and implications of colloid and microorganism retention hysteresis." *Journal of contaminant hydrology*, Elsevier B.V., 138-139, 83–92.
- Bradford, S. A., Kim, H. N., Haznedaroglu, B. Z., Torkzaban, S., and Walker, S. L. (2009). "Coupled factors influencing concentration-dependent colloid transport and retention in saturated porous media." *Environmental science & technology*, 43(18), 6996–7002.
- Bradford, S. A., Morales, V. L., Zhang, W., Ronald, W., Packman, A. I., Mohanram, A., and Welty, C. (2013). "Transport and Fate of Microbial Pathogens in Agricultural

- Settings." *Environmental science & technology*, 43(February), 775–893.
- Bradford, S. A., Simůnek, J., Bettahar, M., Van Genuchten, M. T., and Yates, S. R. (2003). "Modeling colloid attachment, straining, and exclusion in saturated porous media." *Environmental science & technology*, 37(10), 2242–50.
- Bradford, S. A., Simůnek, J., Bettahar, M., van Genuchten, M. T., and Yates, S. R. (2006). "Significance of straining in colloid deposition: Evidence and implications." *Water Resources Research*, 42(12), 1–16.
- Bradford, S. A., and Torkzaban, S. (2008). "Colloid Transport and Retention in Unsaturated Porous Media: A Review of Interface-, Collector-, and Pore-Scale Processes and Models." *Vadose Zone Journal*, 7(2), 667.
- Bradford, S. A., and Torkzaban, S. (2012). "Colloid adhesive parameters for chemically heterogeneous porous media." *Langmuir: the ACS journal of surfaces and colloids*, 28(38), 13643–51.
- Bradford, S. A., Torkzaban, S., and Shapiro, A. (2013). "A Theoretical Analysis of Colloid Attachment and Straining in Chemically Heterogeneous Porous Media." *Langmuir*, 29(23), 6944–6952.
- Bradford, S. A., Torkzaban, S., and Walker, S. L. (2007). "Coupling of physical and chemical mechanisms of colloid straining in saturated porous media." *Water research*, 41(13), 3012–24.
- Bradford, S. A., Yates, S. R., Bettahar, M., and Simůnek, J. (2002). "Physical factors affecting the transport and fate of colloids in saturated porous media." *Water Resources Research*, 38(12), 1–12.
- Bridge, J. W., Heathwaite, A. L., and Banwart, S. A. (2009). "Measurement of colloid mobilization and redeposition during drainage in quartz sand." *Environmental science & technology*, 43(15), 5769–75.
- Brooks, R., and Corey, A. (1964). "Hydraulic properties of porous media." *Hydrology*

Papers, Colorado State University, 3(March), 37 pp.

- Brown, D. G., Stencel, J. R., and Jaffé, P. R. (2002). "Effects of porous media preparation on bacteria transport through laboratory columns." *Water research*, 36(1), 105–14.
- Buddemeier, R. W., and Hunt, J. R. (1988). "Transport of colloidal contaminants in groundwater: Radionuclide migration at the Nevada test site." *Applied Geochemistry*, 3, 535–548.
- Burbank, M., Kavazanjian, E., Weaver, T., Montoya, B. M., Hamdan, N., Bang, S. S., Esnault-Filet, A., Tsesarsky, M., Aydilek, A., Ciurli, S., Tanyu, B., Manning, D. A. C., Larrahondo, J., Soga, K., Chu, J., Dejong, J. T., Cheng, X., Kuo, M., Al Qabany, A., Seagren, E. ., Van Paassen, L. a., Renforth, P., Laloui, L., Nelson, D. C., Hata, T., Burns, S., Chen, C. Y., Caslake, L. F., Fauriel, S., Jefferis, S., Santamarina, J. C., Inagaki, Y., Martinez, B., and Palomino, A. (2013). "Biogeochemical processes and geotechnical applications: progress, opportunities and challenges." *Géotechnique*, 63(4), 287–301.
- Burdine, N. T. (1953). "Relative Permeability Calculations From Pore Size Distribution Data." *Journal of Petroleum Technology*, 5, 71–78.
- Carraro, J., Bandini, P., and Salgado, R. (2003). "Liquefaction resistance of clean and nonplastic silty sands based on cone penetration resistance." *Journal of Geotechnical and Geoenvironmental Engineering*, 129(11), 965–976.
- Castro, F. D., and Tufenkji, N. (2008). "Role of oxygen tension on the transport and retention of two pathogenic bacteria in saturated porous media." *Environmental science & technology*, 42(24), 9178–9183.
- Cey, E. E., Rudolph, D. L., and Passmore, J. (2009). "Influence of macroporosity on preferential solute and colloid transport in unsaturated field soils." *Journal of Contaminant Hydrology*, 107, 45–57.

- Champion, J. A., Katare, Y. K., and Mitragotri, S. (2007). "Making polymeric micro- and nanoparticles of complex shapes." *Proceedings of the National Academy of Sciences of the United States of America*, 104(29), 11901–4.
- Chang, N.-B., Hossain, F., and Wanielista, M. (2010). "Filter Media for Nutrient Removal in Natural Systems and Built Environments: I—Previous Trends and Perspectives." *Environmental Engineering Science*, 27(9), 689–706.
- Chatterjee, N., and Flury, M. (2013). "Effect of Particle Shape on Capillary Forces Acting on Particles at the Air–Water Interface." *Langmuir*, 29(25), 7903–7911.
- Chatterjee, N., Lapin, S., and Flury, M. (2012a). "Capillary forces between sediment particles and an air-water interface." *Environmental Science and Technology*, 46(8), 4411–4418.
- Chatterjee, N., Lapin, S., and Flury, M. (2012b). "Capillary forces between sediment particles and an air-water interface. Supplement." *Environmental science & technology*, 46(8), 4411–8.
- Chen, G., Abichou, T., Tawfiq, K., and Subramaniam, P. K. (2007). "Impact of surface charge density on colloid deposition in unsaturated porous media." *Colloids and Surfaces A: Physicochemical and Engineering Aspects*, 302(1-3), 342–348.
- Chen, G., and Flury, M. (2005). "Retention of mineral colloids in unsaturated porous media as related to their surface properties." *Colloids and Surfaces A: Physicochemical and Engineering Aspects*, 256(2-3), 207–216.
- Chen, G., and Flury, M. (2006). "Retention of mineral colloids in unsaturated porous media as related to their surface properties ERATUM." *Colloids and Surfaces A: Physicochemical and Engineering Aspects*, 289(1-3), 254–255.
- Chen, G., Liu, J., Tawfiq, K., Yang, K., and Banks, C. (2009). "Colloid Retention in Unsaturated Porous Media as Impacted by Colloid Size." *Particulate Science and Technology*, 27(1), 35–49.

- Chen, L., Sabatini, D. A., and Kibbey, T. C. G. (2008). "Role of the air-water interface in the retention of TiO₂ nanoparticles in porous media during primary drainage." *Environmental science & technology*, 42(6), 1916–21.
- Chen, L., Sabatini, D. A., and Kibbey, T. C. G. (2012). "Transport and retention of fullerene (nC₆₀) nanoparticles in unsaturated porous media: effects of solution chemistry and solid phase coating." *Journal of contaminant hydrology*, Elsevier B.V., 138-139, 104–12.
- Cheng, T., and Sayers, J. E. (2009). "Mobilization and transport of in situ colloids during drainage and imbibition of partially saturated sediments." *Water Resources Research*, 45(8), 1–14.
- Cheng, T., and Sayers, J. E. (2010). "Colloid-facilitated transport of cesium in vadose-zone sediments: the importance of flow transients." *Environmental science & technology*, 44(19), 7443–9.
- Cherrey, K. D., Flury, M., and Harsh, J. B. (2003). "Nitrate and colloid transport through coarse Hanford sediments under steady state, variably saturated flow." *Water Resources Research*, 39(6).
- Cho, G. C., and Santamarina, J. C. (2001). "Unsaturated particulate materials-particle-level studies." *Journal of geotechnical and geoenvironmental engineering*, 127(1), 84.
- Cho, G.-C., Dodds, J., and Santamarina, J. C. (2006). "Particle Shape Effects on Packing Density, Stiffness, and Strength: Natural and Crushed Sands." *Journal of Geotechnical and Geoenvironmental Engineering*, 132(5), 591–602.
- Chu, Y., Jin, Y., Baumann, T., and Yates, M. V. (2003). "Effect of soil properties on saturated and unsaturated virus transport through columns." *Journal of environmental quality*, 32(1980), 2017–2025.
- Chu, Y., Jin, Y., Flury, M., and Yates, M. V. (2001). "Mechanisms of virus removal during

- transport in unsaturated porous media." *Water Resources Research*, 37(2), 253–263.
- Compère, F., Porel, G., and Delay, F. (2001). "Transport and retention of clay particles in saturated porous media. Influence of ionic strength and pore velocity." *Journal of Contaminant Hydrology*, 49(1-2), 1–21.
- Corapcioglu, M. Y., and Choi, H. (1996). "Modeling Colloid Transport in Unsaturated Porous Media and Validation with Laboratory Column Data." *Water Resources Research*, 32(12), 3437–3449.
- Crist, J. T., McCarthy, J. F., Zevi, Y., Baveye, P. C., Throop, J. A., and Steenhuis, T. S. (2004). "Pore-Scale Visualization of Colloid Transport and Retention in Partly Saturated Porous Media." *Vadose Zone Journal*, 3(2), 444–450.
- Crist, J. T., Zevi, Y., McCarthy, J. F., Throop, J. A., and Steenhuis, T. S. (2005). "Transport and Retention Mechanisms of Colloids in Partially Saturated Porous Media." *Vadose Zone Journal*, 4(1), 184–195.
- Dai, M., Kelley, J. M., and Buesseler, K. O. (2002). "Sources and migration of plutonium in groundwater at the Savannah River Site." *Environmental Science and Technology*, 36(17), 3690–3699.
- Dane, J. H., and Topp, G. C. (2002). *Methods of Soil Analysis. Part 4: Physical Methods*. Soil Science Society of America, Inc., Soil Science Society of America, Inc, Madison, WI.
- Darbha, G. K., Fischer, C., Luetzenkirchen, J., and Schäfer, T. (2012). "Site-specific retention of colloids at rough rock surfaces." *Environmental Science and Technology*, 46, 9378–9387.
- DeNovio, N. M., Sainers, J. E., and Ryan, J. N. (2004). "Colloid Movement in Unsaturated Porous Media: Recent Advances and Future Directions." *Vadose Zone Journal*.
- Díaz, J., Rendueles, M., and Díaz, M. (2010). "Straining phenomena in bacteria

- transport through natural porous media." *Environmental science and pollution research international*, 17(2), 400–9.
- Dong, H., Rothmel, R., Onstott, T. C., Fuller, M. E., DeFlaun, M. F., Streger, S. H., Dunlap, R., and Fletcher, M. (2002). "Simultaneous transport of two bacterial strains in intact cores from Oyster, Virginia: Biological effects and numerical modeling." *Applied and Environmental Microbiology*, 68(5), 2120–2132.
- Durner, W., and Iden, S. C. (2011). "Extended multistep outflow method for the accurate determination of soil hydraulic properties near water saturation." *Water Resources Research*, 47(8), W08526.
- Dyer, A. (1988). *An introduction to Zeolite Molecular Sieves*. John Wiley & Sons, Chichester.
- Eching, S., and Hopmans, J. W. (1993). "Optimization of hydraulic functions from transient outflow and soil water pressure data." *Soil Science Society of America ...*, 57(5), 1167–1175.
- Eching, S., Hopmans, J. W., and Wendroth, O. (1994). "Unsaturated hydraulic conductivity from transient multistep outflow and soil water pressure data." *Soil Science Society of ...*, 9, 687–695.
- Elimelech, M. (1994). "Effect of particle size on the kinetics of particle deposition under attractive double layer interactions." *Journal of colloid and interface science*, 164, 190–199.
- Elimelech, M., Gregory, J., Jia, X., and Williams, R. (1995). *Particle Deposition and Aggregation Measurement, Modelling, and Simulation*. Butterworth-Heinemann.
- Elimelech, M., Nagai, M., Ko, C. H., and Ryan, J. N. (2000). "Relative insignificance of mineral grain zeta potential to colloid transport in geochemically heterogeneous porous media." *Environmental Science and Technology*, 34(11), 2143–2148.
- Elimelech, M., and O'Meliae, C. R. (1990). "Effect of particle size on collision efficiency

- in the deposition of Brownian particles with electrostatic energy barriers." *Langmuir*, 6(10), 1153–1163.
- Engström, E., Thunvik, R., Kulabako, R., and Balfors, B. (2014). "Water Transport, Retention, and Survival of *Escherichia coli* in Unsaturated Porous Media: A Comprehensive Review of Processes, Models, and Factors." *Critical Reviews in Environmental Science and Technology*, 45(1), 1–100.
- Erickson, A. J., Weiss, P. T., Gulliver, J. S., and Weiss, P. T. (2006). "Enhanced Sand Filtration for Storm Water Phosphorus Removal." *Journal of Environmental Engineering*, Asce.
- Ersoy, B., and Çelik, M. S. (2002). "Electrokinetic properties of clinoptilolite with mono- and multivalent electrolytes." *Microporous and Mesoporous Materials*, 55(3), 305–312.
- Evans, J., and Ryan, C. (2005). "Time-dependent strength behavior of soil-bentonite slurry wall backfill." *Geotechnical Special Publication*, 3779–3787.
- Ewing, R. P., Hu, Q., and Liu, C. (2010). "Scale dependence of intragranular porosity, tortuosity, and diffusivity." *Water Resources Research*, 46(6), W06513.
- Fang, J., Xu, M., Wang, D., Wen, B., and Han, J. (2013). "Modeling the transport of TiO₂ nanoparticle aggregates in saturated and unsaturated granular media: effects of ionic strength and pH." *Water research*, Elsevier Ltd, 47(3), 1399–408.
- Färm, C. (2002). "Metal sorption to natural filter substrates for storm water treatment--column studies." *The Science of the total environment*, 298(1-3), 17–24.
- Figueras, J., and Gribb, M. M. (2009). "Design of a User-Friendly Automated Multistep Outflow Apparatus." *Vadose Zone Journal*, 8(2), 523.
- Fisher, R. A. (1926). "On the capillary forces in an ideal soil; correction of formulae given by W. B. Haines." *The Journal of Agricultural Science*, 16(03), 492.
- Flury, M., and Qiu, H. (2008). "Modeling Colloid-Facilitated Contaminant Transport in the

- Vadose Zone." *Vadose Zone Journal*, 7(2), 682.
- Fontes, D. E., Mills, A. L., Hornberger, G. M., and Herman, J. S. (1991). "Physical and chemical factors influencing transport of microorganisms through porous media." *Applied and Environmental Microbiology*, 57(9), 2473–2481.
- Foppen, J. W. A., Oklety, S., and Schijven, J. F. (2006). "Effect of goethite coating and humic acid on the transport of bacteriophage PRD1 in columns of saturated sand." *Journal of contaminant hydrology*, 85(3-4), 287–301.
- Franchi, A., and O'Melia, C. R. (2003). "Effects of natural organic matter and solution chemistry on the deposition and reentrainment of colloids in porous media." *Environmental Science and Technology*, 37(6), 1122–1129.
- Fredlund, M. D., and Xing, A. (1994). "Equations for the soil-water characteristic curve." *Canadian Geotechnical Journal*, 31(3), 521–532.
- Frimmel, F. H., Kammer, F., Flemming, H., Schriewer, A., Athanasiadis, K., and Helmreich, B. (2007). *Colloidal Transport in Porous Media*. (F. H. Frimmel, F. Kammer, and H.-C. Flemming, eds.), Springer Berlin Heidelberg, Berlin, Heidelberg.
- Gaber, H. M., Comfort, S. D., Shea, P. J., and Machacek, T. A. (2002). "Metolachlor dechlorination by zerovalent iron during unsaturated transport." *J Environ Qual*, 31(3), 962–969.
- Gamerding, A. P., and Kaplan, D. I. (2001a). "Physical and chemical determinants of colloid transport and deposition in water-unsaturated sand and Yucca Mountain tuff material." *Environmental science & technology*, 35(12), 2497–504.
- Gamerding, A. P., and Kaplan, D. I. (2001b). "Colloid transport and deposition in water-saturated Yucca Mountain tuff as determined by ionic strength." *Environmental science & technology*, 35(16), 3326–31.
- Gao, B., Saiers, J. E., and Ryan, J. N. (2006). "Pore-scale mechanisms of colloid

- deposition and mobilization during steady and transient flow through unsaturated granular media." *Water Resources Research*, 42(1), 1–9.
- Gargiulo, G., Bradford, S. A., Simunek, J., Ustohal, P., Vereecken, H., and Klumpp, E. (2008). "Bacteria Transport and Deposition under Unsaturated Flow Conditions: The Role of Water Content and Bacteria Surface Hydrophobicity." *Vadose Zone Journal*.
- Genç-Fuhrman, H., Mikkelsen, P. S., and Ledin, A. (2007). "Simultaneous removal of As, Cd, Cr, Cu, Ni and Zn from stormwater: Experimental comparison of 11 different sorbents." *Water Research*, 41(3), 591–602.
- Genç-Fuhrman, H., Wu, P., Zhou, Y., and Ledin, A. (2008). "Removal of As, Cd, Cr, Cu, Ni and Zn from polluted water using an iron based sorbent." *Desalination*, 226(1-3), 357–370.
- van Genuchten, M. T. T. (1980). "A Closed-form Equation for Predicting the Hydraulic Conductivity of Unsaturated Soils." *Soil Science Society of America Journal*, 44(5), 892.
- Ginn, T. R., Wood, B. D., Nelson, K. E., Scheibe, T. D., Murphy, E. M., and Clement, T. P. (2002). "Processes in microbial transport in the natural subsurface." *Advances in Water Resources*, 25(8-12), 1017–1042.
- Githinji, L. J. M., Dane, J. H., and Walker, R. H. (2010). "Physical and hydraulic properties of inorganic amendments and modeling their effects on water movement in sand-based root zones." *Irrigation Science*, 29(1), 65–77.
- Goebel, M.-O., Woche, S. K., Abraham, P. M., Schaumann, G. E., and Bachmann, J. (2013). "Water repellency enhances the deposition of negatively charged hydrophilic colloids in a water-saturated sand matrix." *Colloids and Surfaces A: Physicochemical and Engineering Aspects*, Elsevier B.V., 431, 150–160.
- Goldberg, E., Scheringer, M., Bucheli, T. D., and Hungerbühler, K. (2014). "Critical

- Assessment of Models for Transport of Engineered Nanoparticles in Saturated Porous Media.” *Environmental Science & Technology*, 48(21), 12732–12741.
- Gómez-Suárez, C., Busscher, H. J., and van der Mei, H. C. (2001). “Analysis of bacterial detachment from substratum surfaces by the passage of air-liquid interfaces.” *Applied and Environmental Microbiology*, 67(6), 2531–2537.
- Gottardi, G., and Galli, E. (1985). *Natural Zeolites*. Springer-Verlag Berlin, Heidelberg.
- Grasso, D., Subramaniam, K., Butkus, M., Strevett, K., and Bergendahl, J. (2002). “A review of non-DLVO interactions in environmental colloidal systems.” *Reviews in Environmental Science and Biotechnology*, 1, 17–38.
- Gray, D. H. (1966). “Formation Damage in Sandstones caused by Clay Dispersion and Migration.” *Clays and Clay Minerals*.
- Gregory, J. (1981). “Approximate expressions for retarded van der waals interaction.” *Journal of Colloid and Interface Science*.
- Hahn, M. W., and O’Melia, C. R. (2004). “Deposition and Reentrainment of Brownian Particles in Porous Media under Unfavorable Chemical Conditions: Some Concepts and Applications.” *Environmental Science and Technology*, 38(1), 210–220.
- Hajra, M. G., Asce, S. M., Reddi, L. N., Asce, M., Glasgow, L. A., Xiao, M., and Lee, I. M. (2002). “Effects of Ionic Strength on Fine Particle Clogging of Soil Filters.” *Journal of Geotechnical and Geoenvironmental Engineering*, 128(8), 631.
- Haluszczak, L. O., Rose, A. W., and Kump, L. R. (2013). “Geochemical evaluation of flowback brine from Marcellus gas wells in Pennsylvania, USA.” *Applied Geochemistry*, Elsevier Ltd, 28, 55–61.
- Han, J., Jin, Y., and Willson, C. S. (2006). “Virus retention and transport in chemically heterogeneous porous media under saturated and unsaturated flow conditions.” *Environmental Science and Technology*, 40(5), 1547–1555.
- Han, P., Wang, X., Cai, L., Tong, M., and Kim, H. (2014). “Transport and retention

- behaviors of titanium dioxide nanoparticles in iron oxide-coated quartz sand: Effects of pH, ionic strength, and humic acid." *Colloids and Surfaces A: Physicochemical and Engineering Aspects*, Elsevier B.V., 454, 119–127.
- Hansmire, W. H., Russell, H. A., Rawnsley, R. P., and Abbott, E. L. (1989). "Field Performance of Structural Slurry Wall." *Journal of Geotechnical Engineering*.
- Happel, J. (1958). "Viscous flow in multiparticle systems: Slow motion of fluids relative to beds of spherical particles." *AIChE Journal*, 4, 197–201.
- Henderson, A. D., and Demond, A. H. (2007). "Long-Term Performance of Zero-Valent Iron Permeable Reactive Barriers: A Critical Review." *Environmental Engineering Science*, 24(4), 401–423.
- Ho, C., Keller, A., Odell, J., and Ottewill, R. (1993). "Preparation of monodisperse ellipsoidal polystyrene particles." *Colloid & Polymer Science*, Springer, 271(5), 469–479.
- Ho, C., Ottewill, R., Keller, A., and Odell, J. (1993). "Monodisperse ellipsoidal polystyrene latex particles: Preparation and characterisation." *Polymer international*, Wiley Online Library, 30(2), 207–211.
- Ho, C., Ottewill, R., and Yu, L. (1997). "Examination of ellipsoidal polystyrene particles by electrophoresis." *Langmuir*, 7463(28), 1925–1930.
- Hoffman, E. J., Latimer, J. S., Hunt, C. D., Mills, G. L., and Quinn, J. G. (1985). "Stormwater runoff from highways." *Water, Air, & Soil Pollution*, Springer, 25(4), 349–364.
- Hogg, R., Healy, T. W., and Fuerstenau, D. W. (1966). "Mutual coagulation of colloidal dispersions." *Transactions of the Faraday Society*, 62(615), 1638.
- Hopmans, J. W., Simunek, J., Romano, N., and Durner, W. (2002). "Simultaneous determination of water transmission and retention properties. Inverse methods." *Methods of Soil Analysis Part 4: Physical Methods*, J. H. Dane and C. G. Topp,

eds., Soil Science Society of America, Madison, WI.

- Hotze, E. M., Phenrat, T., and Lowry, G. V. (2010). "Nanoparticle aggregation: challenges to understanding transport and reactivity in the environment." *Journal of environmental quality*, 39(6), 1909–1924.
- Huang, X., Bhattacharjee, S., and Hoek, E. M. V. (2010). "Is surface roughness a 'scapegoat' or a primary factor when defining particle-substrate interactions?" *Langmuir*, 26(4), 2528–2537.
- Hwang, S. II, and Powers, S. E. (2003). "Estimating unique soil hydraulic parameters for sandy media from multi-step outflow experiments." *Advances in Water Resources*, 26(4), 445–456.
- Inagaki, Y., Tsukamoto, M., and Mori, H. (2011). "The influence of injection conditions and soil types on soil improvement by microbial functions." *Geo*, 4021–4030.
- Israelachvili, J. N. (2011). "Intermolecular and Surface Forces." *Intermolecular and Surface Forces*, 205–222.
- Jaafar, R., and Likos, W. J. (2014). "Estimating Water Retention Characteristics of Sands from Grain Size Distribution using Idealized Packing Conditions." 34(5), 1–14.
- Jacobs, A., Lafolie, F., Herry, J. M., and Debroux, M. (2007). "Kinetic adhesion of bacterial cells to sand: Cell surface properties and adhesion rate." *Colloids and Surfaces B: Biointerfaces*, 59(1), 35–45.
- Jaisi, D. P., Saleh, N. B., Blake, R. E., and Elimelech, M. (2008). "Transport of single-walled carbon nanotubes in porous media: Filtration mechanisms and reversibility." *Environmental Science and Technology*, 42(22), 8317–8323.
- Jaradat, A. Q., Fowler, K., Grimberg, S. J., Holsen, T. M., and Ghosh, R. S. (2009). "Treatment of Storm Water Containing Low Levels of PCBs Using Natural Media Filtration." *Environmental Engineering Science*.

- Jarvie, H. P., Neal, C., Rowland, A. P., Neal, M., Morris, P. N., Lead, J. R., Lawlor, A. J., Woods, C., Vincent, C., Guyatt, H., and Hockenhull, K. (2012). "Role of riverine colloids in macronutrient and metal partitioning and transport, along an upland-lowland land-use continuum, under low-flow conditions." *Science of the Total Environment*, 434, 171–185.
- Johansson Westholm, L. (2006). "Substrates for phosphorus removal - Potential benefits for on-site wastewater treatment?" *Water Research*.
- Johnson, W. P., and Elimelech, M. (1995). "Dynamics of Colloid Deposition in Porous Media: Blocking Based on Random Sequential Adsorption." *Langmuir*, 11(33), 801–812.
- Johnson, W. P., Li, X., and Yal, G. (2007). "Colloid retention in porous media: Mechanistic confirmation of wedging and retention in zones of flow stagnation." *Environmental Science and Technology*, 41(4), 1279–1287.
- Johnson, W. P., Ma, H., and Pazmino, E. (2011). "Straining Credibility: A General Comment Regarding Common Arguments Used to Infer Straining As the Mechanism of Colloid Retention in Porous Media." *Environmental Science & Technology*, 45(9), 3831–3832.
- Johnson, W. P., Pazmino, E., and Ma, H. (2010). "Direct observations of colloid retention in granular media in the presence of energy barriers, and implications for inferred mechanisms from indirect observations." *Water Research*, Elsevier Ltd, 44(4), 1158–1169.
- Johnson, W. P., Sun, N., and Elimelech, M. (1996). "Colloid Transport in Geochemically Heterogeneous Porous Media: Modeling and Measurements." *Environmental Science & Technology*, 30(11), 3284–3293.
- de Jonge, H., Jacobsen, O. H., de Jonge, L. W., and Moldrup, P. (1998). "Particle-Facilitated Transport of Prochloraz in Undisturbed Sandy Loam Soil Columns."

- Journal of Environment Quality*, 27(6), 1495–1503.
- de Jonge, L. W., Kjaergaard, C., and Moldrup, P. (2004). “Colloids and colloid-facilitated transport of contaminants in soils.” *Vadose Zone Journal*, 3(2), 321–325.
- de Jonge, L. W., Moldrup, P., Rubæk, G. H., Schelde, K., and Djurhuus, J. (2004). “Particle Leaching and Particle-Facilitated Transport of Phosphorus at Field Scale.” *Vadose Zone Journal*, 3(2), 462.
- Ju-Nam, Y., and Lead, J. R. (2008). “Manufactured nanoparticles: An overview of their chemistry, interactions and potential environmental implications.” *Science of the Total Environment*, Elsevier B.V., 400(1-3), 396–414.
- Kargbo, D. M., Wilhelm, R. G., and Campbell, D. J. (2010). “Natural gas plays in the marcellus shale: Challenges and potential opportunities.” *Environmental Science and Technology*.
- Karraker, K. A., and Radke, C. J. (2002). “Disjoining pressures, zeta potentials and surface tensions of aqueous non-ionic surfactant/electrolyte solutions: Theory and comparison to experiment.” *Advances in Colloid and Interface Science*, 96, 231–264.
- Kasel, D., Bradford, S. A., Šimůnek, J., Heggen, M., Vereecken, H., and Klumpp, E. (2013). “Transport and retention of multi-walled carbon nanotubes in saturated porous media: Effects of input concentration and grain size.” *Water Research*, 47(2), 933–944.
- Keller, A., and Sirivithayapakorn, S. (2004). “Transport of colloids in unsaturated porous media: Explaining large-scale behavior based on pore-scale mechanisms.” *Water Resources Research*, 40(12), 1–8.
- Kenst, A. B., Perfect, E., Wilhelm, S. W., Zhuang, J., McCarthy, J. F., and McKay, L. (2008). “Virus transport during infiltration of a wetting front into initially unsaturated sand columns.” *Environmental Science and Technology*, 42(4), 1102–1108.

- Kersting, A. B., Efurud, D. W., Finnegan, D. L., Rokop, D. J., Smith, D. K., and Thompson, J. L. (1999). "Migration of plutonium in ground water at the Nevada Test Site." *Nature*, 397(1), 56–59.
- Khilar, K. ., and Fogler, H. . (1984). "The existence of a critical salt concentration for particle release." *Journal of Colloid and Interface Science*, 101(I), 214–224.
- Kietlińska, A., and Renman, G. (2005). "An evaluation of reactive filter media for treating landfill leachate." *Chemosphere*, 61(7), 933–40.
- Kim, J. I. (1991). "Actinide Colloid Generation in Groundwater." *Radiochimica Acta*, 52-53(1), 71–81.
- Kjær, J., Ersten, V., Jacobsen, O. H., Hansen, N., de Jonge, L. W., and Olsen, P. (2011). "Transport modes and pathways of the strongly sorbing pesticides glyphosate and pendimethalin through structured drained soils." *Chemosphere*, 84, 471–479.
- Kjaergaard, C., Moldrup, P., de Jonge, L. W., and Jacobsen, O. . (2004). "Colloid mobilization and transport in undisturbed soil columns. II. The role of colloid dispersibility and preferential flow." *Vadose Zone Journal*, Soil Sci Soc America, 3(2), 424.
- Kjaergaard, C., Poulsen, T. G., Moldrup, P., and de Jonge, L. W. (2004). "Colloid Mobilization and Transport in Undisturbed Soil Columns. I. Pore Structure Characterization and Tritium Transport." *Vadose Zone Journal*, 3(2), 413–423.
- Klaine, S. J., Alvarez, P. J. J., Batley, G. E., Fernandes, T. F., Handy, R. D., Lyon, D. Y., Mahendra, S., McLaughlin, M. J., and Lead, J. R. (2008). "Nanomaterials in the environment: behavior, fate, bioavailability, and effects." *Environmental toxicology and chemistry / SETAC*, Wiley Online Library, 27(9), 1825–1851.
- Knappenberger, T., Flury, M., Mattson, E. D., and Harsh, J. B. (2014). "Does water content or flow rate control colloid transport in unsaturated porous media?"

- Environmental science & technology*, 48(7), 3791–9.
- Knox, A. S., Paller, M., Reible, D., Ma, X., and Petrisor, I. (2008). “Sequestering Agents for Active Caps—Remediation of Metals and Organics.” *Soil and Sediment Contamination*.
- Ko, C. H., and Elimelech, M. (2000). “The ‘shadow effect’ in colloid transport and deposition dynamics in granular porous media: Measurements and mechanisms.” *Environmental Science and Technology*, 34(17), 3681–3689.
- Koerner, G. R., and Koerner, R. (1992). “Leachate flow rate behavior through geotextile and soil filters and possible remediation methods.” *Geotextiles and Geomembranes*.
- Köhne, J. M., Köhne, S., and Šimůnek, J. (2009). “A review of model applications for structured soils: a) Water flow and tracer transport.” *Journal of Contaminant Hydrology*, Elsevier B.V., 104(1-4), 4–35.
- Korkuna, O., Leboda, R., Skubiszewska-Zieba, J., Vrublevs’ka, T., Gun’ko, V. M., and Ryzkowski, J. (2006). “Structural and physicochemical properties of natural zeolites: clinoptilolite and mordenite.” *Microporous and Mesoporous Materials*, 87(3), 243–254.
- Kosugi, K. (1994). “Three-parameter lognormal distribution model for soil water retention.” *Water Resources Research*, 30(4), 891–901.
- Kosugi, K. (1996). “Lognormal distribution model for unsaturated soil hydraulic properties.” *Water Resources Research*, M. T. van Genuchten, F. J. Leij, and L. Wu, eds., U.C. Riverside Press, Riverside, CA., Riverside, CA, 2697–2703.
- Kosugi, K. (1999a). “General model for unsaturated hydraulic conductivity for soils with lognormal pore-size distribution.” *Soil Science Society of America Journal*, 63(2), 270–277.
- Kosugi, K. (1999b). “Lognormal distribution model for unsaturated soil hydraulic

- properties.” *Proceedings of the International Workshop on Characterization and Measurement of the Hydraulic Properties of Unsaturated Porous Media*. Oct. 22-24, 1997, M. T. van Genuchten, F. J. Leij, and L. Wu, eds., U.C. Riverside Press, Riverside, CA., Riverside, CA, 1602.
- Kowalczyk, P., Sprynskyy, M., Terzyk, A. P., Lebedynets, M., Namieśnik, J., and Buszewski, B. (2006). “Porous structure of natural and modified clinoptilolites.” *Journal of colloid and interface science*, 297(1), 77–85.
- Krishna Darbha, G., Fischer, C., Michler, A., Luetzenkirchen, J., Schäfer, T., Heberling, F., and Schild, D. (2012). “Deposition of latex colloids at rough mineral surfaces: An analogue study using nanopatterned surfaces.” *Langmuir*, 28, 6606–6617.
- Kutílek, M., Jendele, L., and Krejca, M. (2009). “Comparison of empirical, semi-empirical and physically based models of soil hydraulic functions derived for bi-modal soils.” *Journal of contaminant hydrology*, 104(1-4), 84–9.
- Laegdsmand, M., de Jonge, L. W., Moldrup, P., and Keiding, K. (2004). “Pyrene Sorption to Water-Dispersible Colloids.” *Vadose Zone Journal*.
- Lamy, E., Lassabatère, L., Bechet, B., and Andrieu, H. (2013). “Effect of a nonwoven geotextile on solute and colloid transport in porous media under both saturated and unsaturated conditions.” *Geotextiles and Geomembranes*, Elsevier Ltd, 36, 55–65.
- Larrahondo, J. M., Choo, H., and Burns, S. E. (2011). “Laboratory-prepared iron oxide coatings on sands: Submicron-scale small-strain stiffness.” *Engineering Geology*, 121(1-2), 7–17.
- Lazouskaya, V., and Jin, Y. (2008). “Colloid retention at air–water interface in a capillary channel.” *Colloids and Surfaces A: Physicochemical and Engineering Aspects*, 325(3), 141–151.
- Lazouskaya, V., Wang, L.-P., Or, D., Wang, G., Caplan, J. L., and Jin, Y. (2013). “Colloid mobilization by fluid displacement fronts in channels.” *Journal of colloid and*

- interface science*, Elsevier Inc., 406, 44–50.
- Lecoanet, H. F., Bottero, J. Y., and Wiesner, M. R. (2004). “Laboratory assessment of the mobility of nanomaterials in porous media.” *Environmental Science and Technology*, 38(19), 5164–5169.
- Lee, S.-H., Jo, H. Y., Yun, S.-T., and Lee, Y. J. (2010). “Evaluation of factors affecting performance of a zeolitic rock barrier to remove zinc from water.” *Journal of hazardous materials*, 175(1-3), 224–34.
- Lee, T., Benson, C. H., and Eykholt, G. R. (2004). “Waste green sands as reactive media for groundwater contaminated with trichloroethylene (TCE).” *Journal of Hazardous Materials*, 109(1-3), 25–36.
- Lenhart, J. J., and Saiers, J. E. (2002). “Transport of silica colloids through unsaturated porous media: experimental results and model comparisons.” *Environmental science & technology*, 36(4), 769–77.
- Lenhart, J. J., and Saiers, J. E. (2003). “Colloid mobilization in water-saturated porous media under transient chemical conditions.” *Environmental Science and Technology*, 37(12), 2780–2787.
- Levin, J. M., Herman, J. S., Hornberger, G. M., and Saiers, J. E. (2006). “Colloid Mobilization from a Variably Saturated, Intact Soil Core.” *Vadose Zone Journal*, 5(2), 564.
- Li, X., and Johnson, W. P. (2005). “Nonmonotonic Variations in Deposition Rate Coefficients of Microspheres in Porous Media under Unfavorable Deposition Conditions.” *Environmental Science & Technology*, 39(6), 1658–1665.
- Li, X., Lin, C. L., Miller, J. D., and Johnson, W. P. (2006). “Role of grain-to-grain contacts on profiles of retained colloids in porous media in the presence of an energy barrier to deposition.” *Environmental Science and Technology*, 40(12), 3769–3774.
- Li, X., Scheibe, T. D., and Johnson, W. P. (2004). “Apparent decreases in colloid

- deposition rate coefficients with distance of transport under unfavorable deposition conditions: A general phenomenon." *Environmental Science and Technology*, 38(21), 5616–5625.
- Lin, D., Tian, X., Wu, F., and Xing, B. (2010). "Fate and transport of engineered nanomaterials in the environment." *Journal of environmental quality*, 39(6), 1896–1908.
- Lin, S., Cheng, Y., Bobcombe, Y., L. Jones, K., Liu, J., and Wiesner, M. R. (2011). "Deposition of silver nanoparticles in geochemically heterogeneous porous media: Predicting affinity from surface composition analysis." *Environmental Science and Technology*, 45, 5209–5215.
- Litton, G. M., and Olson, T. M. (1993). "Colloid deposition rates on silica bed media and artifacts related to collector surface preparation methods." *Environmental Science & Technology*, 27(1), 185–193.
- Liu, Q., Lazouskaya, V., He, Q., and Jin, Y. (2010). "Effect of particle shape on colloid retention and release in saturated porous media." *Journal of environmental quality*, 39(2), 500–508.
- Liu, Y., Zhao, Y., Sun, B., and Chen, C. (2013). "Understanding the toxicity of carbon nanotubes." *Accounts of chemical research*, 46(3), 702–13.
- Loveland, J. P., Bhattacharjee, S., Ryan, J. N., and Elimelech, M. (2003). "Colloid transport in a geochemically heterogeneous porous medium: aquifer tank experiment and modeling." *Journal of contaminant hydrology*, 65(3-4), 161–82.
- Madigan, M. T., Martinko, J. M., Stahl, D., and Clark, D. P. (2010). *Brock Biology of Microorganisms*. Benjamin Cummings, Prentice Hall, NJ.
- Mahmood, T., Amirtharajah, A., Sturm, T. W., and Dennett, K. E. (2001). "A micromechanics approach for attachment and detachment of asymmetric colloidal particles." *Colloids and Surfaces A: Physicochemical and Engineering Aspects*, 99–

110.

- Majdalani, S., Michel, E., Di Pietro, L., and Angulo-Jaramillo, R. (2008). "Effects of wetting and drying cycles on in situ soil particle mobilization." *European Journal of Soil Science*, 59(2), 147–155.
- Martin, J. P., Korkut, E., and Yaman, C. (2006). "Effects of wastewater filtration on geotextile permeability." *Geosynthetics International*.
- Martin, M. J., Logan, B. E., Johnson, W. P., Jewett, D. G., and Arnold, R. G. (1996). "Scaling Bacterial Filtration Rates in Different Sized Porous Media." *Journal of Environmental Engineering*, 122(5), 407–415.
- Massoudieh, A., and Ginn, T. R. (2008). "Modeling Colloid-Enhanced Contaminant Transport in Stormwater Infiltration Basin Best Management Practices." *Vadose Zone Journal*, 7(4), 1261.
- Mays, D. C. (2010). "Contrasting Clogging in Granular Media Filters, Soils, and Dead-End Membranes." *Journal of Environmental Engineering*, 136(5), 475.
- McCarthy, J. F., and McKay, L. (2004). "Colloid Transport in the Subsurface: Past, Present, and Future Challenges." *Vadose Zone Journal*, 3(2), 326–337.
- McDowell-Boyer, L. M., Hunt, J. R., and Sitar, N. (1986). "Particle transport through porous media." *Water Resour. Res.*, 22(13), 1901–1921.
- McGechan, M., and Lewis, D. (2002). "Transport of Particulate and Colloid-sorbed Contaminants through Soil, Part 1: General Principles." *Biosystems Engineering*, 83(3), 255–273.
- Mclsaac, R., and Rowe, R. K. (2006). "Effect of filter–separators on the clogging of leachate collection systems." *Canadian Geotechnical Journal*.
- Mehra, O. P. (1958). "Iron Oxide Removal from Soils and Clays by a Dithionite-Citrate System Buffered with Sodium Bicarbonate." *Clays and Clay Minerals*, 7(1), 317–327.

- Mekonen, A., Sharma, P., and Fagerlund, F. (2014). "Transport and mobilization of multiwall carbon nanotubes in quartz sand under varying saturation." *Environmental Earth Sciences*, 71(8), 3751–3760.
- Melnick, J. L., and Gerba, C. P. (1980). "Viruses in water and soil." *Public Health Review*, 9(3-4), 185–213.
- Mishurov, M., Yakirevich, A., and Weisbrod, N. (2008). "Colloid transport in a heterogeneous partially saturated sand column." *Environmental science & technology*, 42(4), 1066–71.
- Mitchell, J. K., and Soga, K. (2005). *Fundamentals of Soil Behavior*. John Wiley & Sons.
- Mitropoulou, P. N., Syngouna, V. I., and Chrysikopoulos, C. V. (2013). "Transport of colloids in unsaturated packed columns: Role of ionic strength and sand grain size." *Chemical Engineering Journal*, Elsevier B.V., 232, 237–248.
- Mockovčiaková, A., Matik, M., Orolínová, Z., Hudec, P., and Kmecová, E. (2007). "Structural characteristics of modified natural zeolite." *Journal of Porous Materials*, 15(5), 559–564.
- Mohanty, S. K., Torkelson, A. A., Dodd, H., Nelson, K. L., and Boehm, A. B. (2013). "Engineering solutions to improve the removal of fecal indicator bacteria by bioinfiltration systems during intermittent flow of stormwater." *Environmental science & technology*, 47(19), 10791–8.
- Molnar, I. L., Johnson, W. P., Gerhard, J. I., Willson, C. S., and O'Carroll, D. M. (2015). "Predicting colloid transport through saturated porous media: A critical review." *Water Resources Research*, 51(9), 6804–6845.
- Morales, V. L., Gao, B., and Steenhuis, T. S. (2009). "Grain Surface-Roughness Effects on Colloidal Retention in the Vadose Zone." *Vadose Zone Journal*, 8(1), 11.
- Mualem, Y. (1976). "A new model for predicting the hydraulic conductivity of unsaturated porous media." *Water Resources Research*, 12(3), 513–522.

- Mualem, Y., and Dagan, G. (1978). "Hydraulic conductivity of soils: Unified approach to the statistical models." *Soil Science Society of America ...*, 42, 392–395.
- Nasta, P., Huynh, S., and Hopmans, J. W. (2011). "Simplified Multistep Outflow Method to Estimate Unsaturated Hydraulic Functions for Coarse-Textured Soils." *Soil Science Society of America Journal*, 75(2), 418.
- Nelson, K. E., and Ginn, T. R. (2005). "Colloid filtration theory and the happel sphere-in-cell model revisited with direct numerical simulation of colloids." *Langmuir*, 21(2), 2173–2184.
- Nola, M., Ewoti, O. V. N., Nougang, M., Mougang, M. L., Chihib, N.-E., Krier, F., Servais, P., Hornez, J.-P., and Njine, T. (2010). "Involvement of cell shape and flagella in the bacterial retention during percolation of contaminated water through soil columns in tropical region." *Journal of environmental science and health. Part A, Toxic/hazardous substances & environmental engineering*, 45(11), 1297–1306.
- Noordmans, J., Wit, P. J., VanderMei, H. C., and Busscher, H. J. (1997). "Detachment of polystyrene particles from collector surfaces by surface tension forces induced by air-bubble passage through a parallel plate flow chamber." *Journal of Adhesion Science and Technology*, 11, 957–969.
- Novikov, A. P., Kalmykov, S. N., Utsunomiya, S., Ewing, R. C., Horreard, F., Merkulov, A., Clark, S. B., Tkachev, V. V., and Myasoedov, B. F. (2006). "Colloid transport of plutonium in the far-field of the Mayak Production Association, Russia." *Science (New York, N. Y.)*, 314, 638–641.
- Nowack, B., and Bucheli, T. D. (2007). "Occurrence, behavior and effects of nanoparticles in the environment." *Environmental Pollution*.
- Oren, A. H., and Ozdamar, T. (2013). "Hydraulic conductivity of compacted zeolites." *Waste management & research : the journal of the International Solid Wastes and Public Cleansing Association, ISWA*, 31(6), 634–40.

- Palmeira, E. M., Remigio, A. F. N., Ramos, M. L. G., and Bernardes, R. S. (2008). "A study on biological clogging of nonwoven geotextiles under leachate flow." *Geotextiles and Geomembranes*, 26(3), 205–219.
- Park, J.-B., Lee, S.-H., Lee, J.-W., and Lee, C.-Y. (2002). "Lab scale experiments for permeable reactive barriers against contaminated groundwater with ammonium and heavy metals using clinoptilolite (01-29B)." *Journal of hazardous materials*, 95(1-2), 65–79.
- Park, S.-J., Lee, C.-G., Kim, S. B., and Chang, Y.-Y. (2012). "Bacterial removal in flow-through columns packed with iron-manganese bimetallic oxide-coated sand." *Journal of environmental science and health. Part A, Toxic/hazardous substances & environmental engineering*, 47(January 2015), 1364–1371.
- Parks, G. A. (1965). "The Isoelectric Points of Solid Oxides, Solid Hydroxides, and Aqueous Hydroxo Complex Systems." *Chemical Reviews*, 65(2), 177–198.
- Pazmino, E. F., Ma, H., and Johnson, W. P. (2011). "Applicability of colloid filtration theory in size-distributed, reduced porosity, granular media in the absence of energy barriers." *Environmental science & technology*, 45(24), 10401–7.
- Pazmino, E., Trauscht, J., and Johnson, W. P. (2014). "Release of Colloids from Primary Minimum Contact under Unfavorable Conditions by Perturbations in Ionic Strength and Flow Rate." *Environmental Science & Technology*, 48(16), 9227–9235.
- Penrose, W. R., Polzer, W. L., Essington, E. H., Nelson, D. M., and Orlandini, K. a. (1990). "Mobility of plutonium and americium through a shallow aquifer in a semiarid region." *Environ. Sci. Technol.*, 24(2), 228–234.
- Peters, A., Durner, W., and Wessolek, G. (2011). "Consistent parameter constraints for soil hydraulic functions." *Advances in Water Resources*, Elsevier Ltd, 34(10), 1352–1365.
- Petosa, A. R., Jaisi, D. P., Quevedo, I. R., Elimelech, M., and Tufenkji, N. (2010).

- “Aggregation and deposition of engineered nanomaterials in aquatic environments: Role of physicochemical interactions.” *Environmental Science and Technology*, 44(17), 6532–6549.
- Pitcher, S. K., Slade, R. C. T., and Ward, N. I. (2004). “Heavy metal removal from motorway stormwater using zeolites.” *Science of The Total Environment*, 334-335, 161–166.
- Porubcan, A. A., and Xu, S. (2011). “Colloid straining within saturated heterogeneous porous media.” *Water research*, Elsevier Ltd, 45(4), 1796–806.
- Potter, J. M., and W.E., D. (1985). “Chemical Aspects of Iron Colloid Plugging in Quartz Sands and Implications for Formation Damage.” *Journal of Petroleum Technology*.
- Ramachandran, V., and Fogler, H. S. (1999). “Plugging by hydrodynamic bridging during flow of stable colloidal particles within cylindrical pores.” *Journal of Fluid Mechanics*, 385, 129–156.
- Reddi, L. N. (1997). “Particle Transport in Soils: Review of Significant Processes in Infrastructure Systems.” *Journal of Infrastructure Systems*.
- Reddi, L. N., Ming, X., Hajra, M. G., and Lee, I. M. (2000). “Permeability Reduction of Soil Filters due to Physical Clogging.” *Journal of Geotechnical and Geoenvironmental Engineering*, 126(3), 236–246.
- Reddi, L. N., Xiao, M., Hajra, M. G., and Lee, I. M. (2005). “Physical clogging of soil filters under constant flow rate versus constant head.” *Canadian Geotechnical Journal*.
- Rockhold, M. L., Yarwood, R. R., and Selker, J. S. (2004). “Coupled Microbial and Transport Processes in Soils.” *Vadose Zone Journal*, 3(2), 368–383.
- Rostad, C. E., Leenheer, J. A., and Daniel, S. R. (1998). “Organic carbon and nitrogen content associated with colloids and suspended particulates from the Mississippi River and some of its tributaries.” *Environmental Science and Technology*, 31,

3218–3225.

- Rousseau, M., Di Pietro, L., Angulo-Jaramillo, R., Tessier, D., and Cabibel, B. (2004). "Preferential Transport of Soil Colloidal Particles: Physicochemical Effects on Particle Mobilization." *Vadose Zone Journal*.
- Roy, S. B., and Dzombak, D. A. (1998). "Sorption nonequilibrium effects on colloid-enhanced transport of hydrophobic organic compounds in porous media." *Journal of Contaminant Hydrology*, 30, 179–200.
- Russell, T. L., Yamahara, K. M., and Boehm, A. B. (2012). "Mobilization and transport of naturally occurring enterococci in beach sands subject to transient infiltration of seawater." *Environmental science & technology*, 46(11), 5988–96.
- Ryan, J., and Gschwend, P. (1992). "Effect of iron diagenesis on the transport of colloidal clay in an unconfined sand aquifer." *Geochimica et Cosmochimica Acta*, 56(4), 1507–1521.
- Ryan, J. N., Elimelech, M., Ard, R. A., Harvey, R. W., and Johnson, W. P. (1999). "Bacteriophage PRD1 and silica colloid transport and recovery in an iron oxide-coated sand aquifer." *Environmental Science and Technology*, 33(1), 63–73.
- Ryan, J. N., and Gschwend, P. M. (1994). "Effect of Solution Chemistry on Clay Colloid Release from an Iron Oxide-Coated Aquifer Sand." *Environmental Science & Technology*, 28(9), 1717–1726.
- Saiers, J. E., Hornberger, G., and Harvey, C. (1994). "Colloidal silica transport through structured, heterogeneous porous media." *Journal of Hydrology*, 163, 271–288.
- Saiers, J. E., Hornberger, G. M., Gower, D. B., and Herman, J. S. (2003). "The role of moving air-water interfaces in colloid mobilization within the vadose zone." *Geophysical Research Letters*, 30(21), 1–5.
- Saiers, J. E., and Lenhart, J. J. (2003a). "Ionic-strength effects on colloid transport and interfacial reactions in partially saturated porous media." *Water Resources*

Research, 39(9).

Saiers, J. E., and Lenhart, J. J. (2003b). "Colloid mobilization and transport within unsaturated porous media under transient-flow conditions." *Water Resources Research*.

Saiers, J. E., and Ryan, J. (2005). "Colloid deposition on non-ideal porous media: The influences of collector shape and roughness on the single-collector efficiency." *Geophysical Research Letters*, 32(21), 1–5.

Salerno, M. B., Flamm, M., Logan, B. E., and Velegol, D. (2006). "Transport of rodlike colloids through packed beds." *Environmental Science and Technology*, 40(20), 6336–6340.

Sang, W., Morales, V. L., Zhang, W., Stooft, C. R., Gao, B., Schatz, A. L., Zhang, Y., and Steenhuis, T. S. (2013). "Quantification of colloid retention and release by straining and energy minima in variably saturated porous media." *Environmental Science and Technology*, 47, 8256–8264.

Sang, W., Stooft, C. R., Zhang, W., Morales, V. L., Gao, B., Kay, R. W., Liu, L., Zhang, Y., and Steenhuis, T. S. (2014). "Effect of hydrofracking fluid on colloid transport in the unsaturated zone." *Environmental science & technology*, 48(14), 8266–74.

Sansalone, J. J. (1999). "Adsorptive infiltration of metals in urban drainage - Media characteristics." *Science of the Total Environment*, 179–188.

Santore, M. M., and Kozlova, N. (2007). "Micrometer scale adhesion on nanometer-scale patchy surfaces: adhesion rates, adhesion thresholds, and curvature-based selectivity." *Langmuir : the ACS journal of surfaces and colloids*, 23(9), 4782–91.

Schaap, M. G., and van Genuchten, M. T. (2006). "A Modified Mualem–van Genuchten Formulation for Improved Description of the Hydraulic Conductivity Near Saturation." *Vadose Zone Journal*, 5(1), 27.

Scheidegger, A., Borkovec, M., and Sticher, H. (1993). "Coating of silica sand with

- goethite: preparation and analytical identification." *Geoderma*, 58(1-2), 43–65.
- Schelde, K., de Jonge, L. W., Kjaergaard, C., Laegdsmand, M., and Rubæk, G. H. (2006). "Effects of Manure Application and Plowing on Transport of Colloids and Phosphorus to Tile Drains." *Vadose Zone Journal*, 5(1), 445–458.
- Schijven, J., and Hassanizadeh, S. (2000). "Removal of viruses by soil passage: Overview of modeling, processes, and parameters." *Critical Reviews in Environmental Science and Technology*, 30(1), 49–127.
- Sen, R. (2008). "Biotechnology in petroleum recovery: The microbial EOR." *Progress in Energy and Combustion Science*, 34(6), 714–724.
- Sen, T. K. (2011). "Processes in pathogenic biocolloidal contaminants transport in saturated and unsaturated porous media: A review." *Water, Air, and Soil Pollution*.
- Sen, T. K., and Khilar, K. C. (2006). "Review on subsurface colloids and colloid-associated contaminant transport in saturated porous media." *Advances in Colloid and Interface Science*.
- Seymour, M. B., Chen, G., Su, C., and Li, Y. (2013). "Transport and retention of colloids in porous media: does shape really matter?" *Environmental science & technology*, 47(15), 8391–8.
- Shang, J., Flury, M., Chen, G., and Zhuang, J. (2008). "Impact of flow rate, water content, and capillary forces on in situ colloid mobilization during infiltration in unsaturated sediments." *Water Resources Research*, 44(6), 1–12.
- Shang, J., Flury, M., and Deng, Y. (2009). "Force measurements between particles and the air-water interface: Implications for particle mobilization in unsaturated porous media." *Water Resources Research*, 45(6), n/a–n/a.
- Shani, C., Weisbrod, N., and Yakirevich, A. (2008). "Colloid transport through saturated sand columns: Influence of physical and chemical surface properties on deposition." *Colloids and Surfaces A: Physicochemical and Engineering Aspects*, 316, 142–150.

- Shaoping, H., Xincui, C., Jiyan, S., Yingxu, C., and Qi, L. (2008). "Particle-facilitated lead and arsenic transport in abandoned mine sites soil influenced by simulated acid rain." *Chemosphere*, 71, 2091–2097.
- Sharma, M. M., Chamoun, H., Sarma, D. S. H. S. R., and Schechter, R. S. (1992). "Factors controlling the hydrodynamic detachment of particles from surfaces." *Journal of Colloid and Interface Science*, 149(1), 121–134.
- Sharma, P., Abdou, H. M., and Flury, M. (2008). "Effect of the Lower Boundary Condition and Flotation on Colloid Mobilization in Unsaturated Sandy Sediments." *Vadose Zone Journal*, 7(3), 930.
- Sharma, P., Flury, M., and Zhou, J. (2008). "Detachment of colloids from a solid surface by a moving air-water interface." *Journal of colloid and interface science*, 326(1), 143–50.
- Shein, E. V., and Devin, B. A. (2007). "Current problems in the study of colloidal transport in soil." *Eurasian Soil Science*, 40(4), 399–408.
- Shellenberger, K., and Logan, B. E. (2002). "Effect of molecular scale roughness of glass beads on colloidal and bacterial deposition." *Environmental science & technology*, 36(2), 184–9.
- Shen, C., Huang, Y., Li, B., and Jin, Y. (2008). "Effects of solution chemistry on straining of colloids in porous media under unfavorable conditions." *Water Resources Research*, 44(5), 1–12.
- Shen, C., Lazouskaya, V., Zhang, H., Wang, F., Li, B., Jin, Y., and Huang, Y. (2012). "Theoretical and experimental investigation of detachment of colloids from rough collector surfaces." *Colloids and Surfaces A: Physicochemical and Engineering Aspects*, Elsevier B.V., 410, 98–110.
- Shen, C., Li, B., Huang, Y., and Jin, Y. (2007). "Kinetics of Coupled Primary- and Secondary-Minimum Deposition of Colloids under Unfavorable Chemical

- Conditions." *Environmental Science & Technology*, 41(20), 6976–6982.
- Shen, C., Li, B., Wang, C., Huang, Y., and Jin, Y. (2011). "Surface Roughness Effect on Deposition of Nano- and Micro-Sized Colloids in Saturated Columns at Different Solution Ionic Strengths." *Vadose Zone Journal*, 10(3), 1071.
- Shen, C., Wang, F., Li, B., Jin, Y., Wang, L.-P., and Huang, Y. (2012). "Application of DLVO energy map to evaluate interactions between spherical colloids and rough surfaces." *Langmuir: the ACS journal of surfaces and colloids*, 28(41), 14681–92.
- Shen, C., Wang, L.-P., Li, B., Huang, Y., and Jin, Y. (2012). "Role of Surface Roughness in Chemical Detachment of Colloids Deposited at Primary Energy Minima." *Vadose Zone Journal*, 11(1).
- Sherard, B. J. L., and Dunnigan, L. P. (1989). "Critical Filters for Impervious Soils." *Journal of Geotechnical and Geoenvironmental Engineering*, 115(7), 927–947.
- Sherard, J. L., Dunnigan, L. P., and Talbot, J. R. (1984a). "Filters for Silts and Clays." *Journal of Geotechnical Engineering*, 110(6), 701.
- Sherard, J. L., Dunnigan, L. P., and Talbot, J. R. (1984b). "Basic Properties of Sand and Gravel Filters." *Journal of Geotechnical Engineering*, 110(6), 684.
- Shi, W., Wang, J., Fan, X., and Gao, H. (2008). "Size and shape effects on diffusion and absorption of colloidal particles near a partially absorbing sphere: Implications for uptake of nanoparticles in animal cells." *Physical Review E - Statistical, Nonlinear, and Soft Matter Physics*, 78(6), 1–11.
- Silliman, S. (1995). "Particle transport through two-dimensional, saturated porous media: influence of physical structure of the medium." *Journal of Hydrology*, 167, 79–98.
- Simon-Deckers, A., Loo, S., Mayne-L'Hermite, M., Herlin-Boime, N., Menguy, N., Reynaud, C., Gouget, B., and Carriere, M. (2009). "Size-, composition- and shape-dependent toxicological impact of metal oxide nanoparticles and carbon nanotubes toward bacteria." *Environmental Science and Technology*, 43(21), 8423–8429.

- Simunek, J., Sejna, M., Saito, H., Sakai, M., and van Genuchten, M. T. (2013). "The Hydrus-1D Software Package for Simulating the Movement of Water, Heat, and Multiple Solutes in Variably Saturated Media." Department of Environmental Sciences, University of California Riverside, Riverside, CA.
- Sirivithayapakorn, S., and Keller, A. (2003a). "Transport of colloids in unsaturated porous media: A pore-scale observation of processes during the dissolution of air-water interface." *Water Resources Research*, 39(12).
- Sirivithayapakorn, S., and Keller, A. (2003b). "Transport of colloids in saturated porous media: A pore-scale observation of the size exclusion effect and colloid acceleration." *Water Resources Research*, 39(4), n/a–n/a.
- Song, L., Johnson, P. R., and Elimelech, M. (1994). "Kinetics of colloid deposition onto heterogeneously charged surfaces in porous media." *Environmental science & technology*, 28(6), 1164–1171.
- Sprague, L. A., Herman, J. S., Hornberger, G. M., and Mills, A. L. (2000). "Atrazine Adsorption and Colloid-Facilitated Transport through the Unsaturated Zone." *Journal of Environment Quality*.
- Sprynskyy, M., Golembiewski, R., Trykowski, G., and Buszewski, B. (2010). "Heterogeneity and hierarchy of clinoptilolite porosity." *Journal of Physics and Chemistry of Solids*, 71(9), 1269–1277.
- Srinivasan, R., Hoffman, D. W., Wolfe, J. E., and Prcin, L. J. (2008). "Evaluation of removal of orthophosphate and ammonia from rainfall runoff using aboveground permeable reactive barrier composed of limestone and zeolite." *Journal of environmental science and health. Part A, Toxic/hazardous substances & environmental engineering*, 43(12), 1441–50.
- Steenhuis, T. S., McCarthy, J. F., Crist, J. T., Zevi, Y., Baveye, P. C., Throop, J. A., Fehrman, R. L., Dathe, A., and Richards, B. K. (2005). "Reply to 'Comments on

- “Pore-Scale Visualization of Colloid Transport and Retention in Partly Saturated Porous Media.”” *Vadose Zone Journal*, 4(4), 957.
- Steiner, L. D., Bidwell, V. J., Hong, J. D. I., Cameron, K. C., and Northcott, G. L. (2010). “Transport and modeling of estrogenic hormones in a dairy farm effluent through undisturbed soil lysimeters.” *Environmental Science and Technology*, 44, 2341–2347.
- Stevik, T. K., Aa, K., Ausland, G., and Hanssen, J. F. (2004). “Retention and removal of pathogenic bacteria in wastewater percolating through porous media: A review.” *Water Research*.
- Stockdale, A., and Bryan, N. D. (2013). “The influence of natural organic matter on radionuclide mobility under conditions relevant to cementitious disposal of radioactive wastes: A review of direct evidence.” *Earth-Science Reviews*, Elsevier B.V.
- Sun, N., Sun, N. Z., Elimelech, M., and Ryan, J. (2001). “Sensitivity analysis and parameter identifiability for colloid transport in geochemically heterogeneous porous media.” *Water Resources Research*, 37(2), 209–222.
- Tian, Y., Gao, B., Morales, V. L., Wang, Y., and Wu, L. (2012). “Effect of surface modification on single-walled carbon nanotube retention and transport in saturated and unsaturated porous media.” *Journal of hazardous materials*, Elsevier B.V., 239-240, 333–9.
- Tobler, D. J., Maclachlan, E., and Phoenix, V. R. (2012). “Microbially mediated plugging of porous media and the impact of differing injection strategies.” *Ecological Engineering*, 42, 270–278.
- Tokunaga, T. K. (2011). “Physicochemical controls on adsorbed water film thickness in unsaturated geological media.” *Water Resources Research*, 47(8), 1–12.
- Tong, M., and Johnson, W. P. (2006). “Excess colloid retention in porous media as a

- function of colloid size, fluid velocity, and grain angularity.” *Environmental science & technology*, 40(24), 7725–31.
- Tong, M., Ma, H., and Johnson, W. P. (2008). “Funneling of Flow into Grain-to-grain Contacts Drives Colloid–Colloid Aggregation in the Presence of an Energy Barrier.” *Environmental Science & Technology*, 42(8), 2826–2832.
- Torkzaban, S., Bradford, S. A., van Genuchten, M. T., and Walker, S. L. (2008). “Colloid transport in unsaturated porous media: the role of water content and ionic strength on particle straining.” *Journal of contaminant hydrology*, 96(1-4), 113–27.
- Torkzaban, S., Bradford, S. A., and Walker, S. (2007). “Resolving the coupled effects of hydrodynamics and DLVO forces on colloid attachment in porous media.” *Langmuir*, (17), 9652–9660.
- Torkzaban, S., Hassanizadeh, S. M., Schijven, J. F., and van den Berg, H. H. J. L. (2006). “Role of air-water interfaces on retention of viruses under unsaturated conditions.” *Water Resources Research*, 42(12), W12S14.
- Torkzaban, S., Kim, H. N., Simunek, J., and Bradford, S. A. (2010). “Hysteresis of colloid retention and release in saturated porous media during transients in solution chemistry.” *Environmental science & technology*, 44(5), 1662–9.
- Tufenkji, N. (2007). “Modeling microbial transport in porous media: Traditional approaches and recent developments.” *Advances in Water Resources*, 30(6-7), 1455–1469.
- Tufenkji, N., Dixon, D. R., Considine, R., and Drummond, C. J. (2006). “Multi-scale Cryptosporidium/sand interactions in water treatment.” *Water Research*.
- Tufenkji, N., and Elimelech, M. (2004a). “Deviation from the classical colloid filtration theory in the presence of repulsive DLVO interactions.” *Langmuir*, 20(21), 10818–10828.
- Tufenkji, N., and Elimelech, M. (2004b). “Correlation Equation for Predicting Single-

- Collector Efficiency in Physicochemical Filtration in Saturated Porous Media.”
Environmental Science and Technology, 38(2), 529–536.
- Tufenkji, N., and Elimelech, M. (2005). “Breakdown of Colloid Filtration Theory: Role of the Secondary Energy Minimum and Surface Charge Heterogeneities.” *Langmuir*, 21(3), 841–852.
- Utsumomiya, S., Kersting, A. B., and Ewing, R. C. (2009). “Groundwater nanoparticles in the far-field at the Nevada test site: Mechanism for radionuclide transport.”
Environmental Science and Technology, 43(5), 1293–1298.
- Uyusur, B., Darnault, C. J. G., Snee, P. T., Kokën, E., Jacobson, A. R., and Wells, R. R. (2010). “Coupled effects of solution chemistry and hydrodynamics on the mobility and transport of quantum dot nanomaterials in the vadose zone.” *Journal of contaminant hydrology*, Elsevier B.V., 118(3-4), 184–98.
- Valdes, J. R., and Santamarina, J. C. (2008). “Clogging: bridge formation and vibration-based destabilization.” *Canadian Geotechnical Journal*, 45(2), 177–184.
- Vaughan, D. E. (1976). “Properties of Natural Zeolites.” *Natural Zeolites: Occurrence, Properties, Use*, Pergamon Press, Inc., Elmsford, 353–401.
- Vervoort, R., and Cattle, S. (2003). “Linking hydraulic conductivity and tortuosity parameters to pore space geometry and pore-size distribution.” *Journal of Hydrology*, 272(2003), 36–49.
- Villholth, K. G. (1999). “Colloid characterization and colloidal phase partitioning of polycyclic aromatic hydrocarbons in two creosote-contaminated aquifers in Denmark.” *Environmental Science and Technology*, 33, 691–699.
- Villholth, K. G., Jarvis, N. J., Jacobsen, O. H., and de Jonge, H. (2000). “Field Investigations and Modeling of Particle-Facilitated Pesticide Transport in Macroporous Soil.” *Journal of Environment Quality*.
- Vogel, T., Van Genuchten, M. T., and Cislerova, M. (2000). “Effect of the shape of the

- soil hydraulic functions near saturation on variably-saturated flow predictions.” *Advances in Water Resources*, 24(2), 133–144.
- Vrugt, J. A., and Bouten, W. (2002). “Validity of first-order approximations to describe parameter uncertainty in soil hydrologic models.” *Soil Science Society of America Journal*, 66, 1740–1751.
- Vrugt, J. A., Bouten, W., Gupta, H. V., and Hopmans, J. W. (2003). “Toward Improved Identifiability of Soil Hydraulic Parameters: On the selection of a Suitable Parametric Model.” *Vadose Zone Journal*, 2, 98–113.
- Vrugt, J. A., Bouten, W., and Weerts, A. H. (2001). “Information Content of Data for Identifying Soil Hydraulic Parameters.” *Soil Science Society of America Journal*, 65, 19–27.
- Vrugt, J. A., ter Braak, C. J. F., Clark, M. P., Hyman, J. M., and Robinson, B. A. (2008). “Treatment of input uncertainty in hydrologic modeling: Doing hydrology backward with Markov chain Monte Carlo simulation.” *Water Resources Research*, 44(12), W00B09.
- Vrugt, J. A., ter Braak, C. J. F., Diks, C. G. H., and Robinson, B. A. (2009). “Accelerating Markov chain Monte Carlo simulation by differential evolution with self-adaptive randomized subspace sampling.” *Journal of Nonlinear Sciences & Numerical Simulation*, 10(3), 271–288.
- Vrugt, J. A., ter Braak, C. J. F., Gupta, H. V., and Robinson, B. A. (2008). “Equifinality of formal (DREAM) and informal (GLUE) Bayesian approaches in hydrologic modeling?” *Stochastic Environmental Research and Risk Assessment*, 23(7), 1011–1026.
- Vrugt, J. A., Stauffer, P. H., Wöhling, T., Robinson, B. A., and Vesselinov, V. V. (2008). “Inverse Modeling of Subsurface Flow and Transport Properties: A Review with New Developments.” *Vadose Zone Journal*, 7(2), 843.

- Walz, J. Y. (1998). "The effect of surface heterogeneities on colloidal forces." *Advances in Colloid and Interface Science*, 74(1-3), 119–168.
- Wan, J., and Tokunaga, T. K. (1997). "Film straining of colloids in unsaturated porous media: Conceptual model and experimental testing." *Environmental Science and Technology*, 31(8), 2413–2420.
- Wan, J., and Tokunaga, T. K. (1998). "Measuring Partition Coefficients of Colloids at Air–Water Interfaces." *Environmental Science & Technology*, 32(21), 3293–3298.
- Wan, J., and Tokunaga, T. K. (2002). "Partitioning of clay colloids at air-water interfaces." *Journal of colloid and interface science*, 247(1), 54–61.
- Wan, J., and Tokunaga, T. K. (2005). "Comments on 'Pore-Scale Visualization of Colloid Transport and Retention in Partly Saturated Porous Media.'" *Vadose Zone Journal*, 4(4), 954.
- Wan, J., and Wilson, J. L. (1994a). "Visualization of the role of the gas-water interface on the fate and transport of colloids in porous media." *Water Resources Research*, 30(1), 11.
- Wan, J., and Wilson, J. L. (1994b). "Colloid transport in unsaturated porous media." *Water Resources Research*, American Geophysical Union, 30(4), 857–864.
- Wang, C., Bobba, A. D., Attinti, R., Shen, C., Lazouskaya, V., Wang, L.-P., and Jin, Y. (2012). "Retention and transport of silica nanoparticles in saturated porous media: effect of concentration and particle size." *Environmental science & technology*, 46(13), 7151–8.
- Wang, D., Bradford, S. A., Harvey, R. W., Gao, B., Cang, L., and Zhou, D. (2012). "Humic acid facilitates the transport of ARS-labeled hydroxyapatite nanoparticles in iron oxyhydroxide-coated sand." *Environmental Science and Technology*, 46, 2738–2745.
- Wang, D., Zhang, W., and Zhou, D. (2013). "Antagonistic effects of humic acid and iron

- oxyhydroxide grain-coating on biochar nanoparticle transport in saturated sand.” *Environmental Science and Technology*, 47, 5154–5161.
- Wang, Y., Bradford, S. A., and Šimůnek, J. (2013). “Transport and fate of microorganisms in soils with preferential flow under different solution chemistry conditions.” *Water Resources Research*, 49, 2424–2436.
- Wang, Y., Bradford, S. A., and Šimůnek, J. (2014). “Estimation and upscaling of dual-permeability model parameters for the transport of *E. coli* D21g in soils with preferential flow.” *Journal of Contaminant Hydrology*, 159, 57–66.
- Wang, Y., Hammes, F., Boon, N., and Egli, T. (2007). “Quantification of the filterability of freshwater bacteria through 0.45, 0.22, and 0.1 μm pore size filters and shape-dependent enrichment of filterable bacterial communities.” *Environmental Science and Technology*, 41(20), 7080–7086.
- Wang, Y., Hammes, F., Düggelin, M., and Egli, T. (2008). “Influence of size, shape, and flexibility on bacterial passage through micropore membrane filters.” *Environmental Science and Technology*, 42(17), 6749–6754.
- Wang, Y., Kim, J. H., Baek, J. B., Miller, G. W., and Pennell, K. D. (2012). “Transport behavior of functionalized multi-wall carbon nanotubes in water-saturated quartz sand as a function of tube length.” *Water Research*, Elsevier Ltd, 46(14), 4521–4531.
- Wantanaphong, J., Mooney, S. J., and Bailey, E. H. (2005). “Natural and waste materials as metal sorbents in permeable reactive barriers (PRBs).” *Environmental Chemistry Letters*, 3(1), 19–23.
- Warner, N. R., Christie, C. A., Jackson, R. B., and Vengosh, A. (2013). “Impacts of shale gas wastewater disposal on water quality in Western Pennsylvania.” *Environmental Science and Technology*, 47, 11849–11857.
- Wayllace, A., and Lu, N. (2014). “A transient water release and imbibitions method for

- rapidly measuring wetting and drying soil water retention and hydraulic conductivity functions." *Geotechnical Testing Journal*, 35(1).
- Weggel, J. R., and Dortch, J. (2012). "A model for filter cake formation on geotextiles: Experiments." *Geotextiles and Geomembranes*, Elsevier Ltd, 31, 62–68.
- Weiss, T. H., Mills, A. L., Hornberger, G. M., and Herman, J. S. (1995). "Effect of bacterial cell shape on transport of bacteria in porous media." *Environmental Science & Technology*, 29(7), 1737–1740.
- Wilson, M. J., Wilson, L., and Patey, I. (2014). "The influence of individual clay minerals on formation damage of reservoir sandstones: a critical review with some new insights." *Clay Minerals*, 49, 147–164.
- Wöhling, T., and Vrugt, J. A. (2011). "Multiresponse multilayer vadose zone model calibration using Markov chain Monte Carlo simulation and field water retention data." *Water Resources Research*, 47(4), W04510.
- Wood, F. M., Yamamuro, J. A., and Lade, P. V. (2008). "Effect of depositional method on the undrained response of silty sand." *Canadian Geotechnical Journal*, 45(11), 1525–1537.
- Xu, S., Gao, B., and Saiers, J. E. (2006). "Straining of colloidal particles in saturated porous media." *Water Resources Research*, 42(12), 1–10.
- Xu, S., Liao, Q., and Saiers, J. E. (2008). "Straining of nonspherical colloids in saturated porous media." *Environmental Science and Technology*, 42(3), 771–778.
- Xu, S., and Saiers, J. E. (2009). "Colloid straining within water-saturated porous media: Effects of colloid size nonuniformity." *Water Resources Research*, 45(5), 1–8.
- Yang, X., Deng, S., and Wiesner, M. R. (2013). "Comparison of enhanced microsphere transport in an iron-oxide-coated porous medium by pre-adsorbed and co-depositing organic matter." *Chemical Engineering Journal*, Elsevier B.V., 230(211), 537–546.

- Yates, M. V., Gerba, C. P., and Kelley, L. M. (1985). "Virus persistence in groundwater." *Applied and Environmental Microbiology*, 49(4), 778–781.
- Yi, Q., Yu, J., and Kim, Y. (2010). "Removal patterns of particulate and dissolved forms of pollutants in a stormwater wetland." *Water science and technology : a journal of the International Association on Water Pollution Research*, 61(8), 2083–96.
- Yoon, J. S., Germaine, J. T., and Culligan, P. J. (2006). "Visualization of particle behavior within a porous medium: Mechanisms for particle filtration and retardation during downward transport." *Water Resources Research*, 42(6), W06417.
- Zevi, Y., Dathe, A., Gao, B., Zhang, W., Richards, B. K., and Steenhuis, T. S. (2009). "Transport and retention of colloidal particles in partially saturated porous media: Effect of ionic strength." *Water Resources Research*, 45(12), 1–10.
- Zevi, Y., Dathe, A., McCarthy, J. F., Richards, B. K., and Steenhuis, T. S. (2005). "Distribution of colloid particles onto interfaces in partially saturated sand." *Environmental Science and Technology*, 39(18), 7055–7064.
- Zevi, Y., Gao, B., Zhang, W., Morales, V. L., Cakmak, M. E., Medrano, E. A., Sang, W., and Steenhuis, T. S. (2012). "Colloid retention at the meniscus-wall contact line in an open microchannel." *Water research*, 46(2), 295–306.
- Zhang, L., Seagren, E. A., Davis, A. P., and Karns, J. S. (2010). "The capture and destruction of Escherichia coli from simulated urban runoff using conventional bioretention media and iron oxide-coated sand." *Water environment research : a research publication of the Water Environment Federation*, 82, 701–714.
- Zhang, Q., Hassanizadeh, S. M., Raouf, A., van Genuchten, M. T., and Roels, S. M. (2012). "Modeling Virus Transport and Remobilization during Transient Partially Saturated Flow." *Vadose Zone Journal*, 11(2).
- Zhang, W., Isaacson, C. W., Rattanaudompol, U., Powell, T. B., and Bouchard, D. (2012). "Fullerene nanoparticles exhibit greater retention in freshwater sediment

- than in model porous media.” *Water research*, Elsevier Ltd, 46(9), 2992–3004.
- Zhang, W., Morales, V. L., Cakmak, M. E., Salvucci, A. E., Geohring, L. D., Hay, A. G., Parlange, J. Y., and Steenhuis, T. S. (2010). “Colloid transport and retention in unsaturated porous media: Effect of colloid input concentration.” *Environmental Science and Technology*, 44(13), 4965–4972.
- Zhuang, J., Goeppert, N., Tu, C., McCarthy, J. F., Perfect, E., and McKay, L. (2010). “Colloid transport with wetting fronts: interactive effects of solution surface tension and ionic strength.” *Water research*, Elsevier Ltd, 44(4), 1270–8.
- Zhuang, J., McCarthy, J. F., Tyner, J. S., Perfect, E., and Flury, M. (2007). “In situ colloid mobilization in Hanford sediments under unsaturated transient flow conditions: effect of irrigation pattern.” *Environmental science & technology*, 41(9), 3199–204.
- Zhuang, J., Qi, J., and Jin, Y. (2005). “Retention and transport of amphiphilic colloids under unsaturated flow conditions: effect of particle size and surface property.” *Environmental science & technology*, 39(20), 7853–9.
- Zhuang, J., Tyner, J. S., and Perfect, E. (2009). “Colloid transport and remobilization in porous media during infiltration and drainage.” *Journal of Hydrology*, Elsevier B.V., 377(1-2), 112–119.
- Zou, Y., and Zheng, W. (2013). “Modeling manure colloid-facilitated transport of the weakly hydrophobic antibiotic florfenicol in saturated soil columns.” *Environmental Science and Technology*, 47, 5185–5192.